University of Texas Rio Grande Valley
ScholarWorks @ UTRGV

Theses and Dissertations

5-2021

Design of Multi-Layered Lenses for Resolusion Enhancement

S. M. Zia Uddin
The University of Texas Rio Grande Valley

Follow this and additional works at: https://scholarworks.utrgv.edu/etd

Part of the Electrical and Computer Engineering Commons

Recommended Citation

Uddin, S. M. Zia, "Design of Multi-Layered Lenses for Resolusion Enhancement" (2021). *Theses and Dissertations*. 987.
https://scholarworks.utrgv.edu/etd/987

This Thesis is brought to you for free and open access by ScholarWorks @ UTRGV. It has been accepted for inclusion in Theses and Dissertations by an authorized administrator of ScholarWorks @ UTRGV. For more information, please contact justin.white@utrgv.edu, william.flores01@utrgv.edu.

DESIGN OF MULTI-LAYERED META-LENSES FOR IMAGE RESOLUSION ENHANCEMENT

A Thesis

by

S M ZIA UDDIN

Submitted to the Graduate College of
The University of Texas Rio Grande Valley
In partial fulfillment of the requirements for the degree of

MASTER OF SCIENCE IN ENGINEERING

May 2021

Major Subject: Electrical Engineering

DESIGN OF MULTI-LAYERED META-LENSES FOR IMAGE RESOLUSION ENHANCEMENT

A Thesis
by
S M ZIA UDDIN

COMMITTEE MEMBERS

Dr. Nantakan Wongkasem
Chair of Committee

Dr. Heinrich D. Foltz
Committee Member

Dr. Yong Zhou
Committee Member

May 2021

Copyright 2021 S M ZIA UDDIN

All Rights Reserved

ABSTRACT

Uddin, S M Zia, Design of multi-layered meta-lenses for image resolution enhancement, Master of Science (MS), May 2021, 120 pp., 3 tables, 53figures, references, 50 titles.

Lenses are important optical device having numerous applications in our day-to-day life. As the conventional lenses, we use concave or convex lenses. These lenses are made with natural materials and the image quality imperfect. Furthermore, they are bulky, and design is complex. Consequently, mass production is difficult.

The shapes of entrance and exit faces of lenses has impact on its imaging capability [30]. The Lens material also play a vital role for reconstructing the image. Flat lenses can be considered as a good alternative of the conventional lenses. One of the advantages of this Flat lenses is that it can restore both the propagating and evanescent waves in the image plane. The conventional lenses only restore the information contained by the propagating waves and the evanescent waves that contains small subwavelength information of the object decays in the image plane. Flat Lenses are preferable in terms of image quality.

DEDICATION

My mother REHANA AKTHER, my father SYED MD. NASIM UDDIN and my sister SYEDA NABILA SULTANA wholeheartedly supported and inspired me. I am grateful to them. Thank you for love and patience.

ACKNOWLEDGMENTS

I am truly grateful to my advisor Dr. Nantakan Wongkasem for her remarkable guidance, support, advice, and patience throughout the research. I have learned a lot from her. She taught me how to think in an innovative way. I also would like to thank Dr. Foltz, Dr. Zhou, Dr. Huq, Dr. Ghalia, Dr. Islam for their suggestions and advice throughout the semesters. I should mention especially GM Shashi, Sazid Hasan for their support in pursuing my master's degree. I also would like to mention Md. Ali Zaker Shawon, Md. Shakil Arman, Md.Ashif Hossain Chowdhury and Md Shoriful Islam for their support throughout the master's. I also thank Dr. Parwinder Grewal, who initiated financial support in UTRGV, that helps to prosper in research works. I also got a lot of help from Bangladeshi Students and Community living in the Rio Grande Valley during my research period. My heartiest thanks to them. Finally, I would like to thank Dr. Wongkasem for inspiring me all the time.

TABLE OF CONTENTS

Page

ABSTRACT iii

DEDICATION iv

ACKNOWLEDGEMENTS v

TABLE OF CONTENTS vi

LIST OF TABLES x

LIST OF FIGURES xi

CHAPTER I. INTRODUCTION 1

CHAPTER II. THEORIES AND LITERATURE REVIEWS 3

2.1: Idea of Metamaterials 3

2.2: Meta-Lenses 5

2.3: Classification of Meta-Lenses 10

2.3.1: Patterned Meta-Lenses 10

2.3.2: Layered Meta-Lenses 13

CHAPTER III. RESEARCH METHODOLOGY 18

3.1.1: 1-D electric energy density analysis 19

3.1.2: 3-D Image of the sub-diffractive object Vs. meta-lenses' paraxial image location 41

CHAPTER IV DESIGN AND NUMERICAL STUDIES 75

4.1: Conductor Meta-Lens: PMMA/Ag/PR..... 75

4.1.1. Varying Silver (Ag) Thickness (PMMA and PR fixed at 40nm and 120nm 76

4.1.2. Varying PMMA Thickness (Ag and PR fixed at 10nm and 120nm)..... 77

4.1.3. Varying PR Thickness (Ag and PMMA fixed at 10nm and 8nm)..... 78

4.2: Semiconductor Meta-Lens: Glass/TiO2/PR 79

4.2.1. Varying TiO_2 Thickness (Glass and PR fixed at 100nm and 100nm)..... 80

4.2.2. Varying Glass Thickness (TiO_2 and PR fixed at 80nm and 100nm)..... 81

4.2.3. Varying PR Thickness (TiO_2 and Glass fixed at 80nm and 98nm)..... 83

4.3 Conductive Polymer Meta-Lens: PMMA/PNIPAM/PR..... 84

4.3.1. Varying Polymer (PNIPAM) Thickness

(PMMA and PR fixed at 10nm and 100nm) 85

4.3.2. Varying PMMA Thickness (Polymer and PR fixed at 237nm and 100nm)..... 87

4.3.3. Varying PR Thickness (PMMA and Polymer fixed at 10nm and 237nm)..... 88

4.4: Optimized Single Layered Lenses dimensions 90

4.5: Multi-Layered Meta-Lenses dimensions and graph..... 91

4.5.1: Multi-Layered 1 stack 91

4.5.2: Multi-Layered 2 stack 92

4.5.3: Multi-Layered 4 stack 93

4.5.4: Multi-Layered 8 stack 93

4.6: Proposed Multi-Layered Meta-Lenses dimension and E-energy density of

Multi-Layered Lenses 94

4.7: Focusing 95

4.7.1: Focusing through illuminated object (without 40nm thick Ag layer) 95

4.7.2: Focusing through illuminated object (with 40nm thick Ag layer) (validation) 95

4.7.3: Focusing through Pendry's Ag slab 96

4.8: Focal bar 98

4.9: Focusing through proposed Lenses 99

4.9.1: Focusing through proposed Ag Lenses 99

4.9.2: Focusing through proposed TiO_2 Lenses 101

4.9.3: Focusing through proposed Polymer Lenses 103

4.9.4: Focusing through proposed Multi-Layer (1stack) Lenses.....105

4.9.5: Focusing through Multi-Layer (2 stack) Lenses..... 107

4.9.6: Focusing through Multi-Layer (4 stack) Lenses..... 109

4.9.7: Focusing through Multi-Layer (8 stack) Lenses..... 111

CHAPTER V CONCLUSIONS AND DISCUSSION..... 115

5.1: Conclusion 115

5.2: Discussion 115

5.3: Future works 116

5.3.1: Fabrication and measurement 116

5.3.2: Further optimization 116

5.3.3: Application approach 116

REFERENCES 117

BIOGRAPHICAL SKETCH..... 120

LIST OF TABLES

Table 1: E-energy density of single-layered lenses 90

Table: 2: E-energy density of multi-layered lenses 94

Table: 3: Comparison of E-field among various lenses 114

LIST OF FIGURES

Page

Figure 2.1: Regular Array of thin wires [4] 4

Figure 2.2: Split ring structure [5]..... 4

Figure 2.3: Combination of Split-ring structure and Thin wire [2]..... 5

Figure 2.4: Snell's law for positive ε & μ (1-4) and negative ε & μ (1-3). [9]..... 6

Figure 2.5: Double focusing through negative index material.[7] 6

Figure 2.6: Pendry's silver lens (a) Imaging through silver lens (b) The electrostatic field in the object plane. (c) The electrostatic field in the image plane with and without the silver slab in place.[7] 7

Figure 2.7: (a) Propagating and (b) Evanescent waves through the NIM [8]..... 9

Figure 2.8: Comparison of various types of optical lenses. a, Conventional lens. b, Near-field superlens. c, Far-field superlens. d, Hyperlens. The wavy curves and smooth curves represent propagating waves and evanescent waves, respectively. [8].....10

Figure 2.9: a, Schematic of a metalens element. b, Scanning electron micrograph of a region of a fabricated metalens [12] 11

Figure 2.10: Chromatic metalenses across the electromagnetic spectrum [13] 11

Figure 2.11: (a) Schematic of a single nanofin on a glass substrate. (b) Top-view scanning electron microscope image of a meta-grating comprised of arrays of nanofins [14].....12

Figure 2.12: This table summarizes different solutions proposed to address wavefront control with meta-surfaces [15] 12

Figure 2.13: All-dielectric polarization-independent transmissive meta-lenses [16] 13

Figure 2.14: System geometry. The layers are infinite in extent in the x-y plane. [18]..... 14

Figure 2.15: Schematic diagram of the transmission of normally evanescent waves, showing the role of surface plasmons. The line represents the electric field strength. [18] 15

Figure 2.16: Optical superlensing experiment. [20]..... 16

Figure 2.17: Schematic diagrams of (a) a single-layer and (b) double-layer super lenses [21]..... 17

Figure 2.18: Design of dual-layered meta-surfaces [22] 17

Figure 4.1: variation of Ag thickness from 10-100nm with 10nm gap..... 76

Figure 4.2: variation of Ag thickness from 5-15nm with 1nm gap 77

Figure 4.3: variation of PMMA thickness from 10-100nm with 10nm gap..... 77

Figure 4.4: variation of PMMA thickness from 5-15nm with 1nm gap 78

Figure 4.5: variation of PR thickness from 10-150nm with 10nm gap 78

Figure 4.6: variation of PR thickness from 115-125nm with 1nm gap 79

Figure 4.7: variation of TiO_2 thickness from 10-100nm with 10nm gap 80

Figure 4.8: variation of TiO_2 thickness from 75-85nm with 1nm gap..... 81

Figure 4.9: variation of Glass thickness from 10-100nm with 10nm gap..... 82

Figure 4.10: variation of Glass thickness from 95-105nm with 1nm gap 82

Figure 4.11: variation of PR thickness from 10-100nm with 10nm gap 83

Figure 4.12: variation of PR thickness from 95-105nm with 1nm gap 84

Figure 4.13: variation of polymer thickness from 140-320nm with 20nm gap 86

Figure 4.14: variation of polymer thickness from 220-260nm with 5nm gap 86

Figure 4.15: variation of polymer thickness from 235-255nm with 1nm gap 87

Figure 4.16: variation of PMMA thickness from 5-55nm with 5nm gap 88

Figure 4.17: variation of PMMA thickness from 5-15nm with 1nm gap 88

Figure 4.18: variation of PR thickness from 50-200nm with 10nm gap 89

Figure 4.19: variation of PR thickness from 95-105nm with 1nm gap 89

Figure 4.20: Optimized Single-Layered Lenses 90

Figure 4.21: Multi-Layered 1 stack dimension and E-energy density plot 92

Figure 4.22: Multi-Layered 2 stack dimension and E-energy density plot 92

Figure 4.23: Multi-Layered 4 stack dimension and E-energy density plot 93

Figure 4.24: Multi-Layered 8 stack dimension and E-energy density plot 93

Figure 4.25: Optimized Multi-Layered Lenses 94

Figure 4.26: Focusing without Lenses [30] 95

Figure 4.27: Focusing through Ag Lens [30] 96

Figure 4.28: Pendry's Ag Lens (a) Dimension and Right-side cross-sectional view (b) Thickness vs. E-field plot (c) Perspective view (d) Cross-section at highest E-field..... 98

Figure 4.29: Proposed Ag Lens (a) Dimension and Right-side cross-sectional view (b) Thickness vs. E-field plot (c) Perspective view (d) Cross-section at highest E-field 101

Figure 4.30: Proposed TiO_2 Lens (a) Dimension and Right-side cross-sectional view (b) Thickness vs. E-field plot (c) Perspective view (d) Cross-section at

highest E-field 103

Figure 4.31: Proposed Polymer Lens (a) Dimension and Right-side cross-sectional view (b) Thickness vs. E-field plot (c) Perspective view (d) Cross-section at highest E-field..... 105

Figure 4.32: Proposed Multi-Layer (1stack) (a) Dimension and Right-side cross-sectional view (b) Thickness vs. E-field plot (c) Perspective view (d) Cross- section at highest E-field..... 107

Figure 4.33: Proposed Multi-Layer (2 stack) (a) Dimension and Right-side cross-sectional view (b) Thickness vs. E-field plot (c) Perspective view (d) Cross-section at highest E-field..... 109

Figure 4.34: Proposed Multi-Layer (4 stack) (a) Dimension and Right-side cross-sectional view (b) Thickness vs. E-field plot (c) Perspective view (d) Cross-section at highest E-field.....111

Figure 4.35: Proposed Multi-Layer (8stack) (a) Dimension and Right-side cross-sectional View (b) Thickness vs. E-field plot (c) Perspective view (d) Cross-section at highest E-field..... 113

CHAPTER I

INTRODUCTION

Meta-lenses or metamaterial (MTM)-based lenses, ultra-thin flat lenses, hold the promise to revolutionize optics. Meta-lenses have been proposed by respective consideration of propagating and evanescent waves for far-field and near-field operation, to manipulate light to an aberration-free focus, as well as to amplify evanescent waves. With a complete planar symmetry and no principal optical axis, meta-lenses with an infinite aperture lead to unique imaging possibility. Meta-lenses can be made as a single metallic layer, metal-dielectric multi-layers, and patterned metasurface structures, focusing on developing a planar homogeneous medium that is either isotropic with negative index, or anisotropic with negative diagonal epsilons.

In this research, we propose novel single- and multi-layered flat meta-lenses. The focus is on getting a higher resolution image by enhancing the evanescent waves, which greatly relies on the materials chosen for conductive lens and dielectric substrate layers. Silver (Ag), Titanium oxide (TiO_2), and commercial conductive polymer, poly(N-isopropylacrylamide) (pNIPAM), based on their conductivity and complex permittivity at the operating visible frequency, 821 THz are selected to design for the single-layered lenses. Polymethyl methacrylate (PMMA) is chosen as a substrate for the Ag and conductive polymer, while SCOTT-SF (Dense flint) glass is chosen as a substrate for the TiO2 lens, respectively. It has shown that the enhanced transmission of the evanescent components occurs only in a finite band centered at a surface plasmon wave vector, where the photon impinging on the metal surface can excite a collective oscillation of conduction

electrons, resulting in a surface plasmon with maximum efficiency. The peak enhancement for various thicknesses of the stacked multilayer lens (Ag-TiO2) is investigated. Measuring the electric energy density serves to quantify the transitivity through various points of the meta-lenses. The thickness of each layer is varied to observe its independent changes to the overall transmissivity of the lens. Comparative simulations of the image of the sub-diffractive object, with and without the proposed meta-lenses proves the super-resoling capabilities of the lens slabs at the proposed meta-lenses' paraxial image location. Furthermore, these spatial energy density distribution results highlight the super-resolution imaging found in our proposed single-layered and multi-layered lenses.

CHAPTER II

THEORIES AND LITERATURE REVIEWS

2.1: Idea of Metamaterials

Metamaterials are engineered materials that possess the unconventional material properties. In 1968, Veselago first theoretically proposed the idea of a medium which has both ε and μ negative and this type of medium would show reversal of Doppler shift and Cherenkov radiation, anomalous refraction, or reverse equivalence of Snell's law [1,2,3].

In 1995, Pendry gave the idea that simple metallic microstructure comprising a regular array of thin wires could provide negative permittivity [4] and in 1999, he also presented that a split ring shape placed along the direction of propagation could display negative permeability [5]. In 1999, D. R. Smith and his team experimentally demonstrated that a periodic array of interspaced conducting nonmagnetic split ring resonators and continuous wires forms a composite medium which can be considered as new metamaterial. [2]

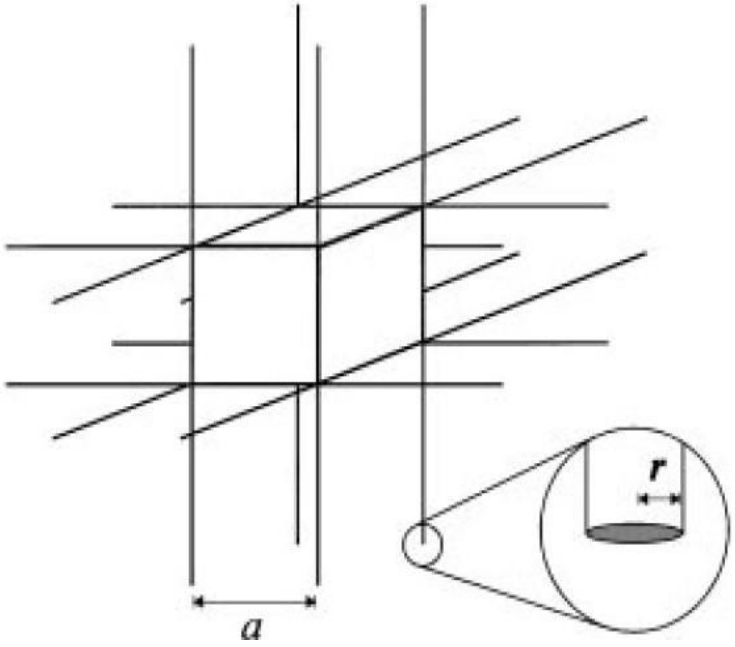

Figure 2.1: Regular Array of thin wires [4]

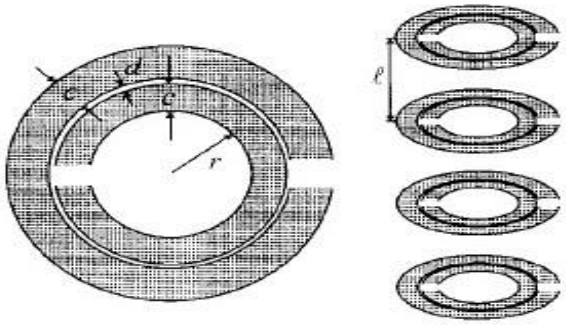

Figure 2.2: Split ring structure [5]

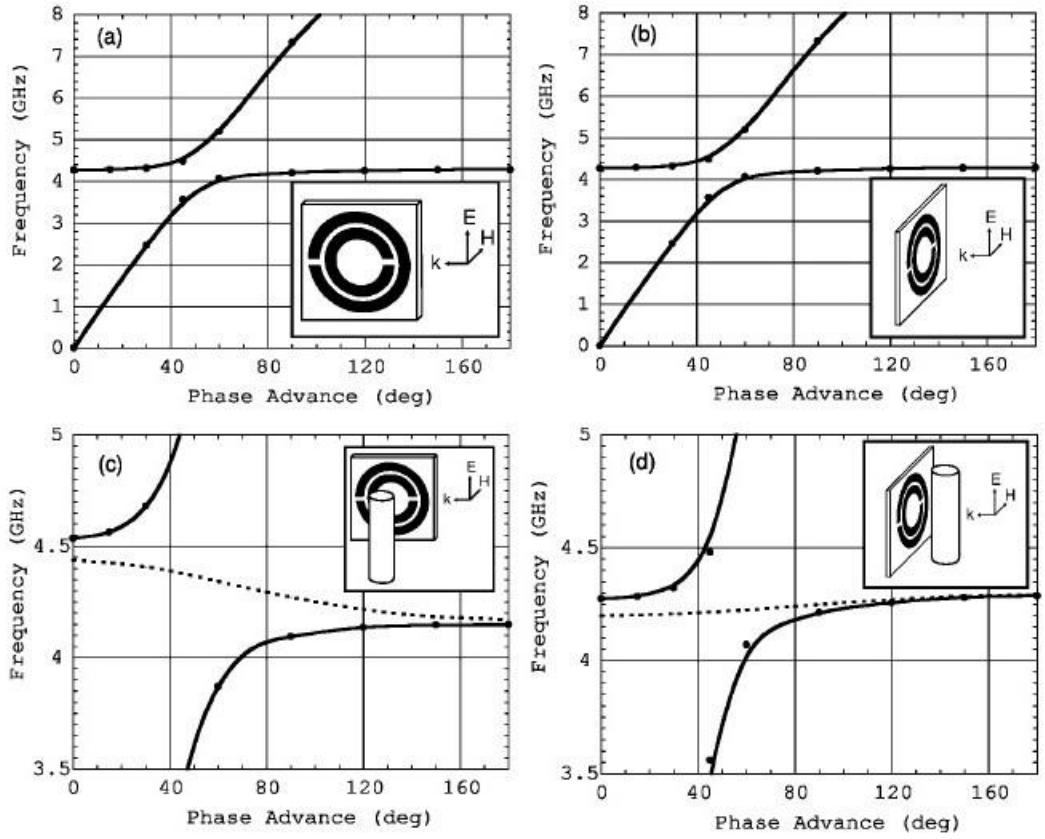

Figure 2.3: Combination of Split-ring structure and Thin wire [2]

2.2: Meta-Lenses

The meta-lenses or metamaterial-based lenses possess the property of super-resolution and desirable features of traditional lenses. [6]. In 2000, Pendry pointed out an idea of "superlens" that is free from the limitation of traditional lenses. He suggested that a negative refractive index material can focus light where both the dielectric function (ε) and magnetic permeability (μ) are negative. It is important to that there is relation between surface plasmon and the focusing action where $\varepsilon = -1$ is required for the existence of surface plasmon. To focus image and to restore amplitude of the higher order Fourier components, Pendry used a silver

slab. In these lenses, both the propagating and evanescent waves has significant contribution for the image resolution [7].

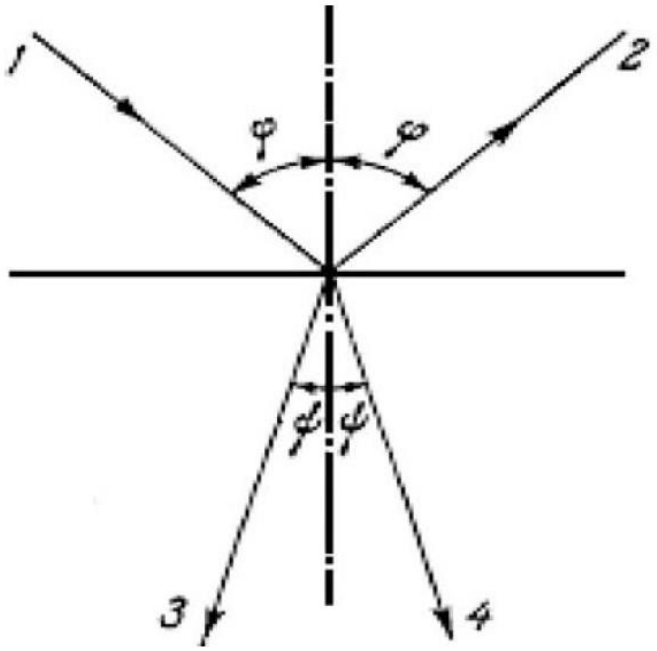

Figure 2.4: Snell's law for positive ε & μ (1-4) and negative ε & μ (1-3). [9]

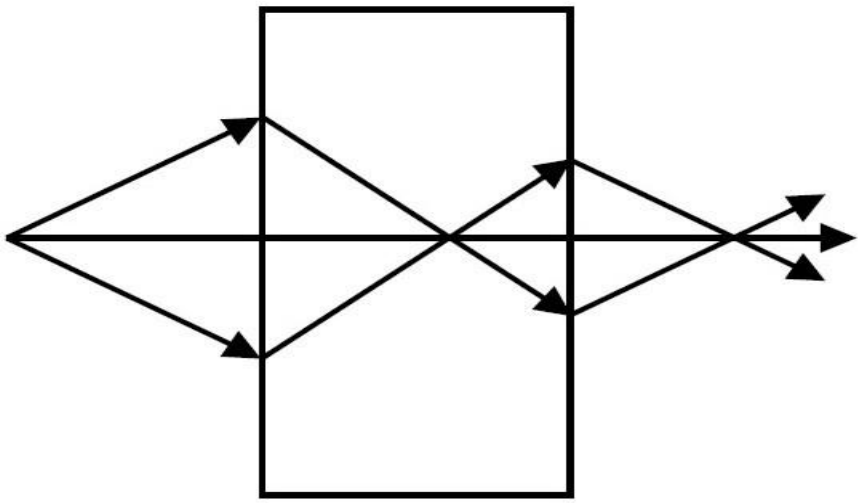

Figure 2.5: Double focusing through negative index material.[7]

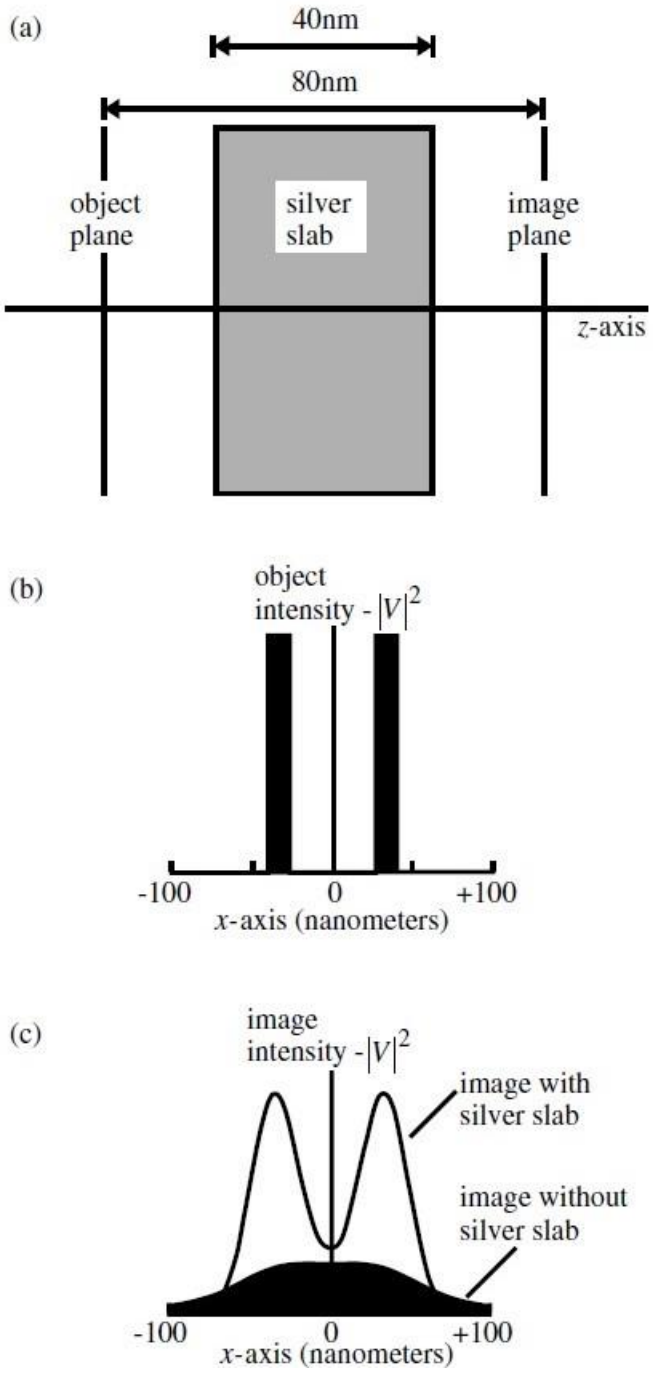

Figure 2.6: Pendry's silver lens (a) Imaging through silver lens (b) The electrostatic field in the object plane. (c) The electrostatic field in the image plane with and without the silver slab in place.[7]

Emitted or scattered light from an object contains both propagating and evanescent waves and these evanescent waves carry the subwavelength detail of the object. In case of positive refractive index medium, the evanescent wave decays exponentially and for this reason they cannot be collected by the traditional lens. As a result, the image becomes diffraction limited. Negative Index Material (NIM) gives a solution to this.

When an object is placed near an NIM lens, the near-field evanescent waves are strongly improved through the lens. After coming out of the lens, evanescent waves deteriorates again until their amplitudes reach their original level at the image plane. In addition to that, the propagating waves go through the NIM lens with the occurrence of negative refraction and reversed phase front simultaneously and in the image plane there is zero phase change. Thus, a perfect image is formed though completely recovering both propagating and evanescent waves in phase and amplitude. The resolution of conventional lens is diffraction limited whereas the resolution of the superlens is determined by the enhancement and by the number of restored evanescent modes.[8]

In case of subwavelength scale, the electrostatic limit can be applied. Here, the electric and magnetic responses of a material decouple. To support resonant surface waves, for one specific polarization (transverse magnetic, TM or transverse electric, TE mode) only one material property (ε or μ) needs to be negative. Single negative index medium can act as a superlens for single polarization of light. A silver slab can be considered as a natural candidate for superlens effect which has negative ε at optical frequency. Superlens properties has been investigated in terms of resolution, inherent loss and so on.

In 2003, it has been found in an optical experiment that silver lens exhibits superlens effect by enhancing the evanescent wave. It has also been observed in the experiment that the optimized thickness of the film/material and surface roughness must be considered to get the best outcome from the superlens.

In microwave and optical frequencies, superlens has different designs. Wires and split ring resonator form a microwave metamaterial which demonstrate superlensing effect in microwave range. Thin slab of silver works as a superlens in optical frequency and could image 60nm features (ƛ/6) which is well below the diffraction limit. [8]

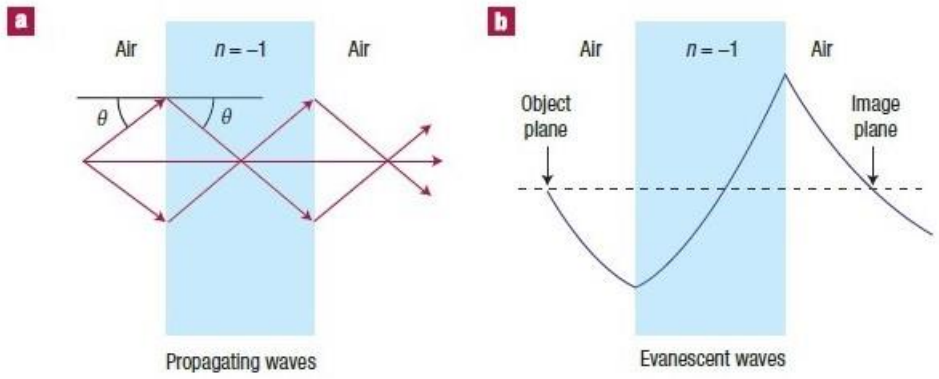

Figure 2.7: (a) Propagating and (b) Evanescent waves through the NIM [8]

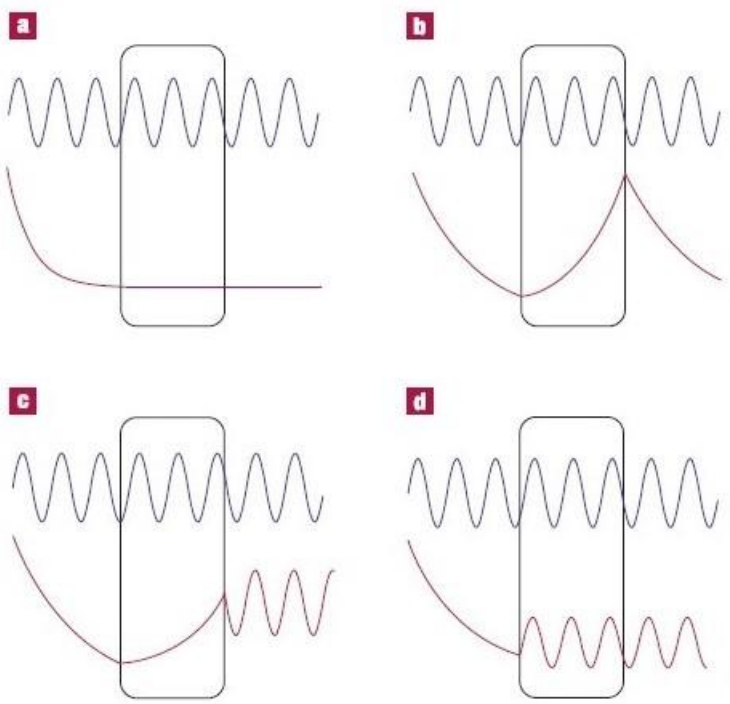

Figure 2.8: Comparison of various types of optical lenses. a, Conventional lens. b, Near-field superlens. c, Far-field superlens. d, Hyperlens. The wavy curves and smooth curves represent propagating waves and evanescent waves, respectively. [8]

2.3: Classification of Meta-Lenses

Meta-lenses can be classified into patterned which is meta-surface based and/or layered lens. [10]

2.3.1: Patterned Meta-Lenses

Subwavelength spaced nanostructures at an interface forms meta-surface which can control properties of light which includes phase, amplitude, and polarization of light. [11]

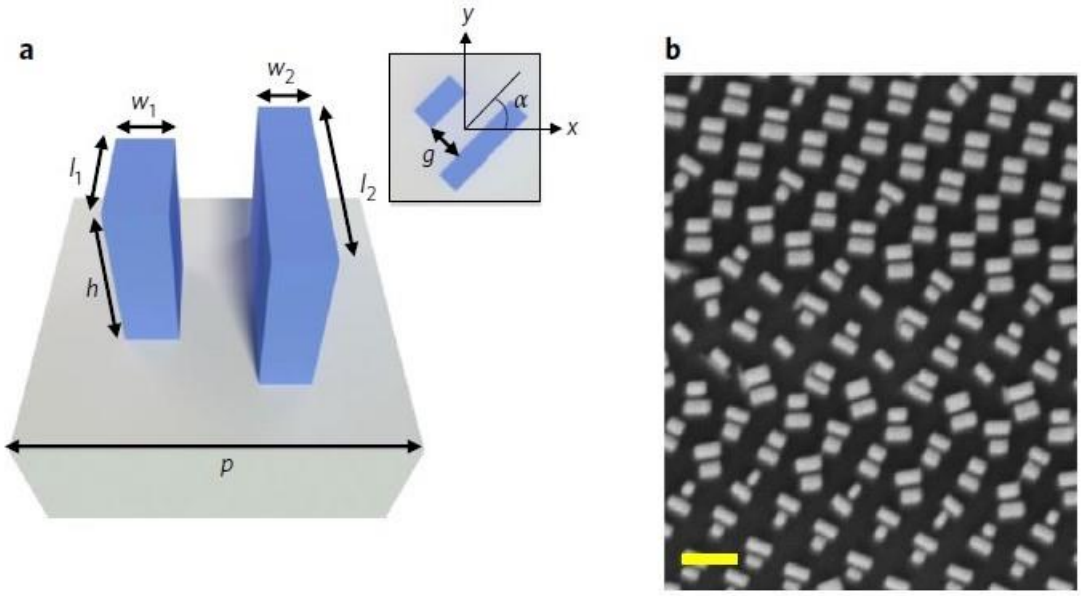

Figure 2.9: a, Schematic of a metalens element. b, Scanning electron micrograph of a region of a fabricated metalens [12]

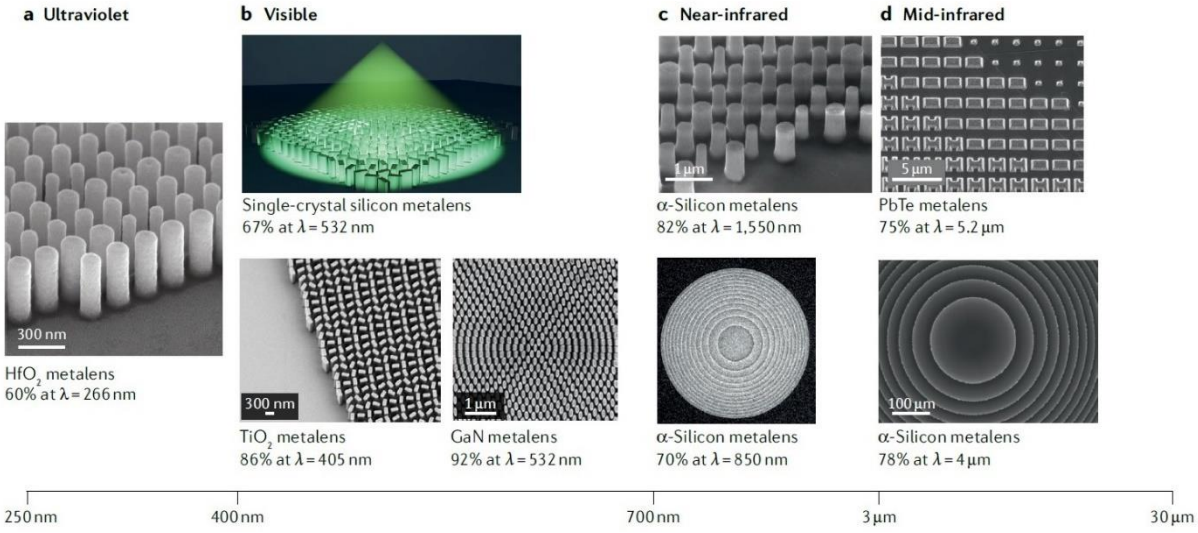

Figure 2.10: Chromatic metalenses across the electromagnetic spectrum [13]

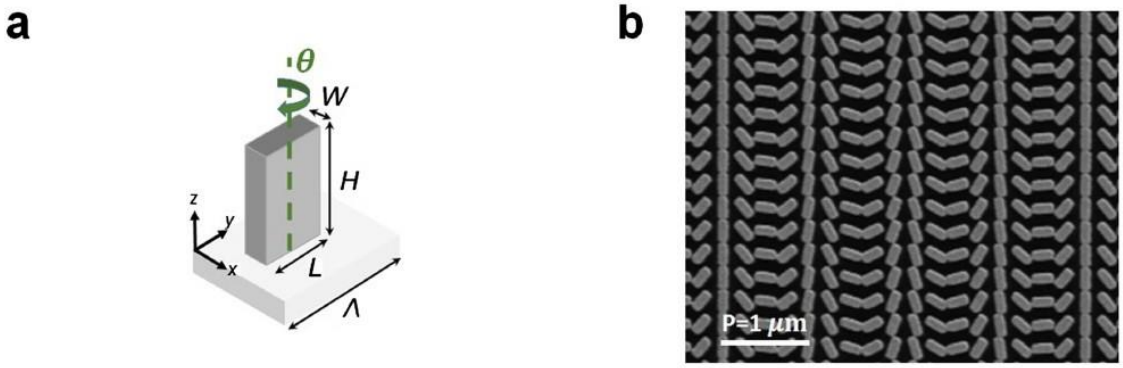

Figure 2.11: (a) Schematic of a single nanofin on a glass substrate. (b) Top-view scanning electron microscope image of a meta-grating comprised of arrays of nanofins [14]

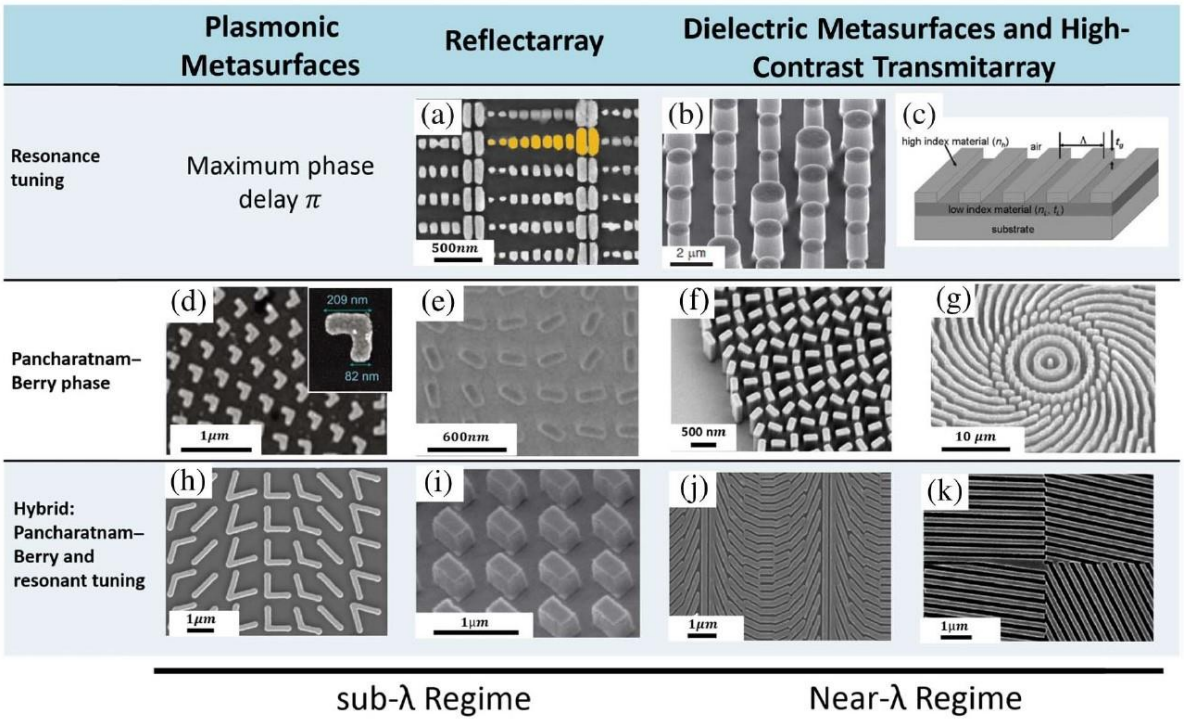

Figure 2.12: This table summarizes different solutions proposed to address wavefront control with metasurfaces [15]

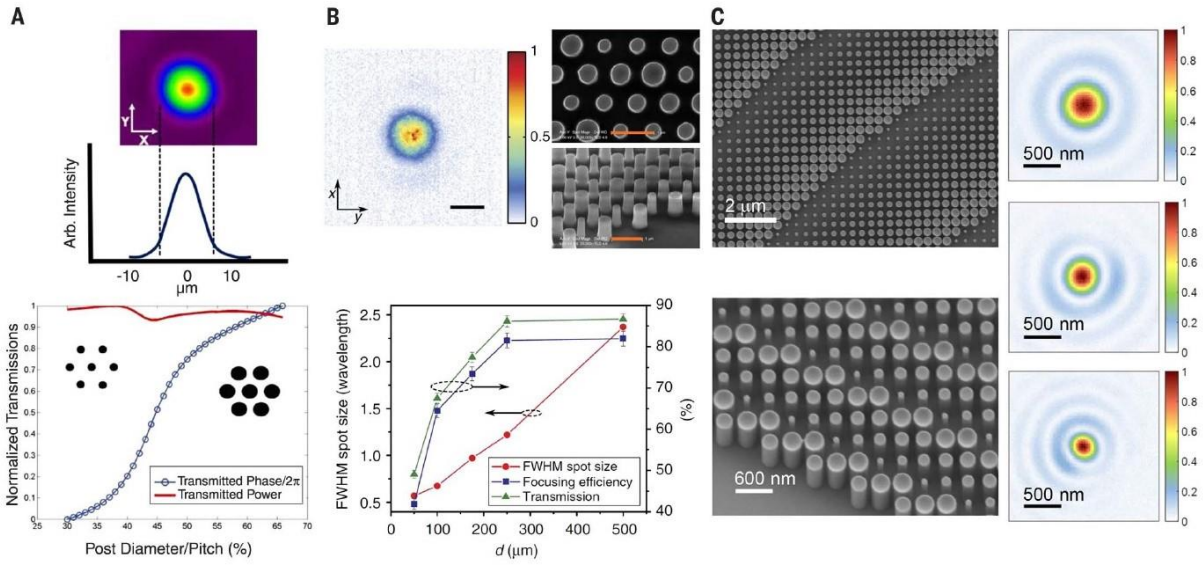

Figure 2.13: All-dielectric polarization-independent transmissive meta-lenses [16]

2.3.2: Layered Meta-Lenses

In these meta-lenses, isotropic medium where n=-1 can be used or anisotropic medium with a constitutive tensor having diagonal components of opposite sign where $\varepsilon_{\parallel}\varepsilon_{\perp}$=-1 can be used.[10]

The following permittivity tensor form is required for the effective propagation of transmission line modes: [17]

$\bar{\bar{\varepsilon}} = xx + yy + \propto zz$ .... (1)

In case of natural materials, it is impossible to get high permittivity value in optical range. But through metamaterial where layered metal-dielectric structures have been used, it is possible to attain high permittivity value. [17]

Ramakrishna *et al* proposed a metamaterial which consists of alternating metal and dielectric layers. This layered system can act as a superlens.[19]

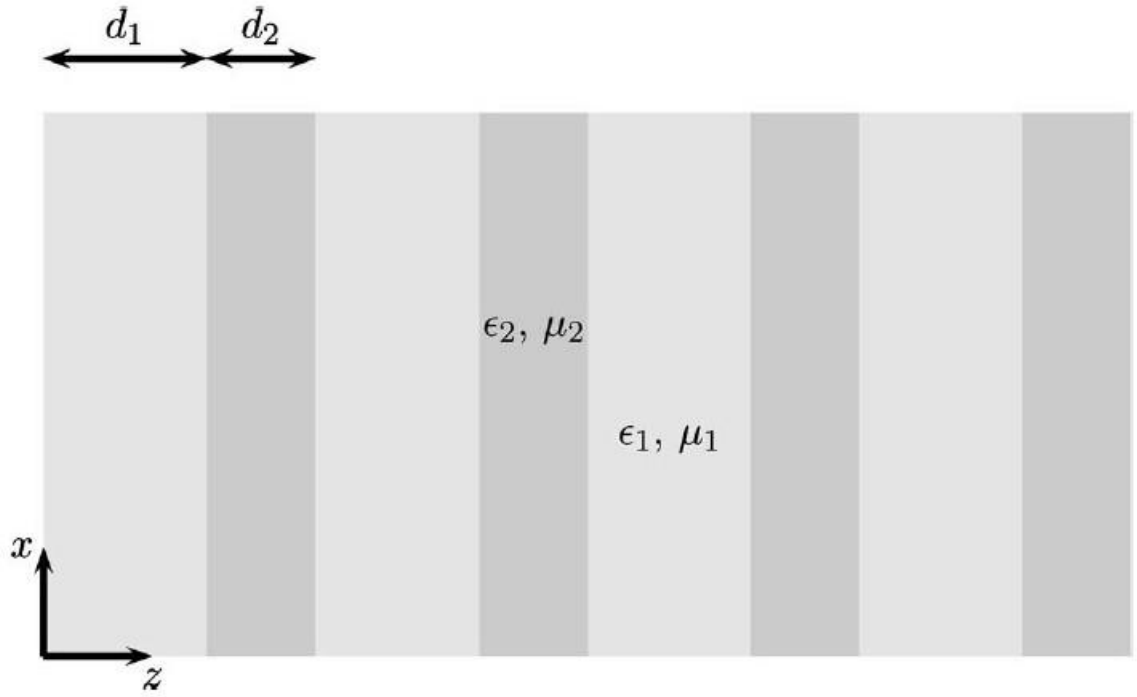

Figure 2.14: System geometry. The layers are infinite in extent in the x-y plane. [18]

In Figure 14, Layered structure has been presented. This type of metamaterial can be described though the following permittivity tensor form: [17]

$$\bar{\bar{\varepsilon}} = \varepsilon_{\parallel}(xx + yy) + \varepsilon_{\perp}\, zz \quad \ldots\ldots (2)$$

where,

$$\varepsilon_{\parallel} = \frac{\varepsilon_1 d_1 + \varepsilon_2 d_2}{d_1 + d_2},\ \ \varepsilon_{\perp} = \left[\frac{\varepsilon_1^{-1} d_1 + \varepsilon_2^{-1} d_2}{d_1 + d_2}\right]^{-1} \ldots\ldots (3)$$

To achieve a permittivity tensor like equation 1, the parameter for the layered metamaterial should be $\varepsilon_1/\varepsilon_2 = -d_1/d_2$ and $\varepsilon_1 + \varepsilon_2 = 1$. From the aforementioned equations, it can be said that one of the layers need to have negative permittivity and so one dielectric and one metallic layer is necessary to form a layered metamaterial structure. For example, $\varepsilon_1 = 2;\ \varepsilon_2 = -1$ and $d_1/d_2 = 2$ can be chosen to design a layered structure. [17]

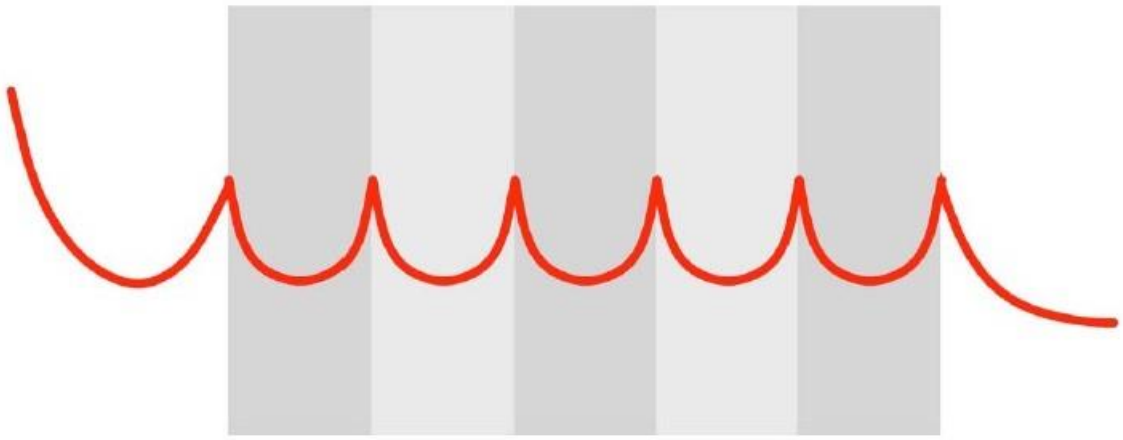

Figure 2.15: Schematic diagram of the transmission of normally evanescent waves, showing the role of surface plasmons. The line represents the electric field strength. [18]

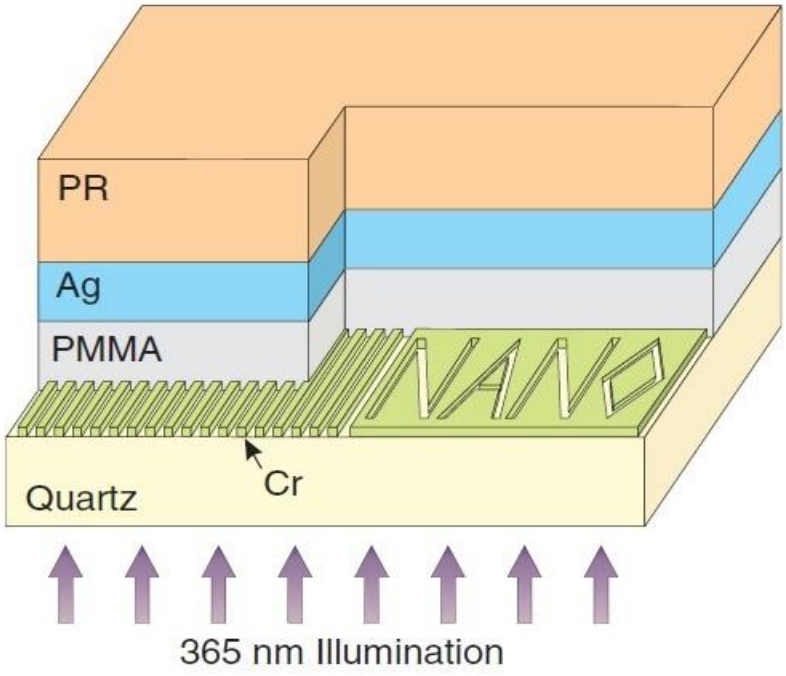

Figure 2.16: Optical superlensing experiment. **[20]**

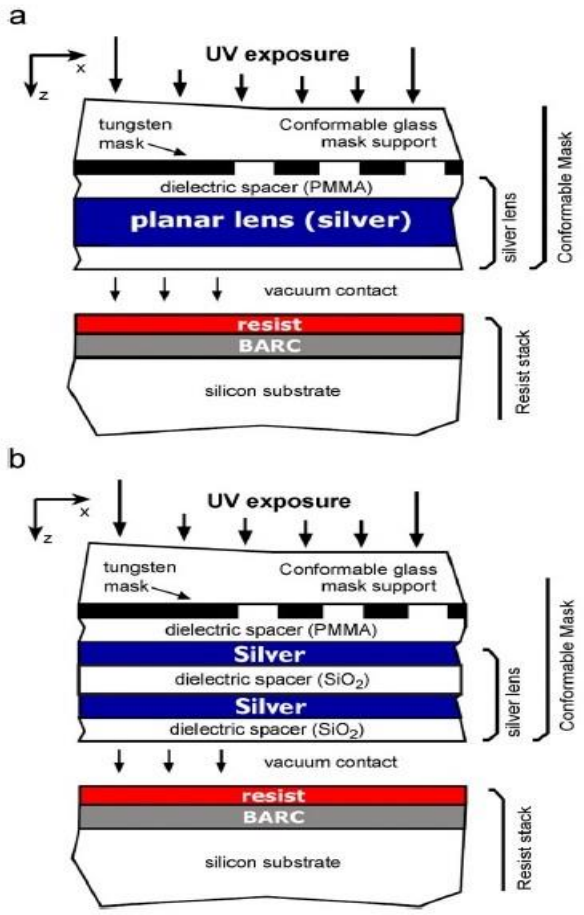

Figure 2.17: Schematic diagrams of (a) a single-layer and (b) double-layer super lenses [21]

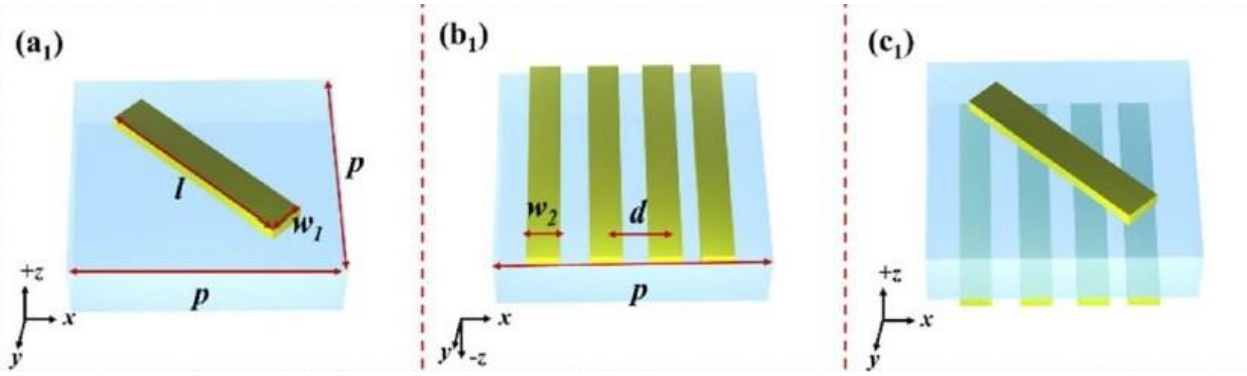

Figure 2.18: Design of dual-layered meta-surfaces [22]

CHAPTER III

RESEARCH METHODOLOGY

The source excitation was set to enter the lens through the substrate material for each 3 lenses. The PR (Photoresist) was used as a common coating material for all the lenses to create image distance. Electric energy density was monitored at the frequency of 821THz to evaluate the effect of evanescent waves.

We observed how the E-energy density has been changed while passing through the prime lens material (Ag, TiO_2 or PNIPAM) as well as the substrate and coating material. The particle size or skin depth of the main lens material for each lens was studied as it points out to the least feasible thickness of the material for fabrication purposes. All the thicknesses were in the nanoscale range. A full-wave excitation, operating from 800-850 THz covering the optical frequency range was run perpendicularly along the z axis to the lens structure plane.

The periodic boundary was set so the structure was repeated in both axes, x, and y, on the structure plane. All the simulations were done using CST Microwave Studio software. TM polarization mode was performed for all the simulations where the value of μ was kept 1 for all three lenses and complex value of ε was used to materialize the property close to the ideal superlens.

Multi-Layered Lenses have been formed though using single layered lenses' materials. The E-energy density of the multi-layered lenses has also been observed. E-energy density demonstrates the amplification of evanescent waves.

The focusing performance of each single-layered and multi-layered meta-lenses has also been observed. The parameter used here is E-field. At the focusing point, the E-field intensity is highest than its surroundings.

The meta-lenses performance has been monitored through its evanescent wave amplification and also, it's focusing.

3.1.1 1-D electric energy density analysis

Step 1: Click on New Template

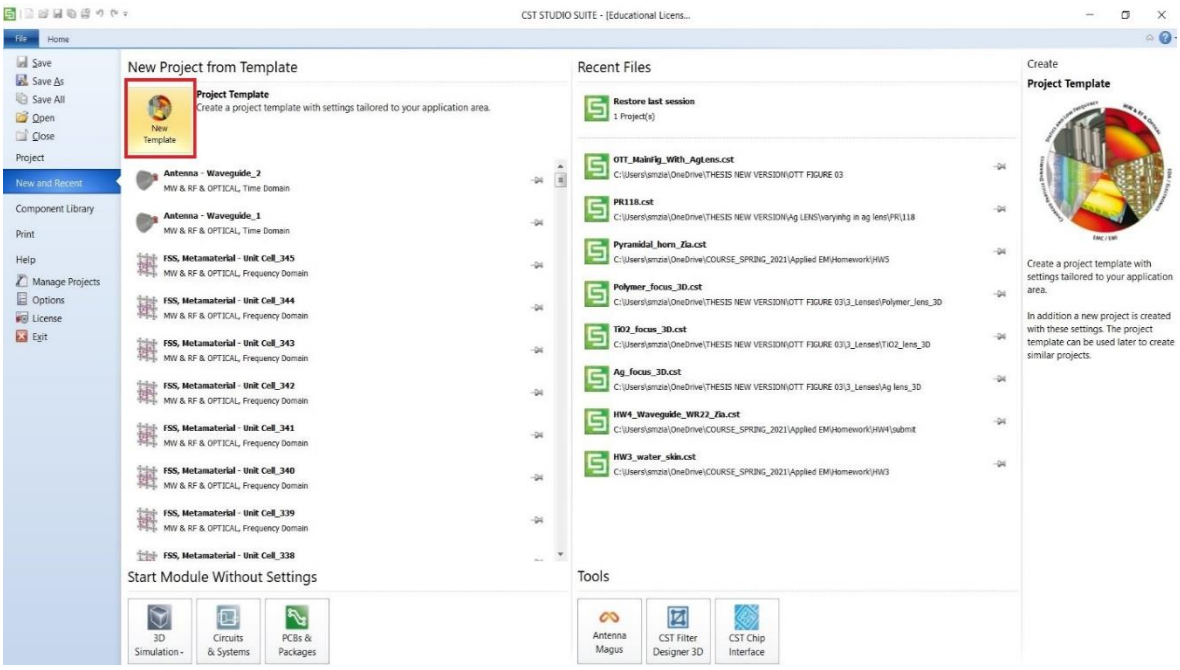

Step 2: Click on MW & RF & Optical

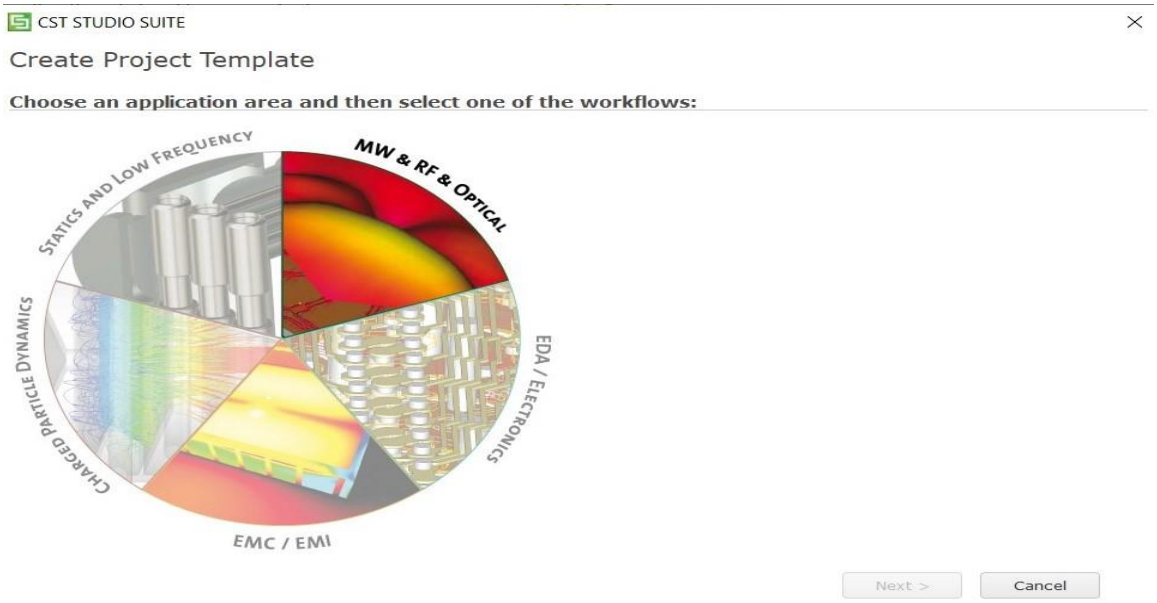

Step 3: Select Periodic structures

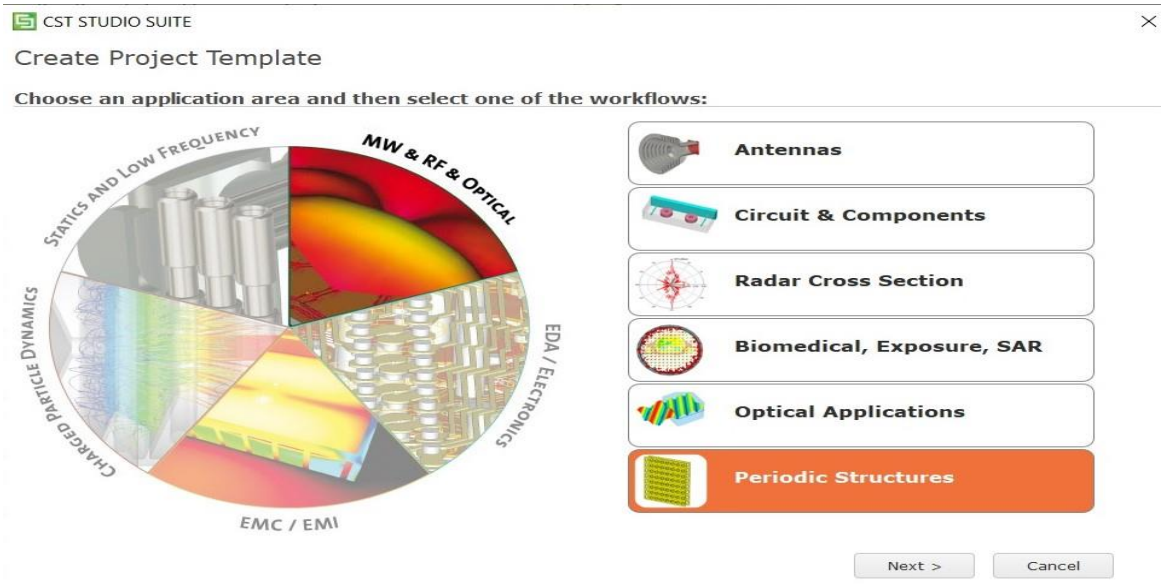

Step 4: Select FSS, Metamaterial-Unit Cell

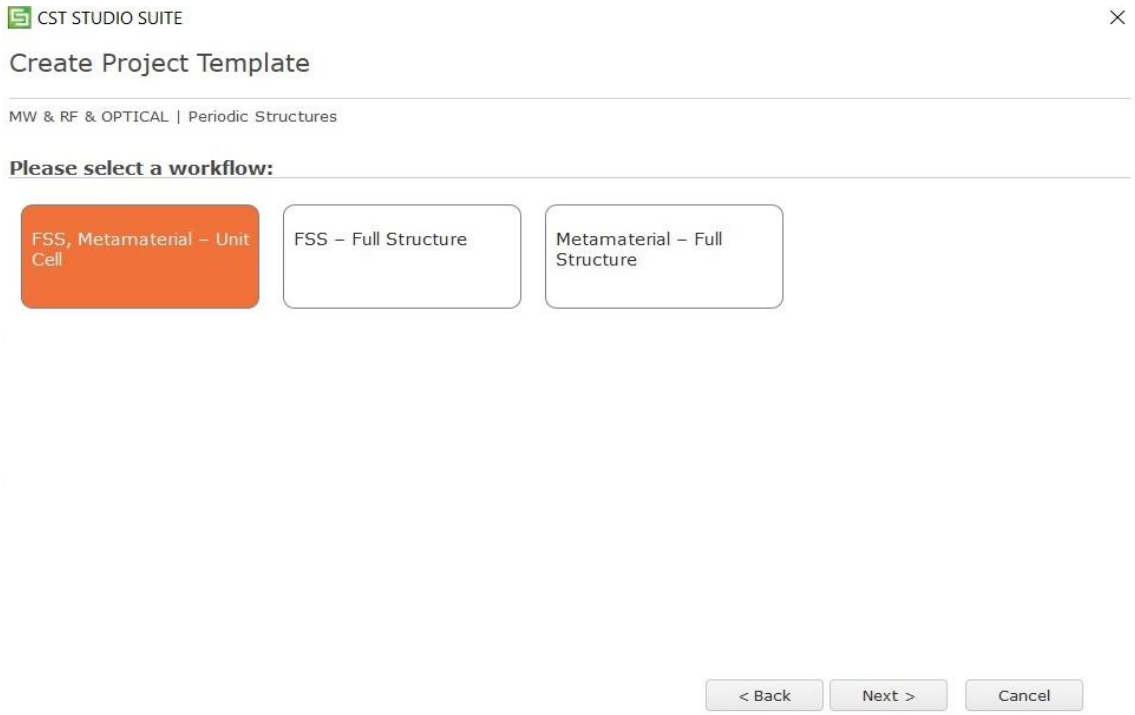

Step 5: Select phase reflection diagram.

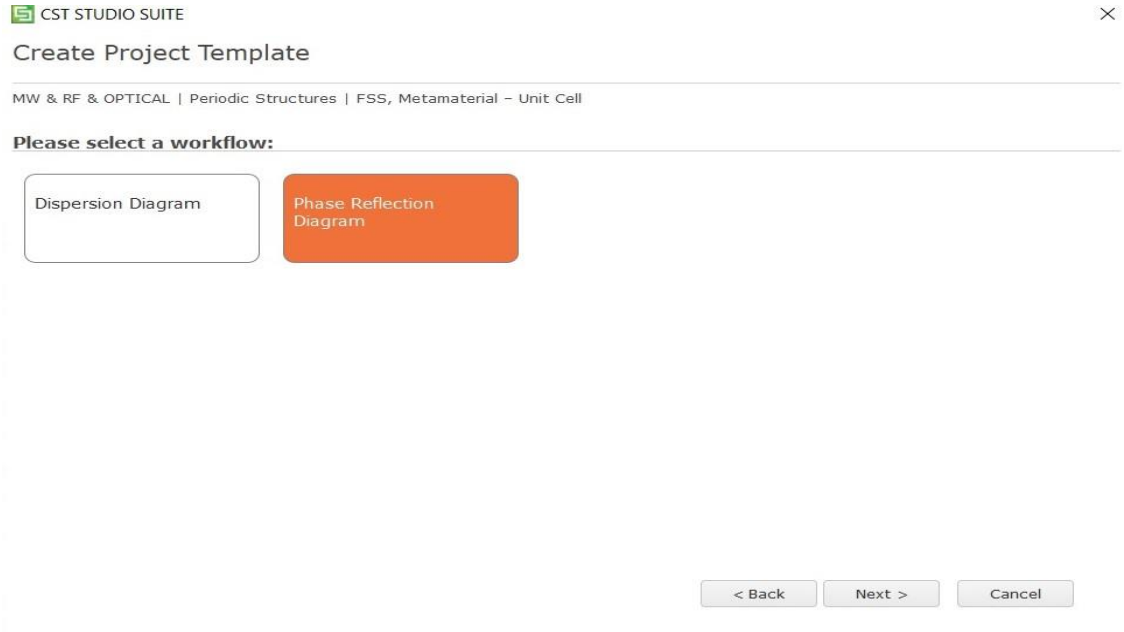

Step 6: Select Frequency Domain

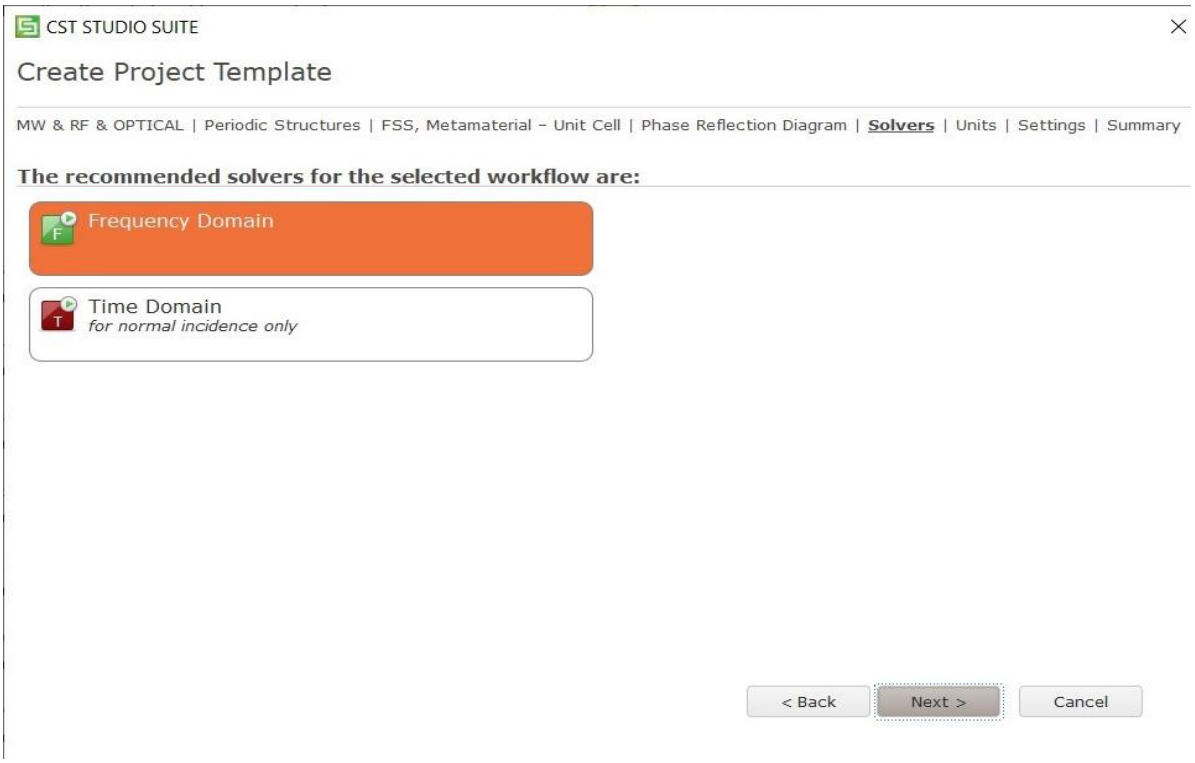

Step 7: Dimensions in nm & frequency in THz:

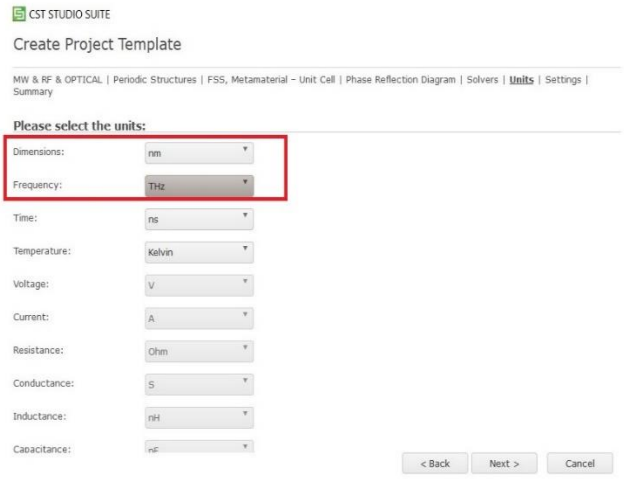

Step 8: Define at 800; 821; 850; 900 THz

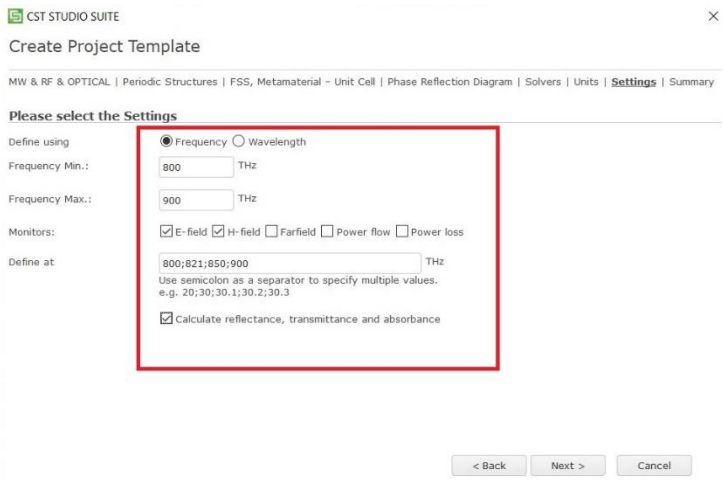

Step 9: New project template has been created.

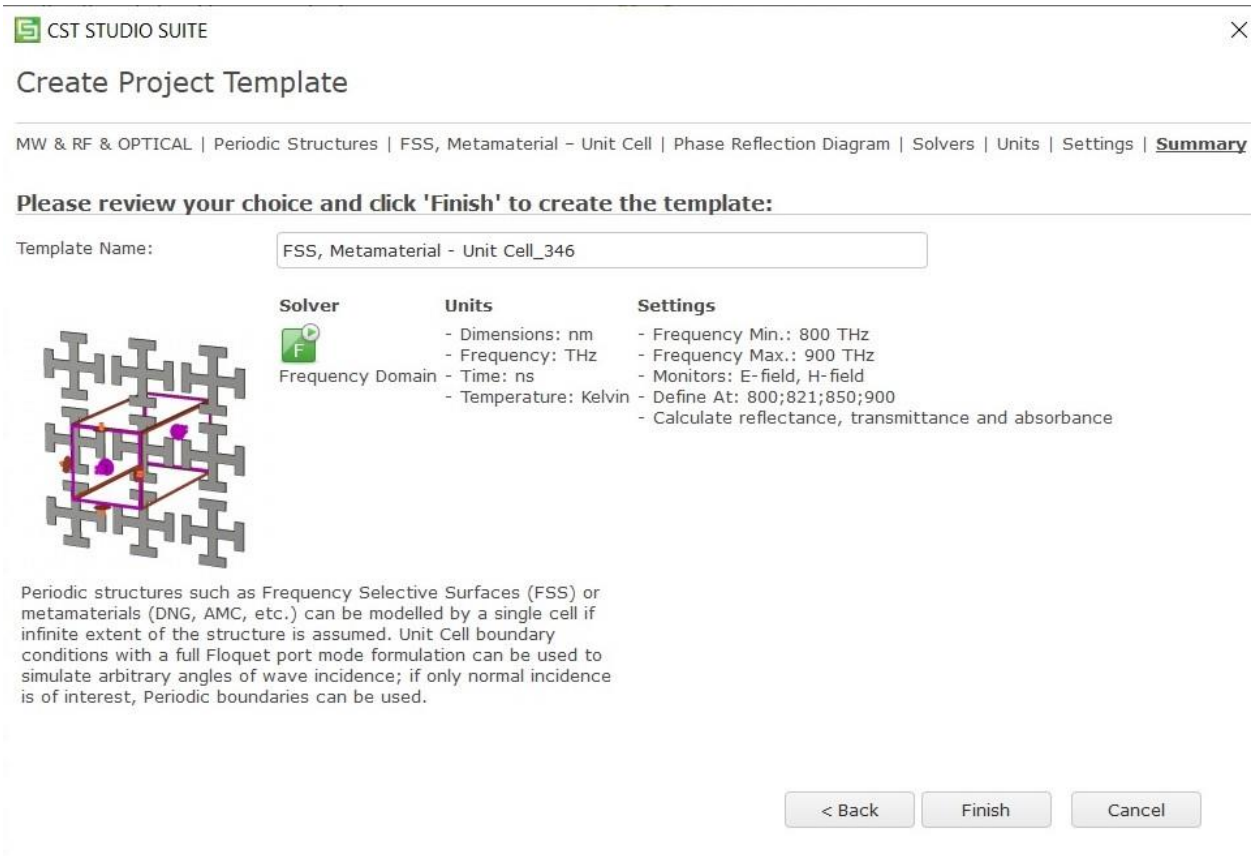

Step 10: Main worksapce

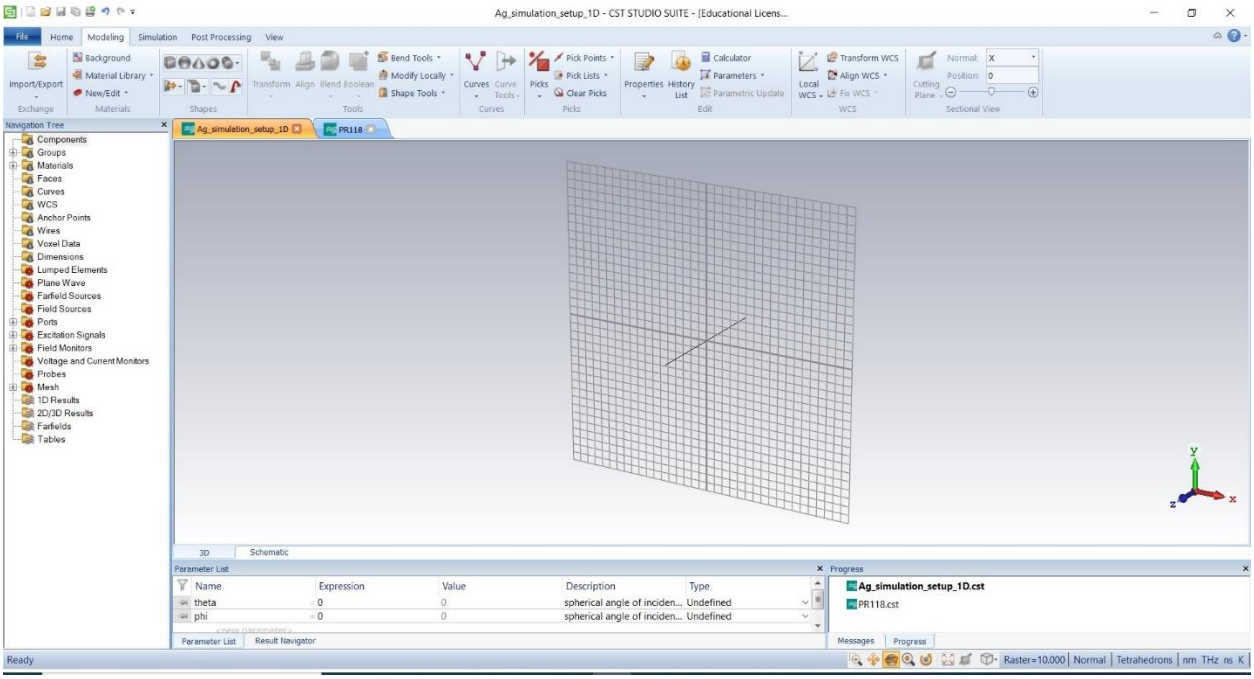

Step 11: Select Brick for a new material

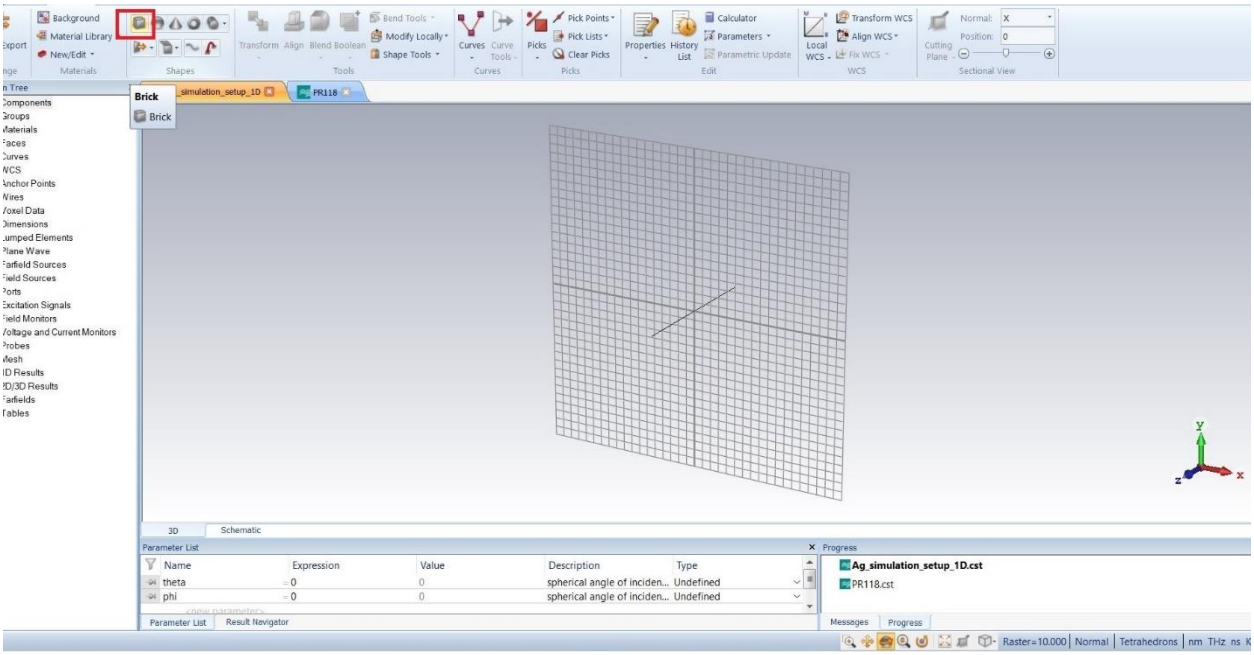

Step 12: Define dimension & Select New Material

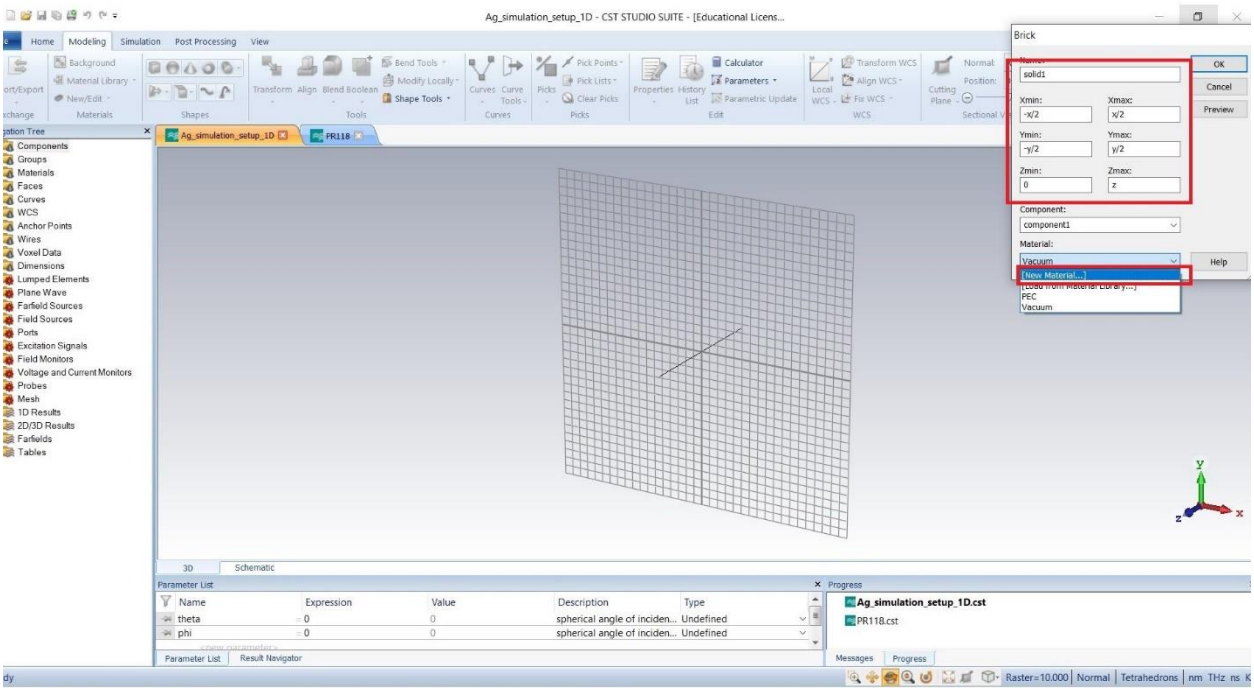

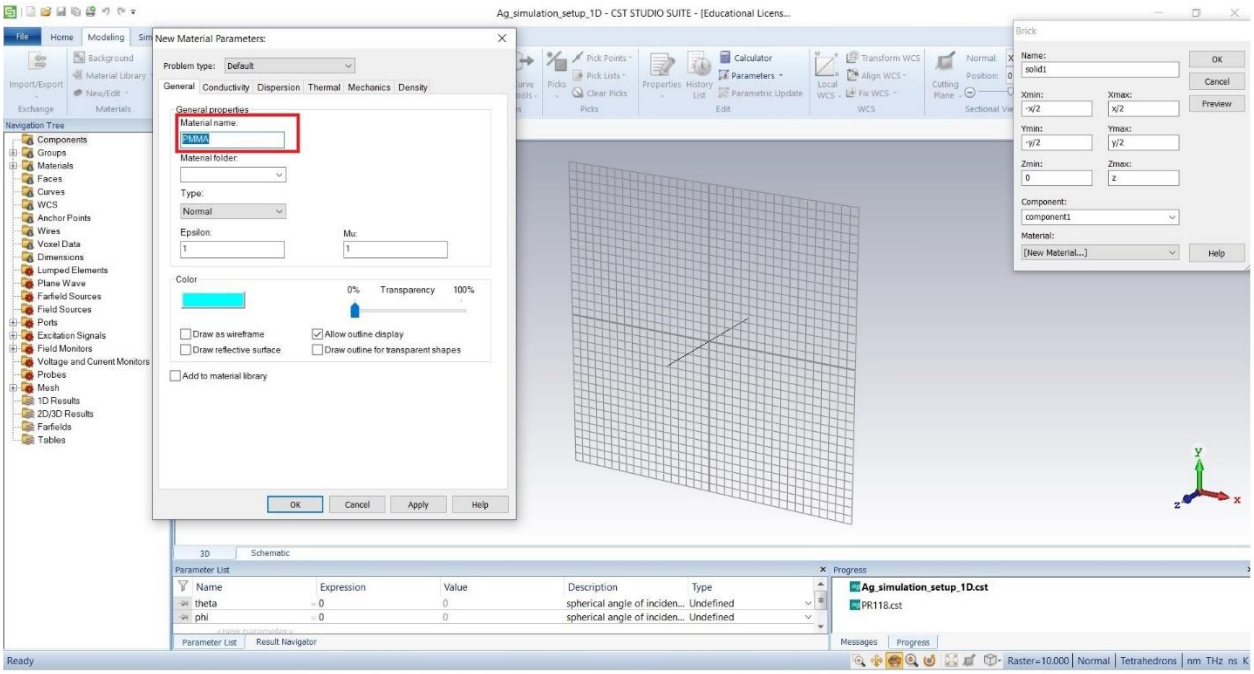

Step 13: Select Dispersion> Dispersion list.

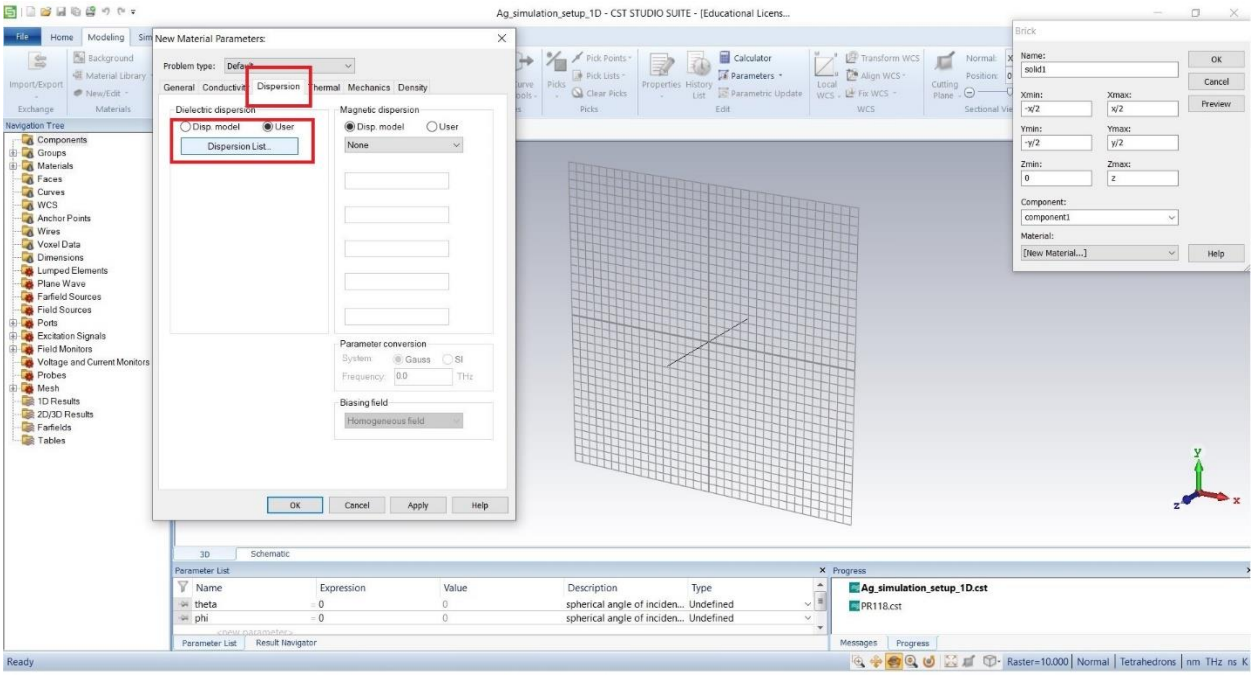

Step 14: Define permittivity at 821 THz for PMMA.

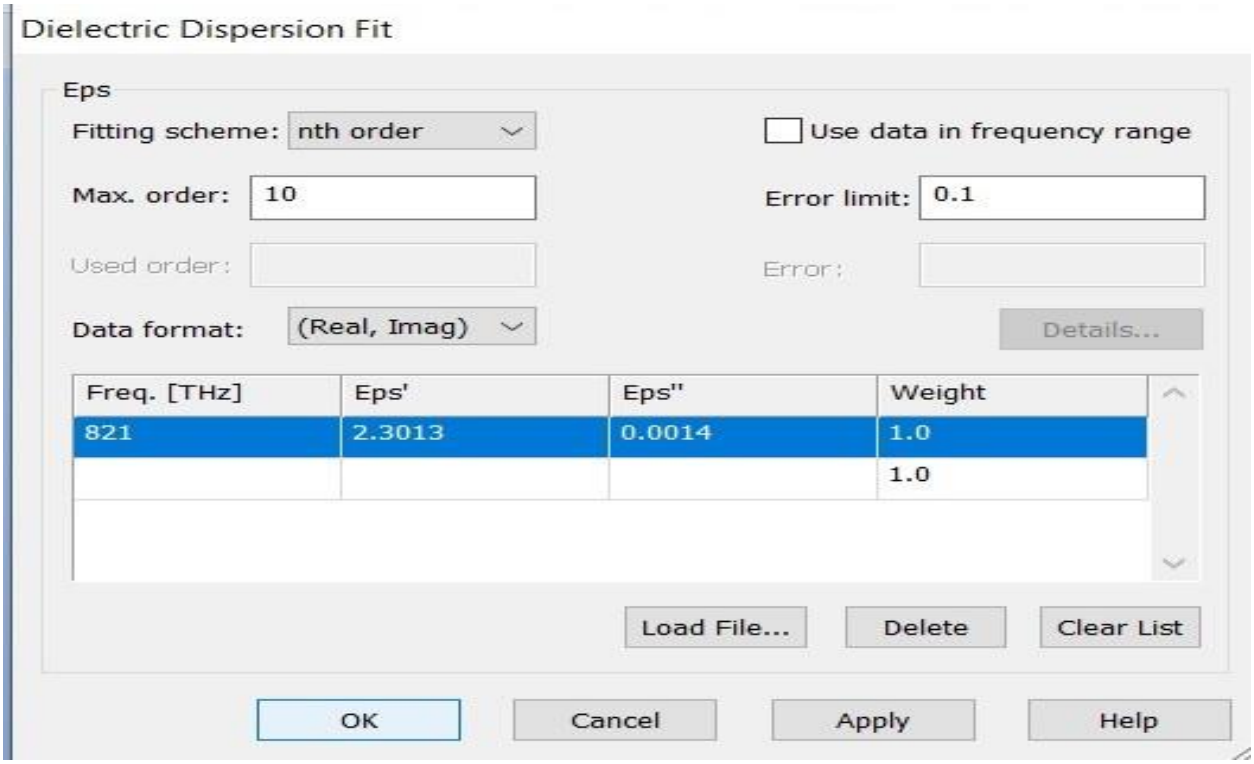

Step 15: Dimension for PMMA

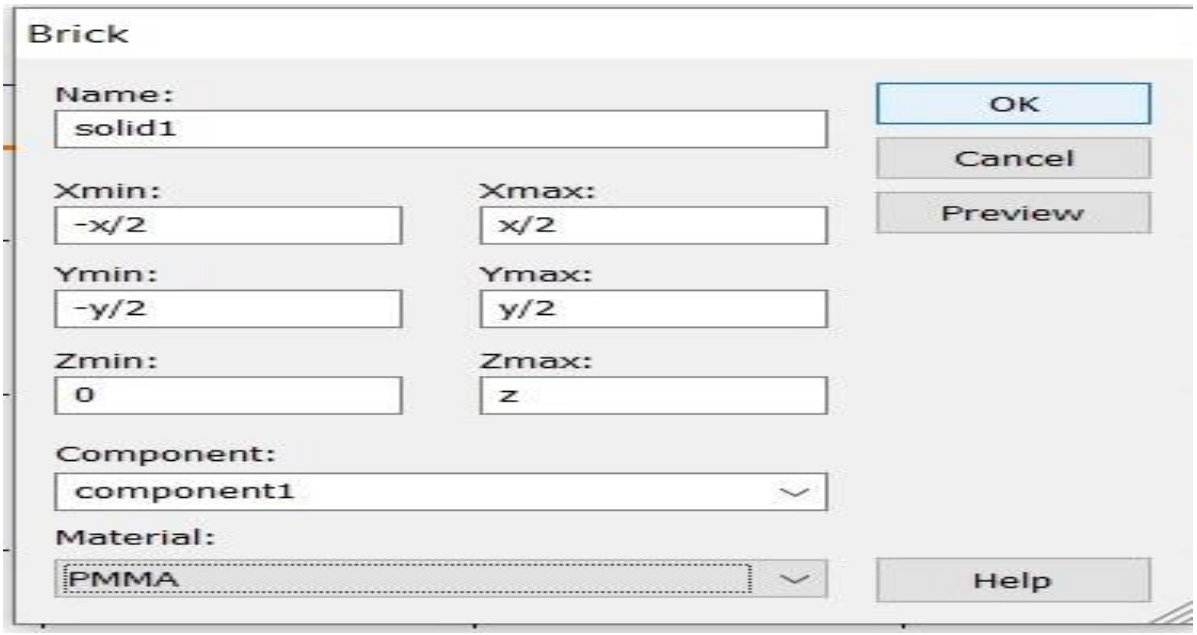

Step 16: Define Parameter value

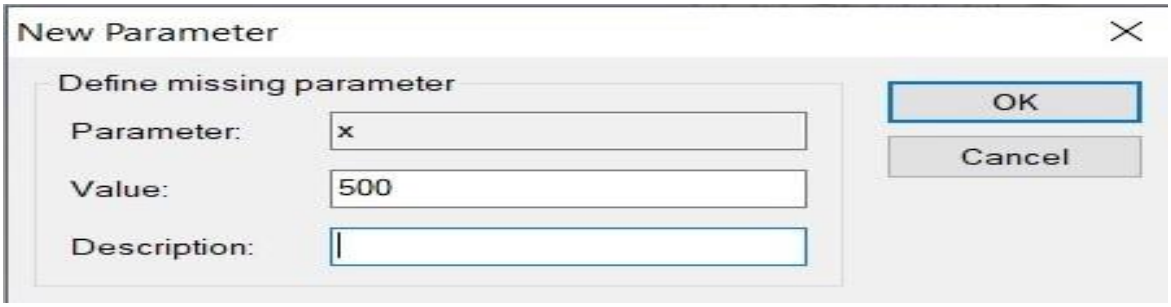

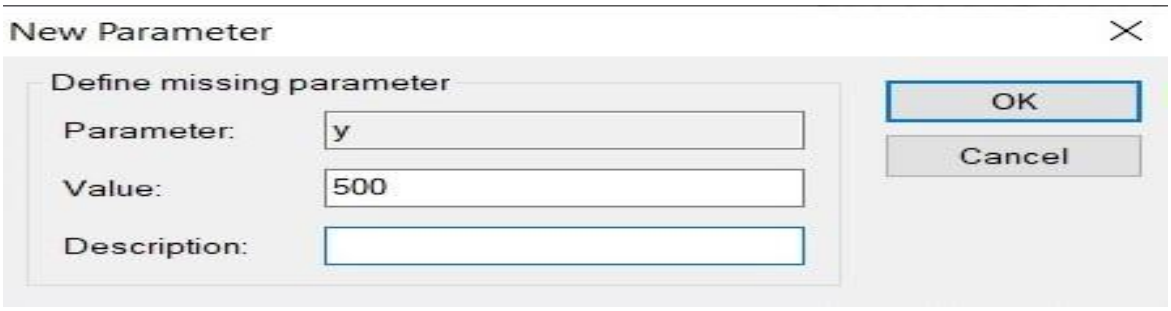

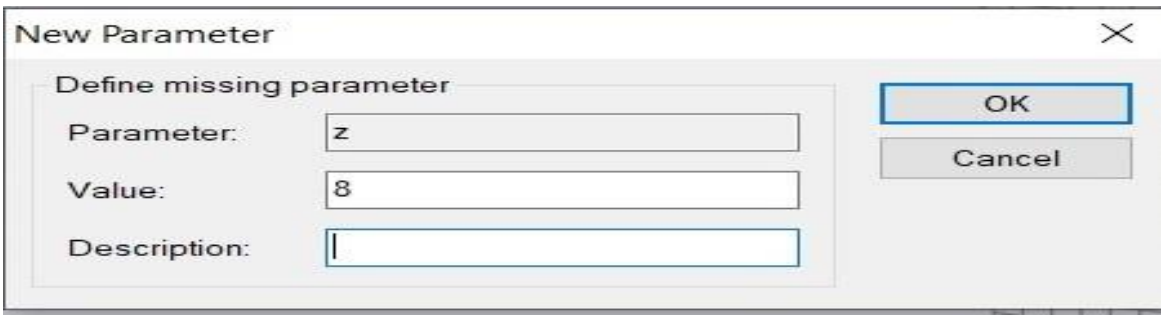

Step 17: Select view > Perspective.

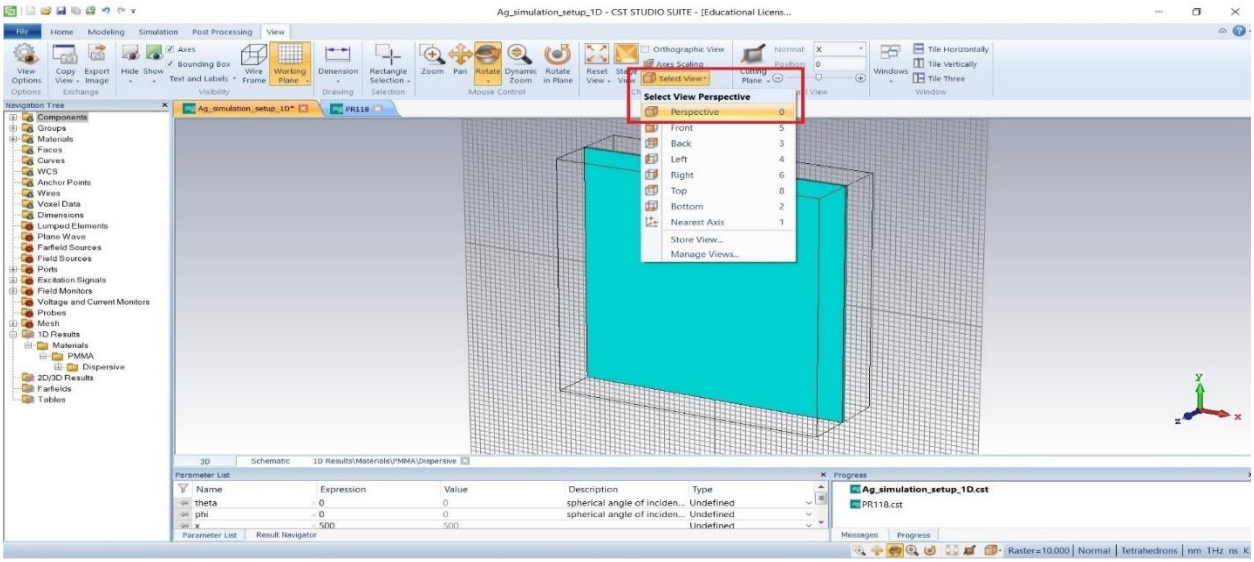

Step 18: Perspective view:

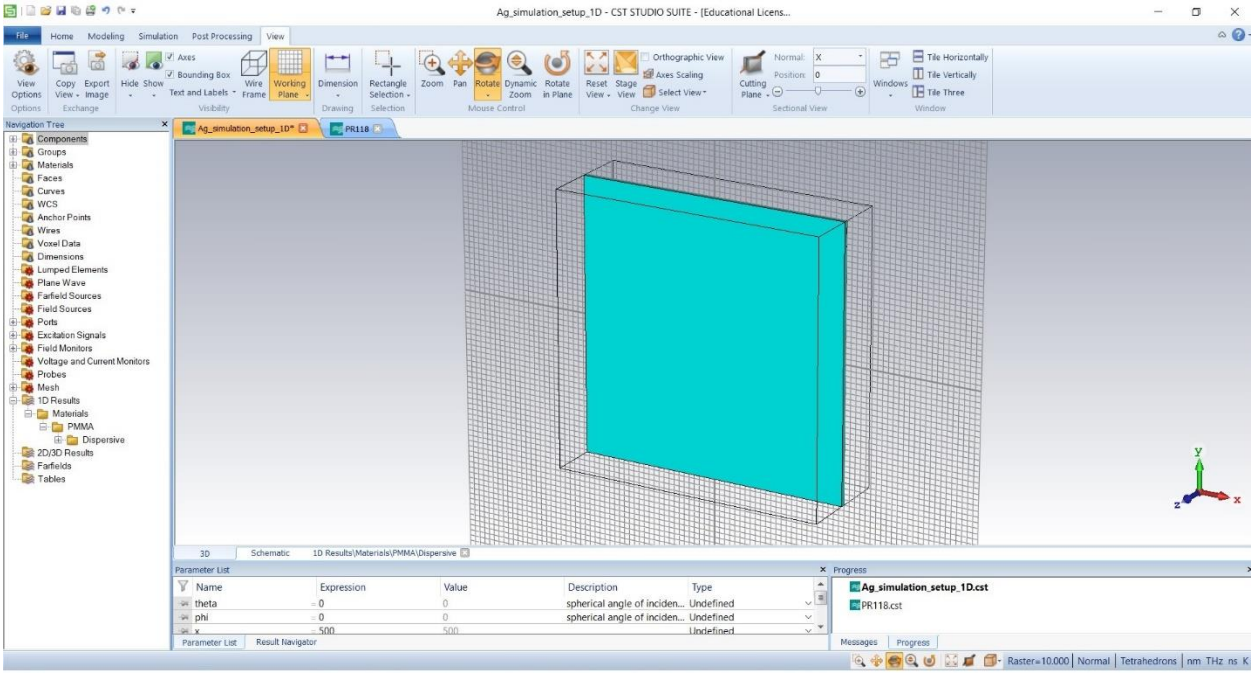

Step 19: Select view > Front to add Ag layer at the front of PMMA.

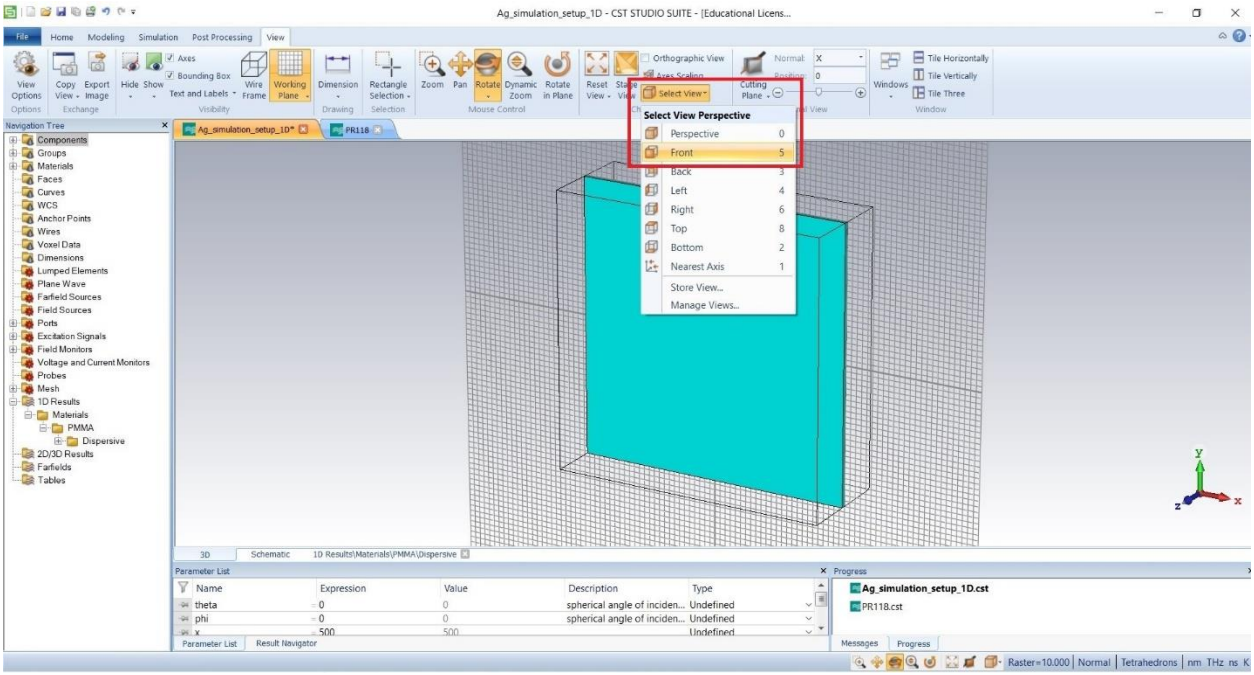

Step 20: Front view

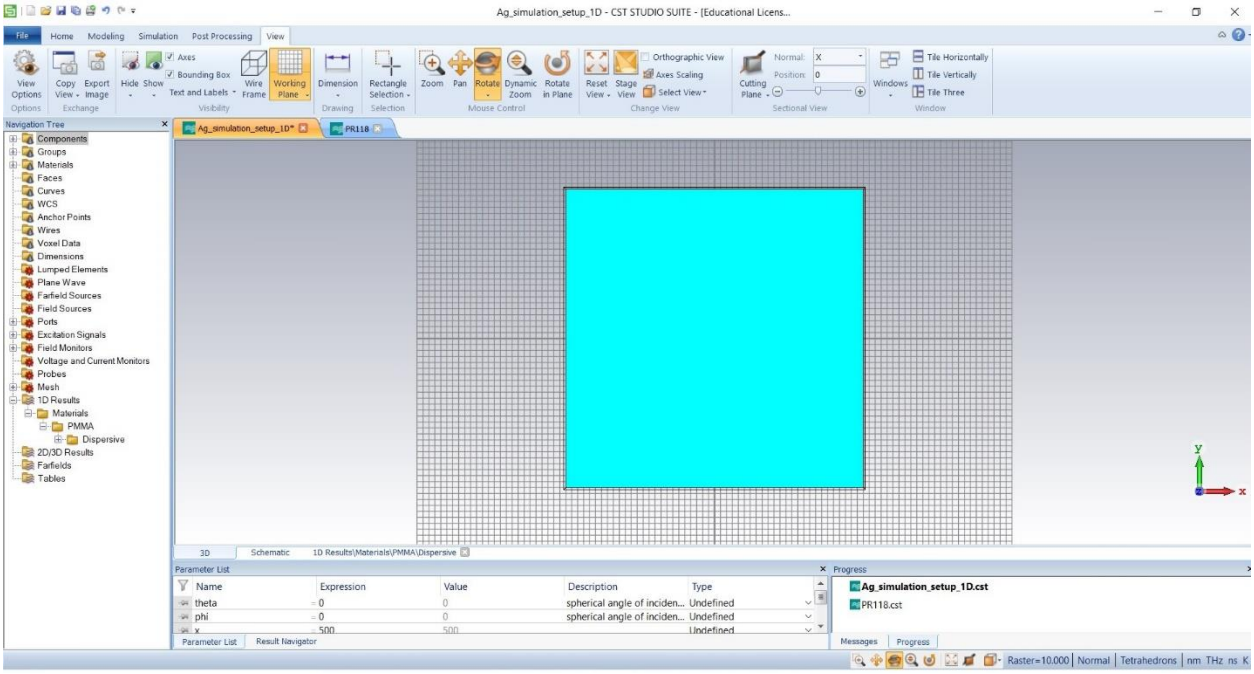

Step 21: Modeling > Picks

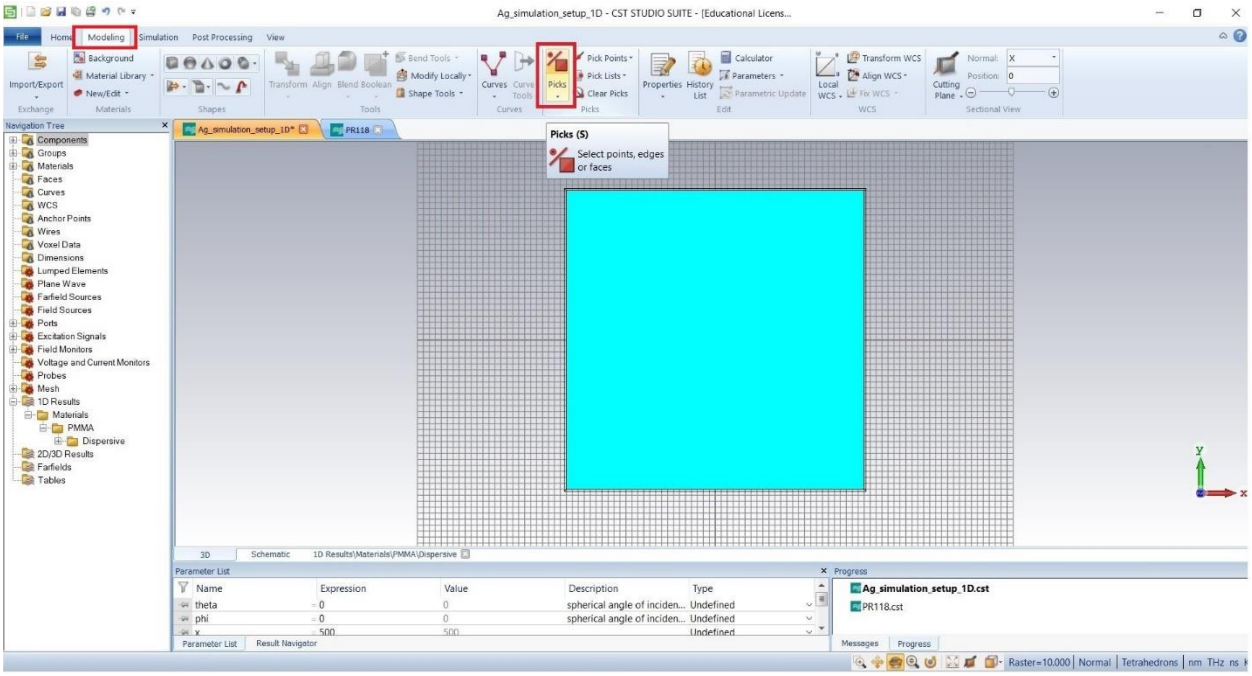

Step 22: Select the desired face to add extra layer.

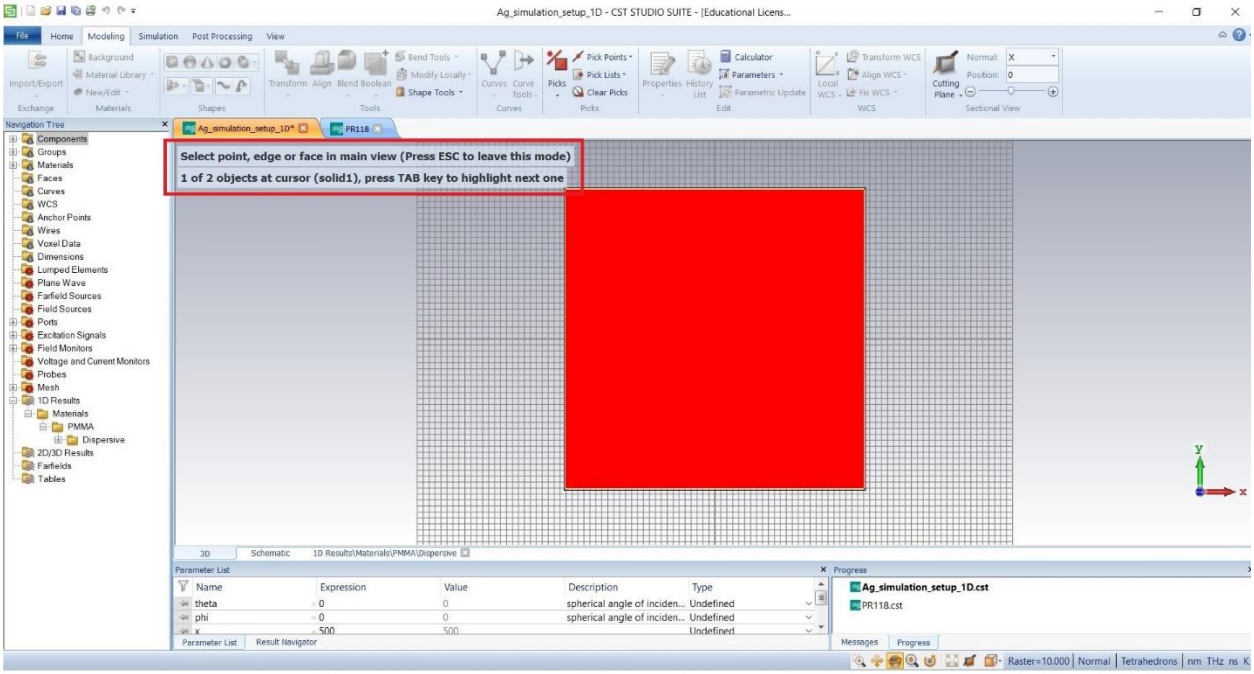

Step 23: After selecting the face click on Extrusions

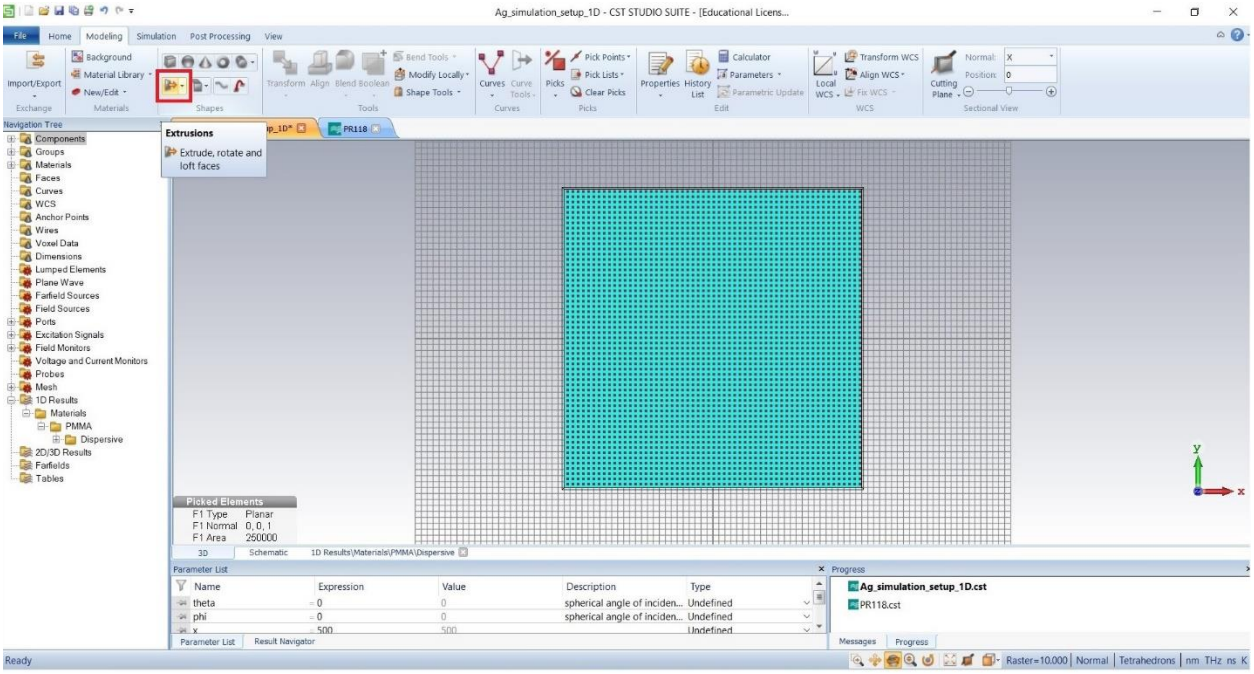

Step 24: Choose New Material (Ag=10nm)

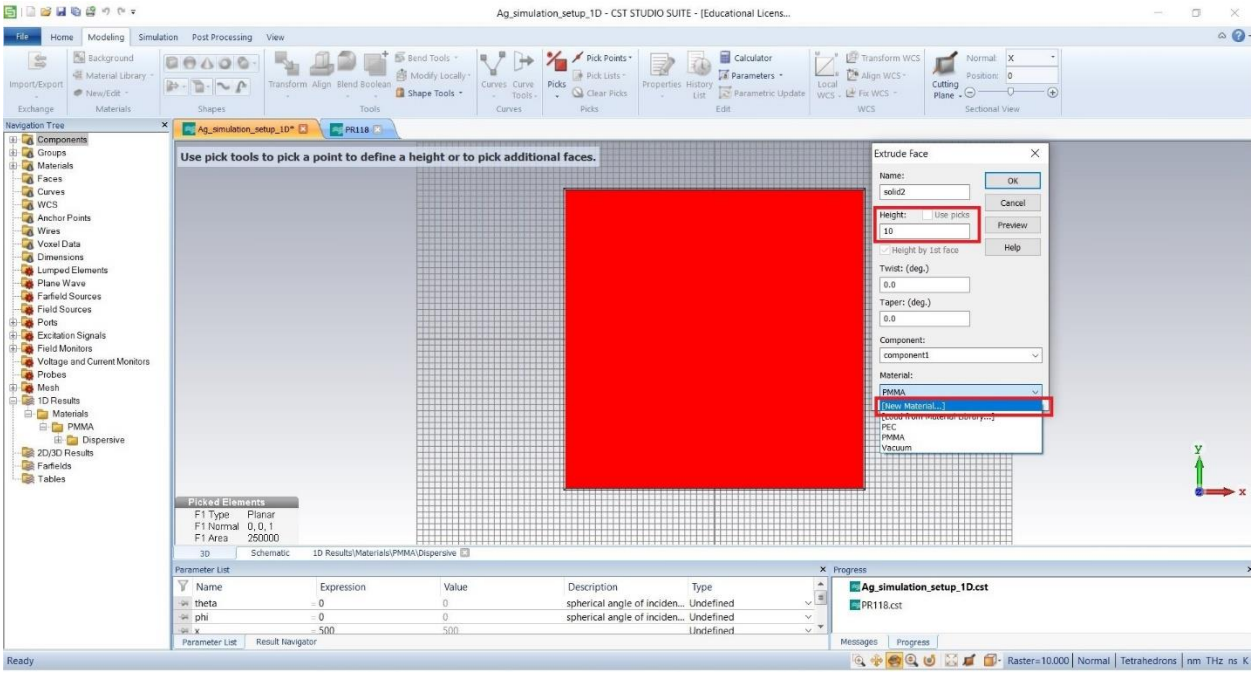

Step 25: Color can be changed.

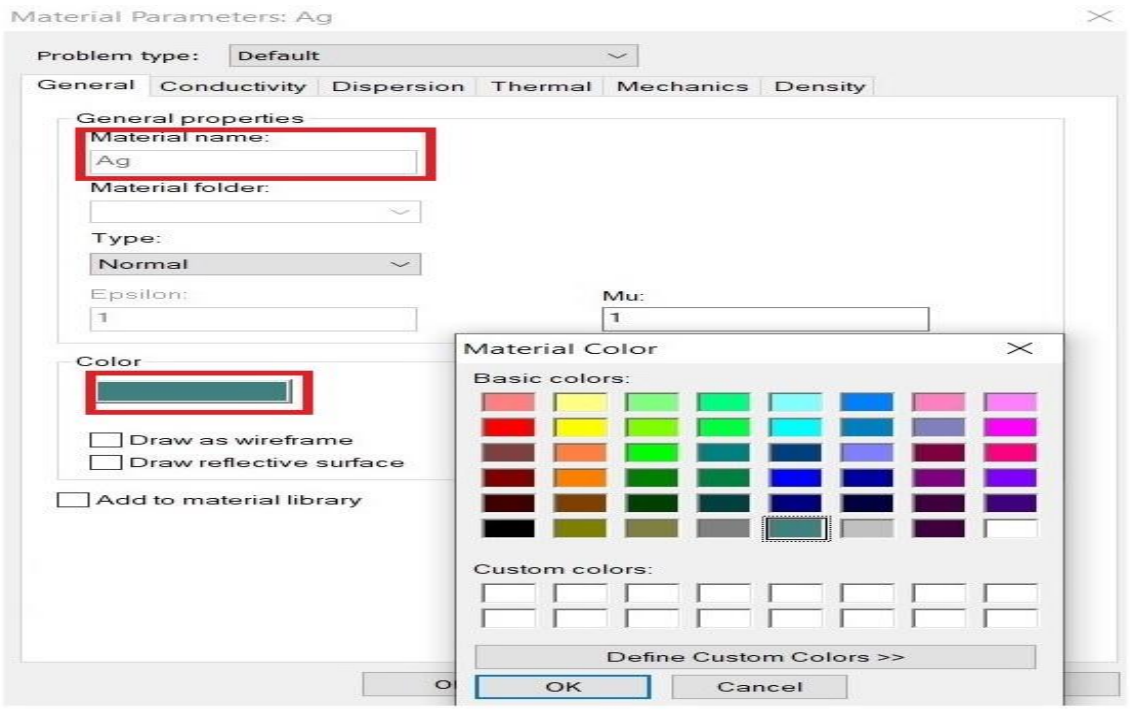

Step 26: Define permittivity for Ag at 821 THz.

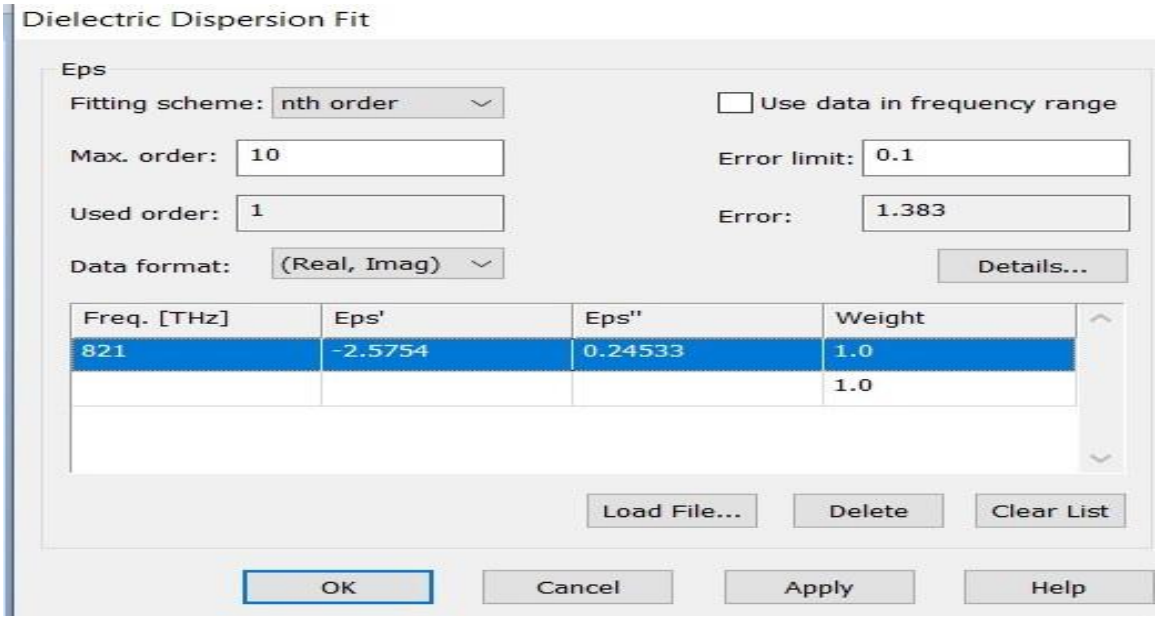

Step 27: Choose Picks and then Extrusion for adding PR (118nm) layer.

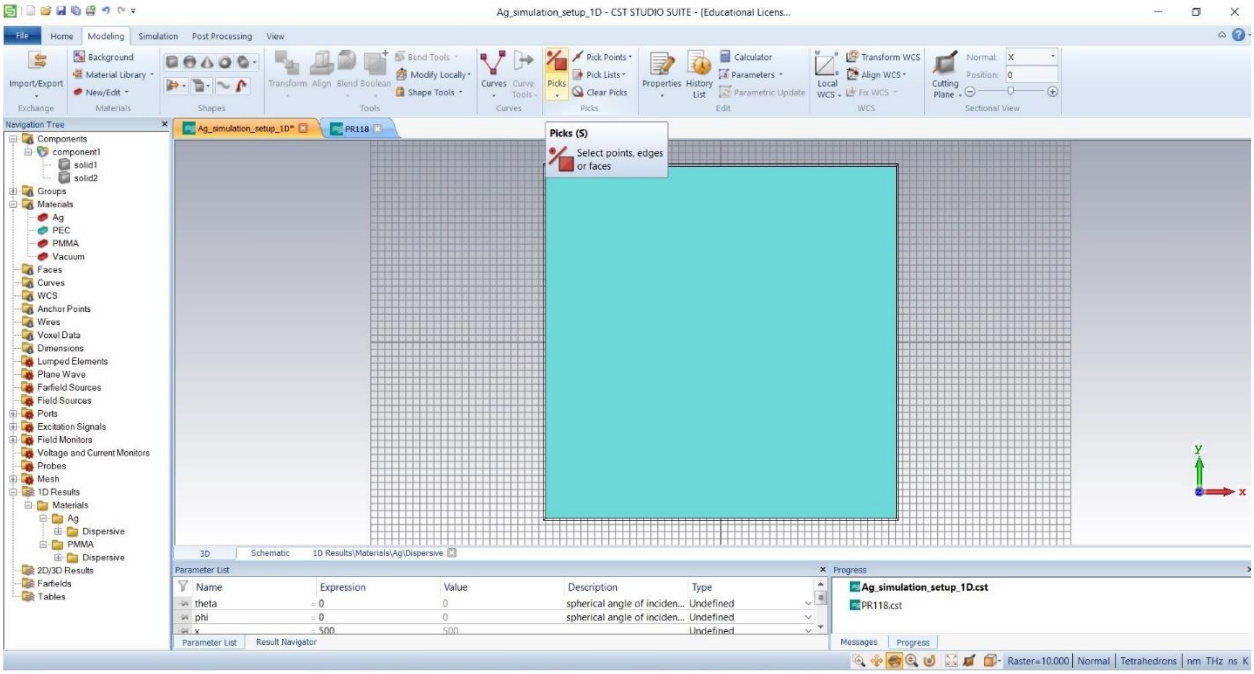
Ag_simulation_setup_1D - CST STUDIO SUITE - [Educational Licens...
Picks (5)
Select points, edges or faces

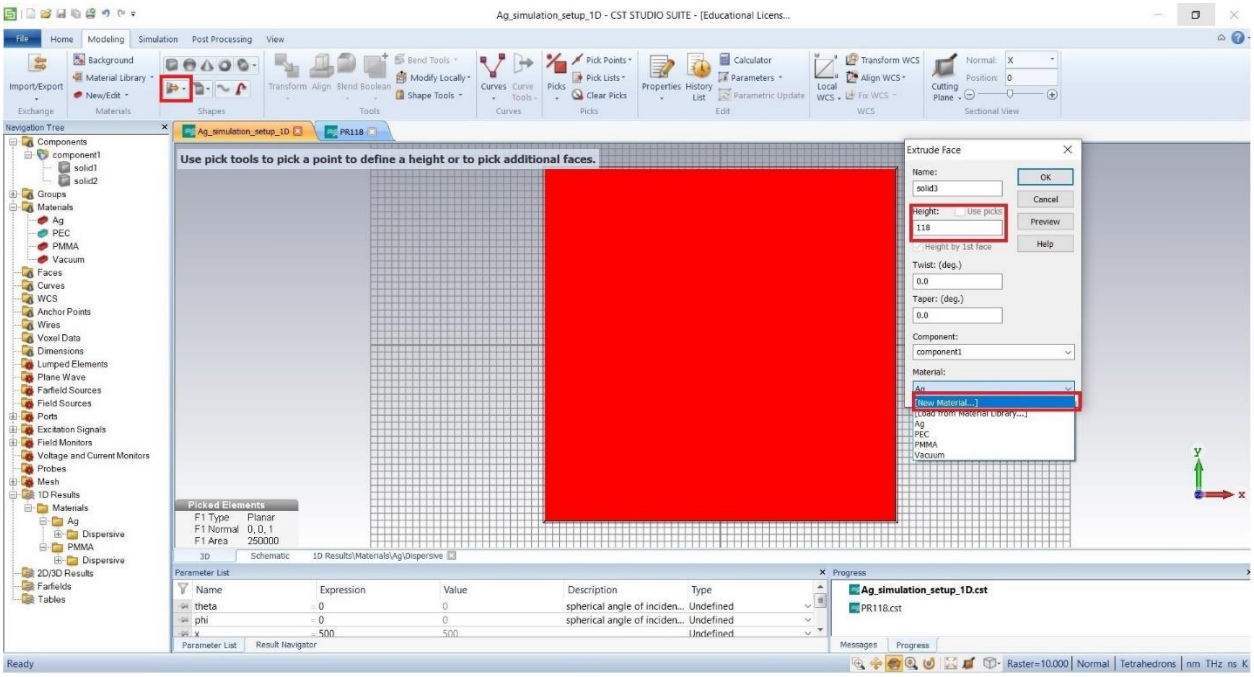
Ag_simulation_setup_1D - CST STUDIO SUITE - [Educational Licens...
Use pick tools to pick a point to define a height or to pick additional faces.
Extrude Face
Name:
solid3
Height:
118
Twist: (deg.)
0.0
Taper: (deg.)
0.0
Component:
component1
Material:
[New Material...]
Ag
PEC
PMMA
Vacuum
OK
Cancel
Preview
Help

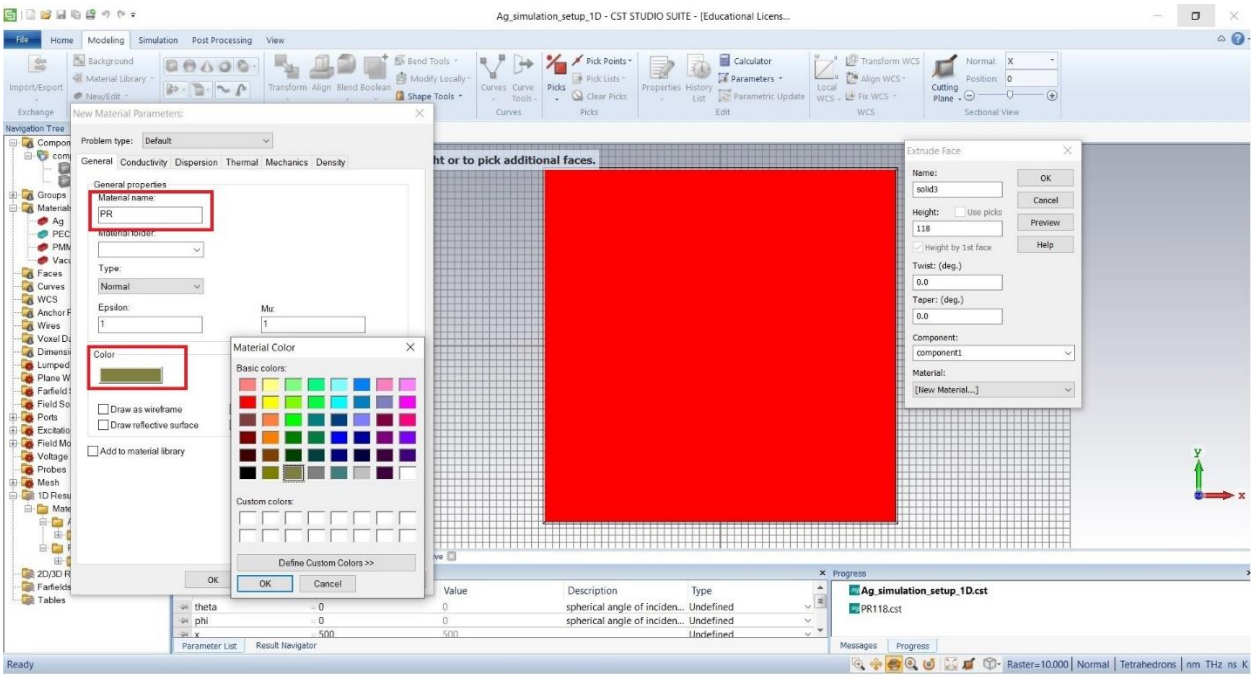

Step 28: Define permittivity for PR layer.

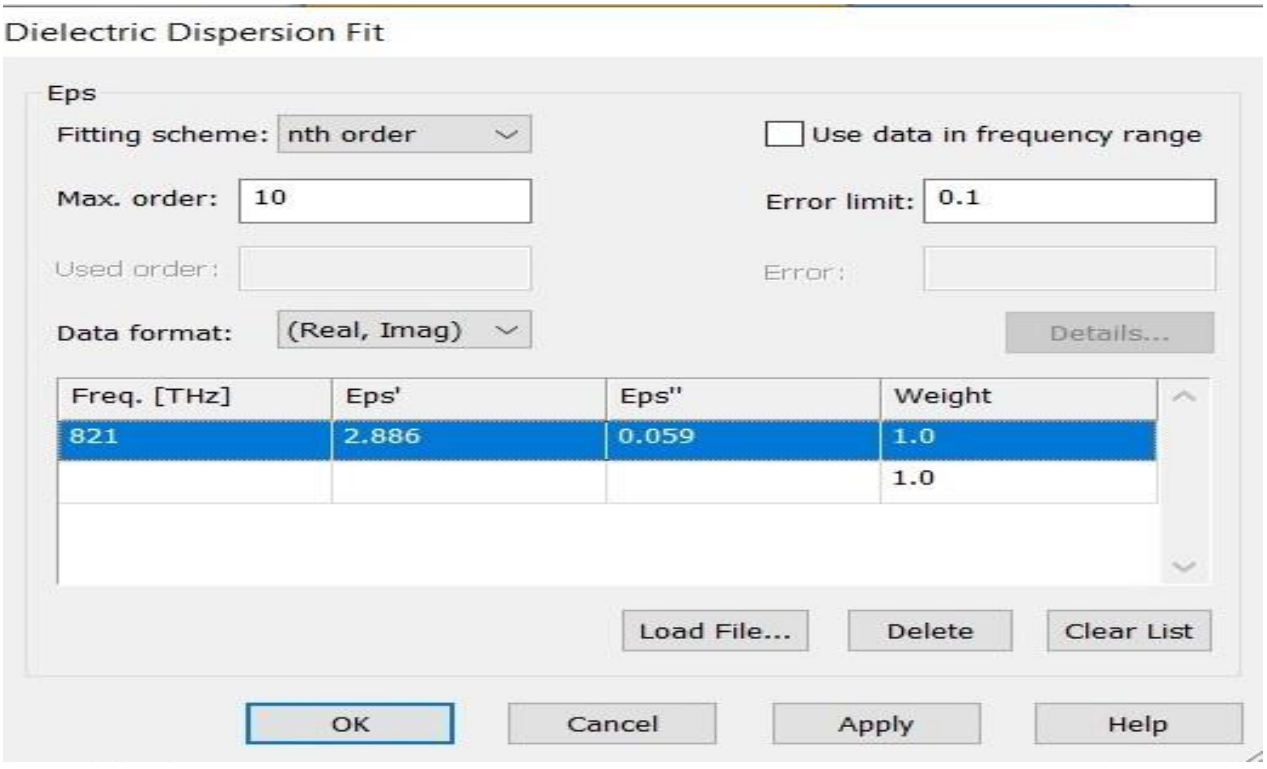

Step 29: Perspective view

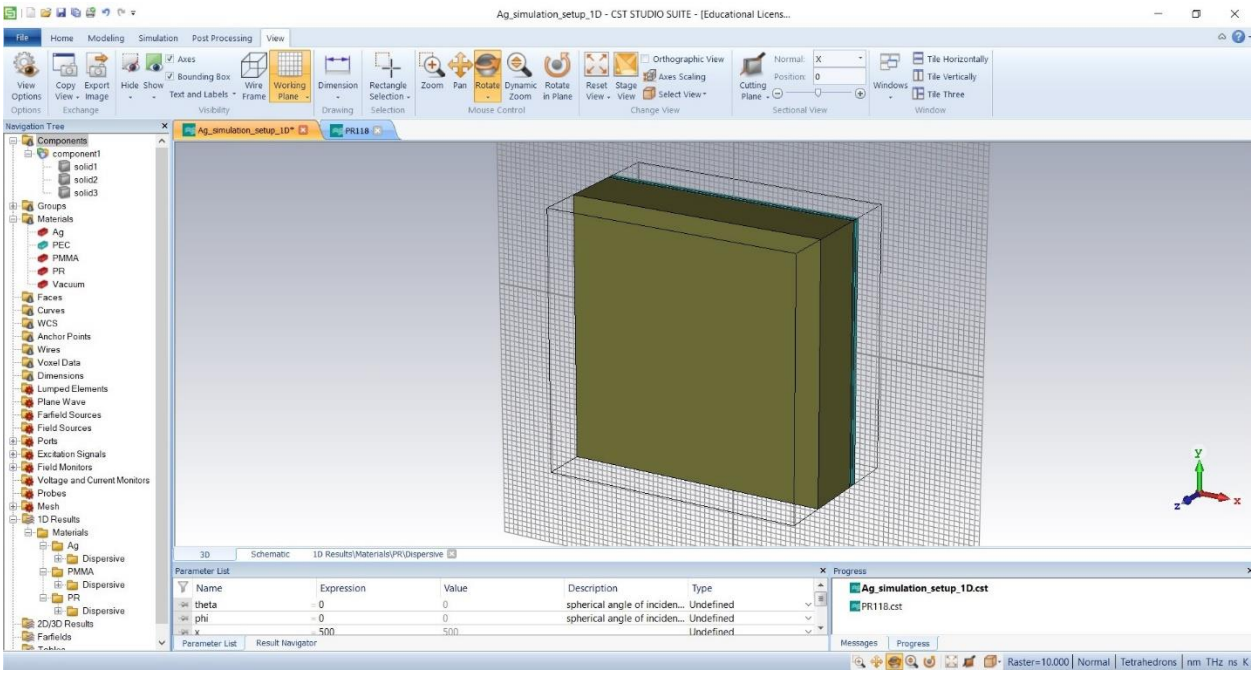

Step 30: Select view > Right.

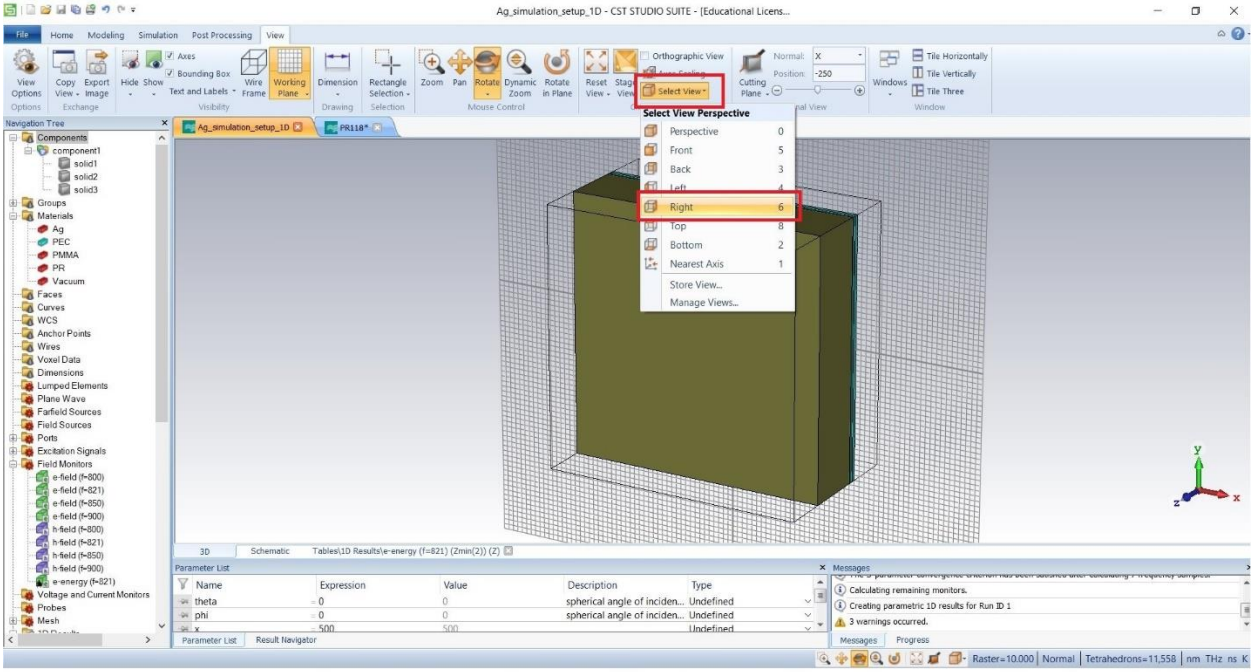

Step 31: Right side view.

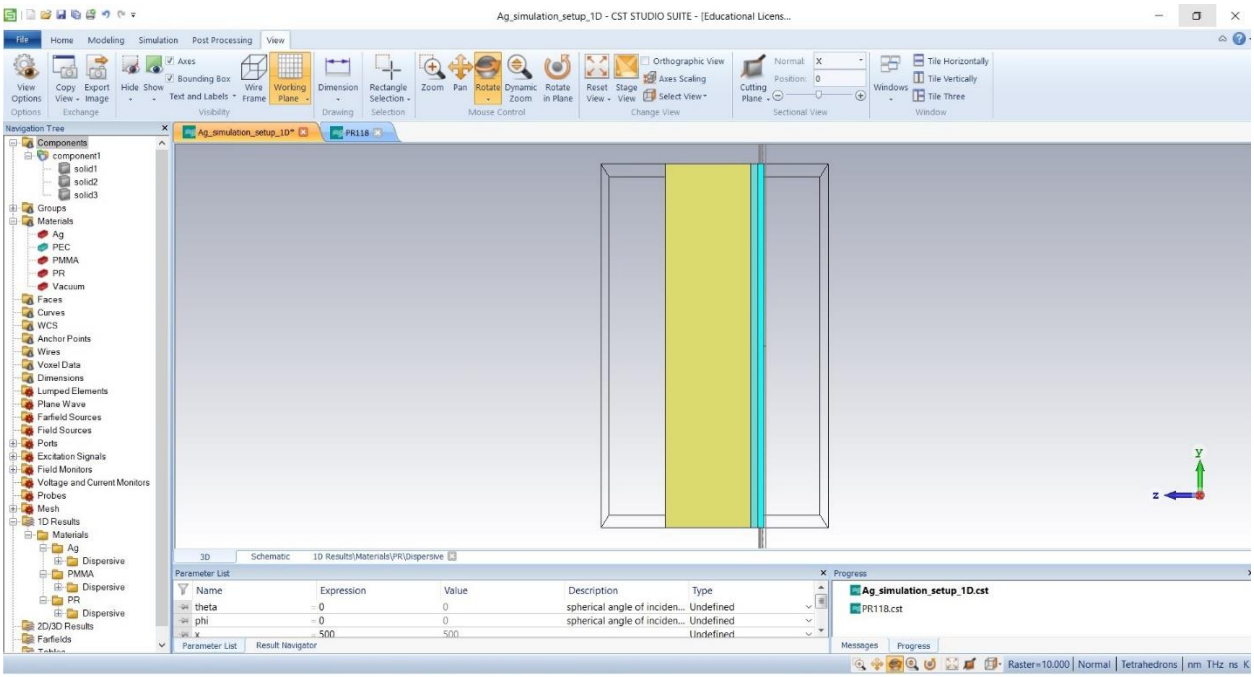

Step 32: Simulation > Boundaries > Define Boundary Conditions

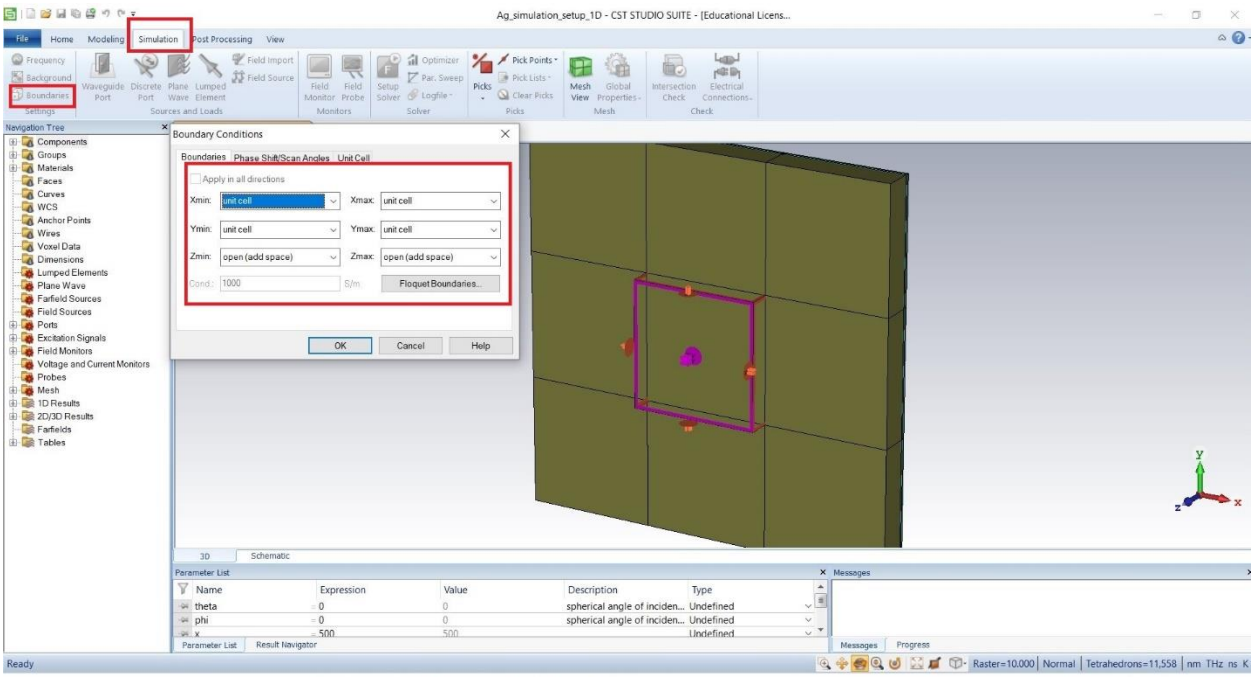

Step 33: Field monitor ＞ Define Electric energy density at 821 THz.

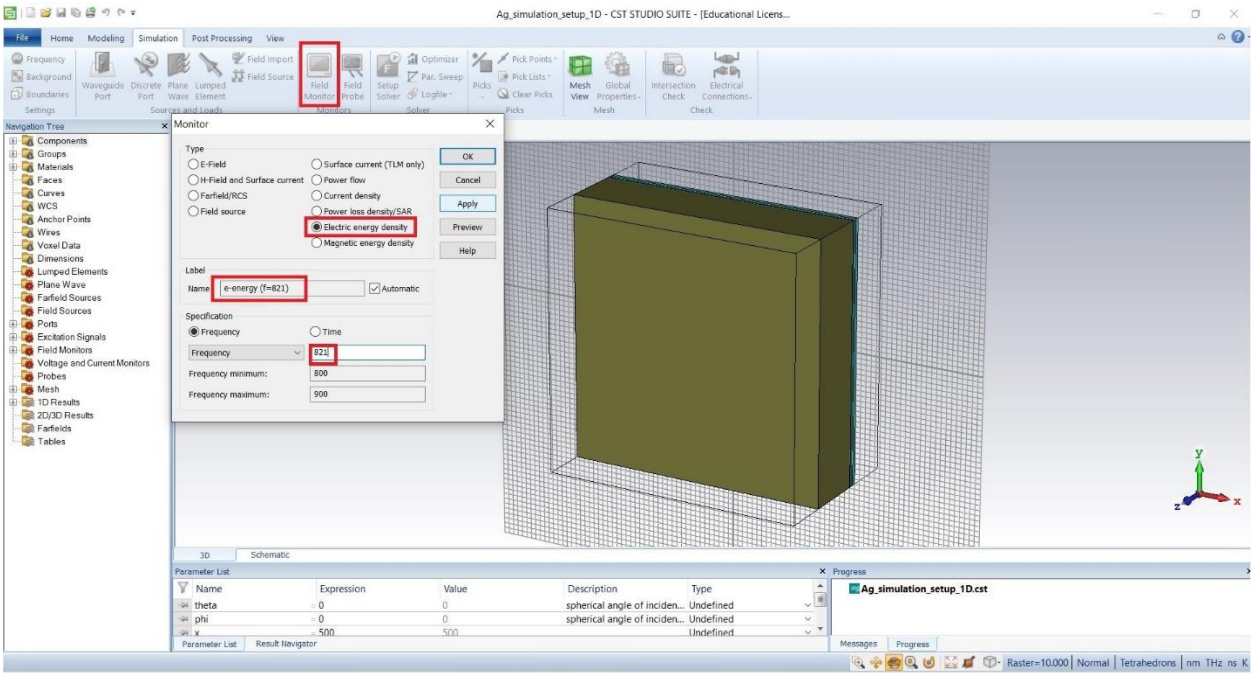

Step 34: Select Zmin as source and TM as mode then Start the simulation.

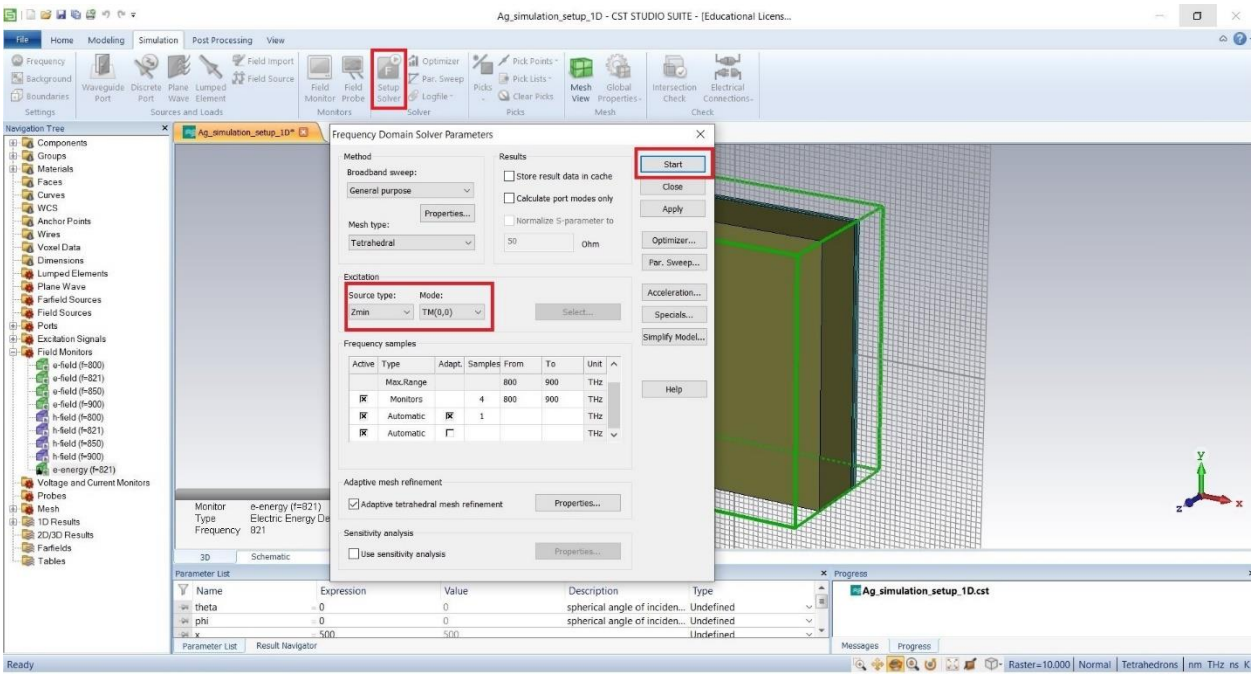

Step 35: Post processing ＞ Result Template ＞ Evaluate field in arbitrary coordinates.

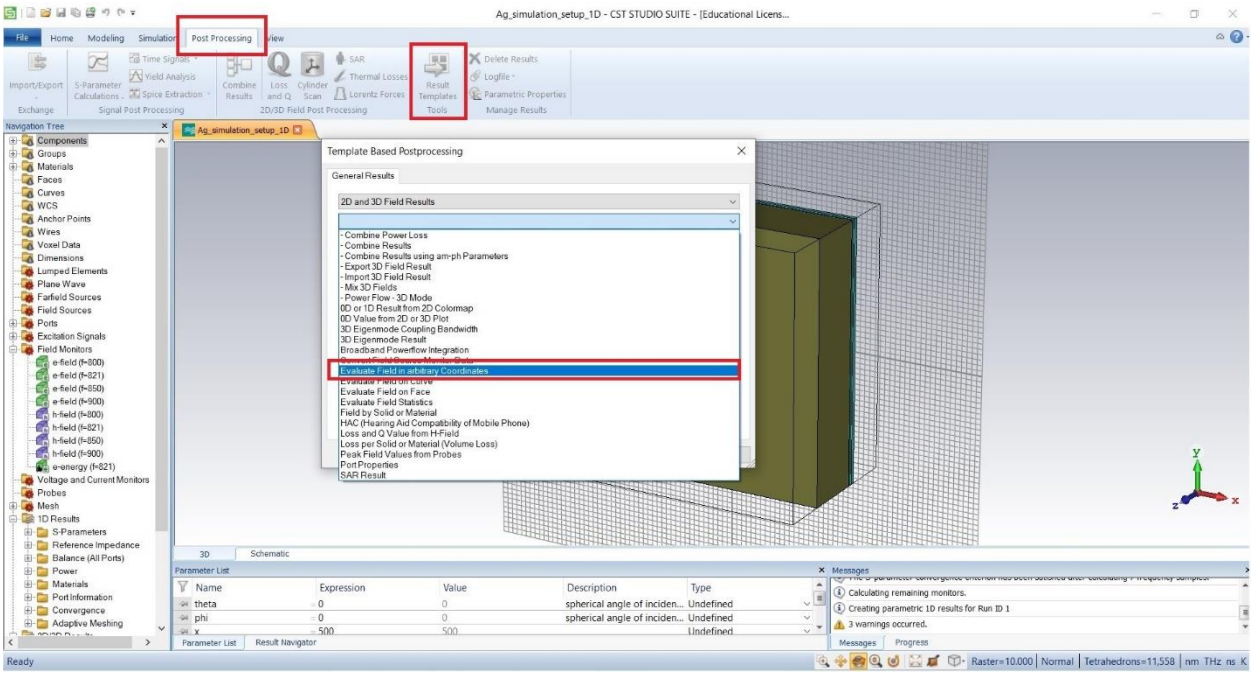

Step 36: Click browse results then select Electric energy density at z direction.

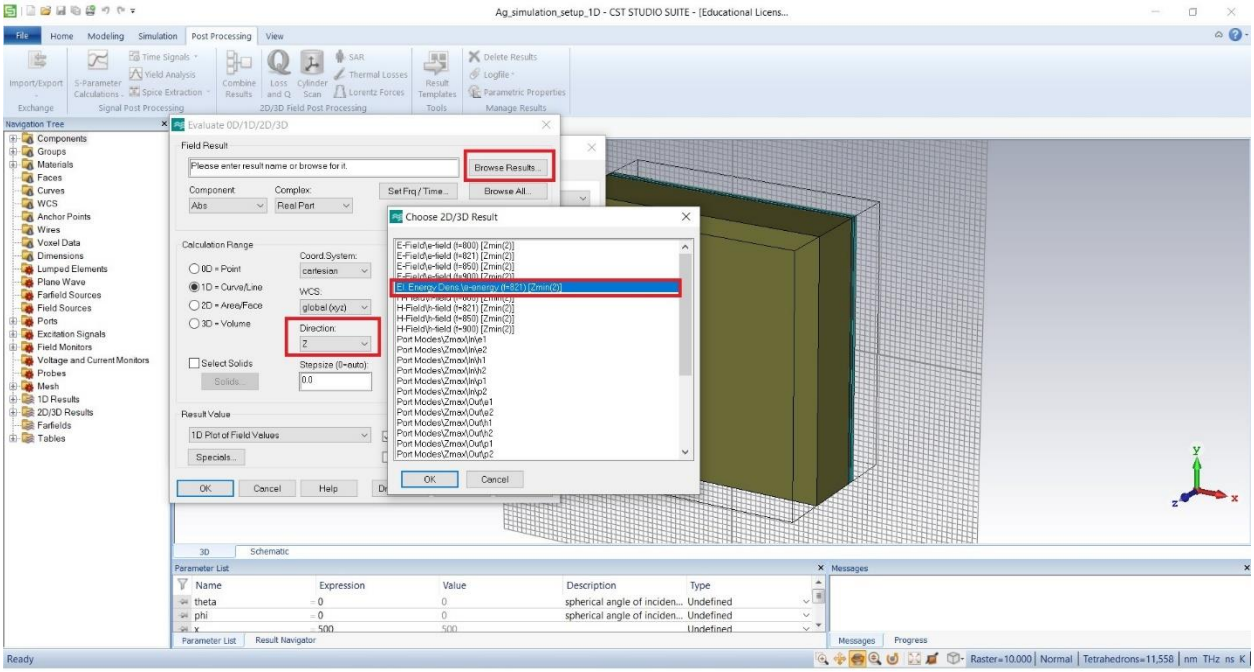

Step 37: Evaluate E-energy density.

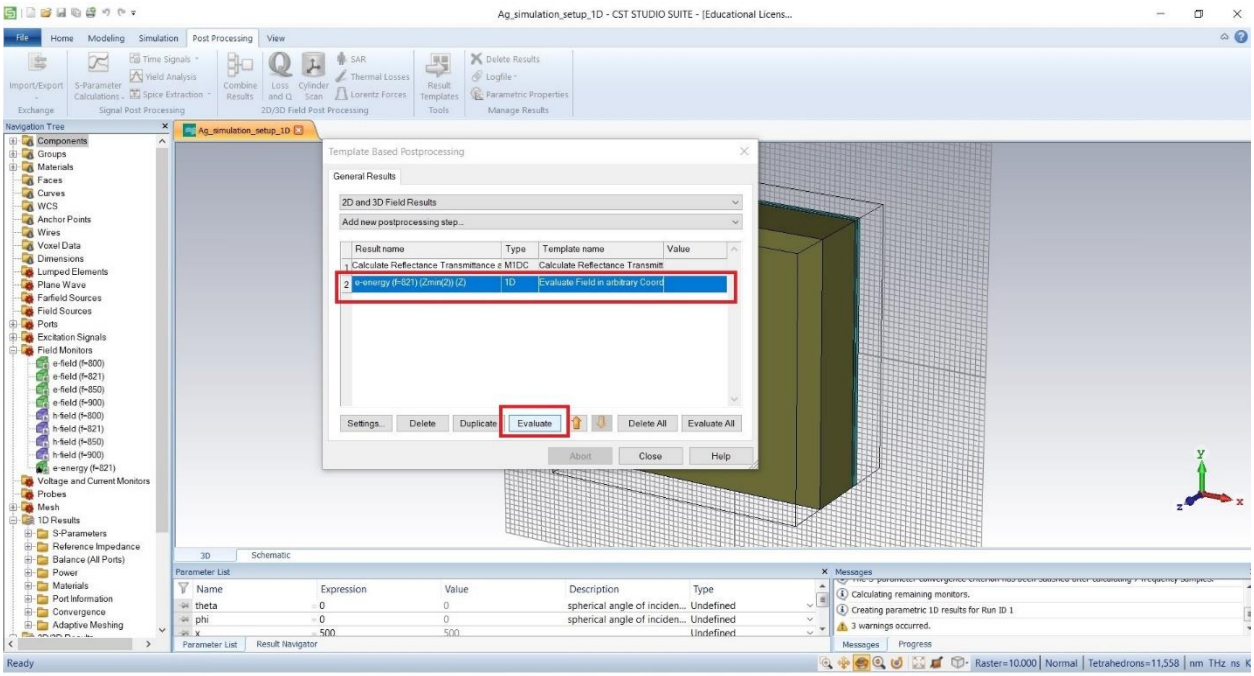

Step 38: Scale can be set in properties.

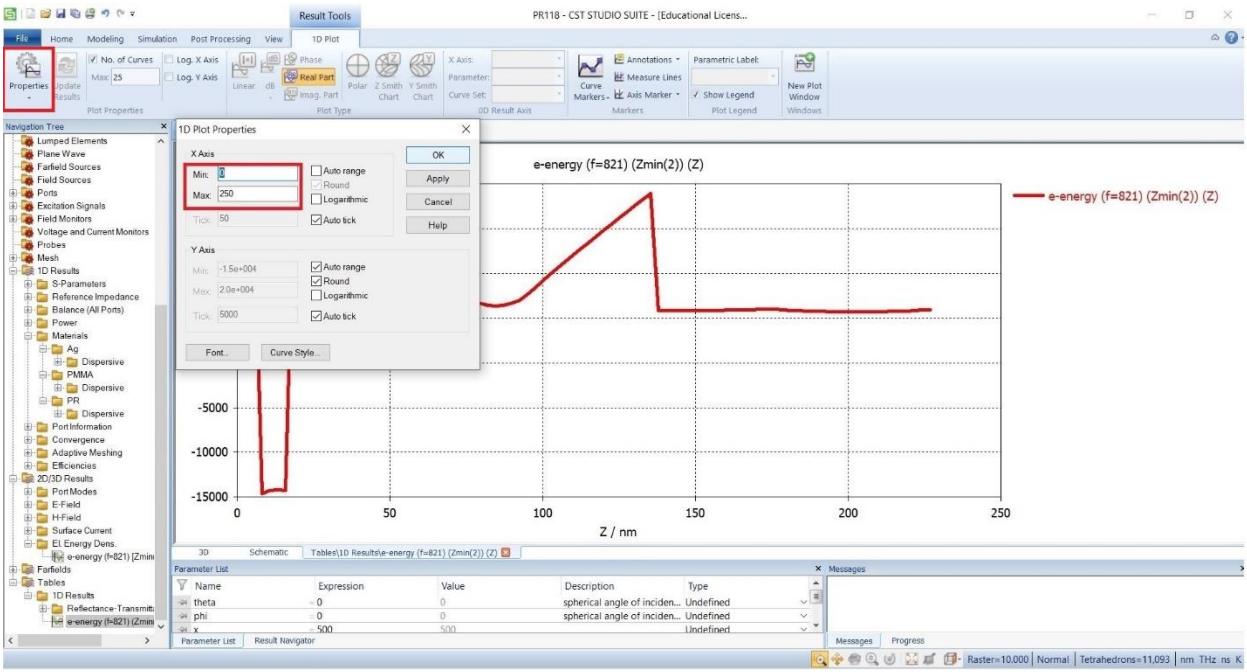

Step 39: Curve markers can be added to define a certain point.

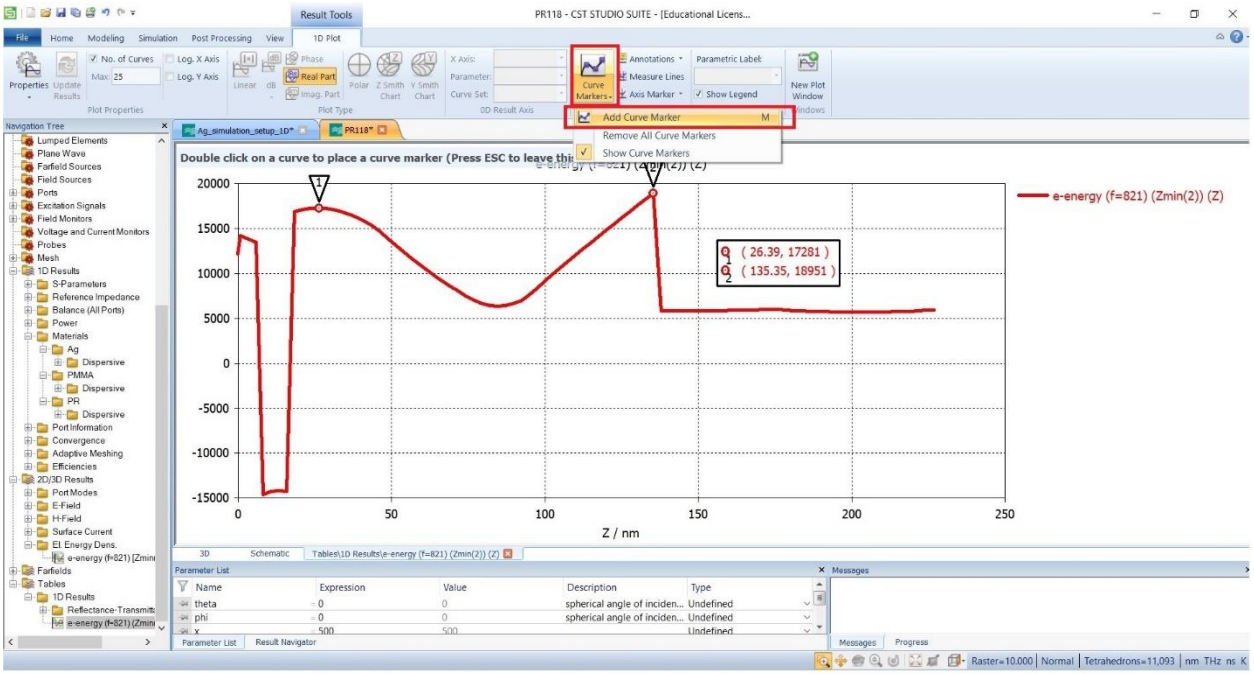

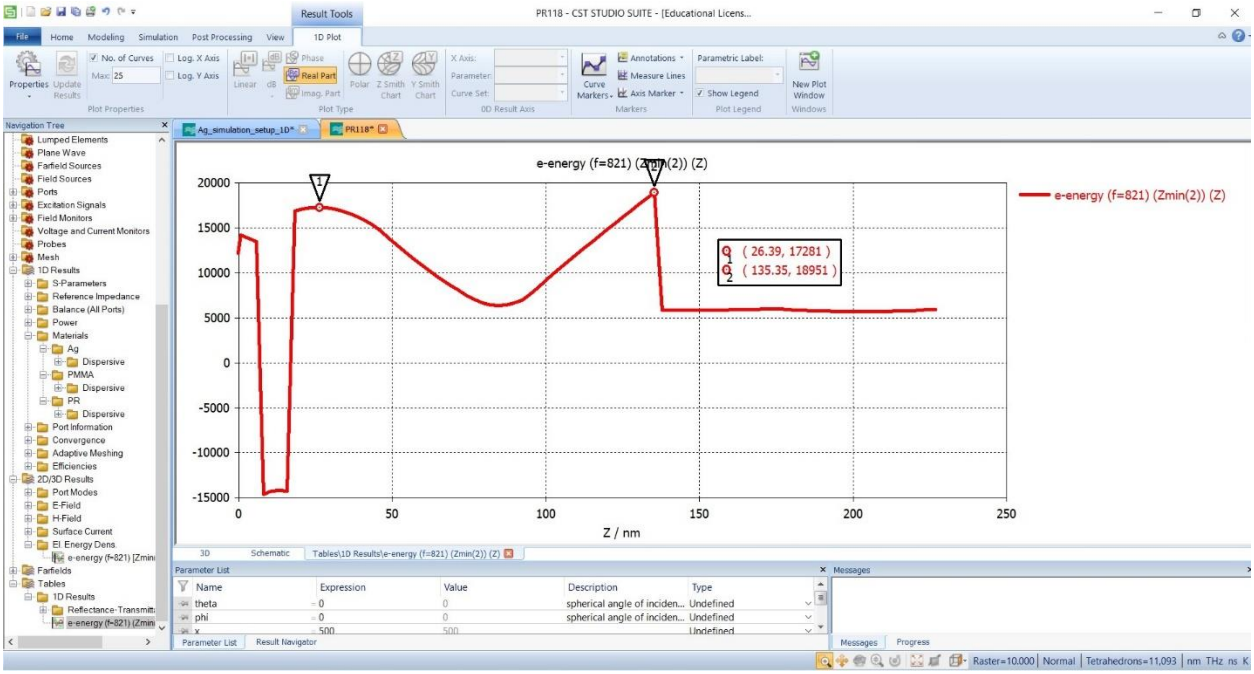

3.1.2: 3-D Image of the sub-diffractive object Vs. meta-lenses' paraxial image location

Repeat step 1 to step 11 from previous section.

Step 12: Selecting 'Cr' as new material

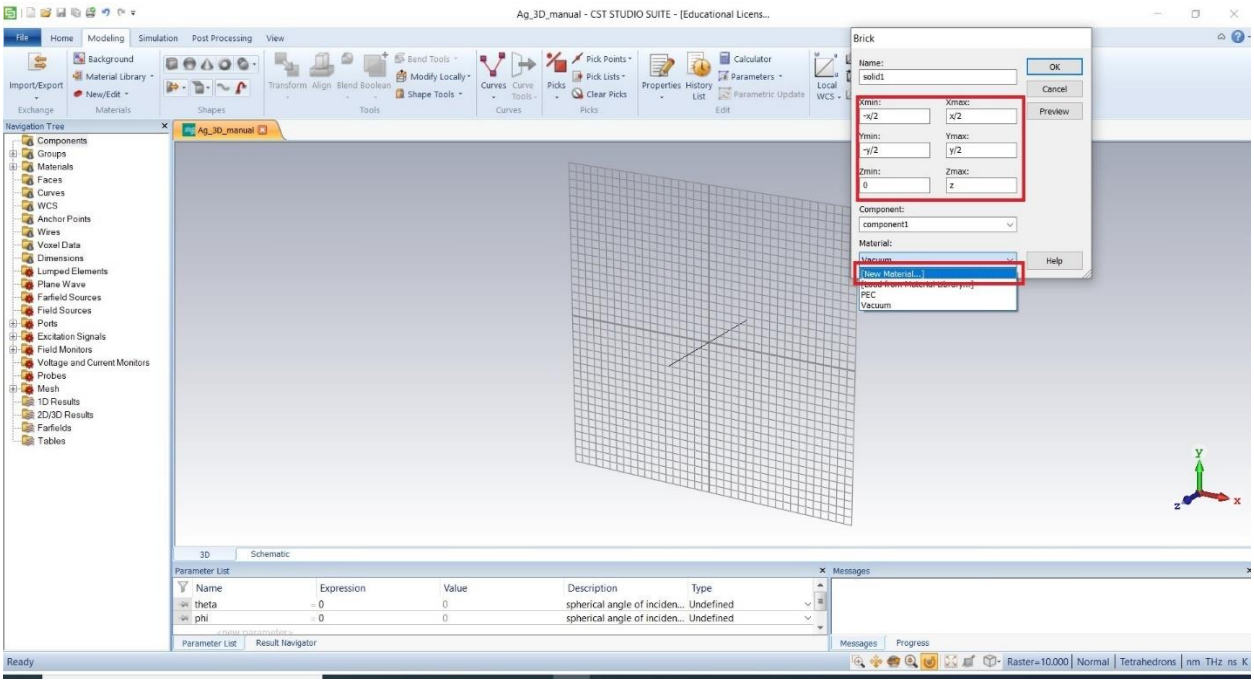

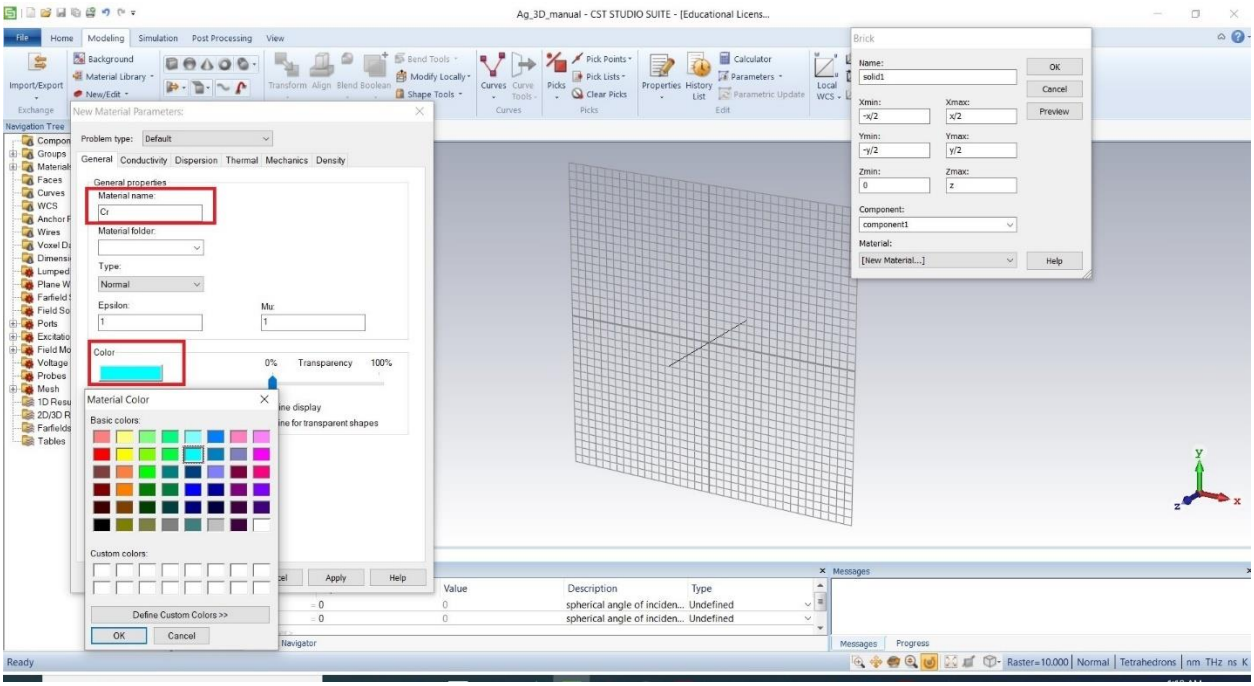

Step 13: Define permittivity of ‘Cr’

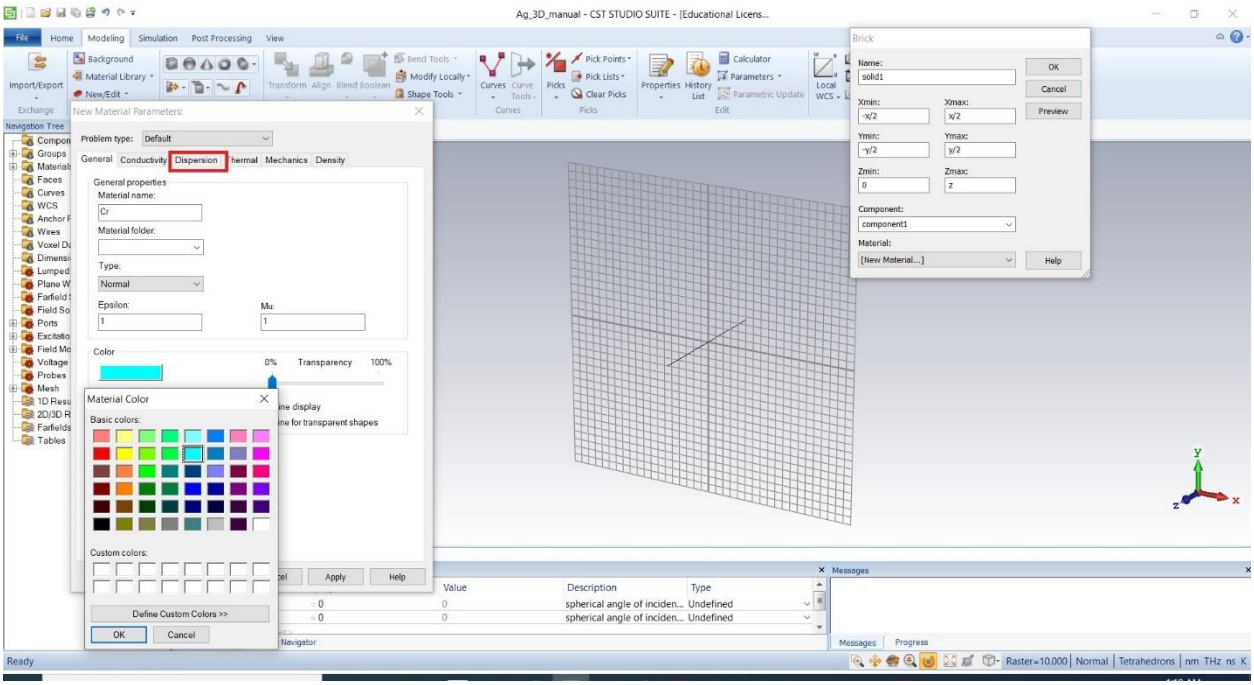

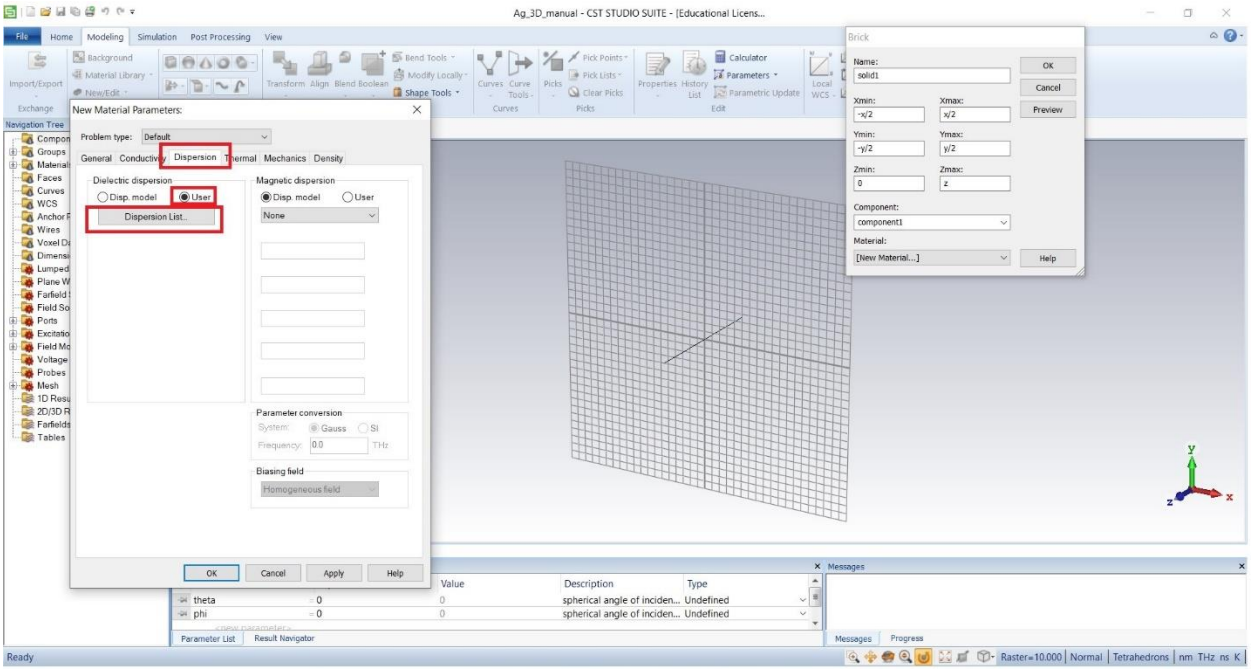

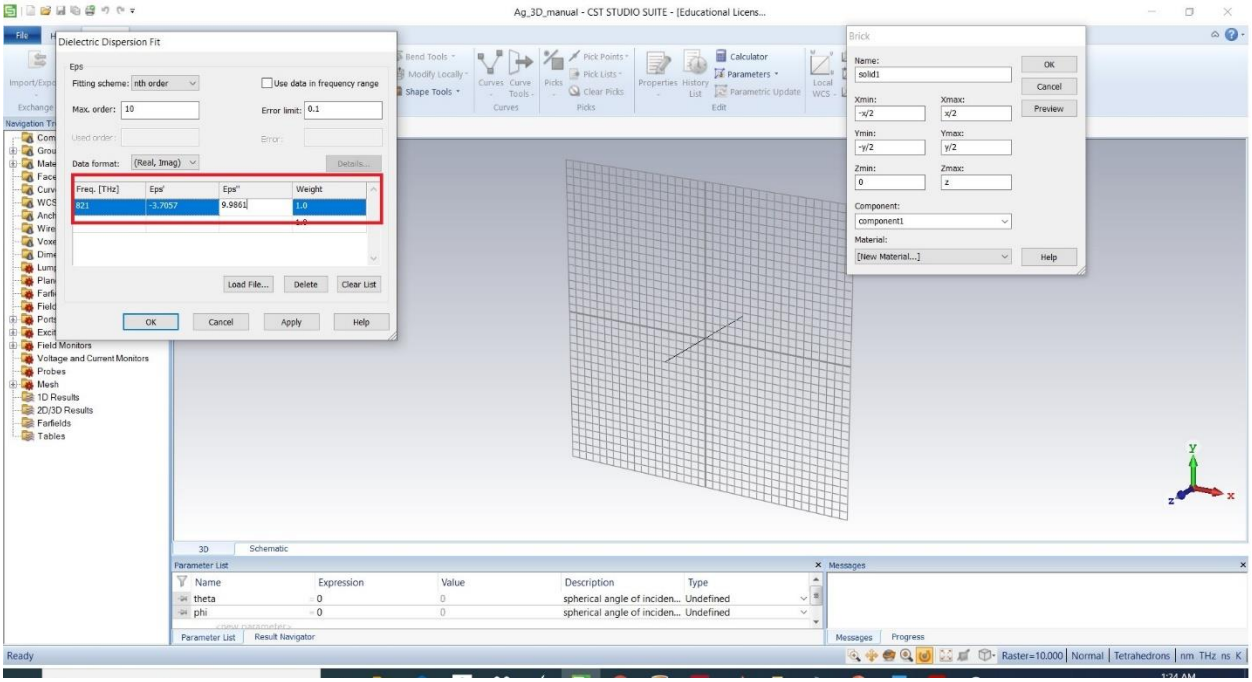

Step 14: Define dimantion of 'Cr'

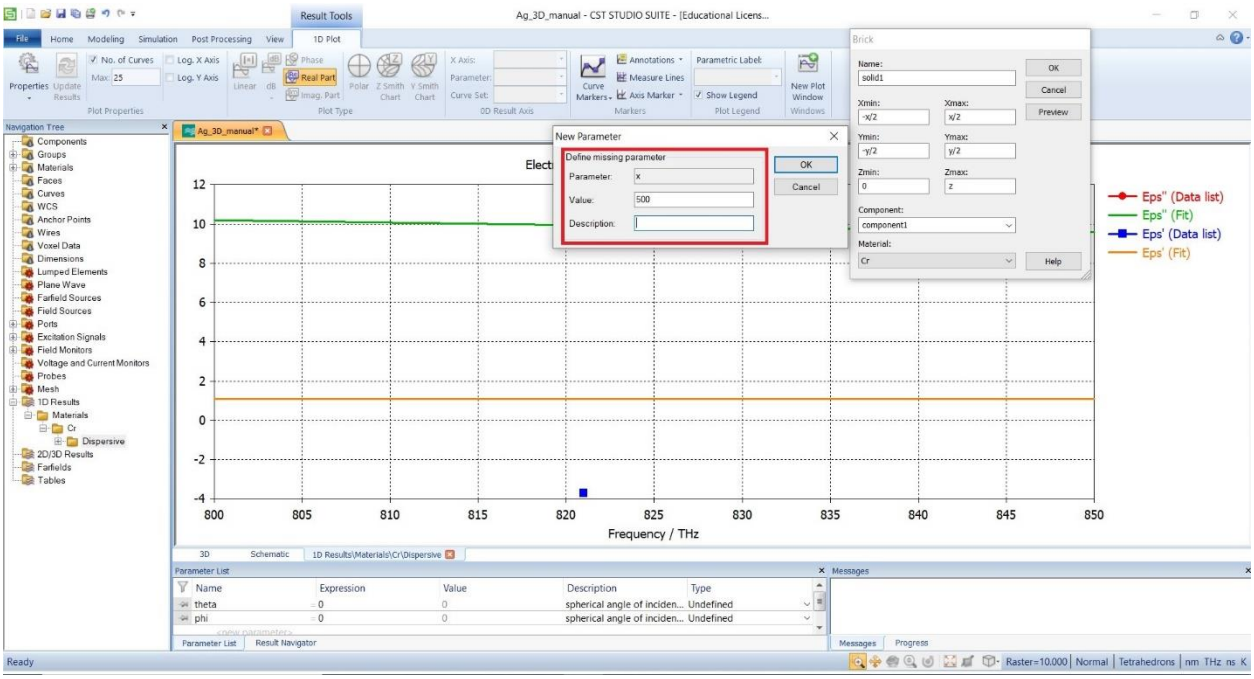

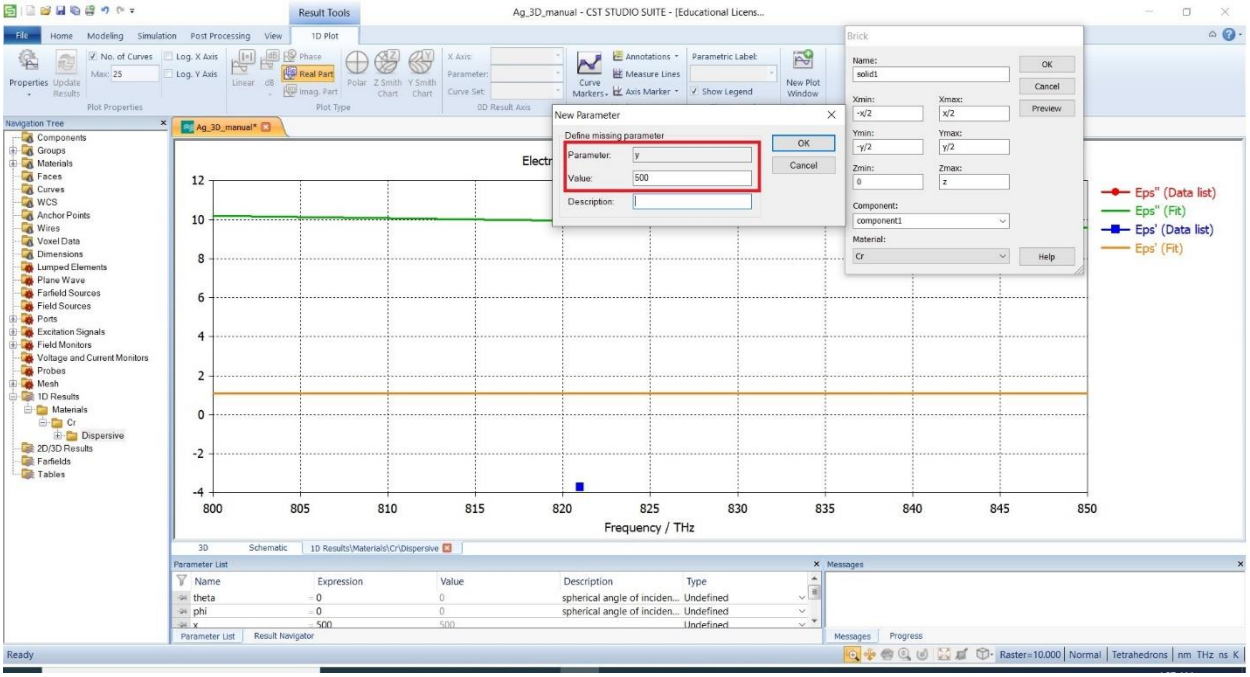
Result Tools
Ag_3D_manual - CST STUDIO SUITE - [Educational Licens...
New Parameter
Define missing parameter
Parameter: y
Value: 500
Description:
OK
Cancel
Brick
Name: solid1
Xmin: -x/2
Xmax: x/2
Ymin: -y/2
Ymax: y/2
Zmin: 0
Zmax: z
Component: component1
Material: Cr
Preview
Help
Eps'' (Data list)
Eps'' (Fit)
Eps' (Data list)
Eps' (Fit)
Frequency / THz
Navigation Tree
Parameter List
Messages
Ready

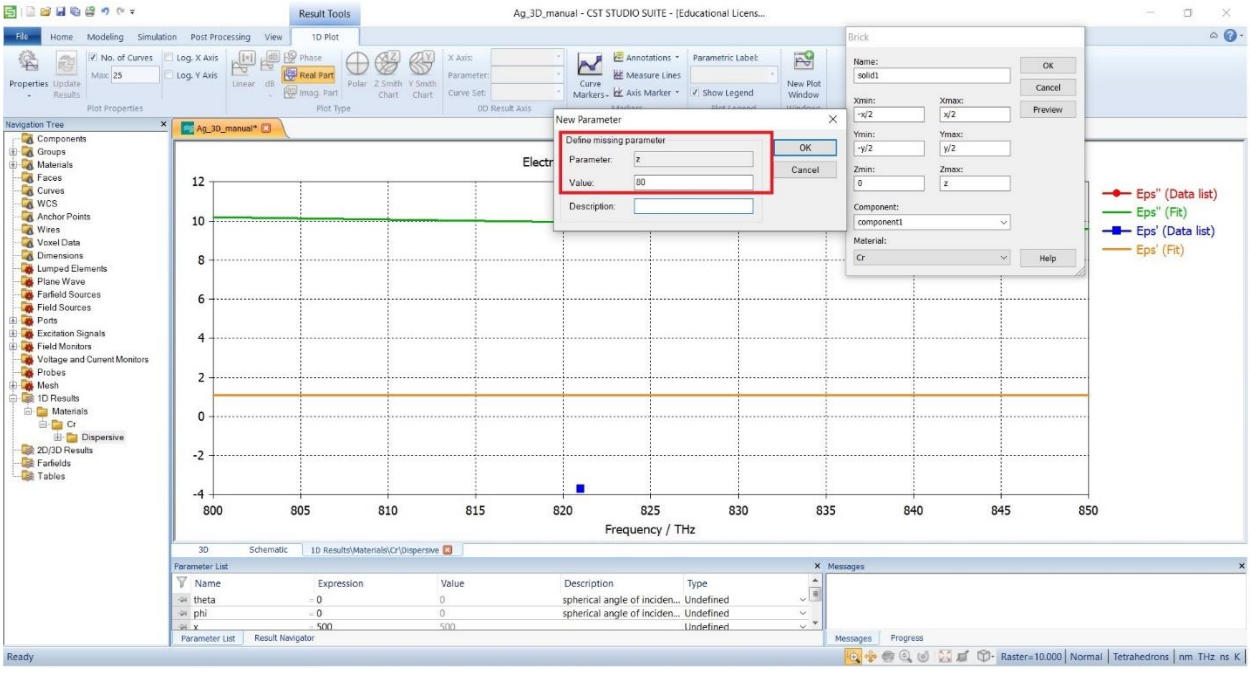
Result Tools
Ag_3D_manual - CST STUDIO SUITE - [Educational Licens...
New Parameter
Define missing parameter
Parameter: z
Value: 80
Description:
OK
Cancel
Brick
Name: solid1
Xmin: -x/2
Xmax: x/2
Ymin: -y/2
Ymax: y/2
Zmin: 0
Zmax: z
Component: component1
Material: Cr
Preview
Help
Eps'' (Data list)
Eps'' (Fit)
Eps' (Data list)
Eps' (Fit)
Frequency / THz
Navigation Tree
Parameter List
Messages
Ready

Step 15: Perspective view

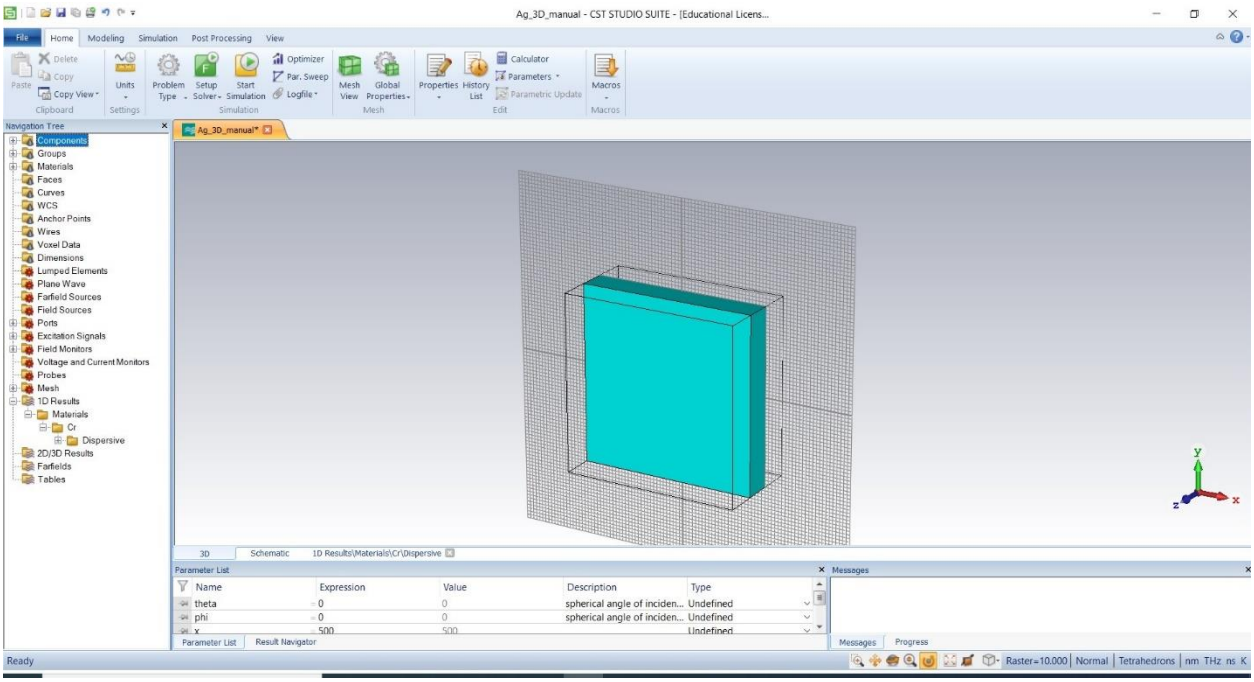

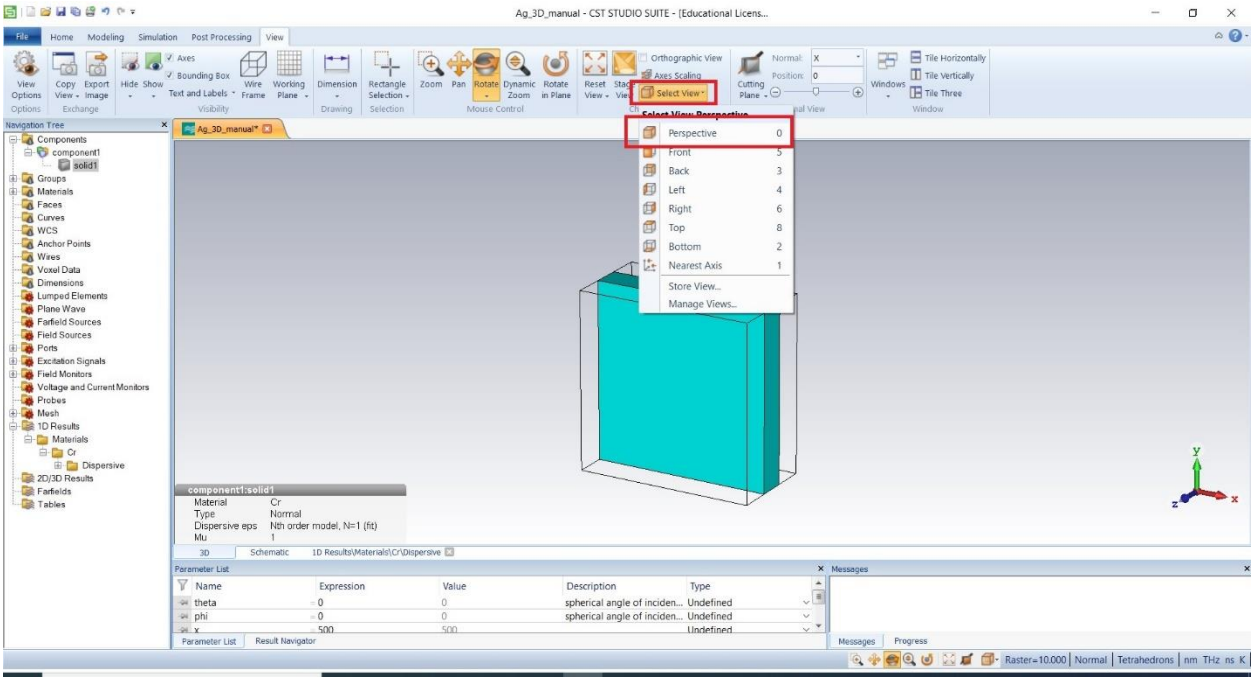

Step 16: Front view

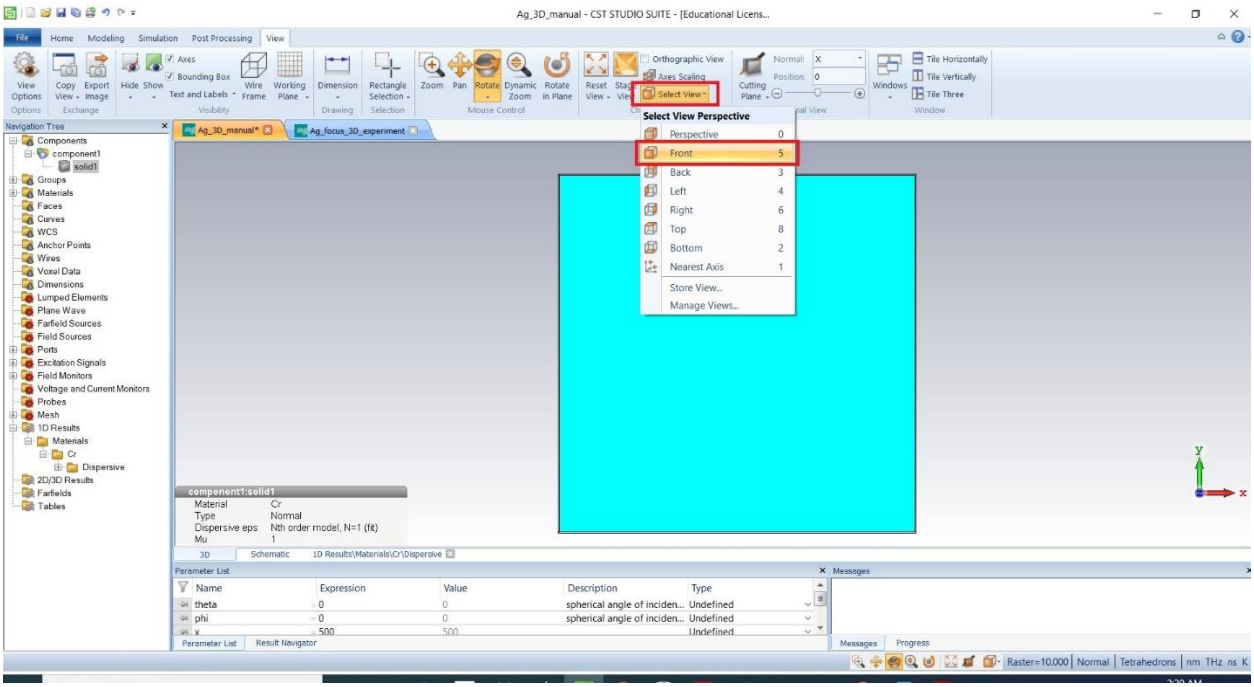

Step 17: Select ‘picks’

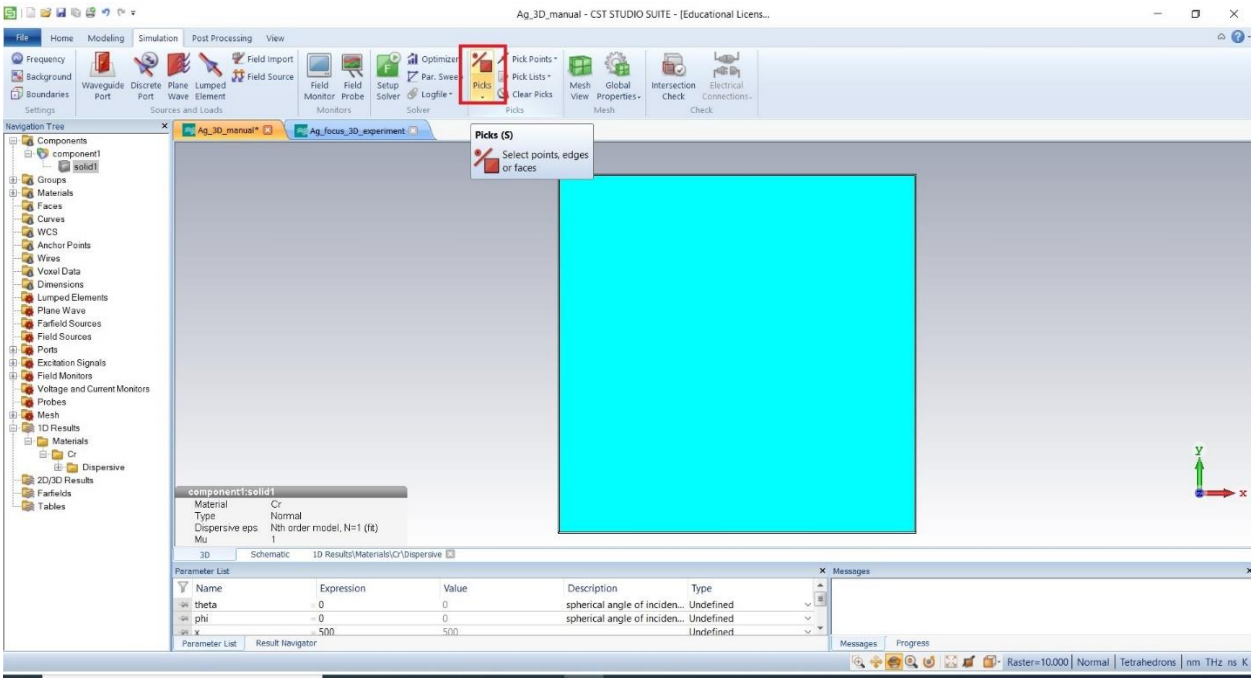

Step 17: Select Front faces of the existing material (Cr)

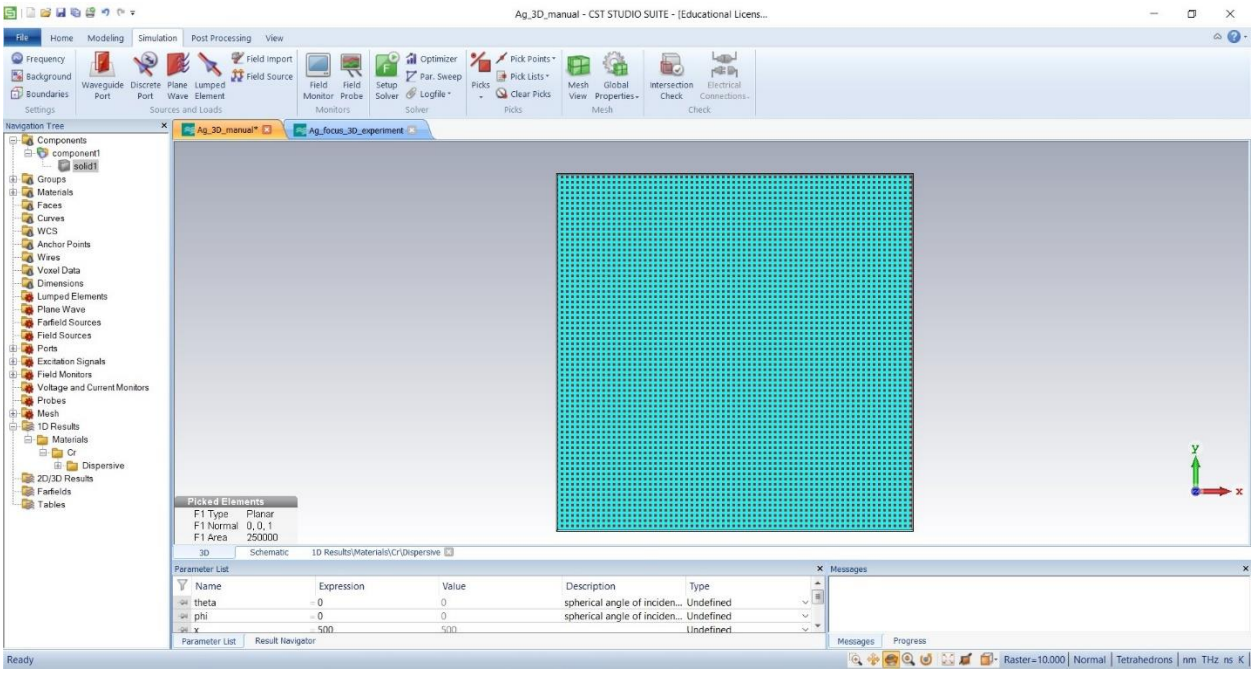

Step 18: select ‘Extrusions’

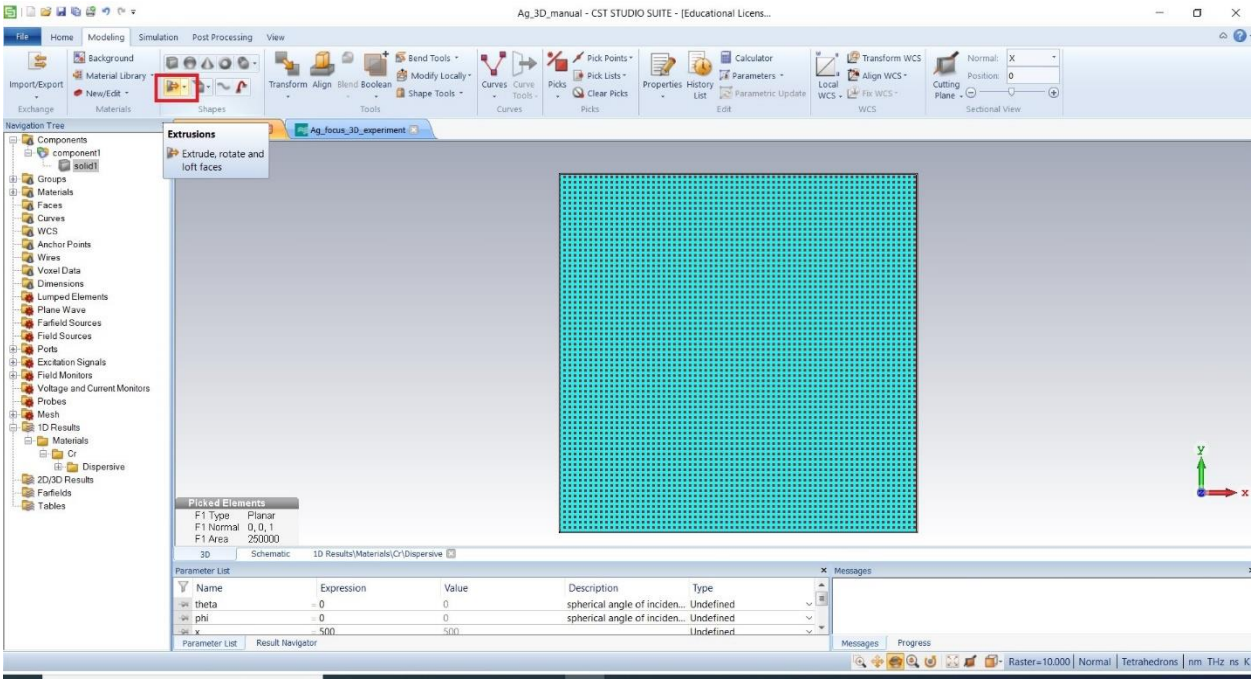

Step 19: Material selection from library.

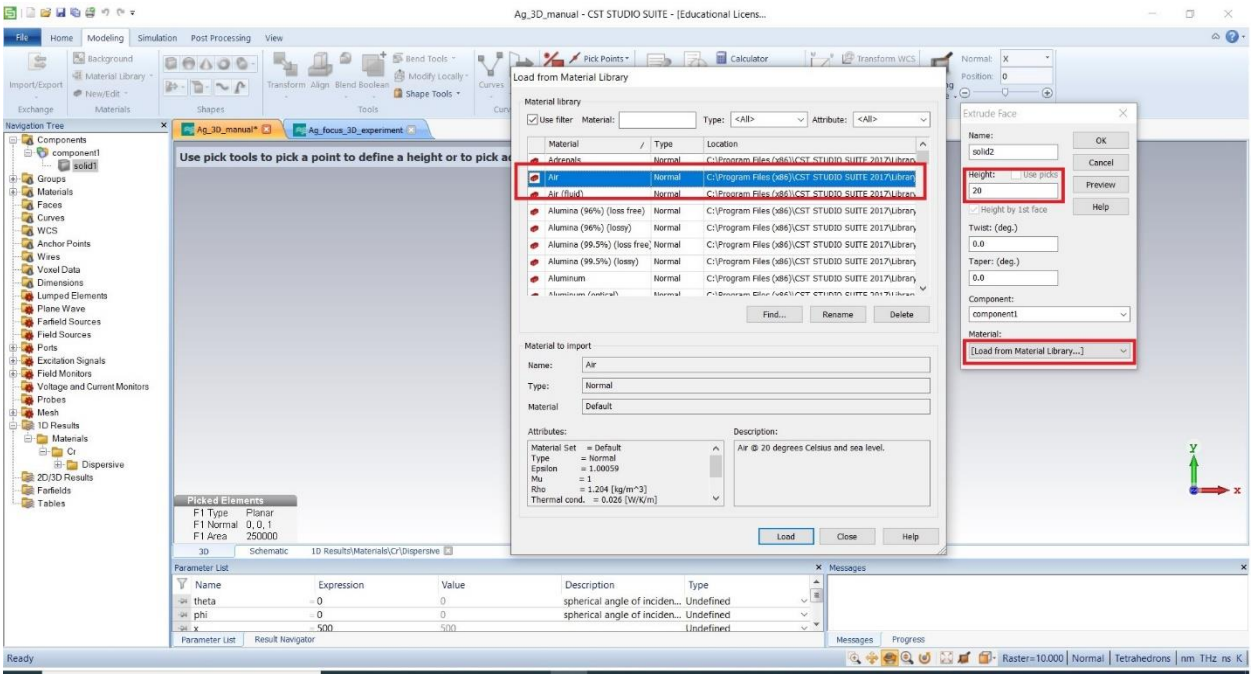

Air has been placed on Cr.

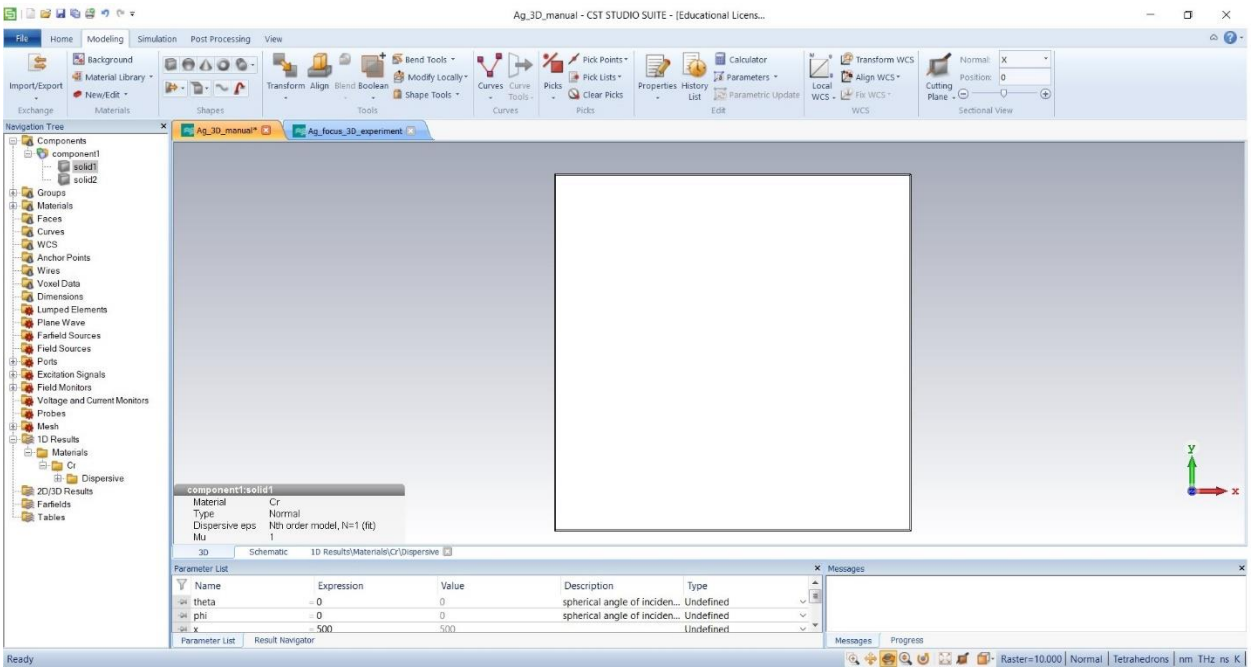

Step 20: select ‘pick’ to introduce new material.

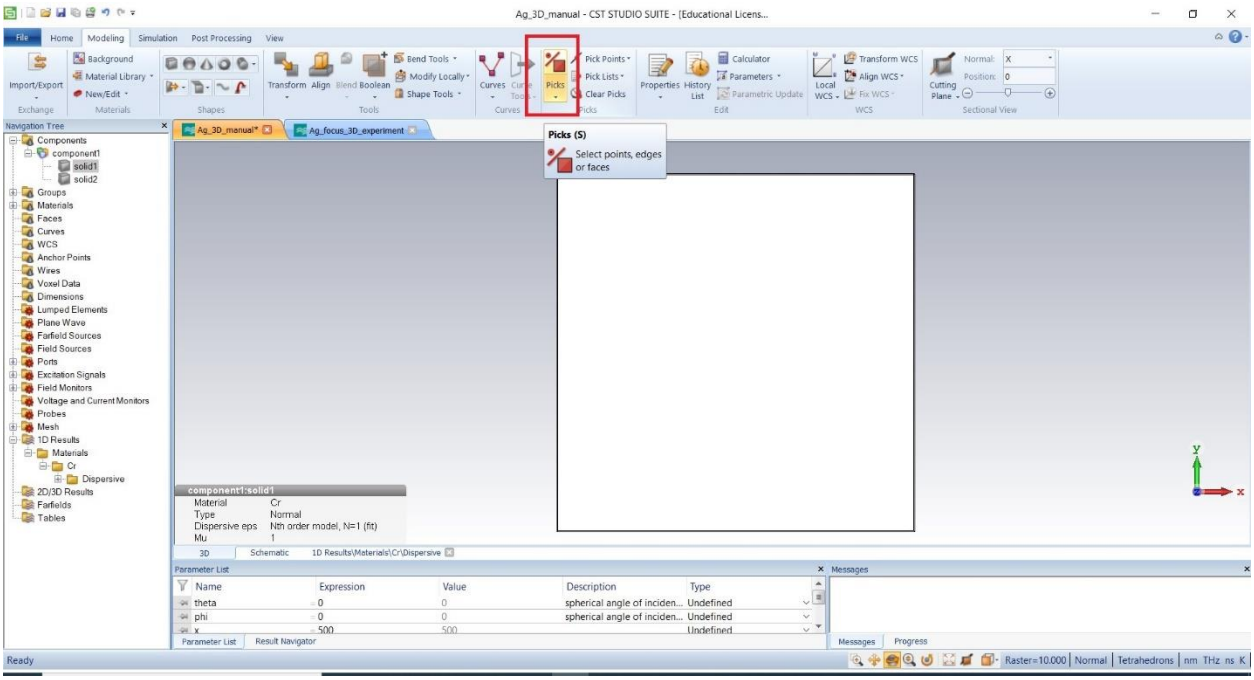

Step 21: select the face

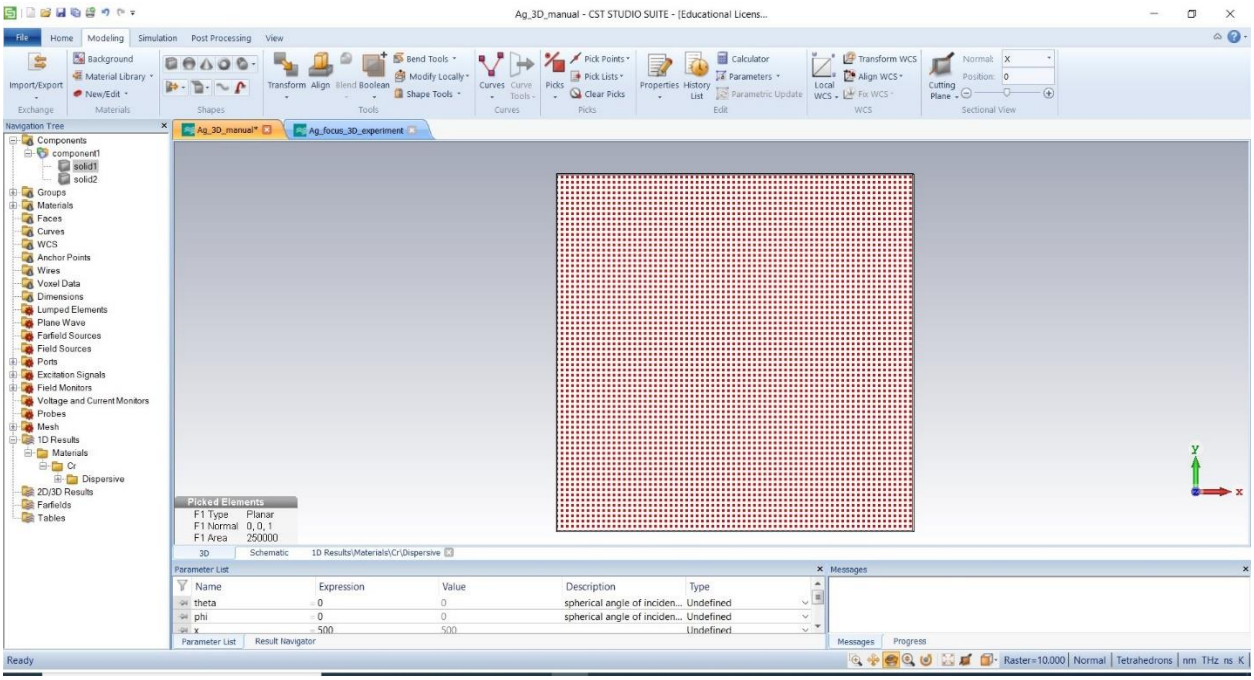

Step 22: select ‘Extrusion’

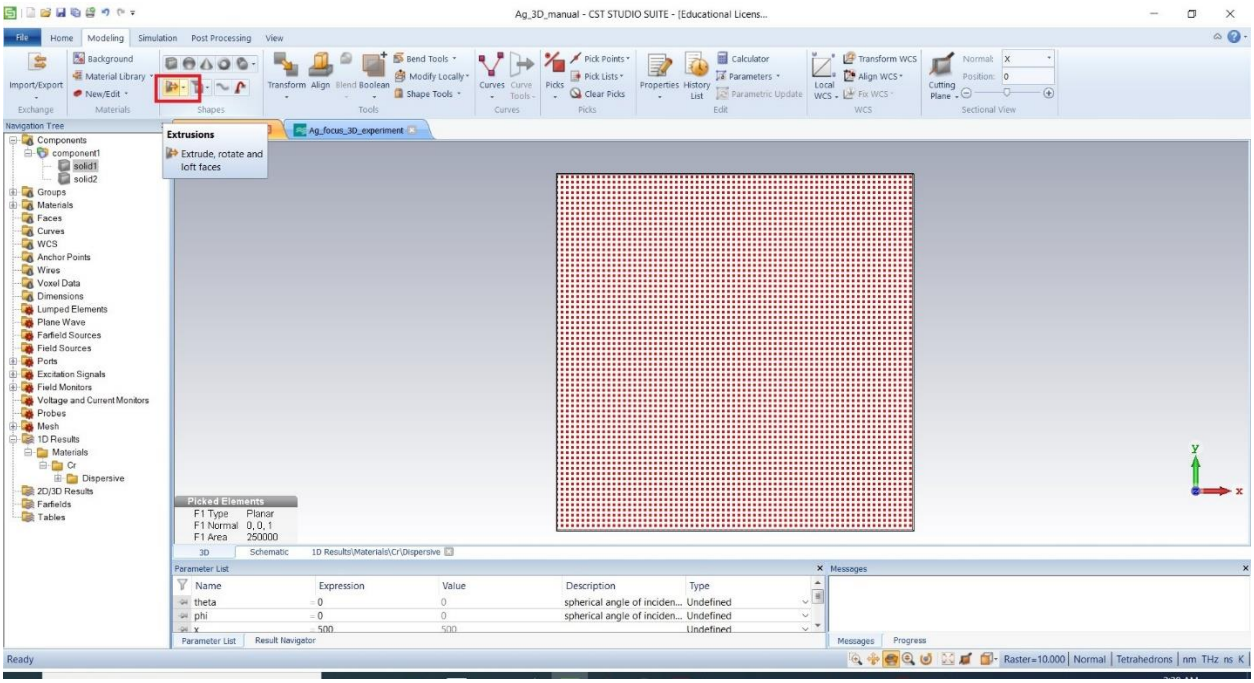

Step 22: Set the dimension and permittivity of new material (PMMA)

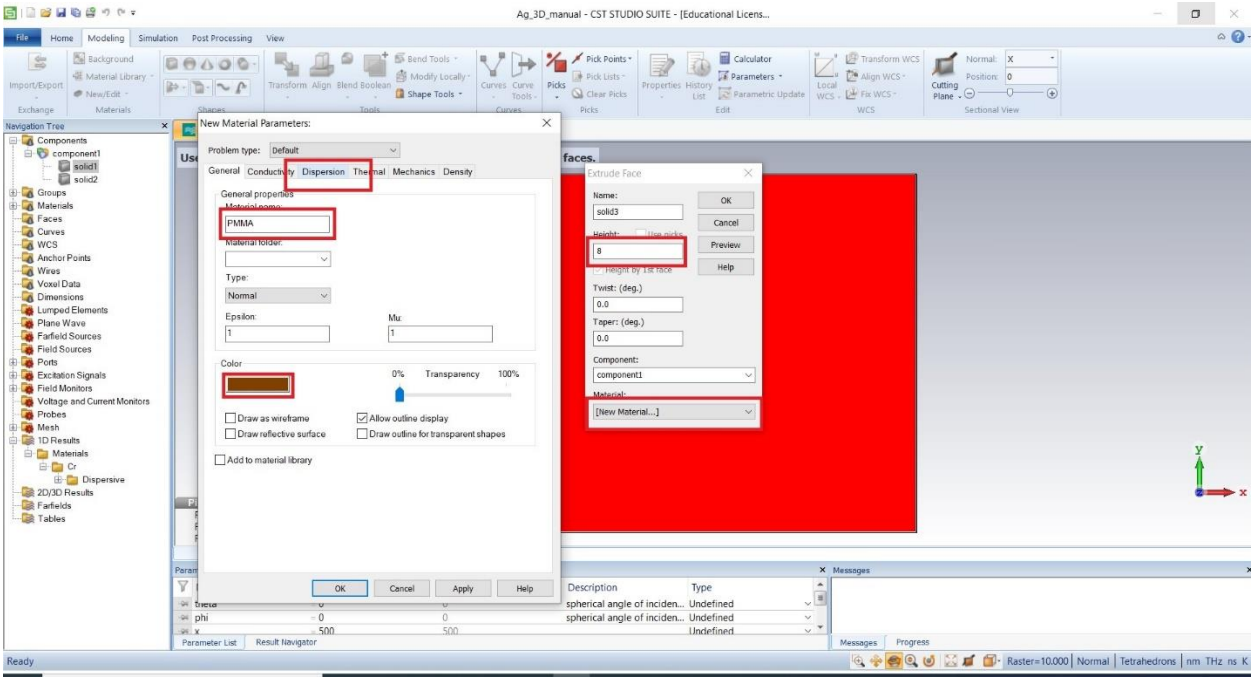

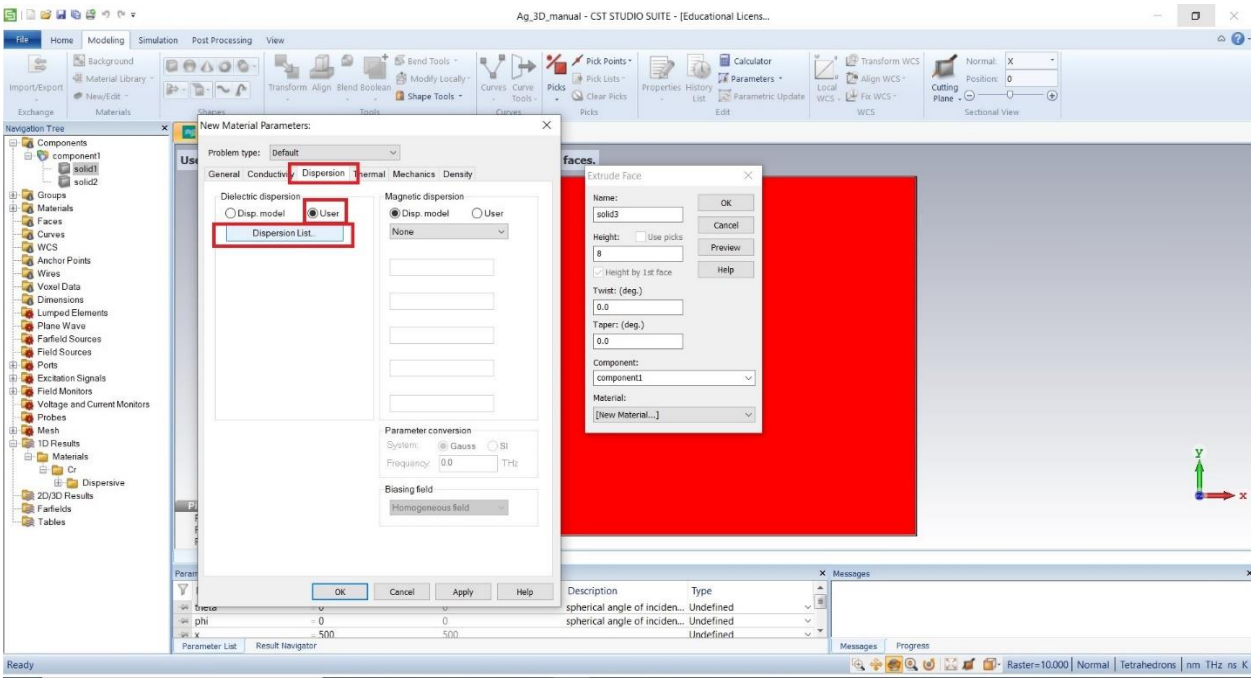
Ag_3D_manual - CST STUDIO SUITE - [Educational Licens...
New Material Parameters:
Problem type: Default
General Conductivity Dispersion Thermal Mechanics Density
Dielectric dispersion
Disp. model
User
Dispersion List...
Magnetic dispersion
Disp. model
User
None
Parameter conversion
System: Gauss SI
Frequency: 0.0 THz
Biasing field
Homogeneous field
OK
Cancel
Apply
Help
Extrude Face
Name: solid3
Height: 8
Twist: (deg.) 0.0
Taper: (deg.) 0.0
Component: component1
Material: [New Material...]
Preview
Navigation Tree
Components
component1
solid1
solid2
Groups
Materials
Faces
Curves
WCS
Anchor Points
Wires
Voxel Data
Dimensions
Lumped Elements
Plane Wave
Farfield Sources
Field Sources
Ports
Excitation Signals
Field Monitors
Voltage and Current Monitors
Probes
Mesh
1D Results
Materials
Cr
Dispersive
2D/3D Results
Farfields
Tables
Description
Type
theta
phi
x
spherical angle of inciden...
Undefined
Parameter List
Result Navigator
Messages
Progress
Ready

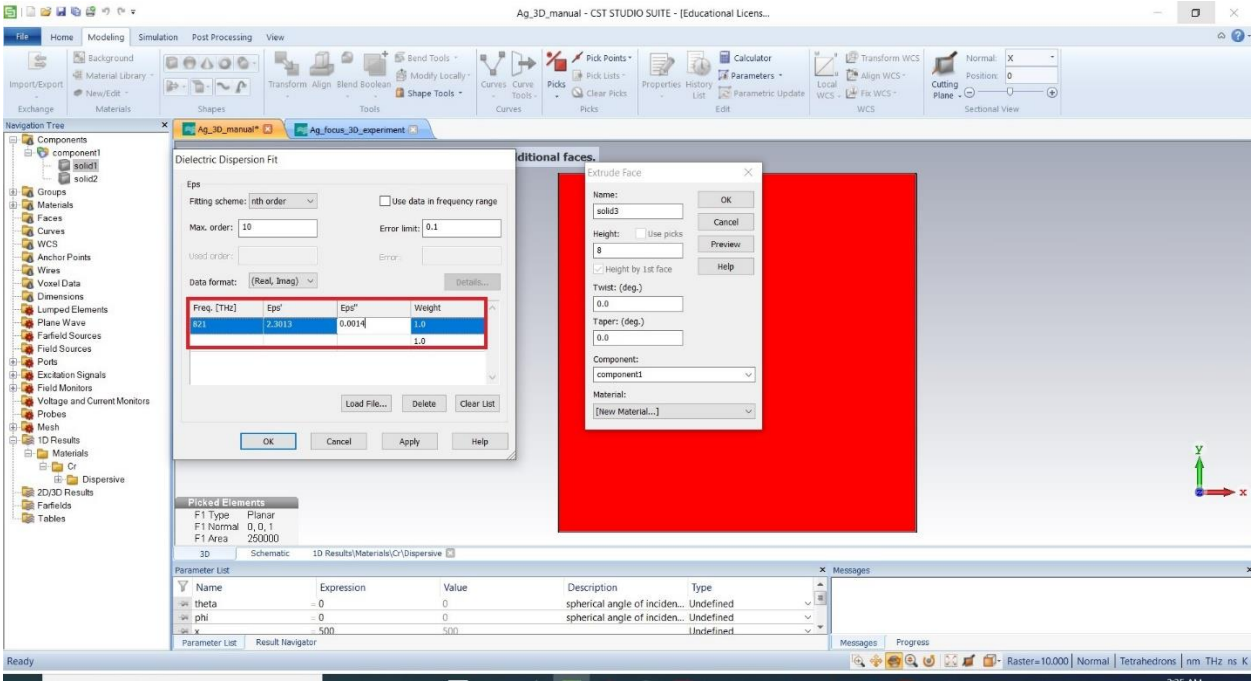
Ag_3D_manual - CST STUDIO SUITE - [Educational Licens...
Ag_3D_manual*
Ag_focus_3D_experiment
Dielectric Dispersion Fit
Eps
Fitting scheme: nth order
Use data in frequency range
Max. order: 10
Error limit: 0.1
Used order:
Error:
Data format: (Real, Imag)
Details...
Freq. [THz] Eps' Eps'' Weight
821 2.3013 0.0014 1.0
1.0
Load File...
Delete
Clear List
OK
Cancel
Apply
Help
Extrude Face
Name: solid3
Height: 8
Twist: (deg.) 0.0
Taper: (deg.) 0.0
Component: component1
Material: [New Material...]
Preview
Picked Elements
F1 Type Planar
F1 Normal 0, 0, 1
F1 Area 250000
3D
Schematic
1D Results\Materials\Cr\Dispersive
Navigation Tree
Parameter List
Name
Expression
Value
Description
Type
theta
phi
x
spherical angle of inciden...
Undefined
Result Navigator
Messages
Progress
Ready

Step 23: Three materials (Cr, Air, PMMA) have been formed, select pick again

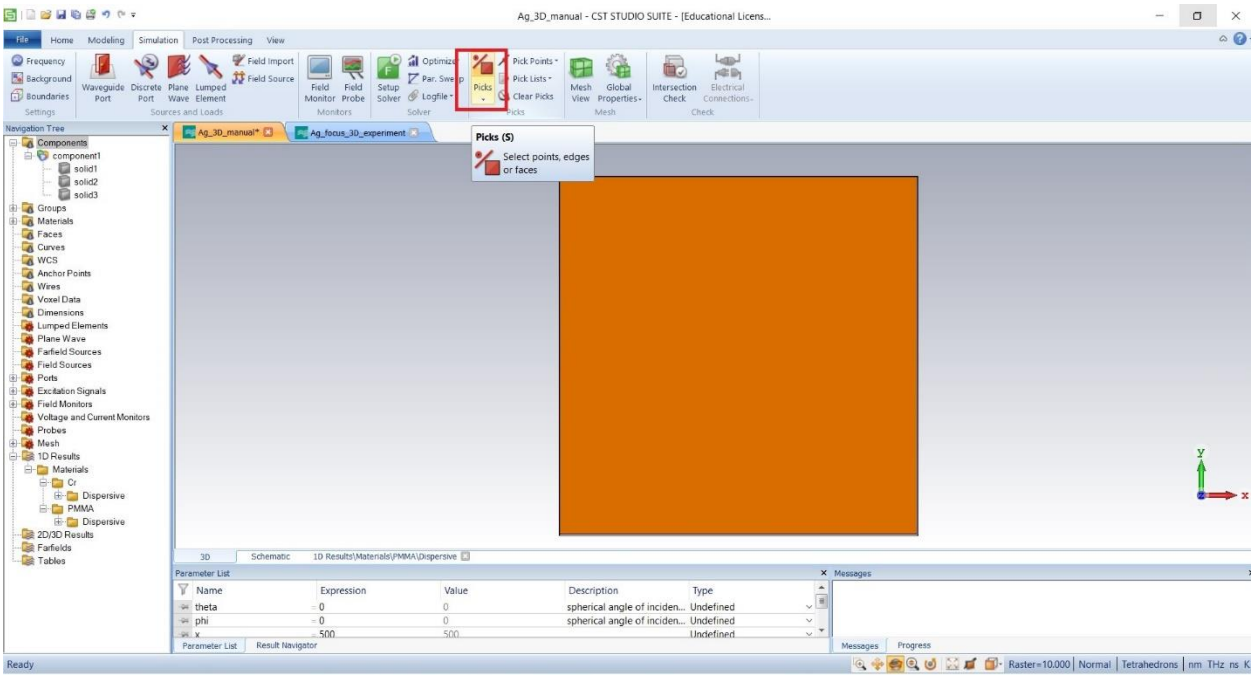

Step 24: Select ‘Face’

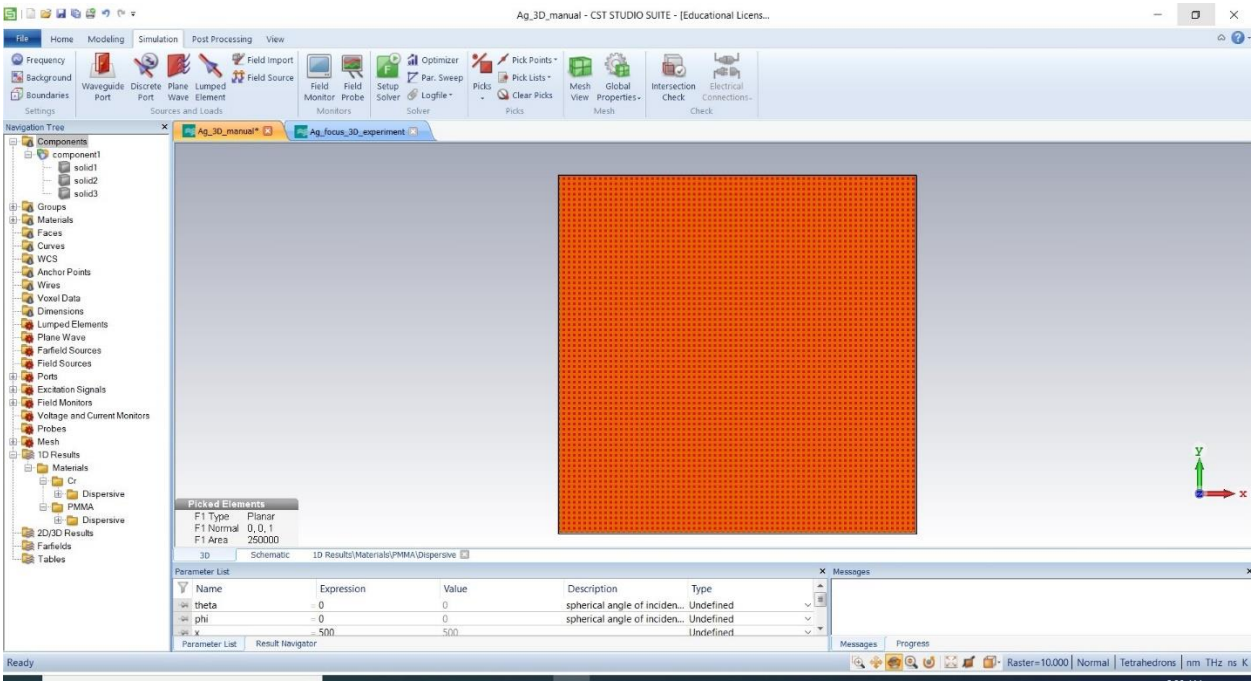

Step 25: Select ‘Extrusion’

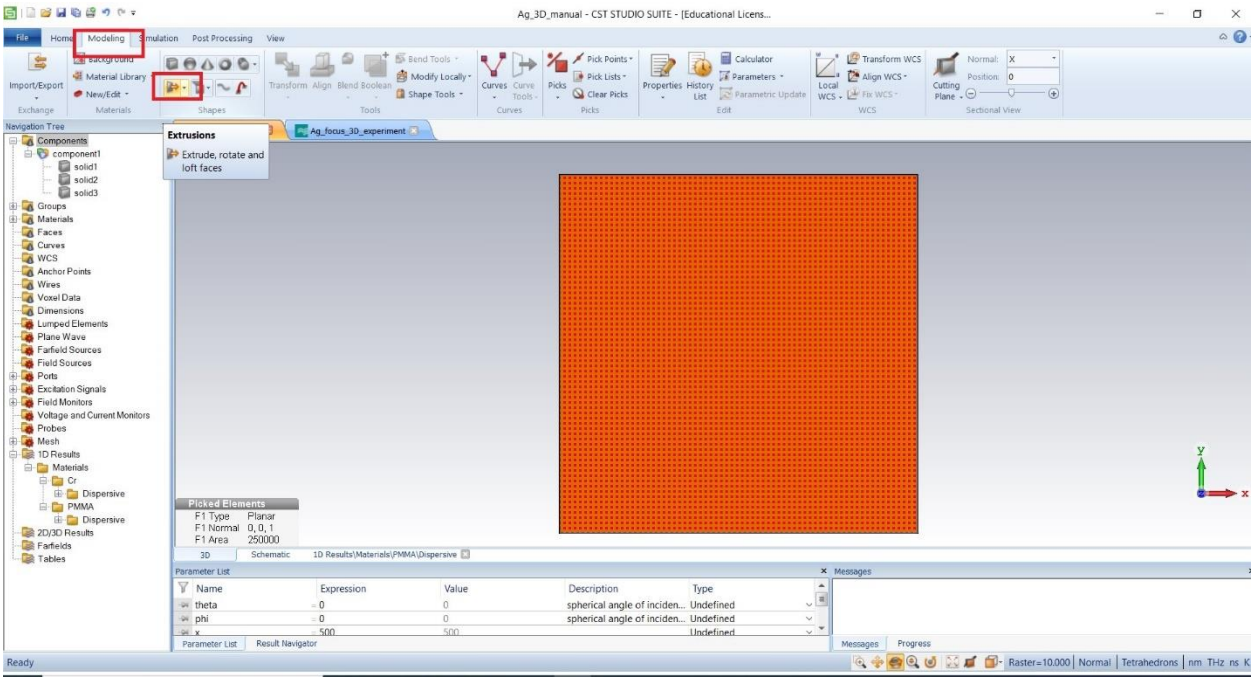

Step 26: Set the dimension and permittivity of new material (Ag)

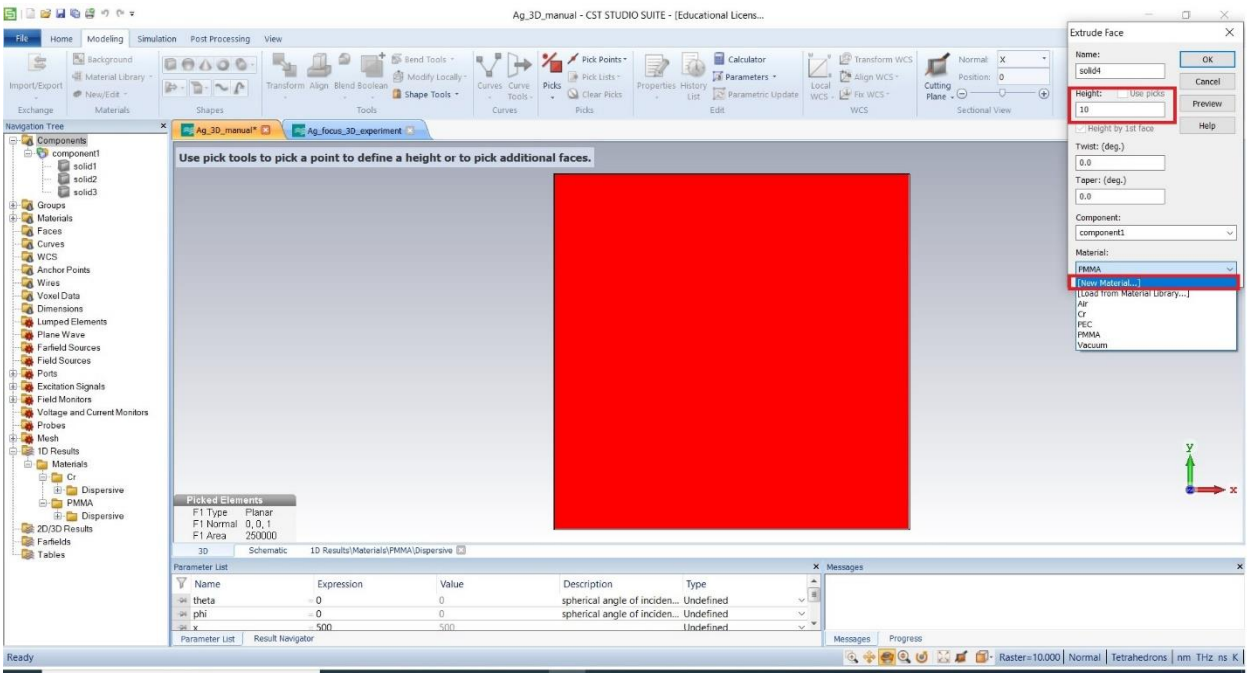

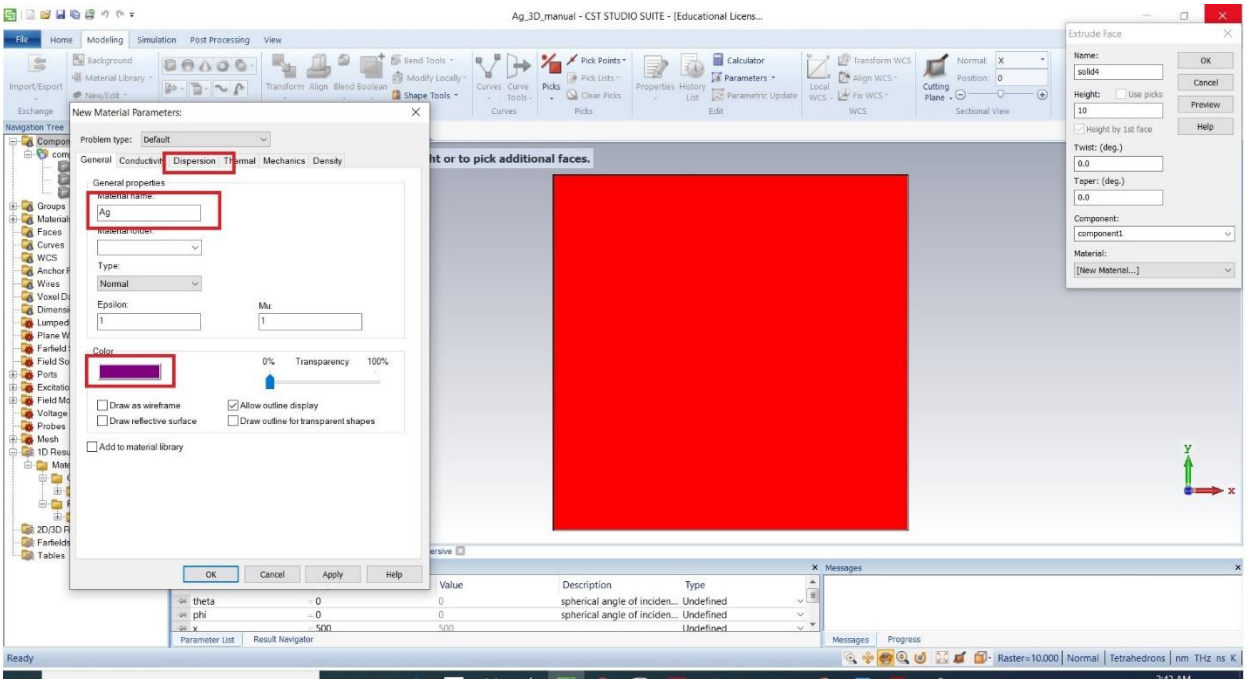
Ag_3D_manual - CST STUDIO SUITE - [Educational Licens...
New Material Parameters:
Problem type: Default
General Conductivity Dispersion Thermal Mechanics Density
General properties
Material name:
Ag
Type:
Normal
Epsilon:
1
Mu:
1
Color:
0% Transparency 100%
Draw as wireframe
Allow outline display
Draw reflective surface
Draw outline for transparent shapes
Add to material library
OK Cancel Apply Help
Extrude Face
Name:
solid4
Height:
10
Twist: (deg.)
0.0
Taper: (deg.)
0.0
Component:
component1
Material:
[New Material...]
OK Cancel Preview Help
ht or to pick additional faces.
Messages
Progress
Ready

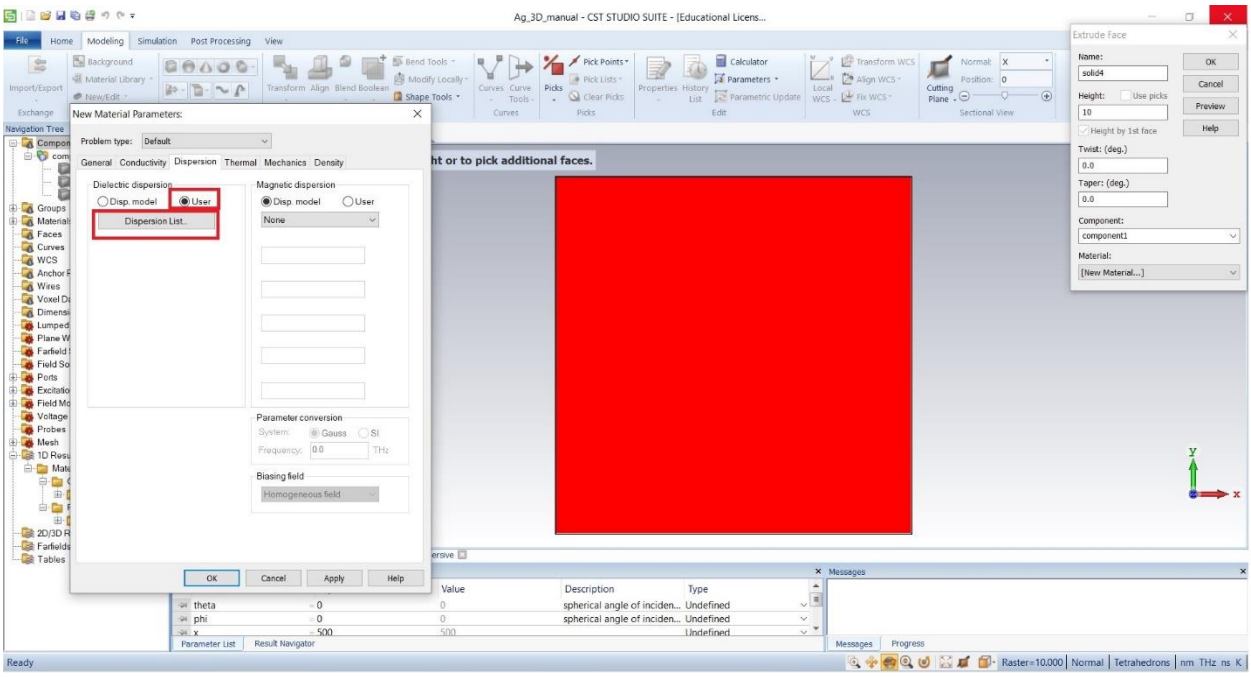
Ag_3D_manual - CST STUDIO SUITE - [Educational Licens...
New Material Parameters:
Problem type: Default
General Conductivity Dispersion Thermal Mechanics Density
Dielectric dispersion
Disp. model
User
Dispersion List...
Magnetic dispersion
Disp. model
User
None
Parameter conversion
Biasing field
Homogeneous field
OK Cancel Apply Help
Extrude Face
Name:
solid4
Height:
10
Twist: (deg.)
0.0
Taper: (deg.)
0.0
Component:
component1
Material:
[New Material...]
OK Cancel Preview Help
ht or to pick additional faces.
Messages
Progress
Ready

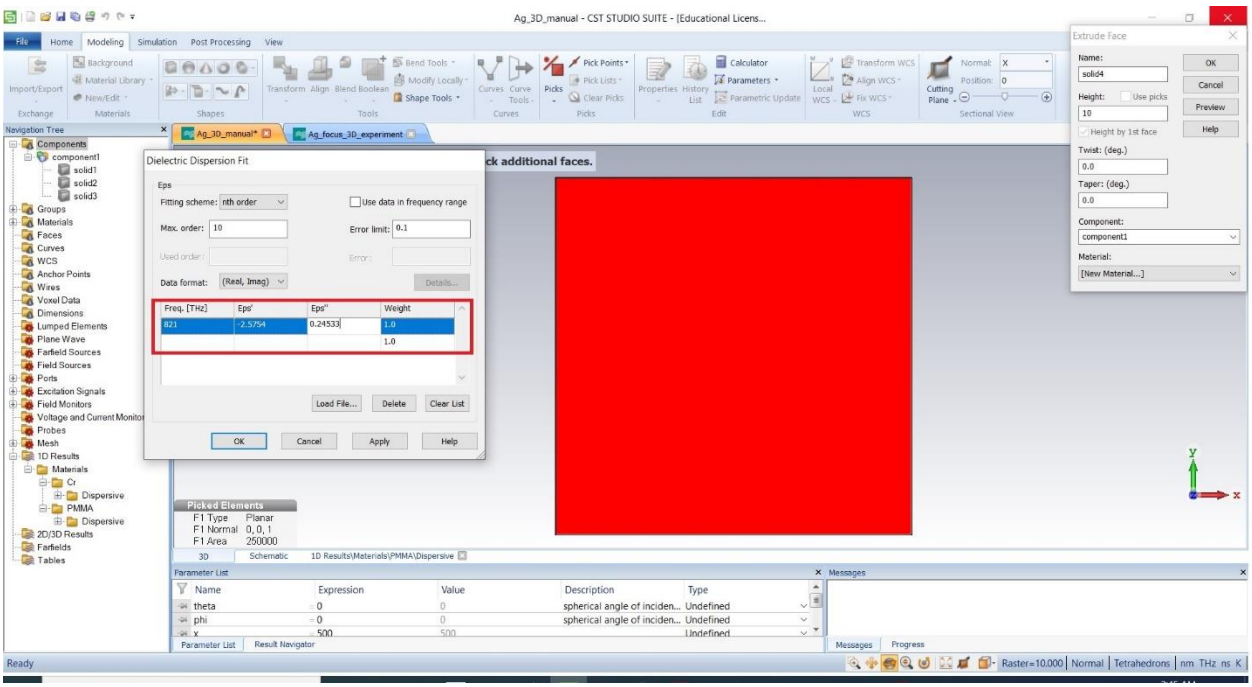

Step 27: Four materials (Cr, Air, PMMA, Ag) have been formed, select pick again

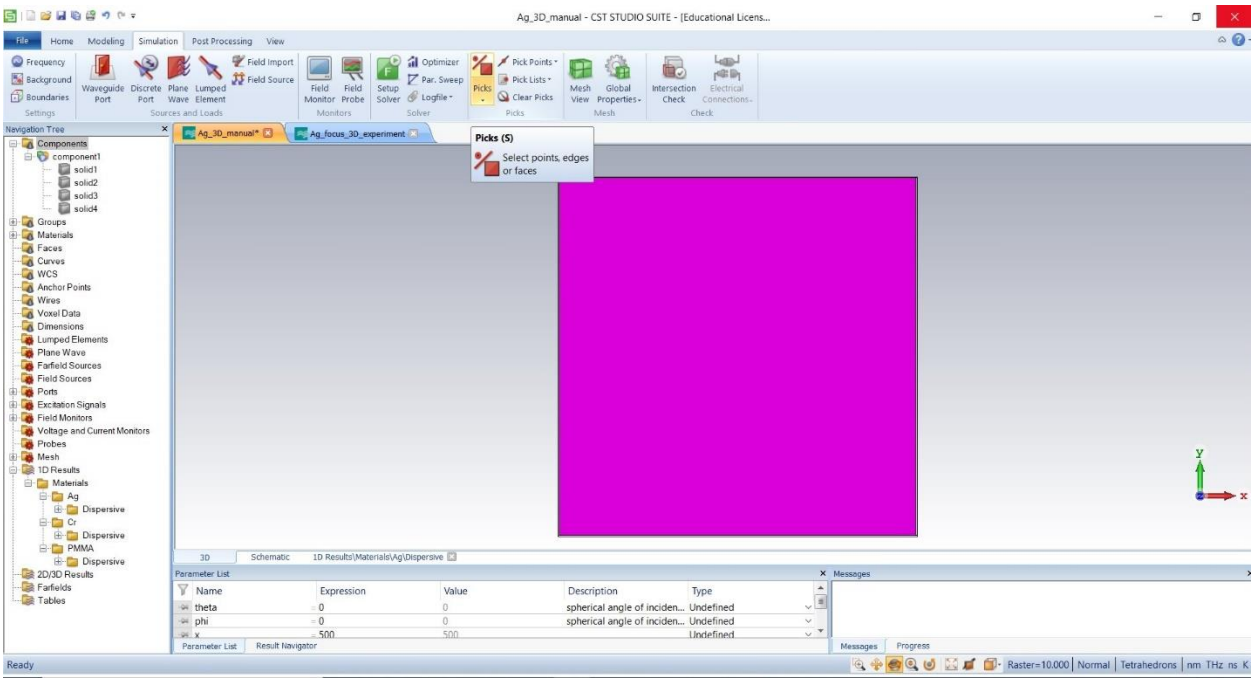

Step 28: Select ‘Face’

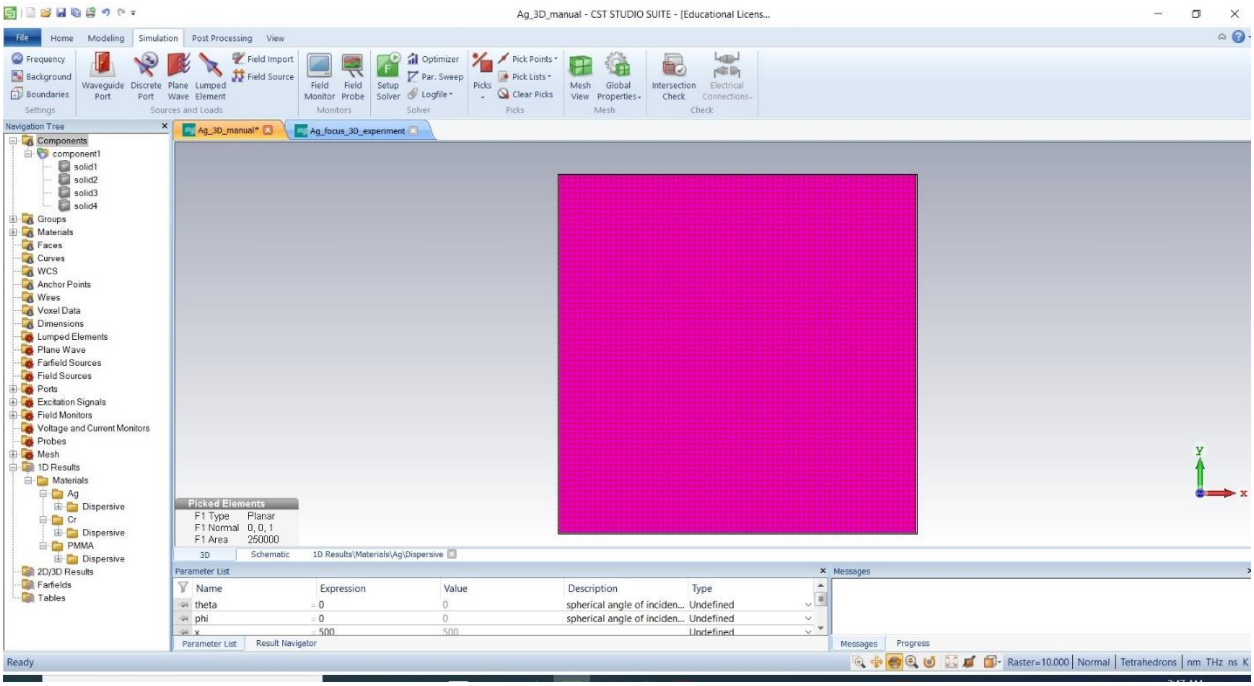

Step 29: Select ‘Extrusion’

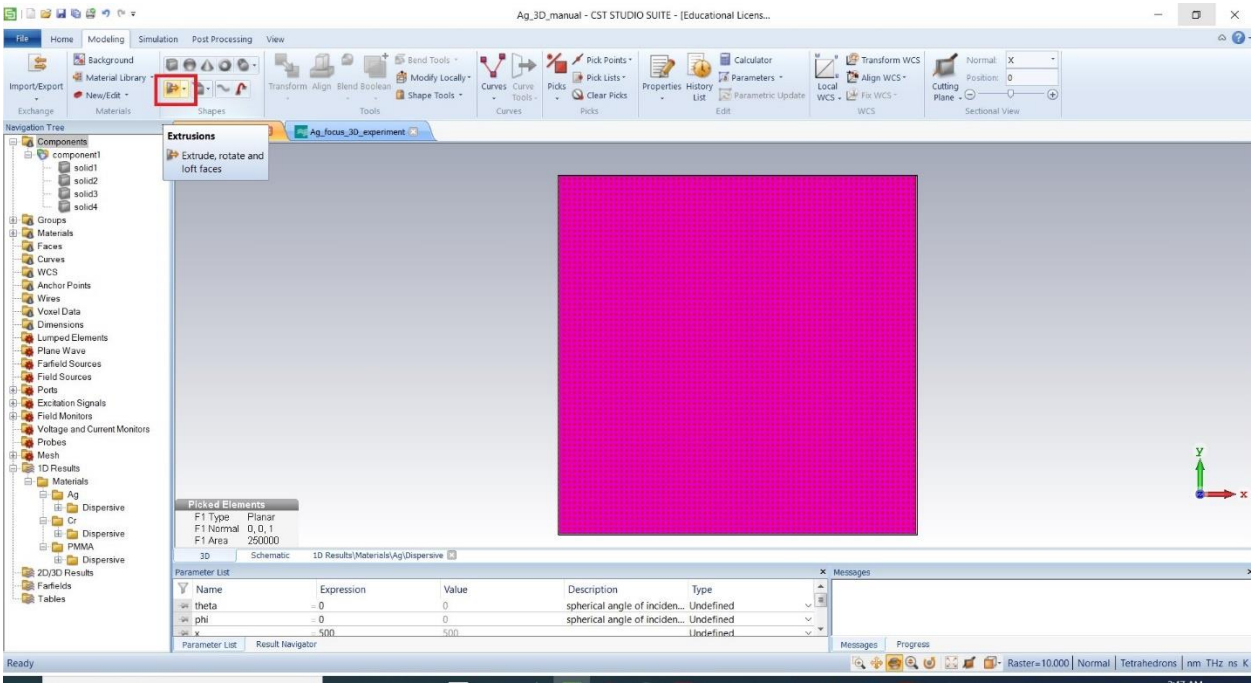

Step 30: Set the dimension and permittivity of new material (PR)

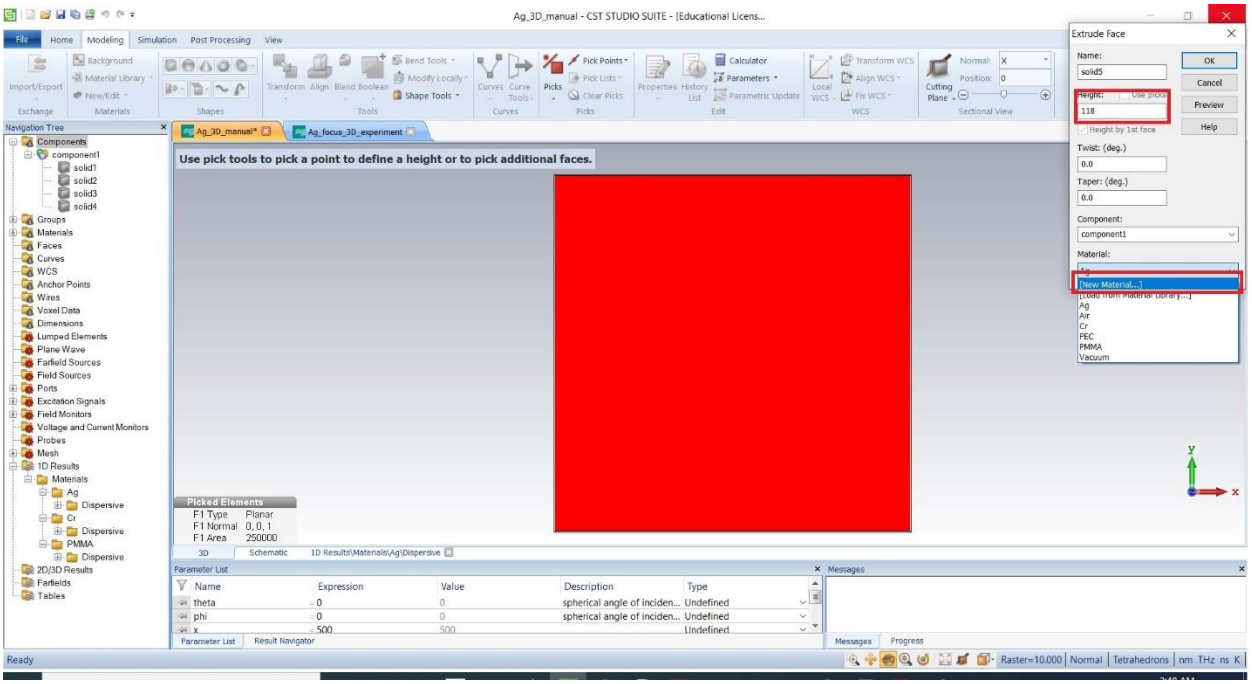

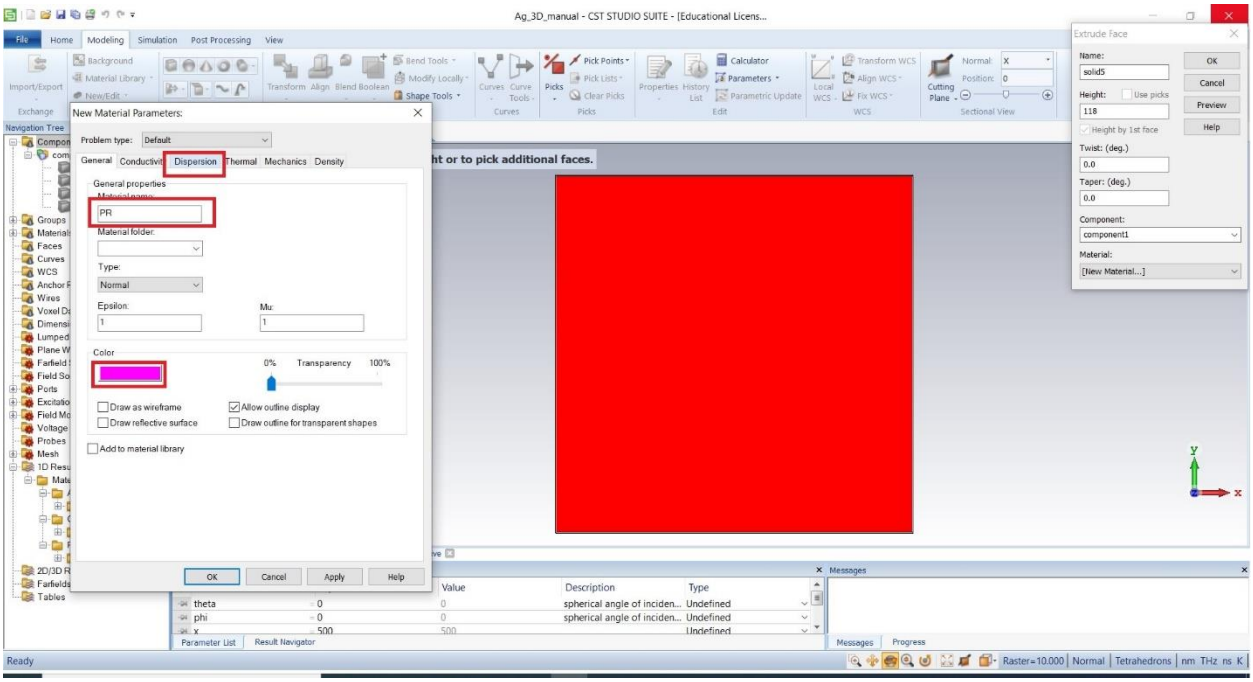

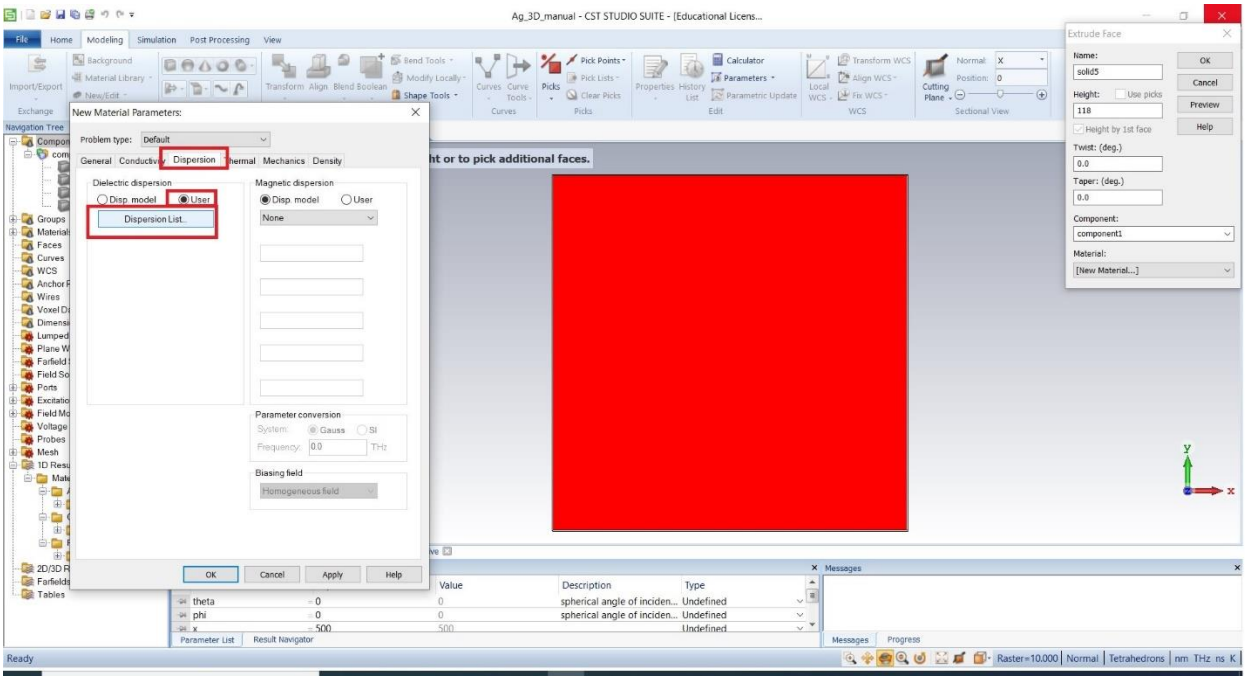
Ag_3D_manual - CST STUDIO SUITE - [Educational Licens...
New Material Parameters:
Problem type: Default
General Conductivity Dispersion Thermal Mechanics Density
Dielectric dispersion
Disp. model
User
Dispersion List...
Magnetic dispersion
Disp. model
User
None
Parameter conversion
Biasing field
Homogeneous field
OK
Cancel
Apply
Help
Extrude Face
Name: solid5
Height: 118
Twist: (deg.) 0.0
Taper: (deg.) 0.0
Component: component1
Material: [New Material...]
Navigation Tree
Parameter List
Result Navigator
Messages
Progress
Ready

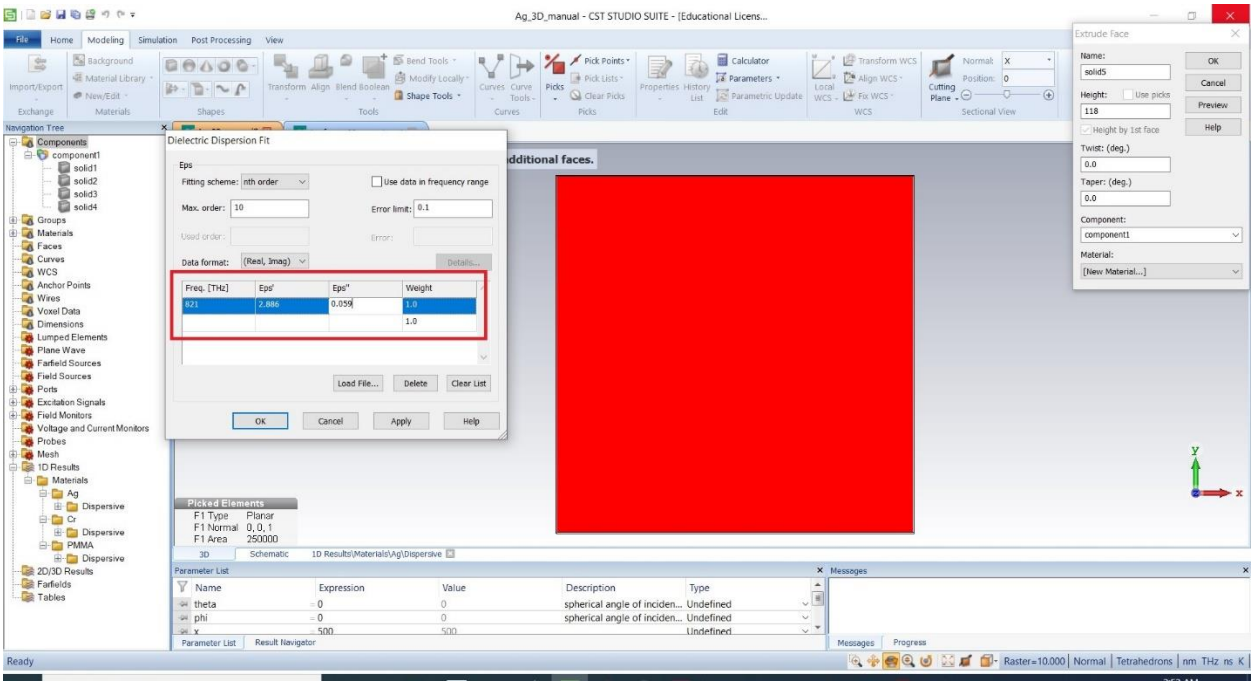
Ag_3D_manual - CST STUDIO SUITE - [Educational Licens...
Dielectric Dispersion Fit
Eps
Fitting scheme: nth order
Use data in frequency range
Max. order: 10
Error limit: 0.1
Data format: (Real, Imag)
Freq. [THz] Eps' Eps'' Weight
821 2.886 0.059 1.0
1.0
Load File...
Delete
Clear List
OK
Cancel
Apply
Help
Extrude Face
Name: solid5
Height: 118
Twist: (deg.) 0.0
Taper: (deg.) 0.0
Component: component1
Material: [New Material...]
Picked Elements
F1 Type Planar
F1 Normal 0, 0, 1
F1 Area 250000
Navigation Tree
Parameter List
Result Navigator
Messages
Progress
Ready

Step 31: Five materials (Cr, Air, PMMA, Ag, PR) have been formed, select pick again

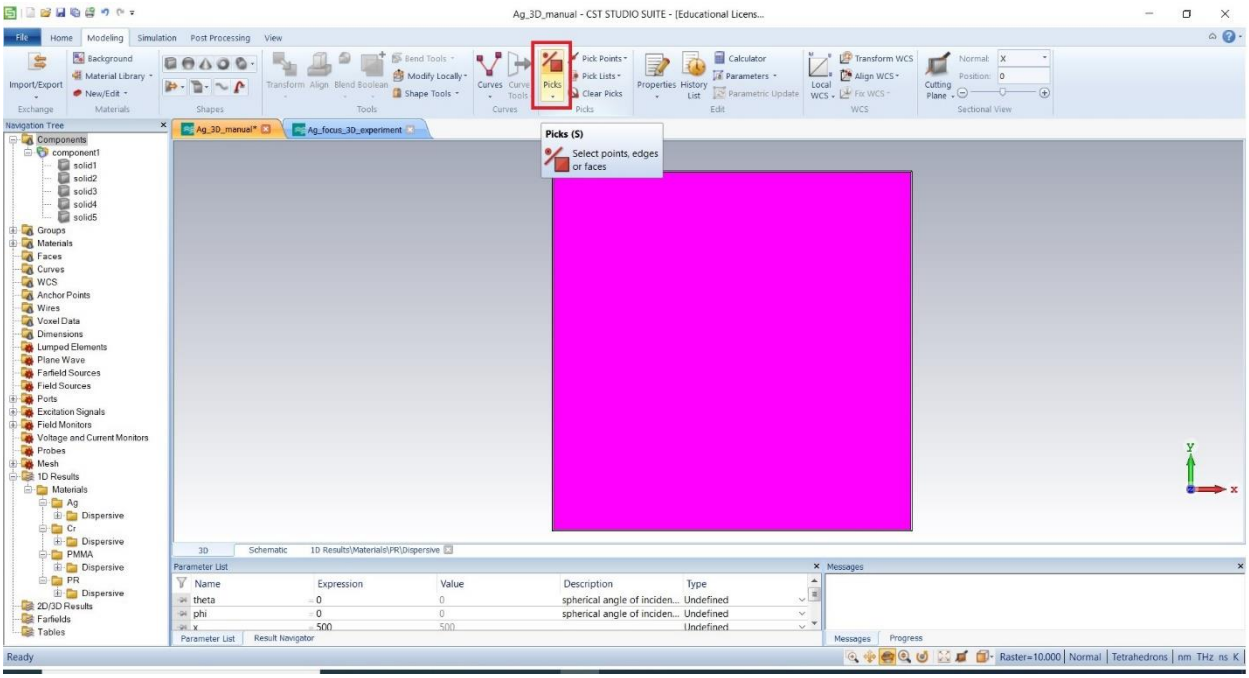

Step 32: Select ‘Face’

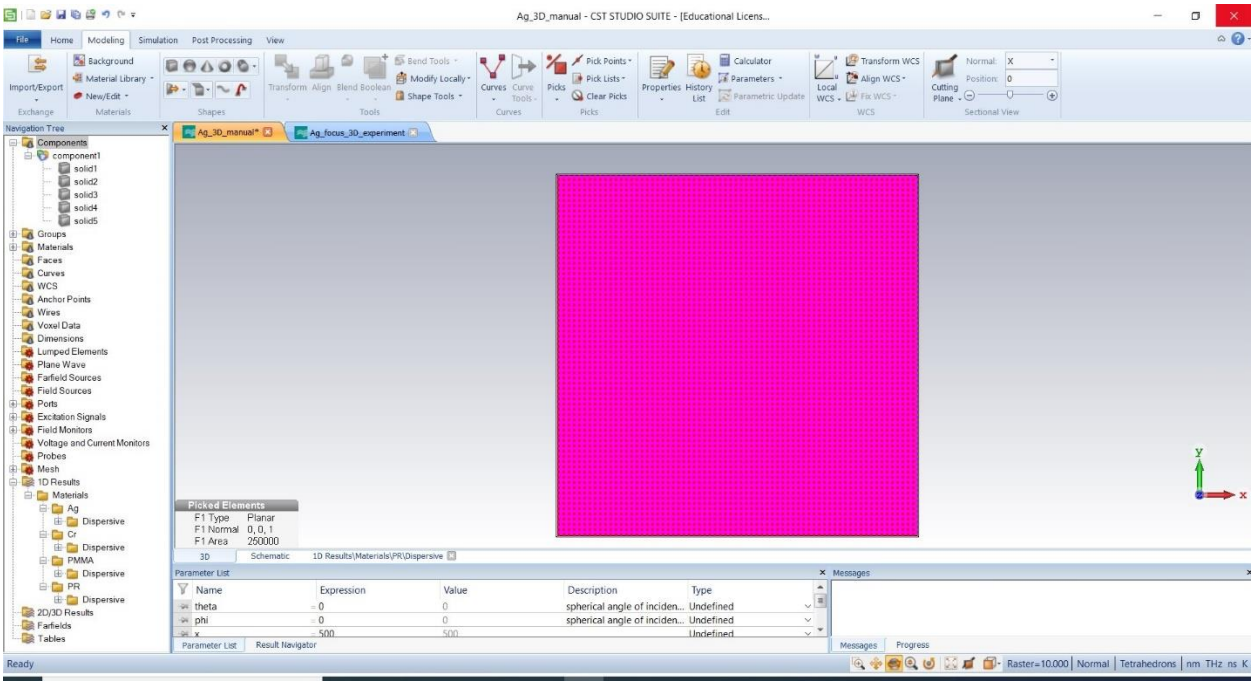

Step 33: Select ‘Extrusion’

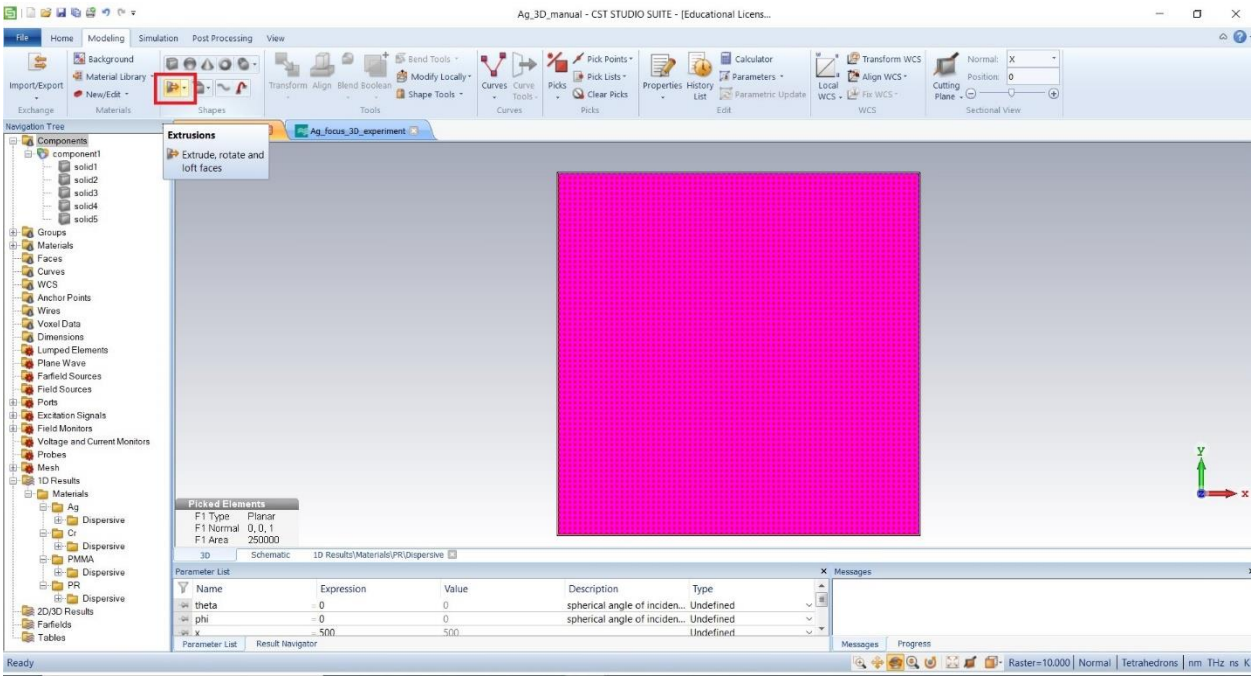

Step 34: Select material ‘Air’ from library and define the dimension

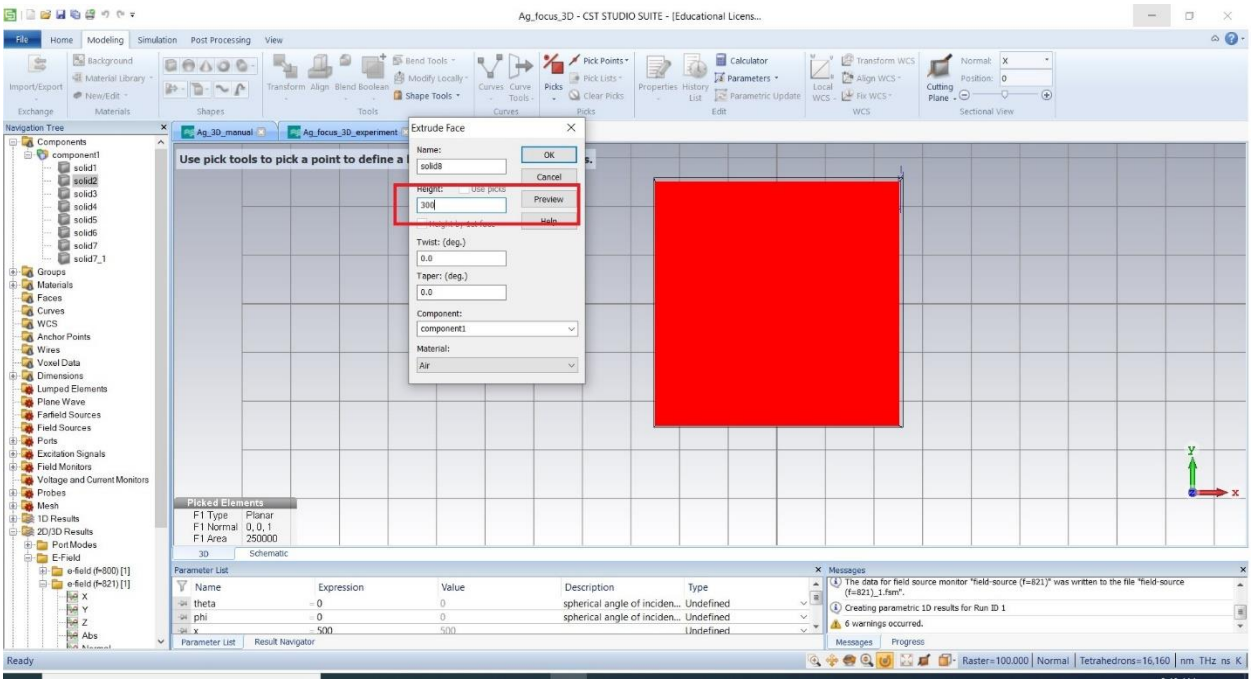

Step 35: Six materials (Cr, Air, PMMA, Ag, PR,Air) have been formed

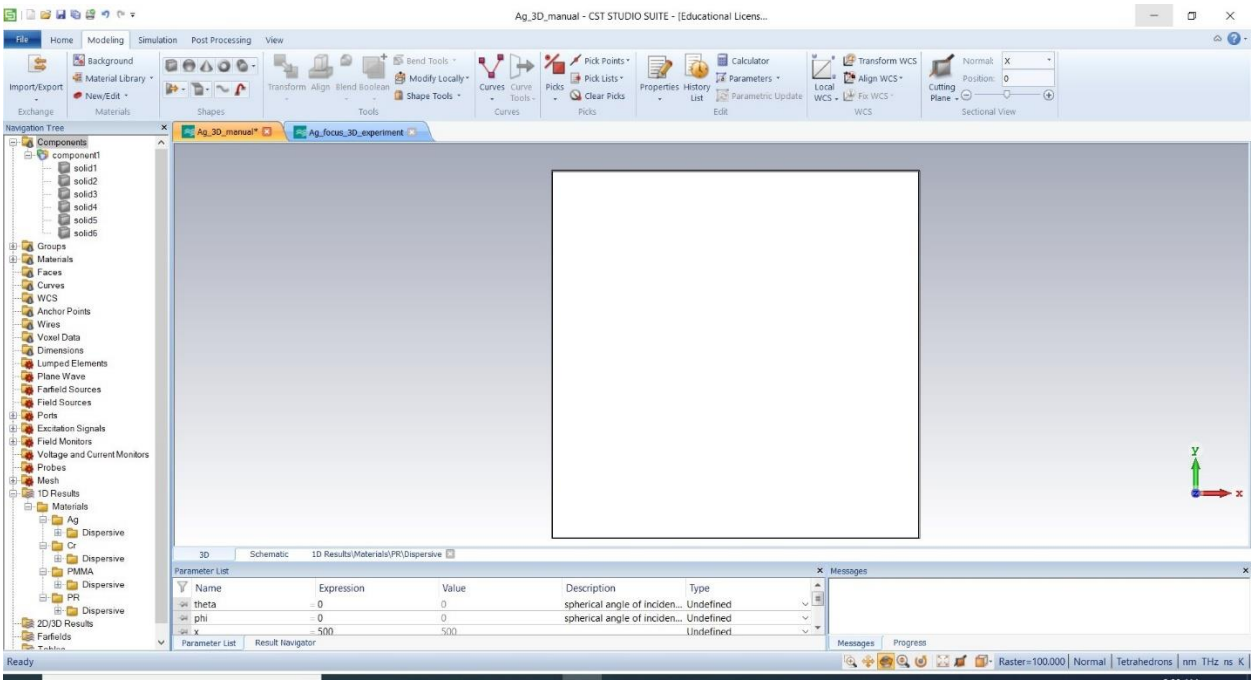

Step 36: Perspective view

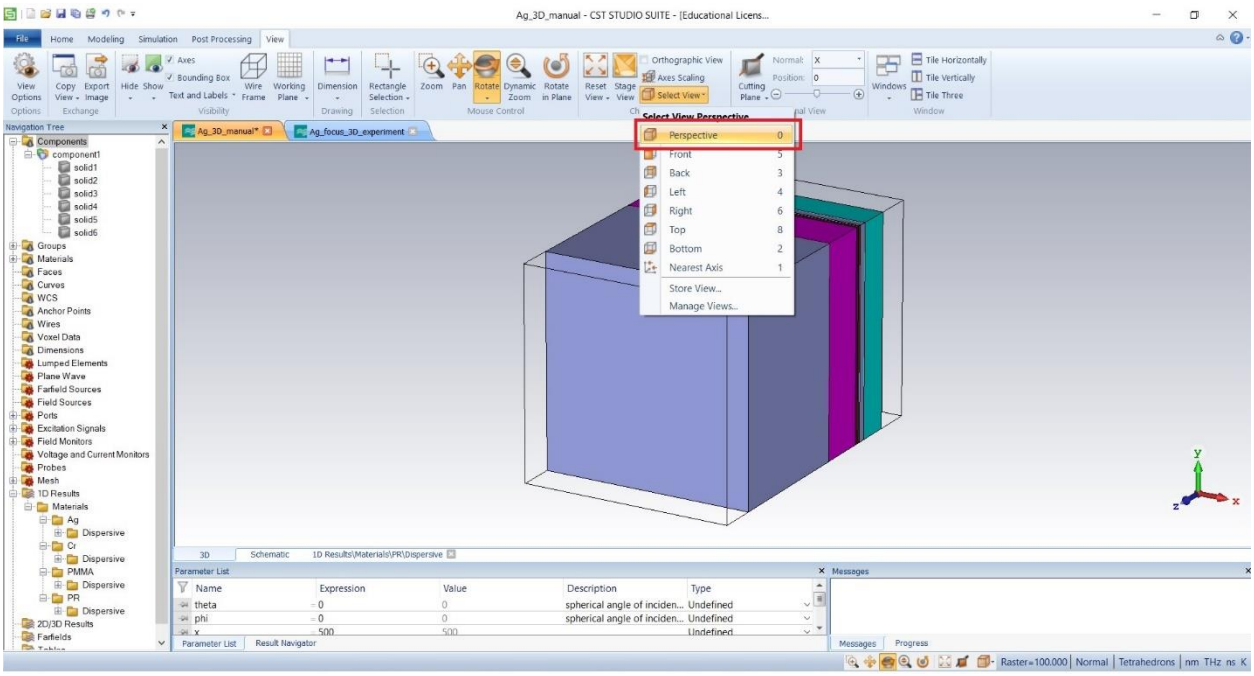

Right side view

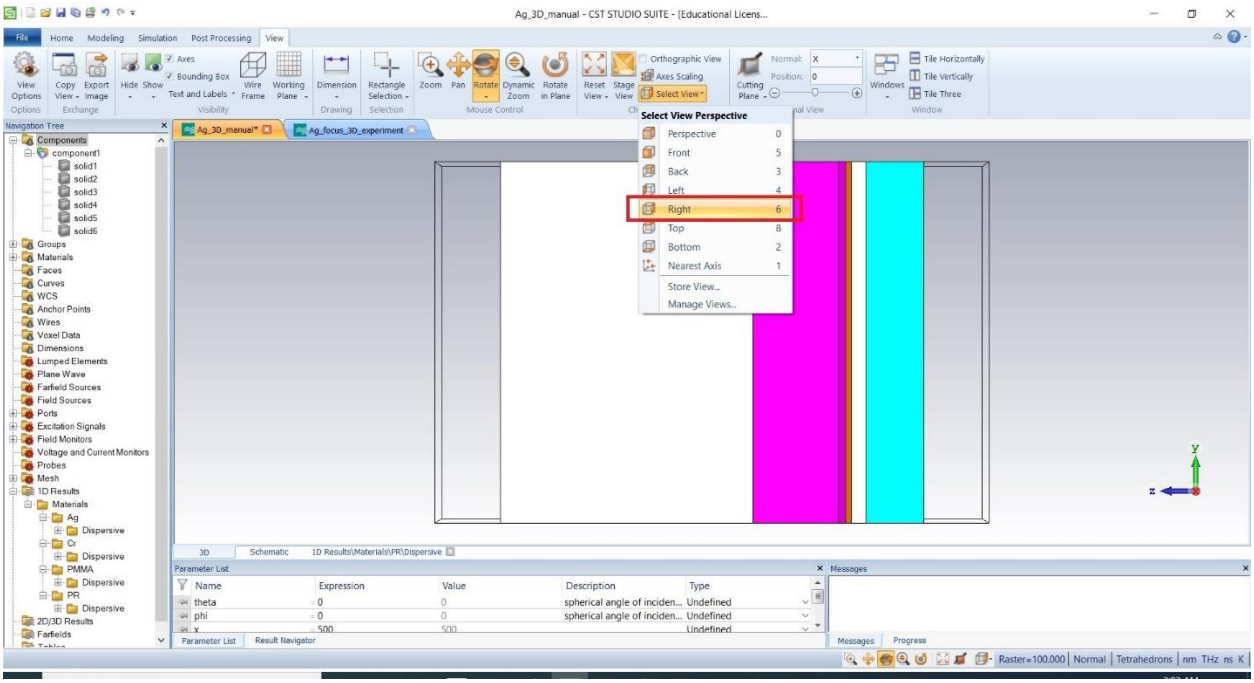

Step 38: Select ‘pick’

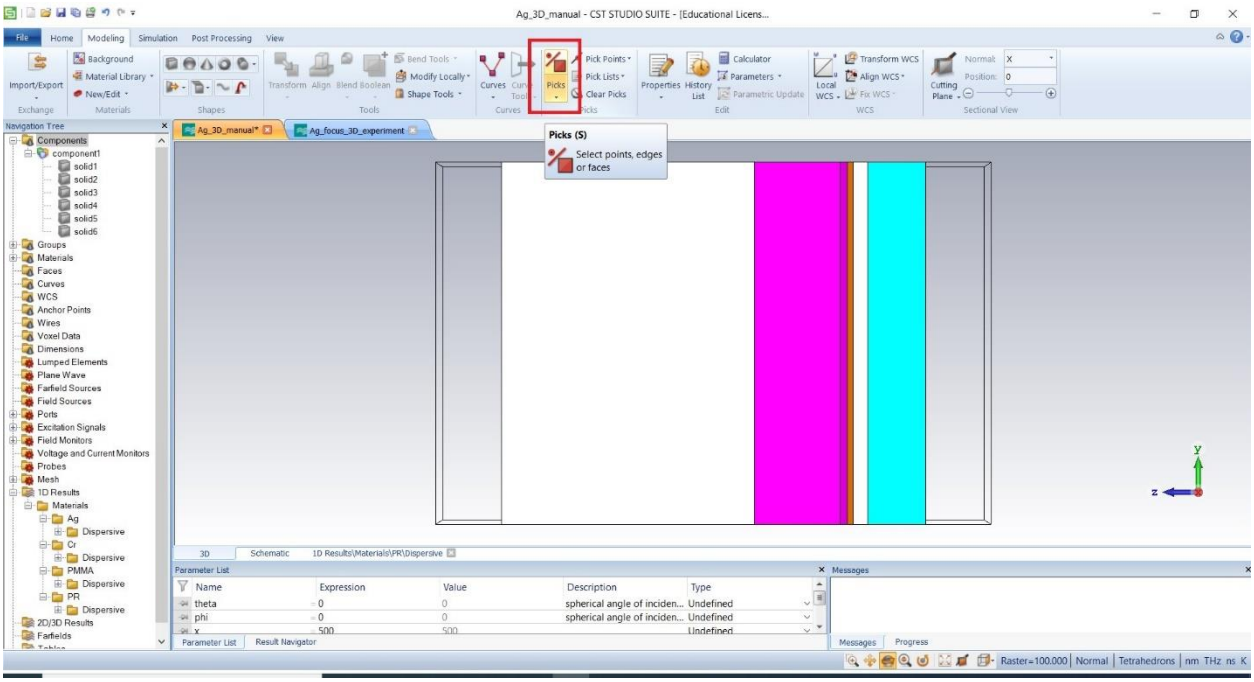

Step 38: Select the side for the alignment of new axis

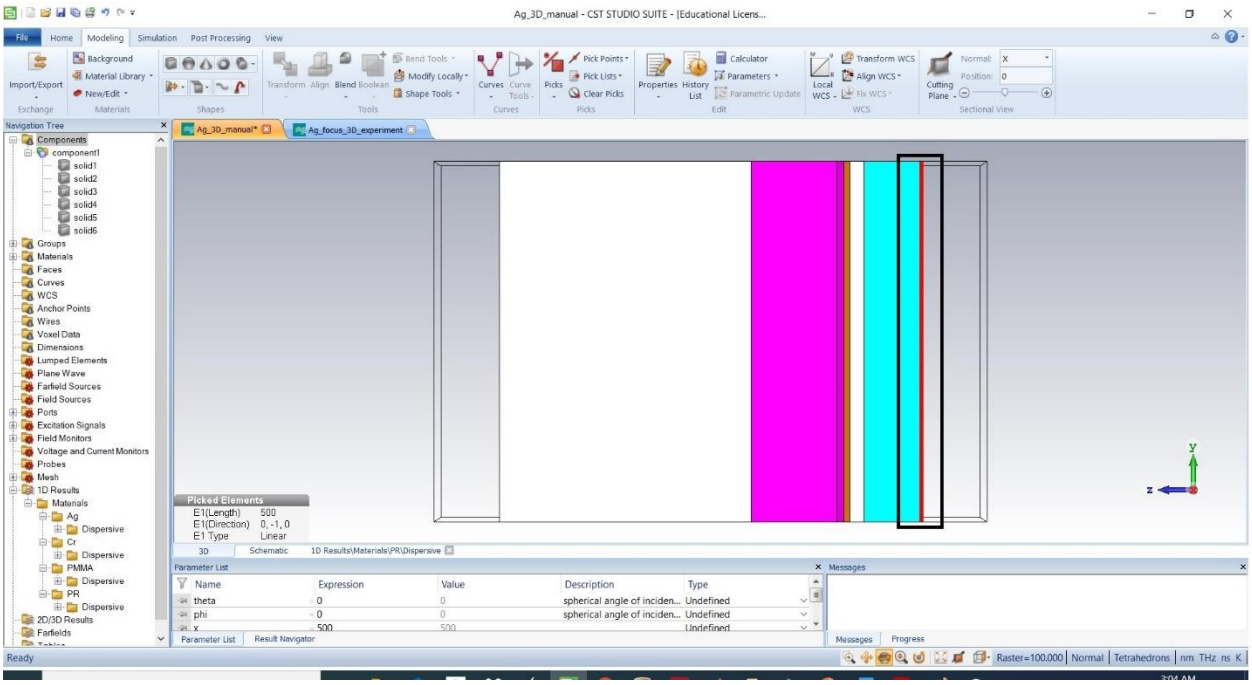

Step 39: Select ‘Align WCS’

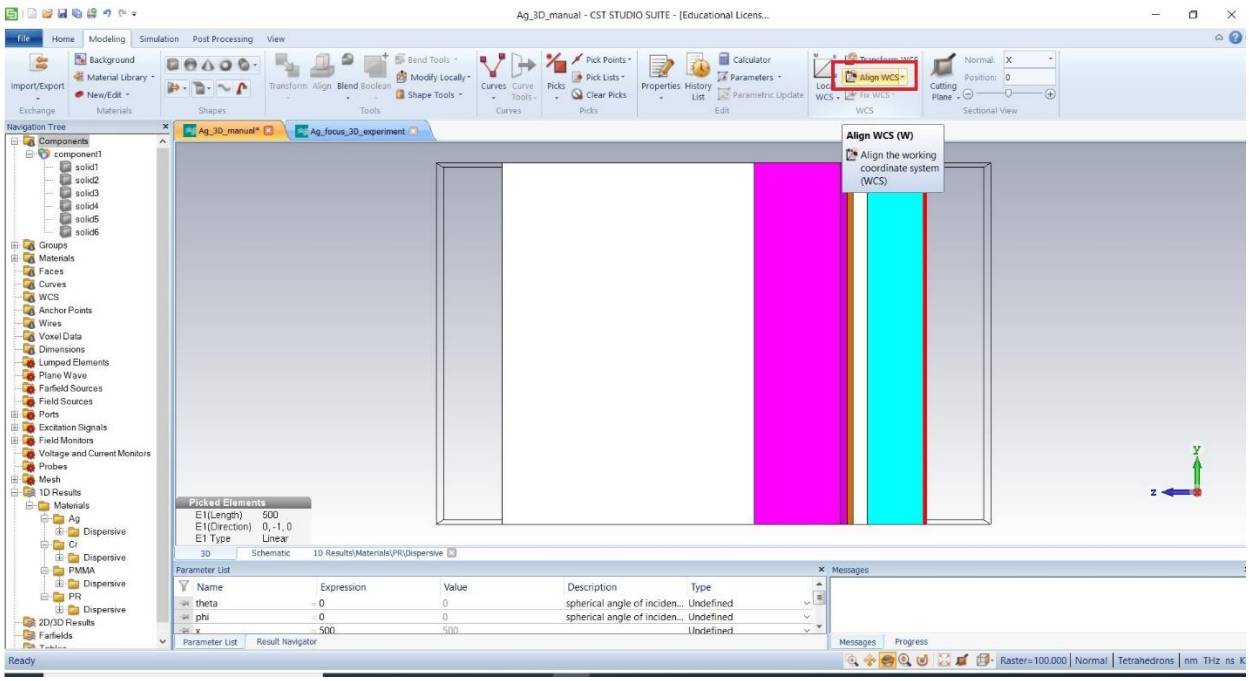

New coordinate has been set.

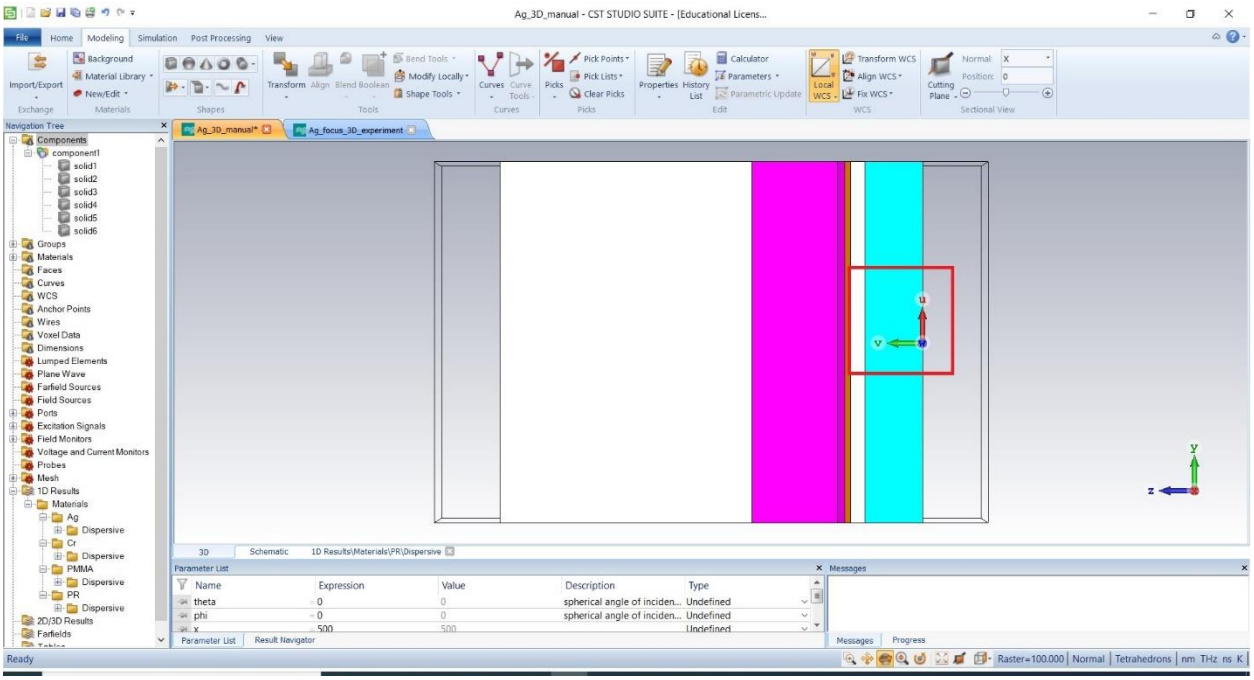

Step 39: Select ‘Brick’ for the aperture

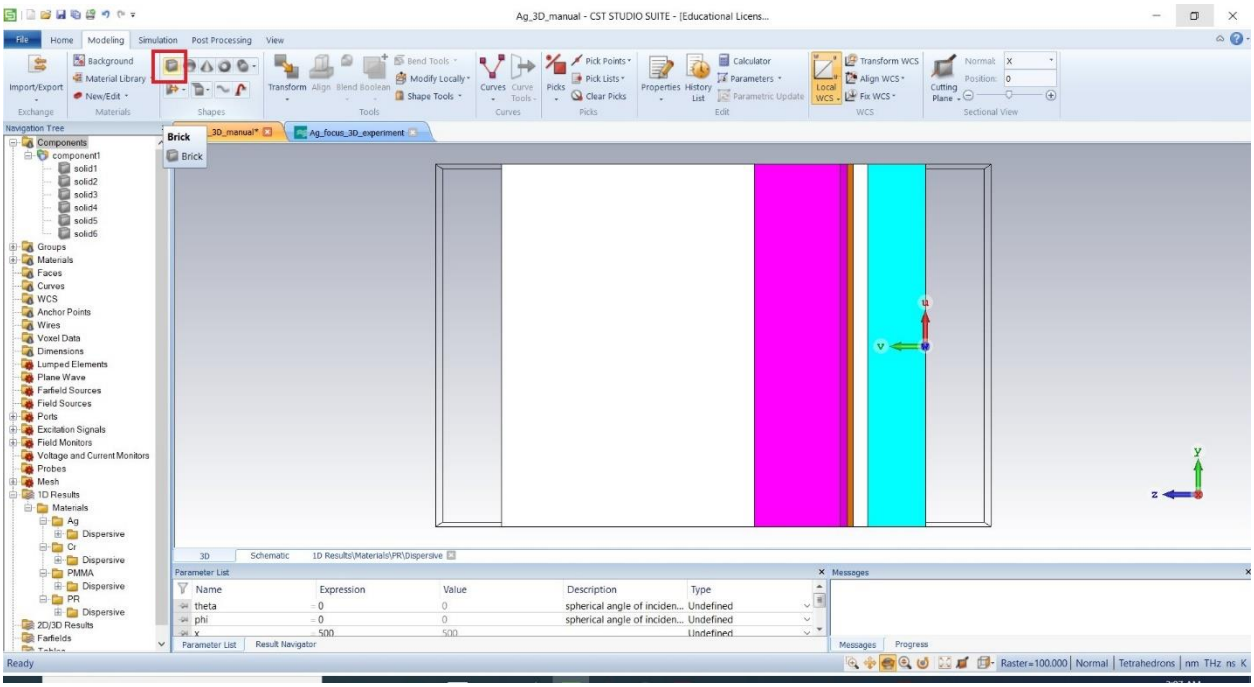

Step 40: Set the dimention of aperture (material-air)

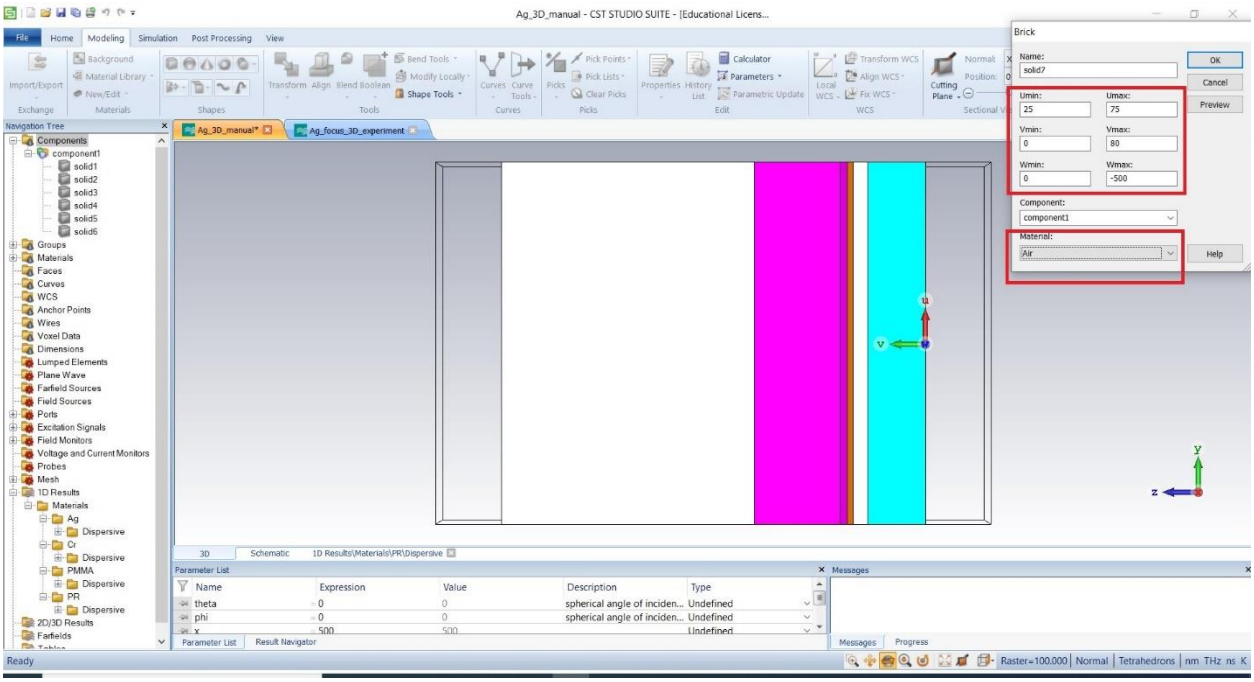

Step 41: Insert the aperture.

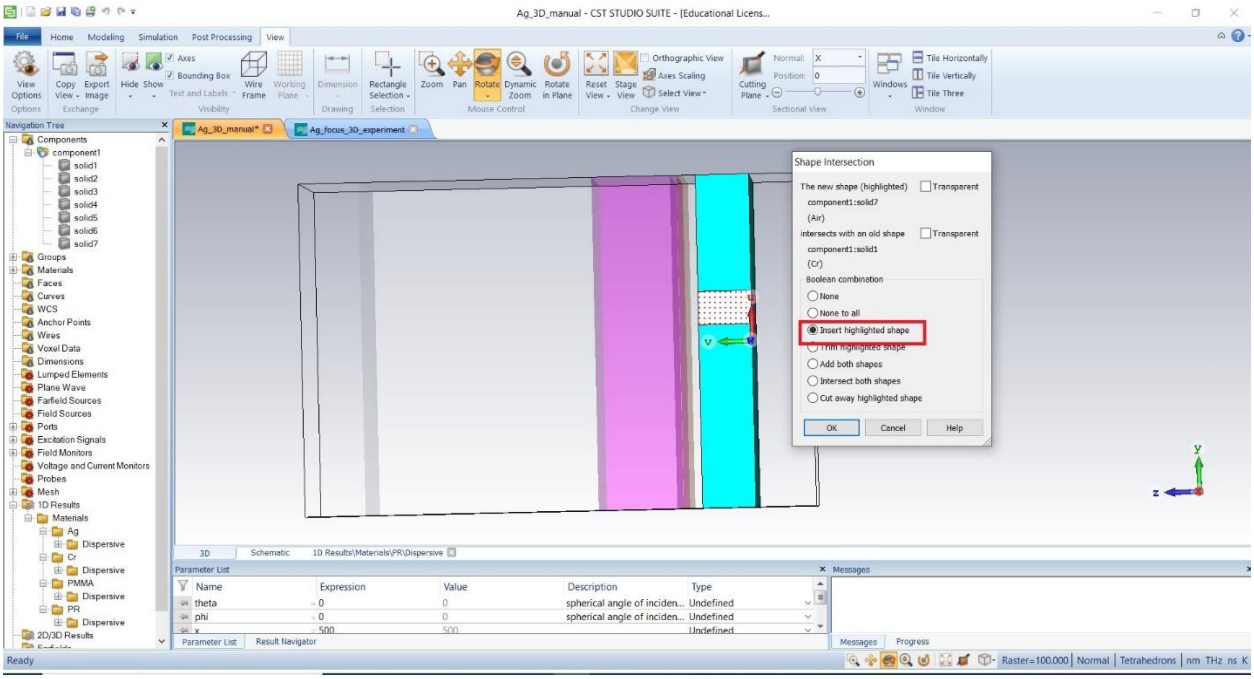

Step 42: Transform and copy the existing aperture to form another aperture

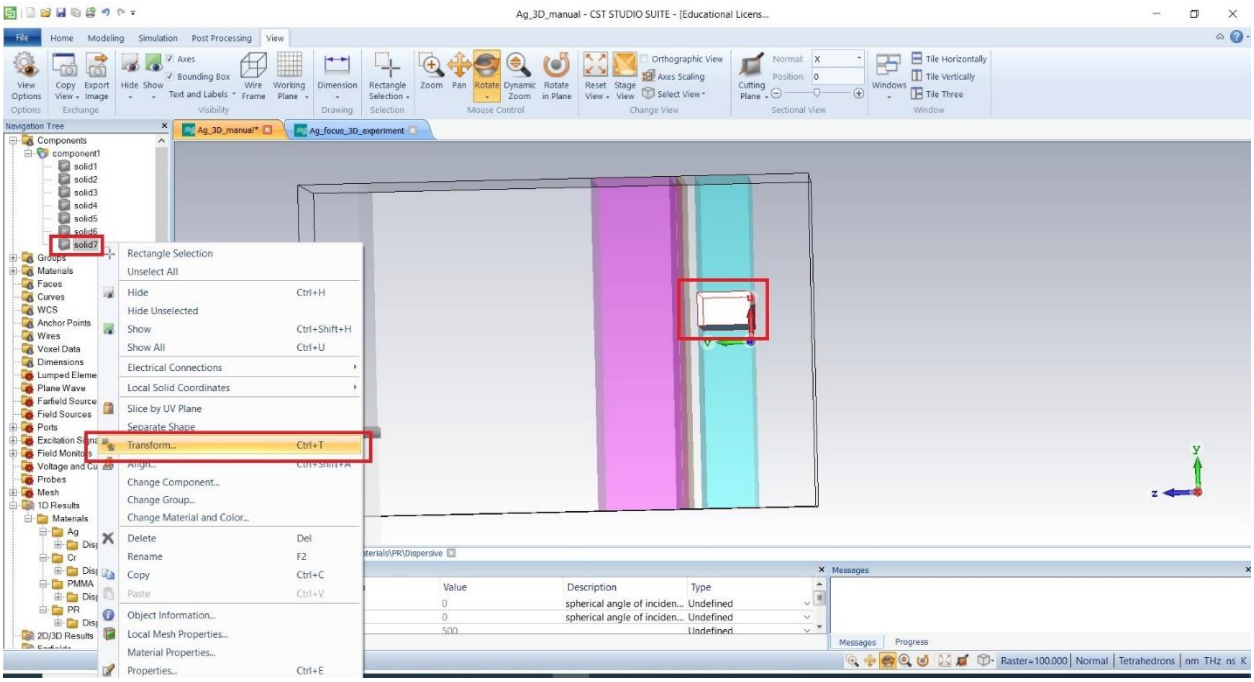

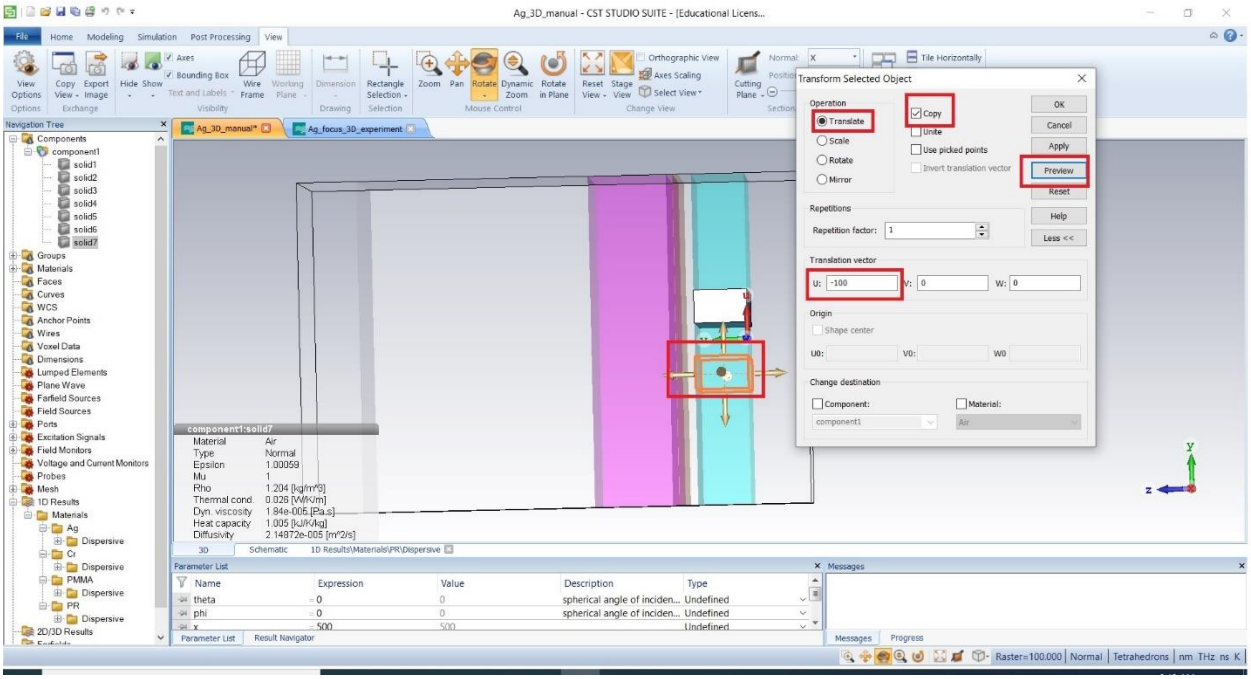

Step 43: Insert the 2nd aperture

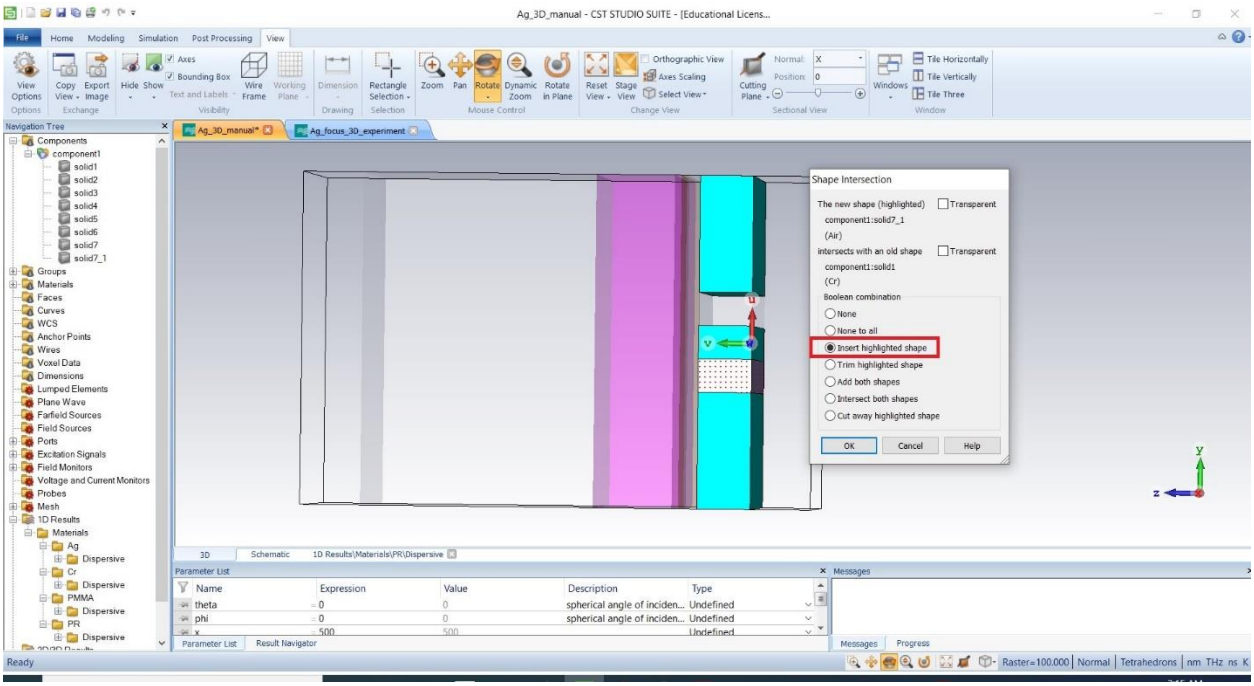

Right side view

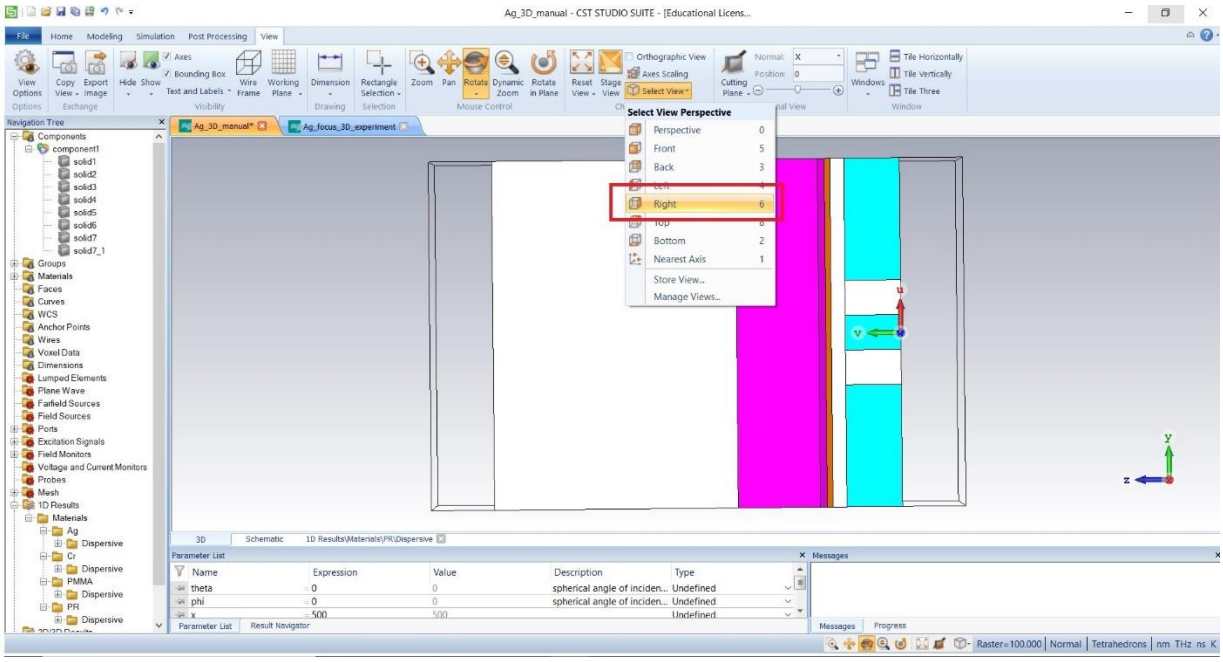

Perspective view

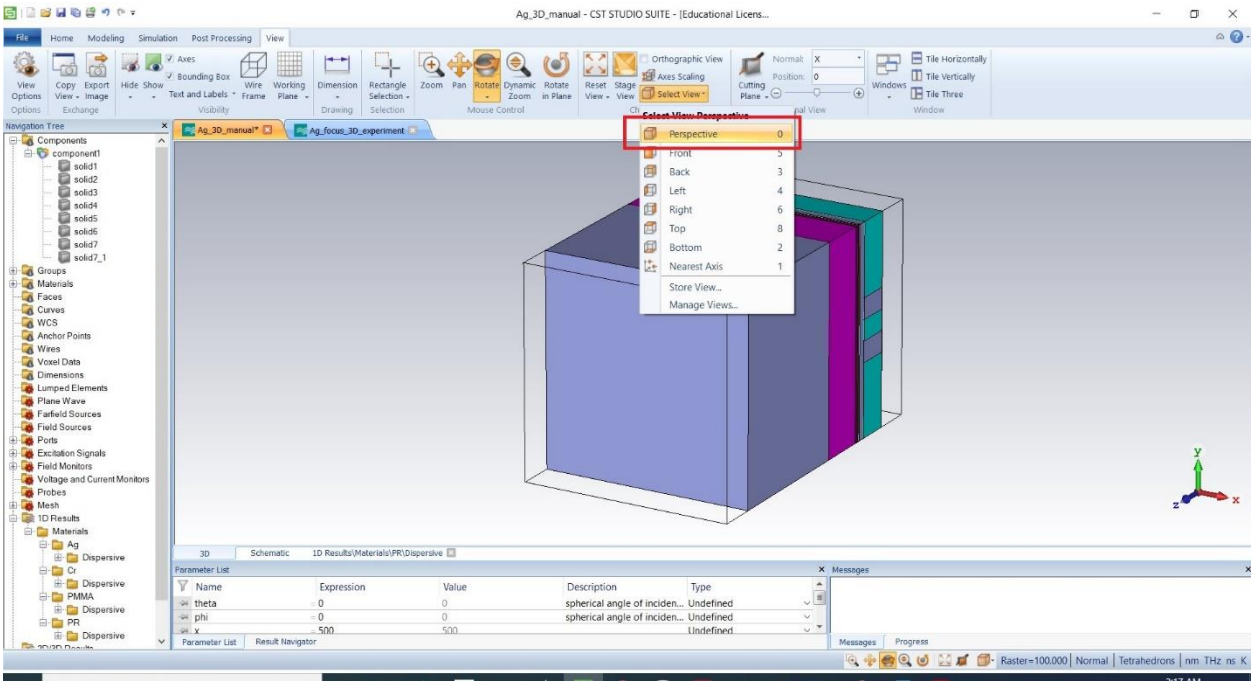

Step 43: Select ‘Waveguide Port’

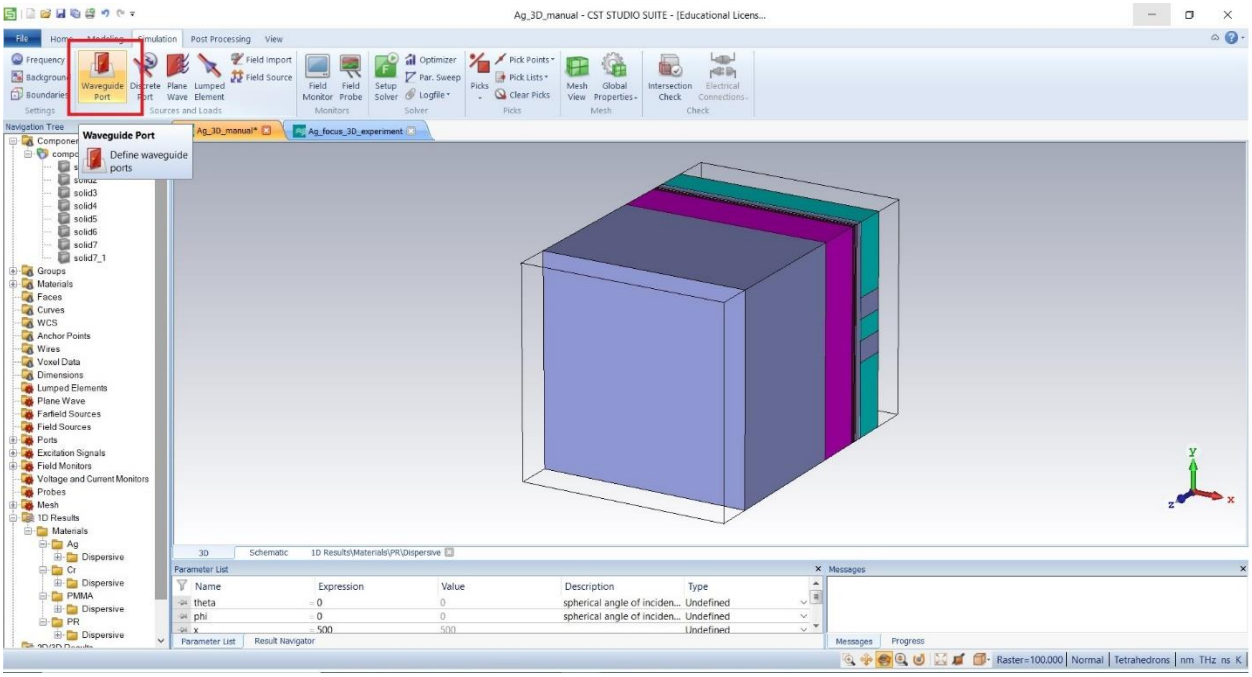

Step 44: Setting ‘Port 1’

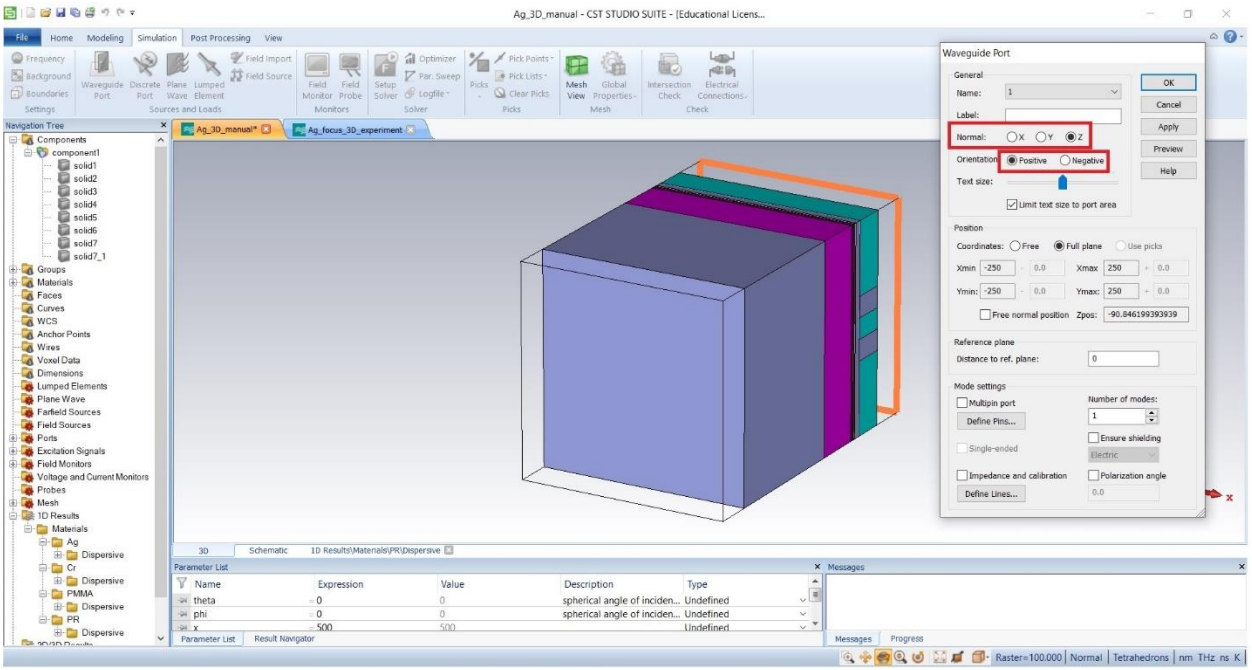

Step 45: Setting ‘Port 2’

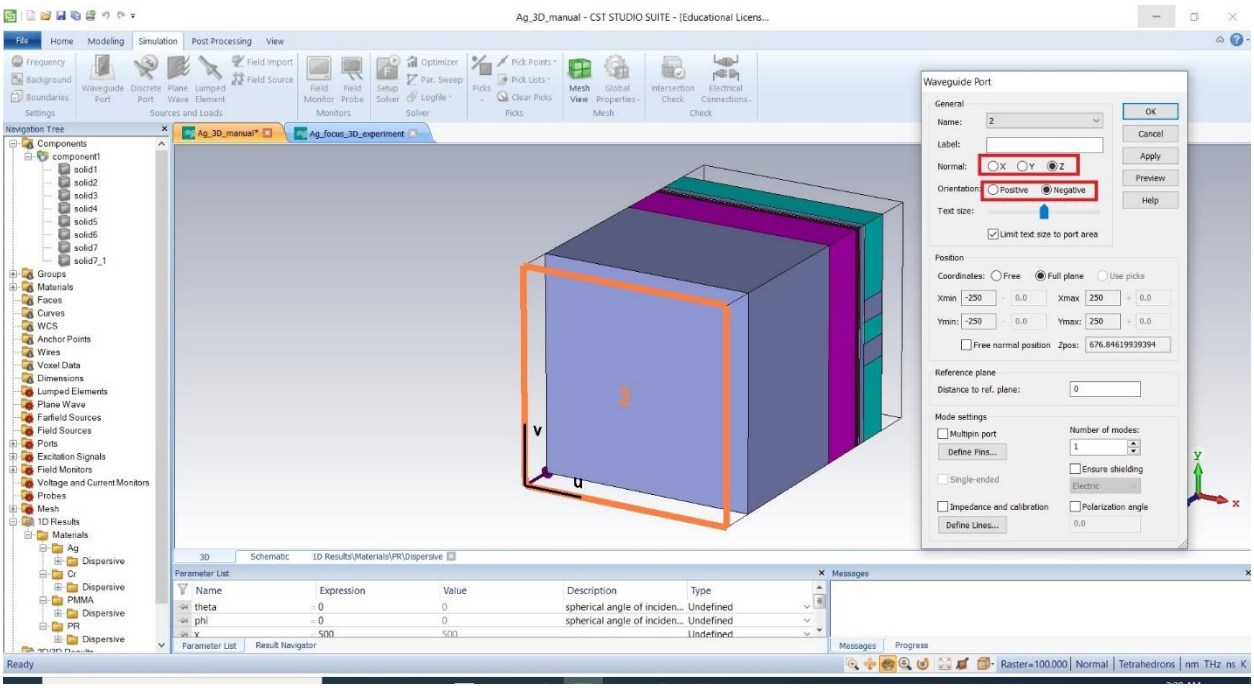

Perspective view with Port

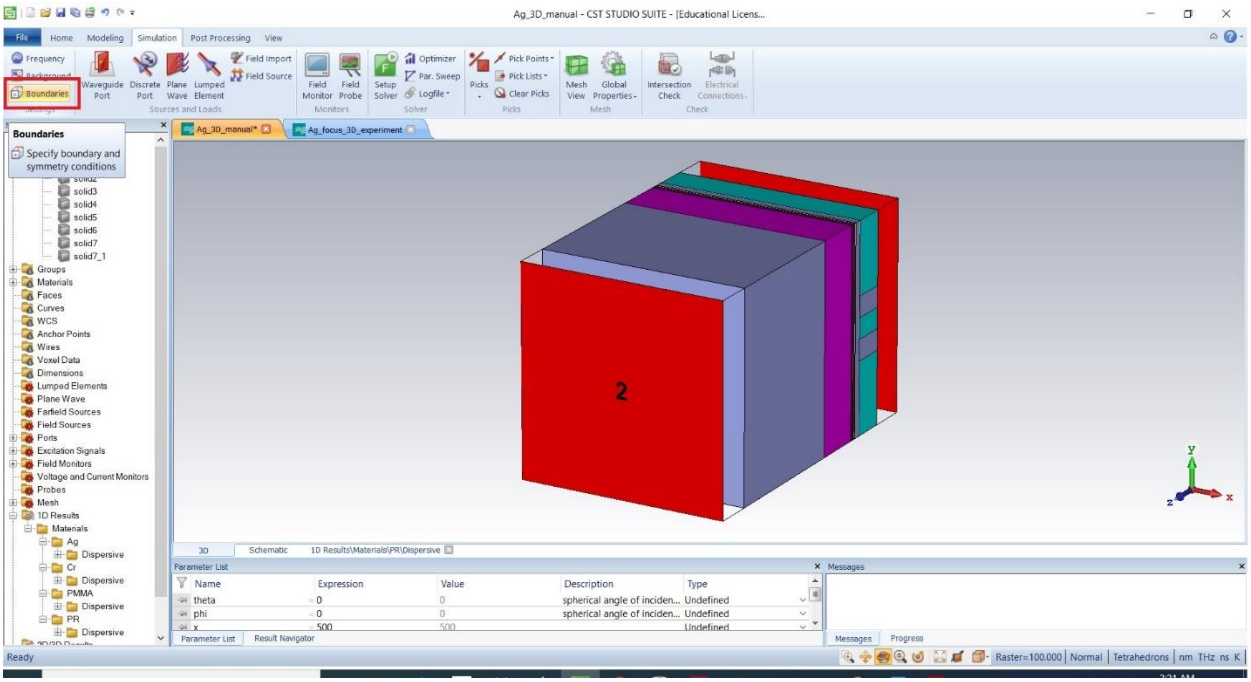

Step 46: Setting Boundary condition

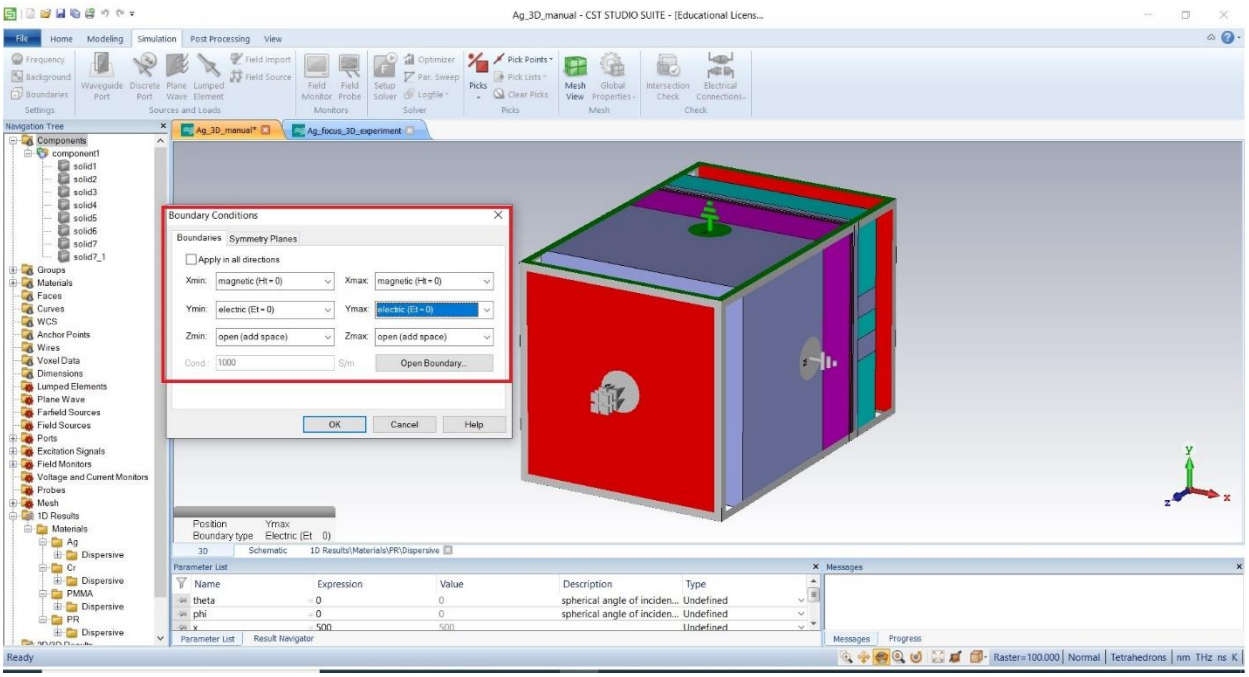

Step 47: Select ‘Field Monitor’

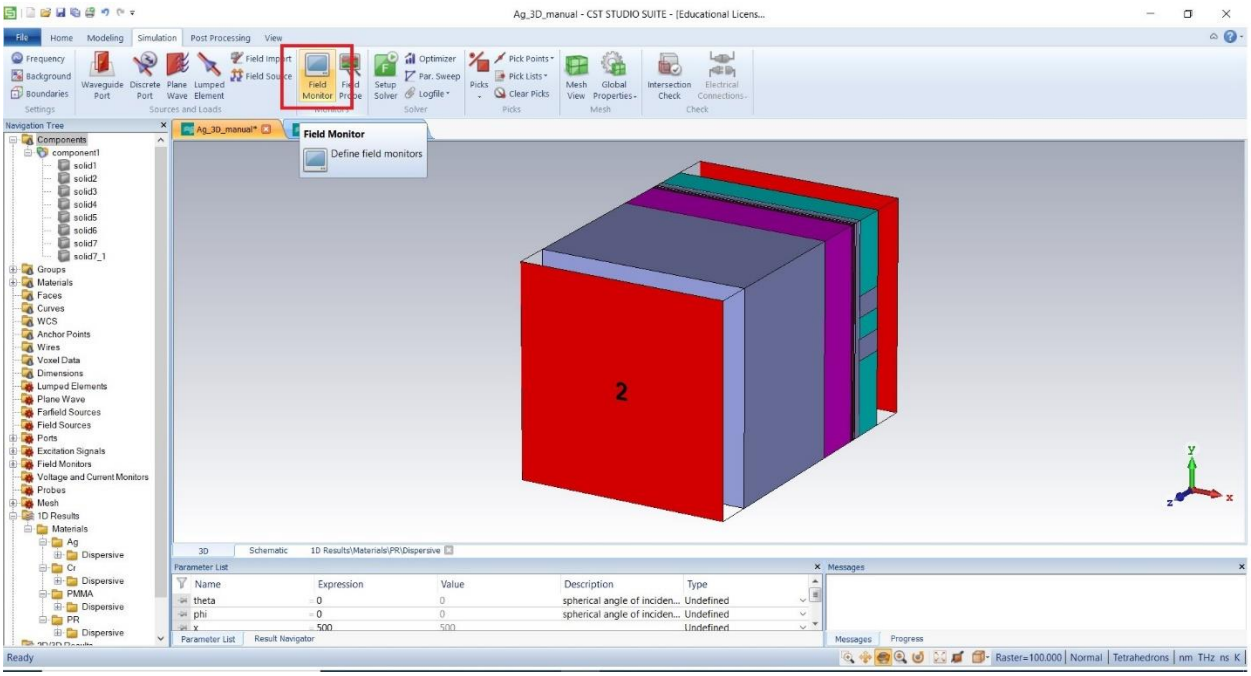

Step 48: Set the property of Monitor

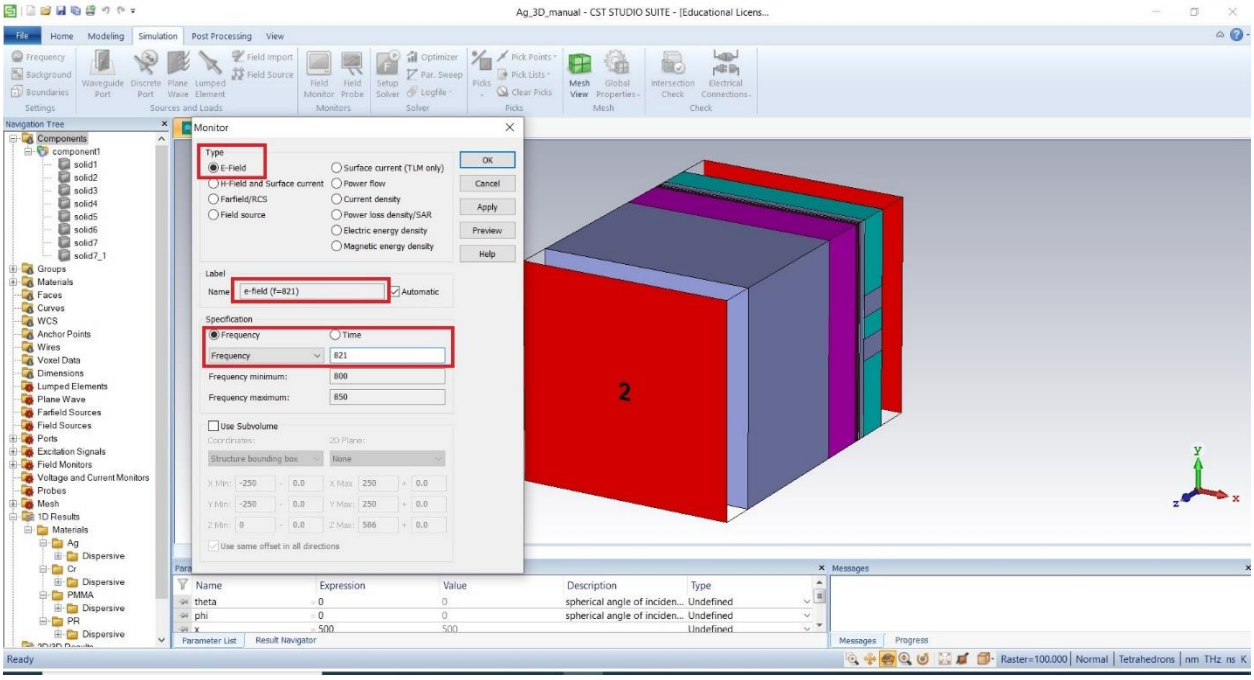

Step 49: Select ‘Source type’ and ‘Mode’

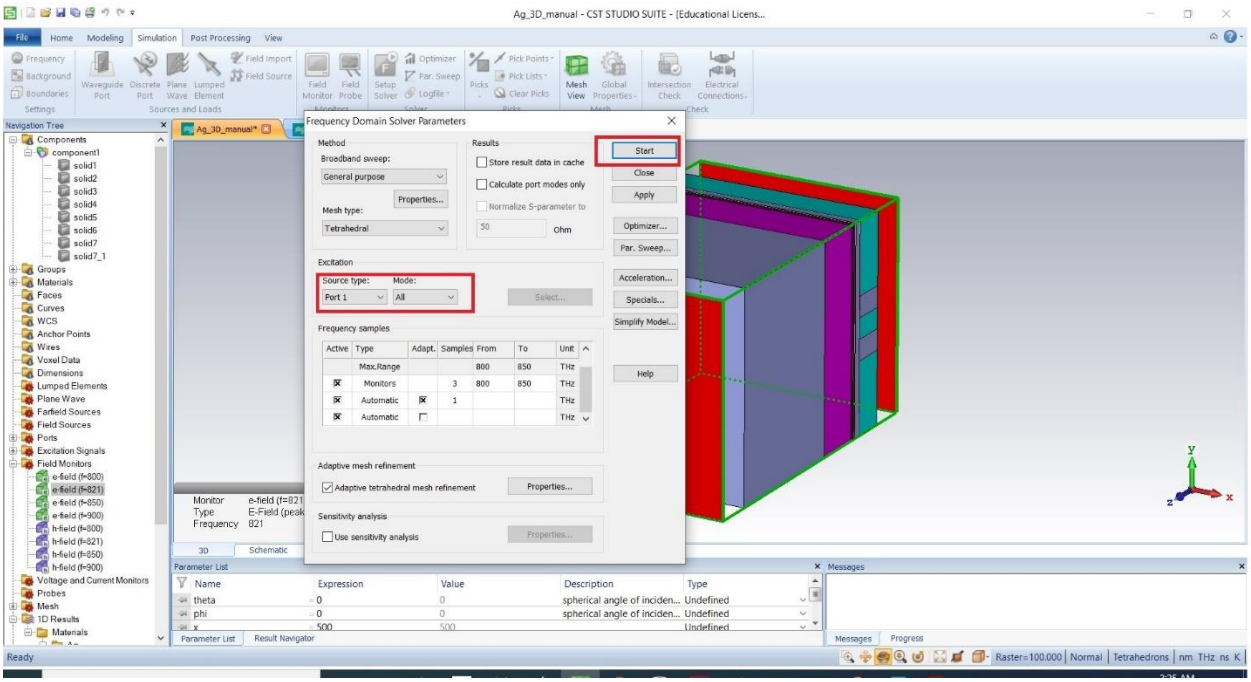

Right side view

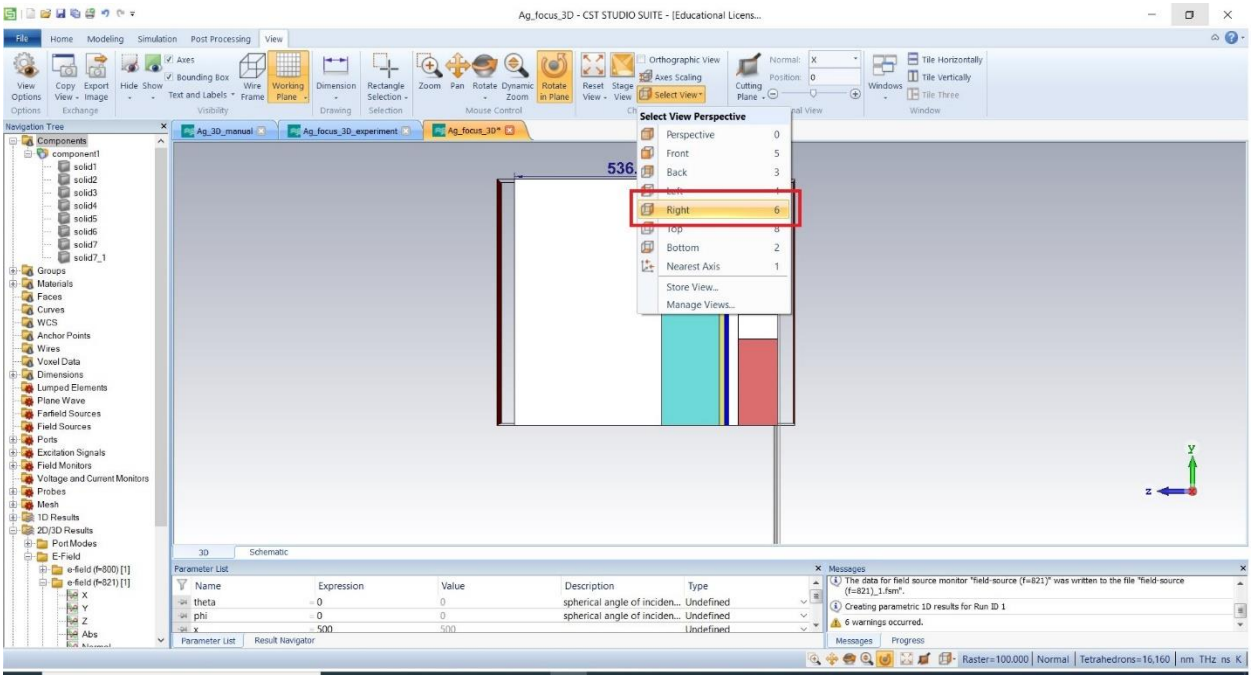

Step 50: Click on the colormap and define the property

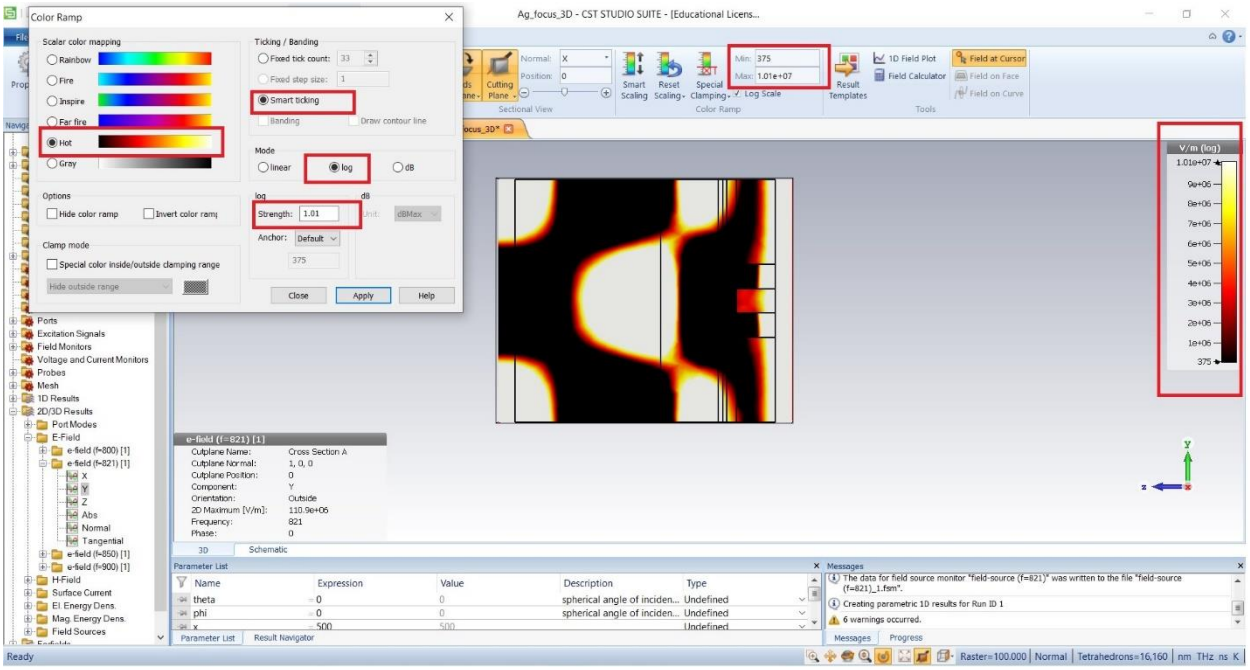

Step 51: Set the phase so that the EM wave enters fully into the aperture. Select ‘Field on view’ and ‘Cutting plane’

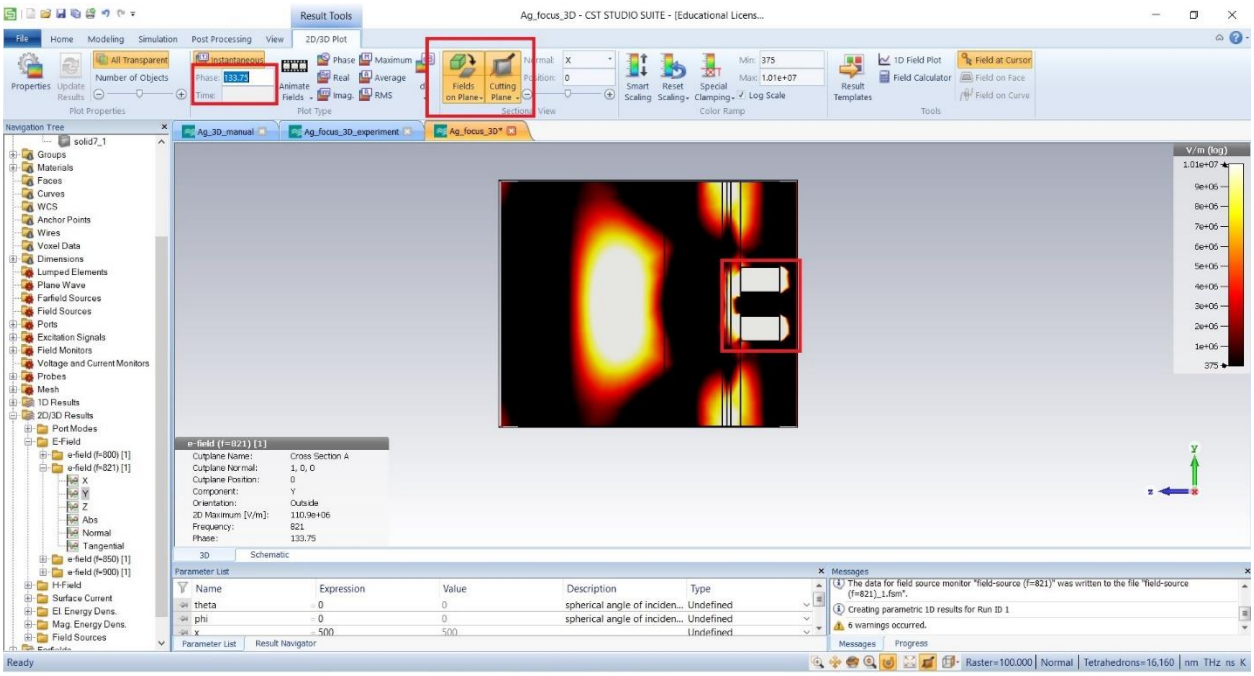

Perspective view

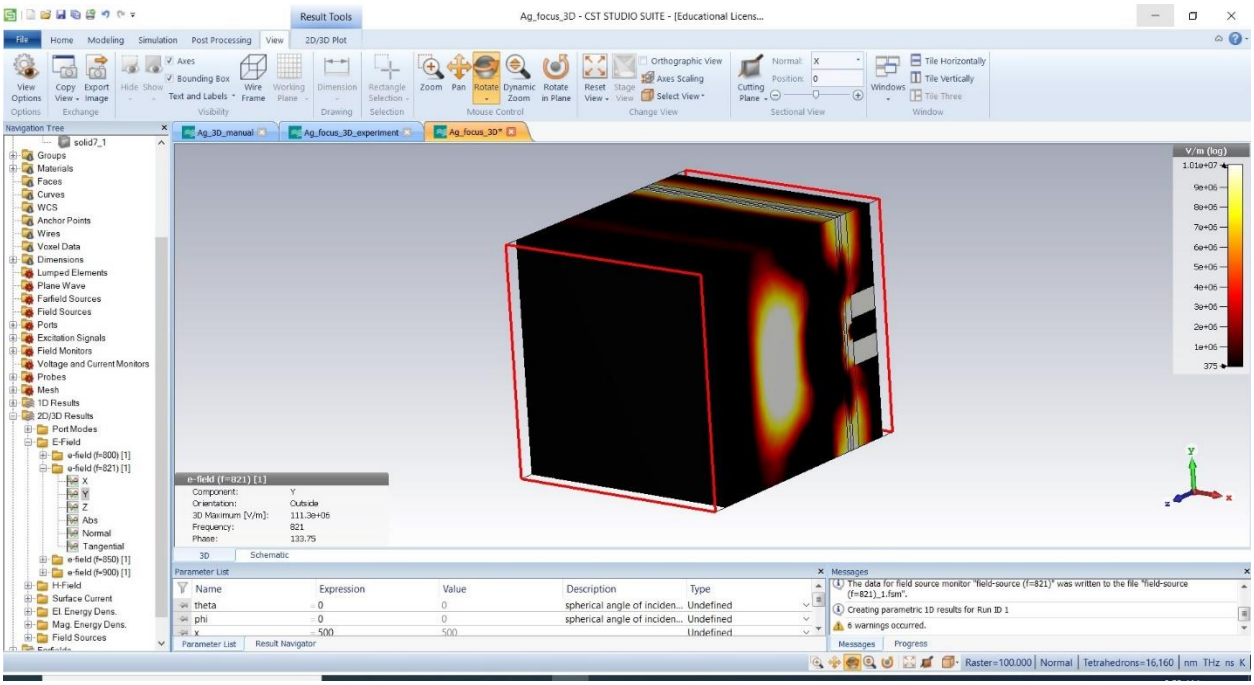

CHAPTER IV

DESIGN AND NUMERICAL STUDIES

4.1 Conductor Meta-Lens: PMMA/Ag/PR

The proposed Ag Lens structure formation is PMMA/Ag/PR. The value of permittivity of PMMA is $\boldsymbol{\varepsilon_{PMMA}} = \mathbf{2.3013} + \mathbf{0.0014}\boldsymbol{i}$ [21] whereas for Ag and Photoresist(PR) it is $\boldsymbol{\varepsilon_{Ag}} = -\mathbf{2.5754} + \mathbf{0.24533}\boldsymbol{i}$ [refractive index.info] and $\boldsymbol{\varepsilon_{PR}} = \mathbf{2.886} + \mathbf{0.059}\boldsymbol{i}$ [23] respectively. The parameters work at the frequency of 821 THz (wavelength, $\lambda = 365nm$). We used the following equation to calculate skin depth.

$$\delta = \sqrt{\frac{\rho}{\pi f \mu_r \mu_0}} \qquad \ldots \quad \ldots \quad \ldots \quad (1)$$

Where, μ_r = relative permeability

μ_0 = permeability in the vacuum

ρ =resistivity of TiO2

δ = skin depth

f = frequency

The skin depth of Ag at this frequency is **2.21nm**. The goal of this experiment is to maximize the enhancement of evanescent waves through varying the thicknesses of the lens materials. The

simulation was performed in three steps where in every step only one material thickness was varied while keeping the thicknesses of other two materials constant.

The simulation was performed in three following steps to reconstruct a quality image.

1. Ag thickness variation

2. PMMA thickness variation

3. PR thickness variation

4.1.1. Varying Silver (Ag) Thickness (PMMA and PR fixed at 40nm and 120nm):

A smaller Ag thickness promotes higher transmittivity of E-energy density [10]. In Figure 1. at 10nm thickness, highest transmittivity is observed which deteriorates gradually with the increment of thickness of the Ag slab. The evanescent amplitude effect is visible up to 60nm Ag layer, after that the effect has been vanished.

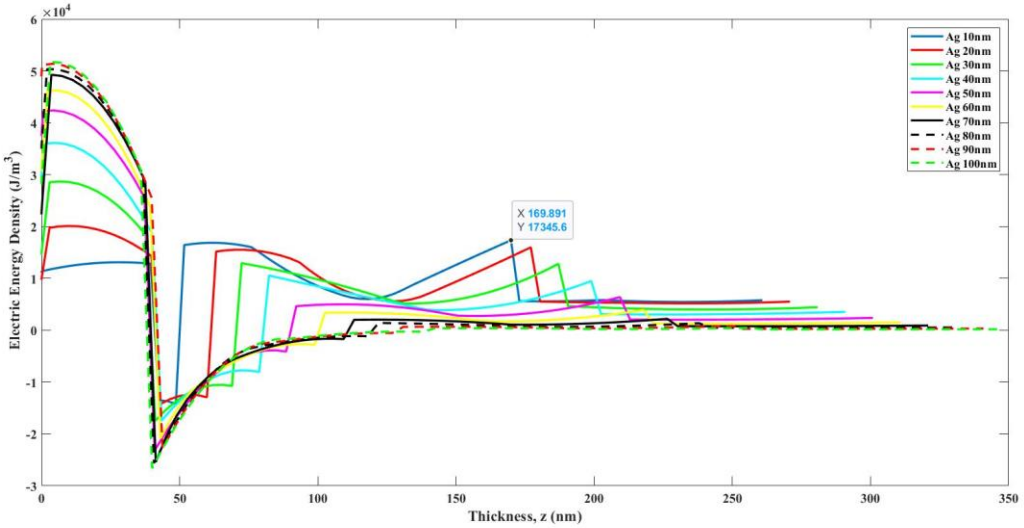

Figure 4.1: variation of Ag thickness from 10-100nm with 10nm gap

Additional simulations have been performed from 5-15nm Ag thickness (Figure 2) where still the 10nm Ag thickness has the highest image resolution feature.

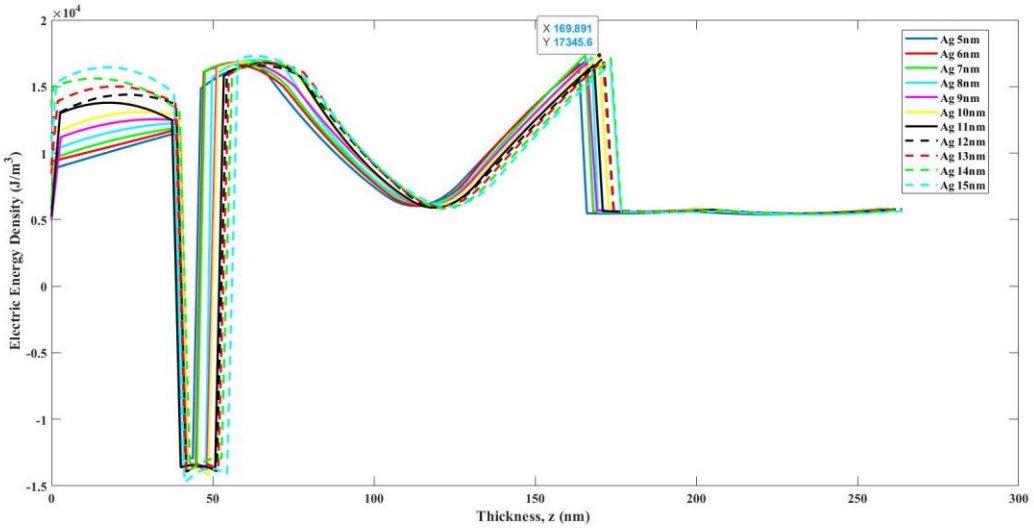

Figure 4.2: variation of Ag thickness from 5-15nm with 1nm gap

4.1.2. Varying PMMA Thickness (Ag and PR fixed at 10nm and 120nm):

Evanescent field enhancement depends also on PMMA layer which determines object distance from the lens [10]. In Figure 3, it is observed that PMMA thickness of 10nm gives peak transmittivity.

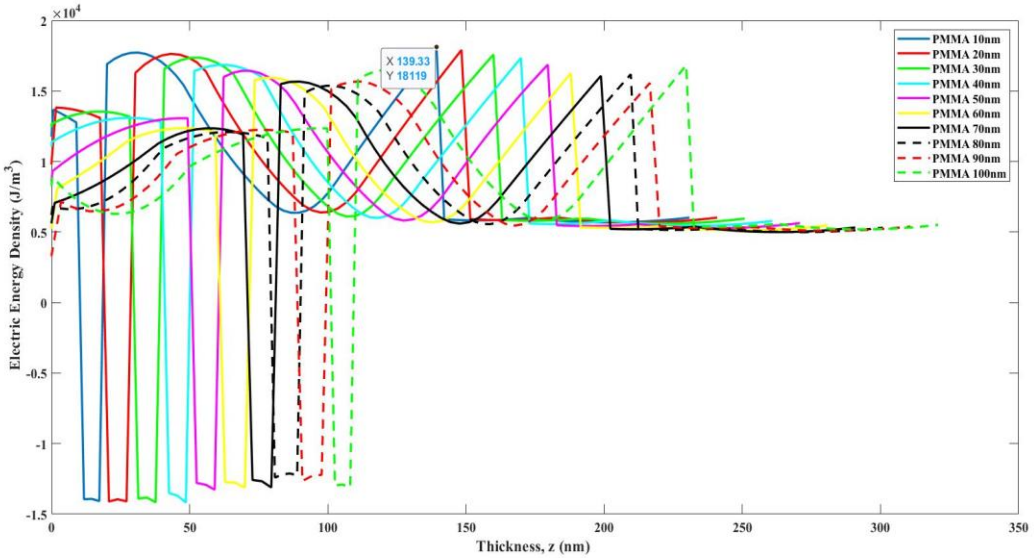

Figure 4.3: variation of PMMA thickness from 10-100nm with 10nm gap

Furthermore, more simulations from 5-15 nm have been conducted to realize better resolution where 8nm PMMA thickness (Figure 4) show maximum enhancement of transmittivity while the result from other thicknesses are very close.

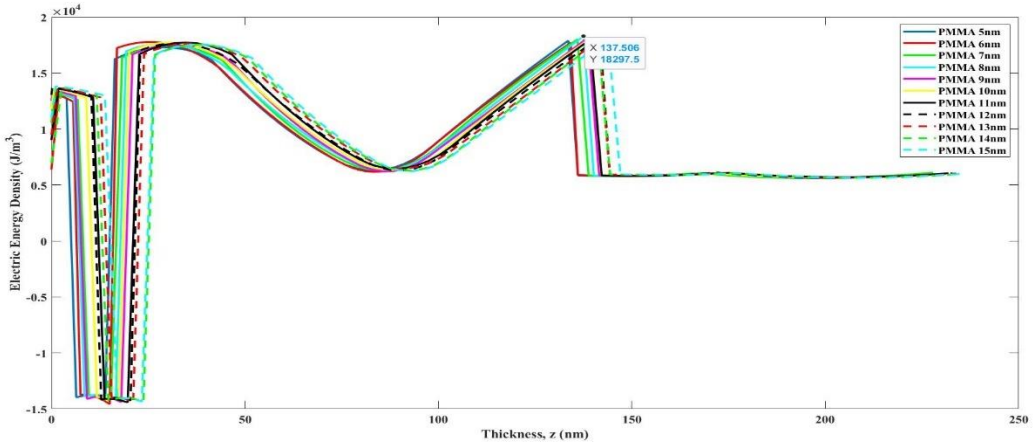

Figure 4.4: variation of PMMA thickness from 5-15nm with 1nm gap

4.1.3. Varying PR Thickness (Ag and PMMA fixed at 10nm and 8nm):

PR increases the image distance and play a vital role in image reconstruction [112]. The PR thickness is altered from 10-150nm (Figure 5 & Figure 6). It is found that 120nm PR thickness generates best field transmission.

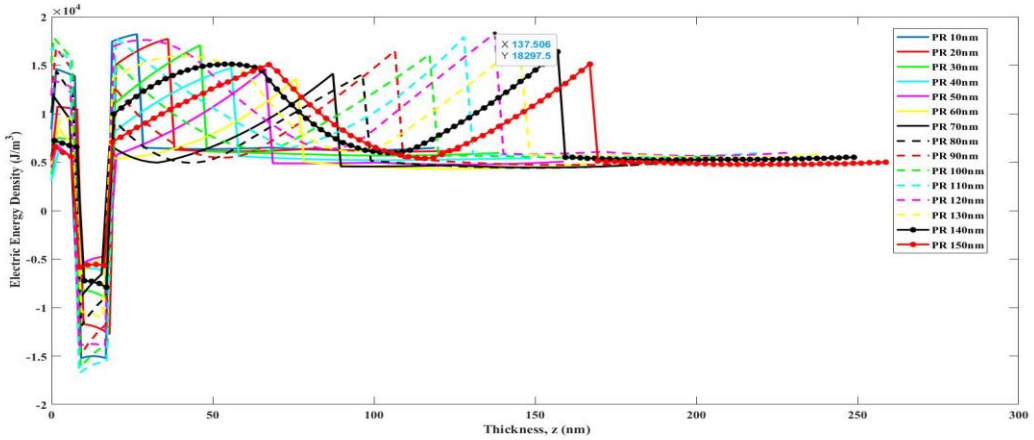

Figure 4.5: variation of PR thickness from 10-150nm with 10nm gap

Besides, simulation has been continued again with PR thickness varying from 115-125nm (**Figure7**). An improved image quality has been found at 118nm.

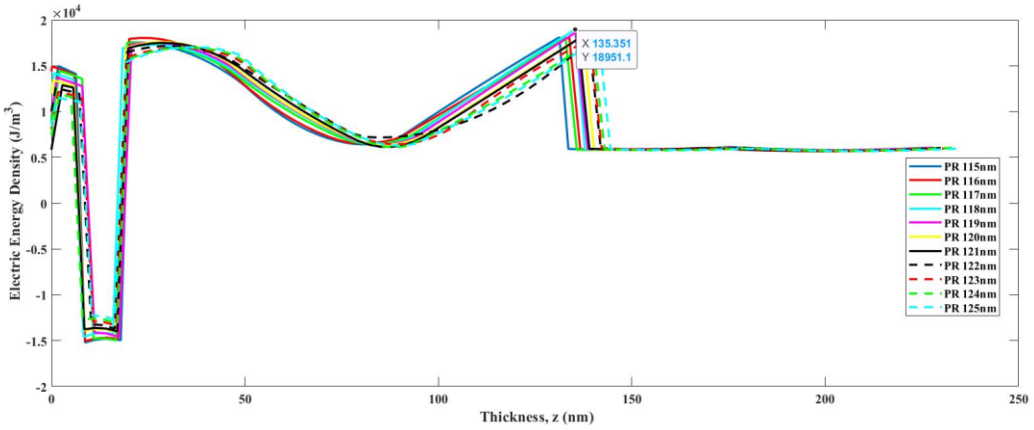

Figure 4.6: variation of PR thickness from 115-125nm with 1nm gap

As a result, the optimized dimension for Ag lens that offers most eminent amplification of evanescent waves is **PMMA/Ag/PR: 8nm/10nm/118nm.**

4.2 Semiconductor Meta-Lens: Glass/TiO2/PR

TiO_2 possesses high refractive index (~2–2.7) and transparency at visible and near-infrared wavelength which make it a suitable medium for optical devices [24]. Titanium dioxide has very good semiconductor properties [25] and it has significant applications such as in optoelectronic devices, photocatalytic systems [26], solar cells, gas sensors, and electrochromic systems [25]. The proposed TiO_2 lens structure formation is **Glass/ TiO_2/PR.** As a glass, we used SCOTT-SF (Dense flint) at 821 THz its permittivity is $\boldsymbol{\varepsilon_{Glass}}$ **= 2.8954+0.000019619i [refractive index.info]**. The small number of imaginary part of glass permittivity indicates to low loss of glass material. Moreover, TiO_2 has permittivity $\boldsymbol{\varepsilon_{TiO_2}}$ **= 6.0965[refractive index.info]**, as TiO_2 has only real part of permittivity and no imaginary part, it has no losses theoretically. PR has permittivity $\boldsymbol{\varepsilon_{PR}}$ **= 2.886+0.059i. [refractive index.info, 23]**. The skin depth of TiO_2 at the working frequency (821 THz) is **1.7565nm [from equation (1)]**. The simulation was conducted in three following steps to increase amplification of evanescent waves.

1. TiO_2 thickness variation

2. Glass thickness variation

3. PR thickness variation

4.2.1. Varying TiO_2 Thickness (Glass and PR fixed at 100nm and 100nm):

In Figure 8, it is noticeable that 80nm TiO_2 provides highest transmittivity. There is a non-linear change of E-energy density till 80nm with respect to thickness. After 80nm, there is gradual decline of evanescent amplitude effect.

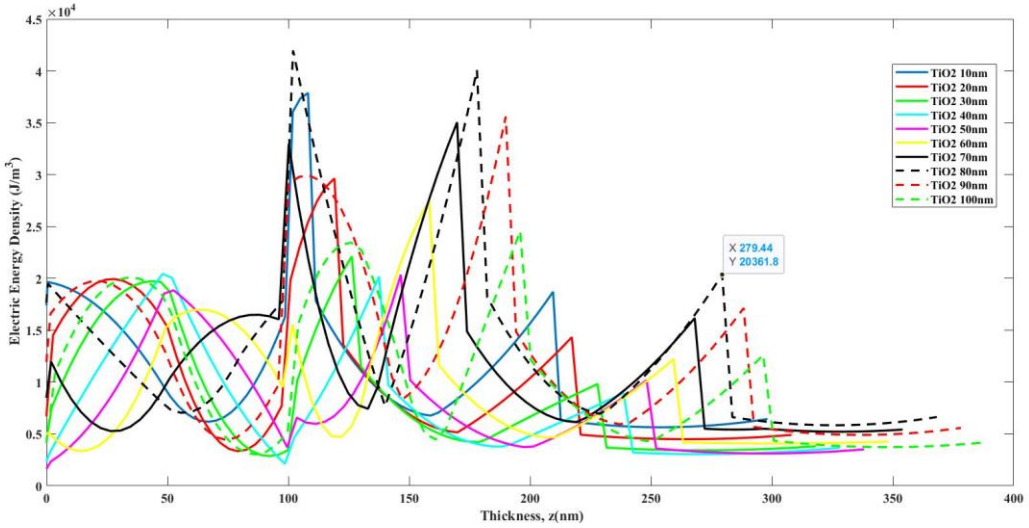

Figure 4.7: variation of TiO_2 thickness from 10-100nm with 10nm gap

In addition to that more simulation for TiO_2 has been performed with view to achieving better image resolution although 80nm TiO_2 (Figure 9) thickness shows peak evanescent wave amplification again.

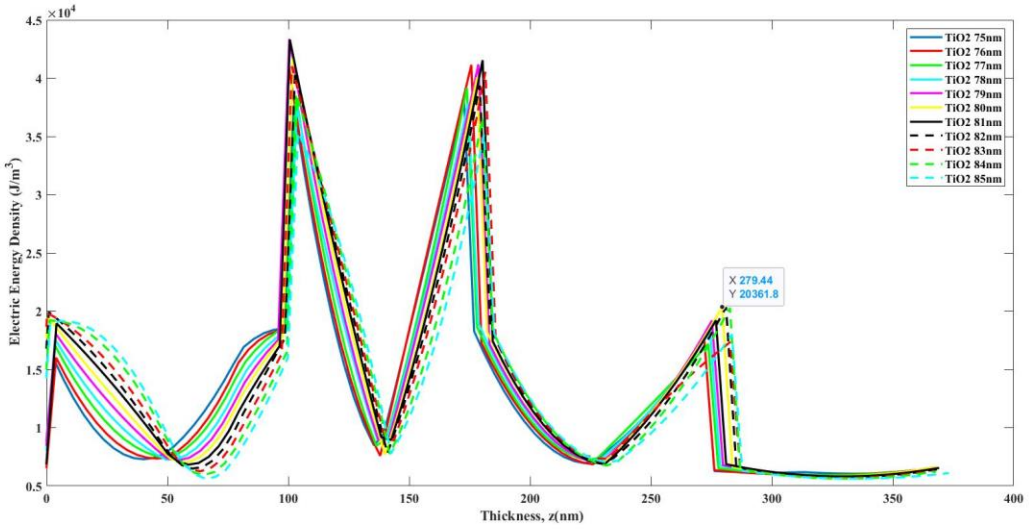

Figure 4.8: variation of TiO_2 thickness from 75-85nm with 1nm gap

4.2.2. Varying Glass Thickness (TiO_2 and PR fixed at 80nm and 100nm):

Electromagnetic wave enters through the glass which is responsible for the object distance. It is noticed (Figure 10) that Glass thickness of 100nm provides highest transmittivity of evanescent waves.

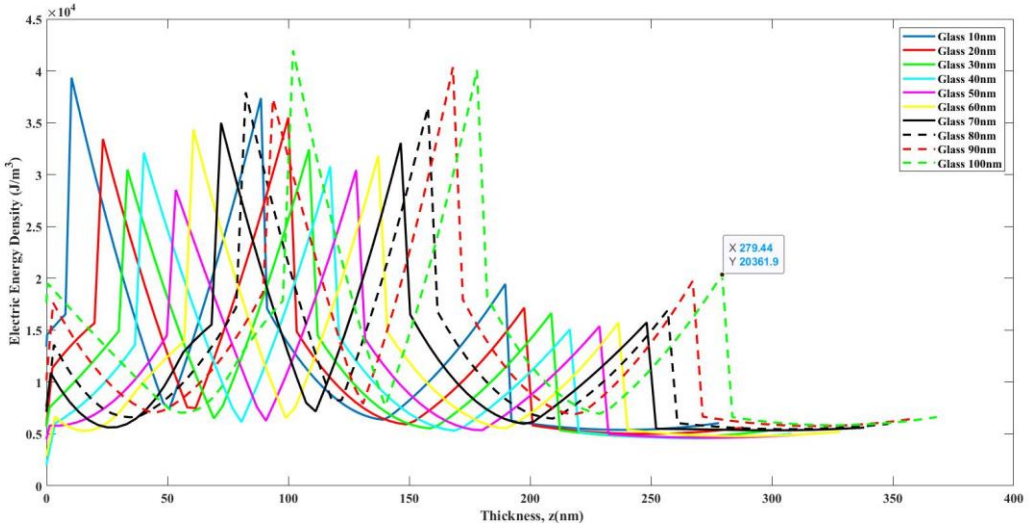

Figure 4.9: variation of Glass thickness from 10-100nm with 10nm gap

We have further run simulations varying glass thickness from 95-105nm (Figure 11) whether a slightly increased transmittivity has found at 98nm Glass thickness.

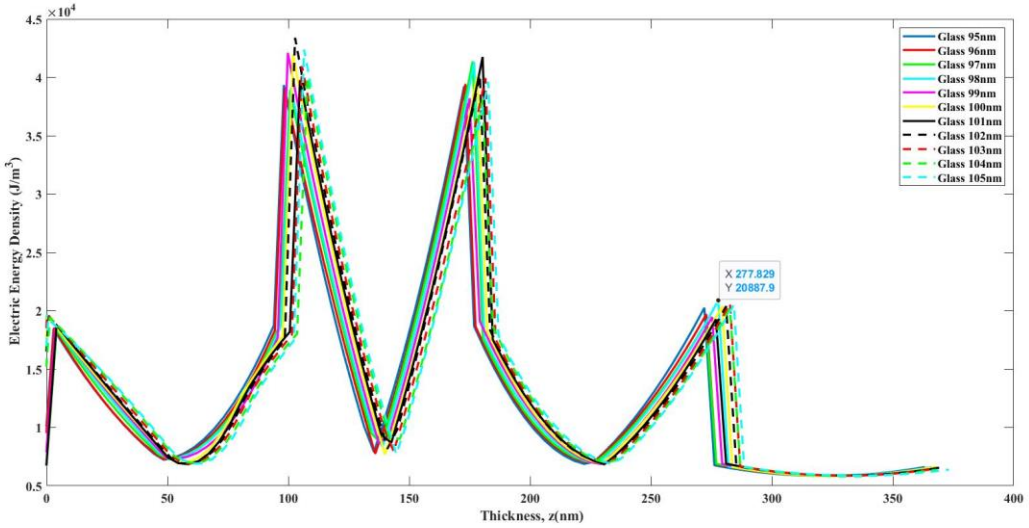

Figure 4.10: variation of Glass thickness from 95-105nm with 1nm gap

4.2.3. Varying PR Thickness (TiO_2 and Glass fixed at 80nm and 98nm)

PR determines the distance of image from the lens and is an inevitable part of the lens structure. It is visible from Figure 12 that after 60nm thickness, the evanescent wave experienced amplification in proportional to the thickness and at 100nm, the transmittivity is at its pinnacle.

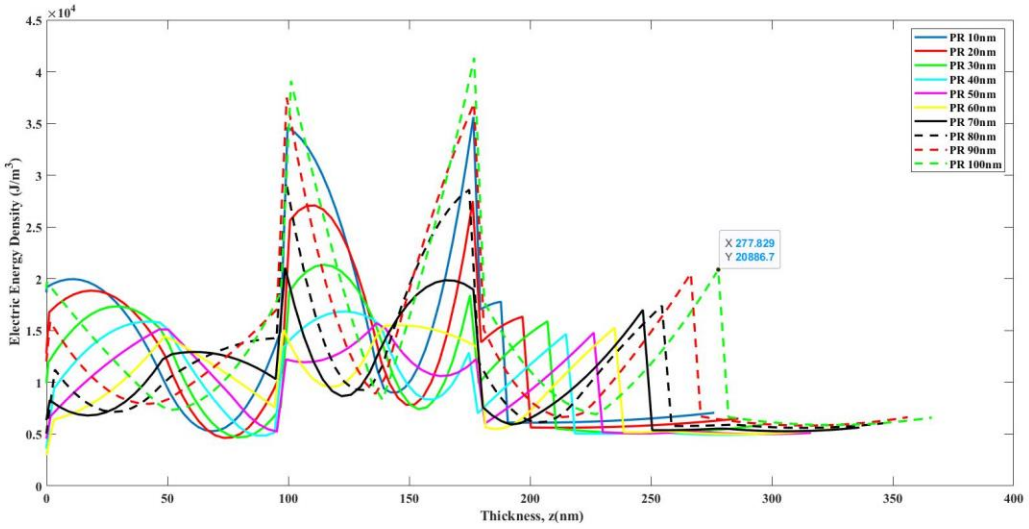

Figure 4.11: variation of PR thickness from 10-100nm with 10nm gap

More simulations are conducted for PR thickness 95-105nm. We have narrowed down the limit to see the possibility of better resolution and we have found that finest transmittivity is still visible at 100nm (Figure 13).

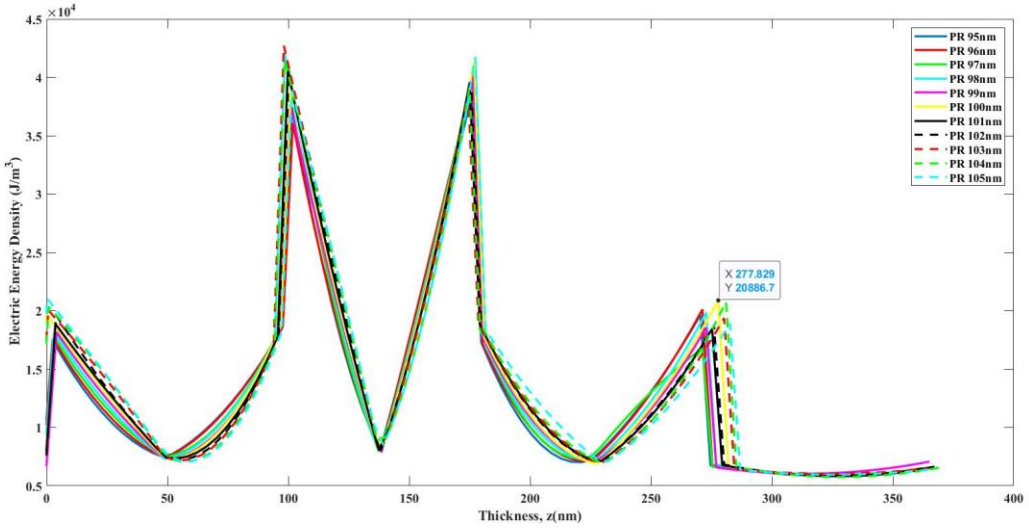

Figure 4.12: variation of PR thickness from 95-105nm with 1nm gap

Finally, the most suitable dimension that we have found from the above simulation is **Glass/ TiO_2/PR: 98nm/80nm/100nm.**

4.3 Conductive Polymer Meta-Lens: PMMA/PNIPAM/PR

poly(N-isopropylacrylamide) (pNIPAM) is a hydrogel that has been studied for thermo responsive polymer applications. It has lower critical solution temperature (LCST) that works in the range of 32-33℃ temperature. When temperature rises above LCST, the hydrogel experiences transition from hydrophilic to hydrophobic state. [27]. The gel particles with micron or submicron sizes can be regarded as microgels or nanogels. As the swelling index of this changes with pH or chemical compositions along with temperature it has application in drug delivery as well as in the field of biosensors and composite nanomaterials. This polymer can be used with metal in composite sensor for the purpose of cell visualization [28].

The particle size of PNIPAM at dried state is 180nm (determined by TEM; see Supporting Information, SI 1), [29].

The proposed Polymer lens structure formation is PMMA/Polymer (PNIPAM)/PR. The value of permittivity of PMMA is $\boldsymbol{\varepsilon_{PMMA} = 2.3013 + 0.0014i}$ [21] whereas for polymer and photoresist(PR) it is $\boldsymbol{\varepsilon_{PNIPAM} = 2.3376 + 0.013402i}$ [refractive index.info] and $\boldsymbol{\varepsilon_{PR} = 2.886 + 0.059i}$ [23] respectively. The parameters work at the frequency of 821 THz (wavelength, $\lambda = 365nm$). The permittivity of both PMMA & PNIPAM are identical.

The simulation has in three following steps to reconstruct a quality image.

1. Polymer (PNIPAM) thickness variation
2. PMMA thickness variation
3. PR thickness variation

4.3.1. Varying Polymer (PNIPAM) Thickness (PMMA and PR fixed at 10nm and 100nm):

In Figure 14, we observe that 240nm polymer thickness ensures peak transmittivity within the range of 140-320nm. As for optimization purpose, further simulation has been conducted between 220-260nm (Figure 15) where highest apex of transmission is found at 240nm. So, we then run simulations between 235-255nm (Figure 16 & Figure 17) seeking better resolution than the previous one and consequently 237nm polymer thickness provides best evanescent wave amplitude.

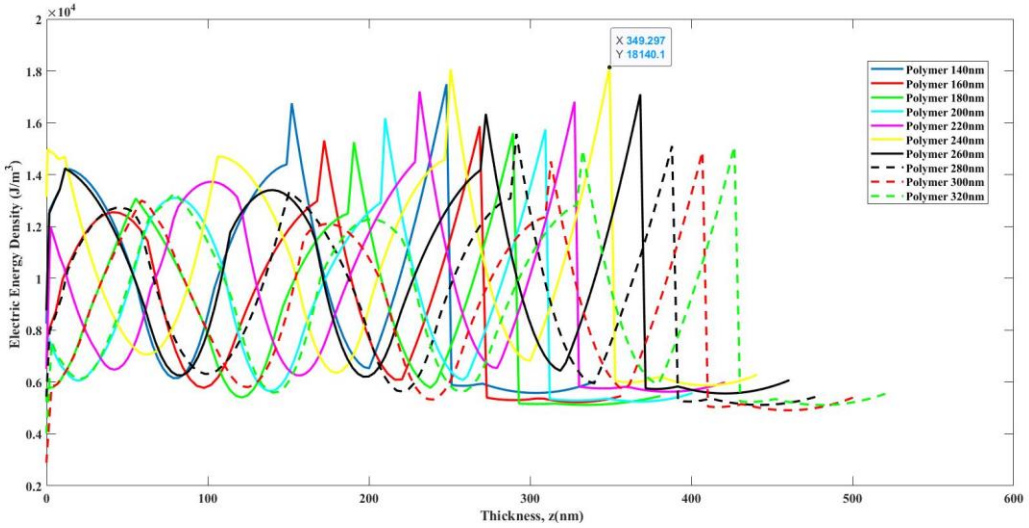

Figure 4.13: variation of polymer thickness from 140-320nm with 20nm gap

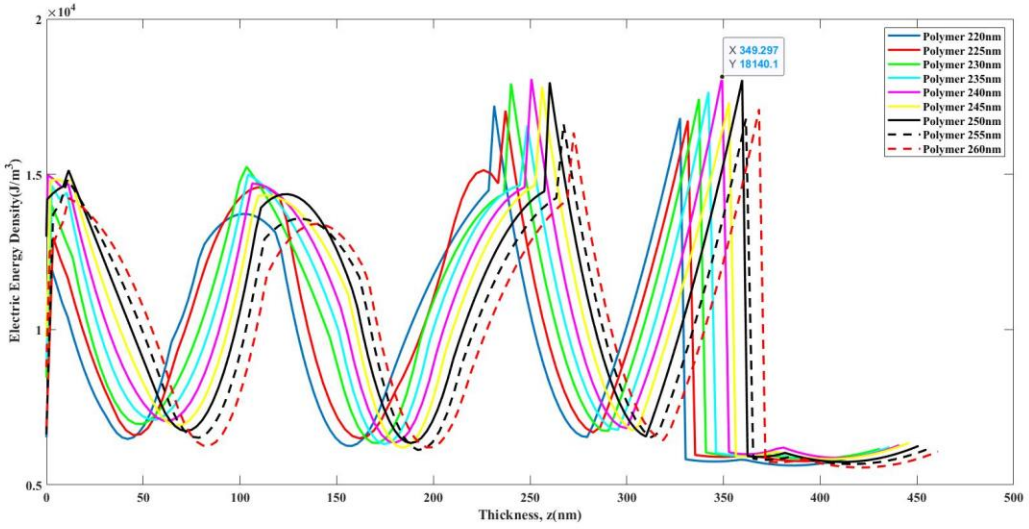

Figure 4.14: variation of polymer thickness from 220-260nm with 5nm gap

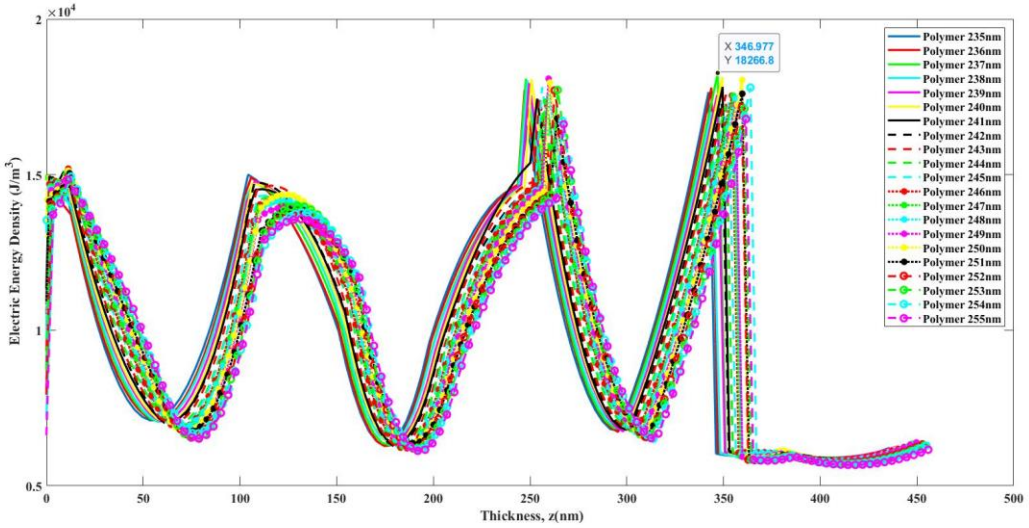

Figure 4.15: variation of polymer thickness from 235-255nm with 1nm gap

4.3.2. Varying PMMA Thickness (Polymer and PR fixed at 237nm and 100nm):

The PMMA thickness has changed in the limit of 5-55nm and 10nm thickness has given best transmittivity so far among other thicknesses (Figure 18). The scale has been narrowed down to 5-15nm where no change has been seen in the previous PMMA thickness and 10nm stands out as the best PMMA thickness (Figure 19).

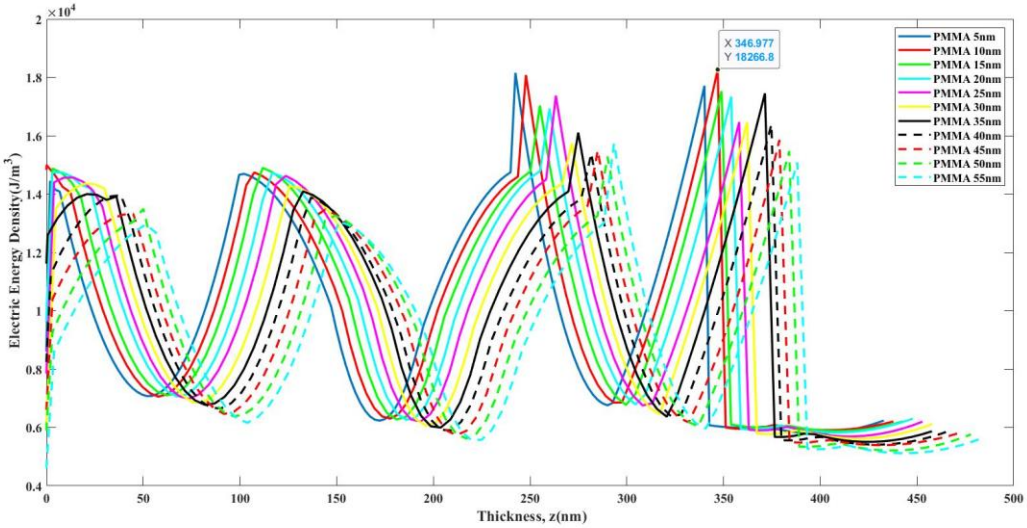

Figure 4.16: variation of PMMA thickness from 5-55nm with 5nm gap

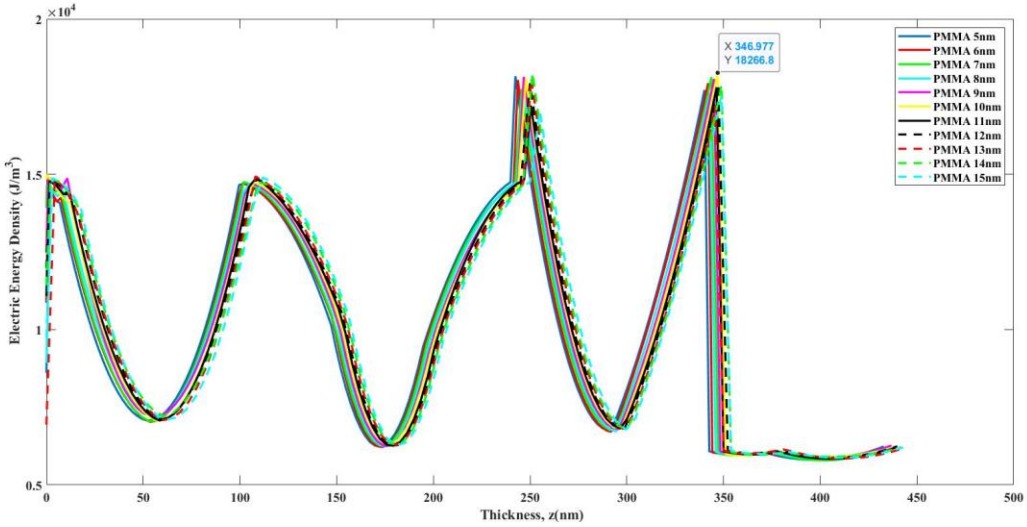

Figure 4.17: variation of PMMA thickness from 5-15nm with 1nm gap

4.3.3. Varying PR Thickness (PMMA and Polymer fixed at 10nm and 237nm):

Finally, PR thickness has been varied between 50-200nm (Figure 20 & Figure 21). The PR thickness of 100nm offers highest transmittivity. Later, additional simulation from 95-105nm has been done and an improved transmittivity has been experienced at 95nm (Figure 22). As a result,

we can say that the optimized polymer lens dimension is **PMMA/Polymer/PR: 10nm/237nm/95nm.**

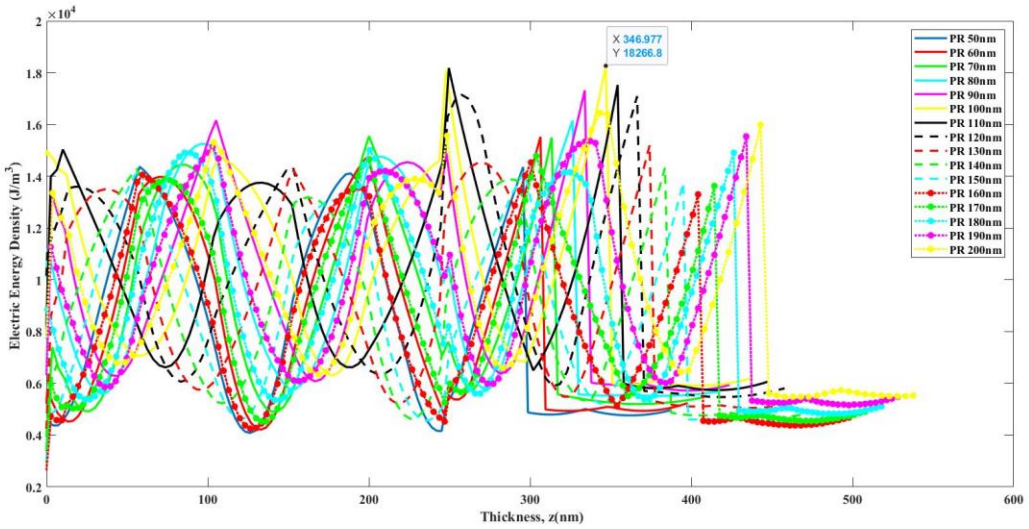

Figure 4.18: variation of PR thickness from 50-200nm with 10nm gap

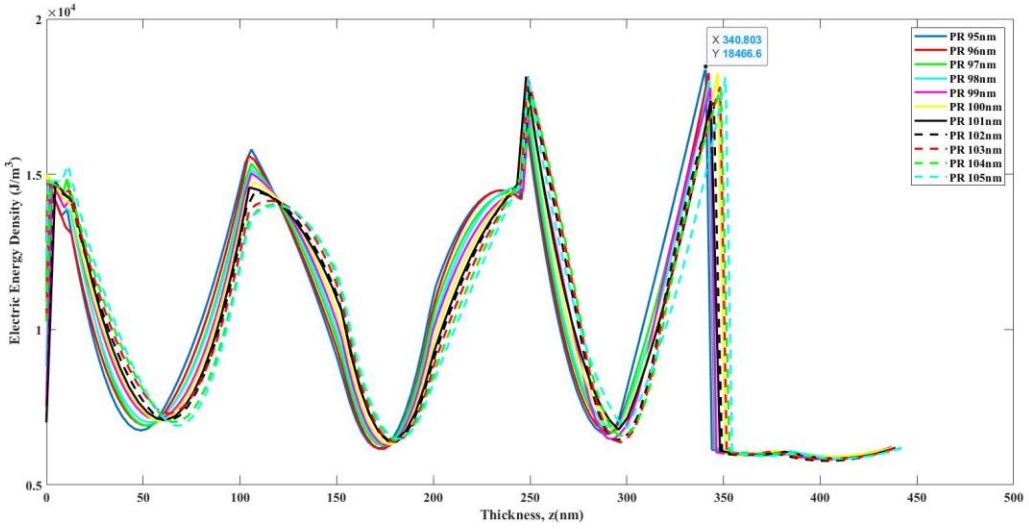

Figure 4.19: variation of PR thickness from 95-105nm with 1nm gap

4.4: Optimized Single Layered Lens dimensions

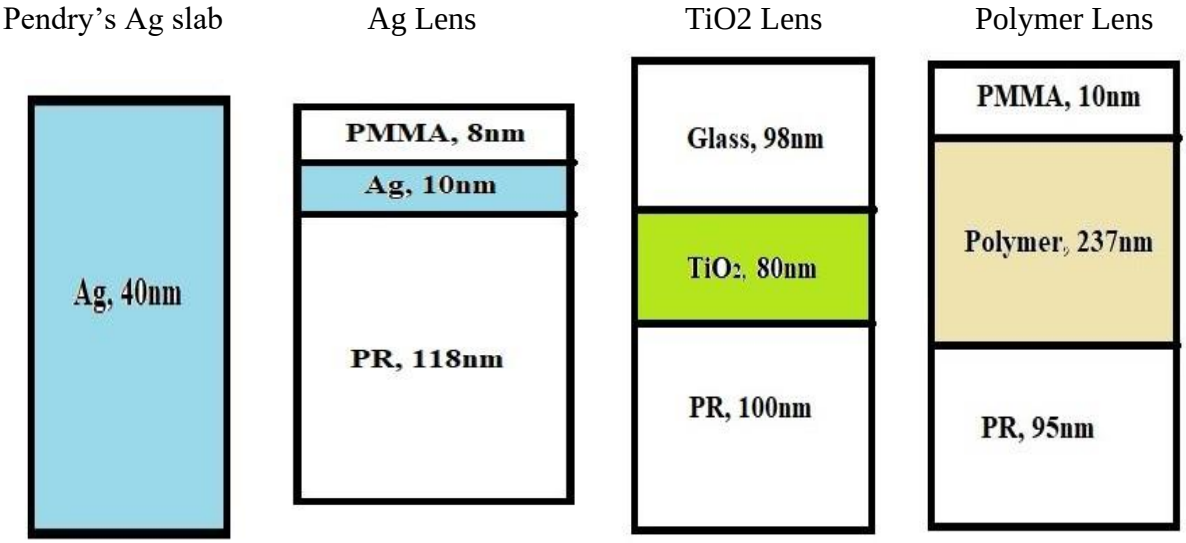

Figure 4.20: Optimized Single-Layered Lenses

Table 1

E-energy density of single-layered lenses

Lens Type (Single-Layered)	E-energy density (J/m^3) (at point D)
Pendry's Ag Lens from OTT et al. [30]	3218.4
Ag Lens	18950
TiO_2 Lens	20890
Polymer Lens	18470

4.5: Multi-Layered Meta-Lens dimensions and graph

4.5.1: Multi-Layered 1 stack:

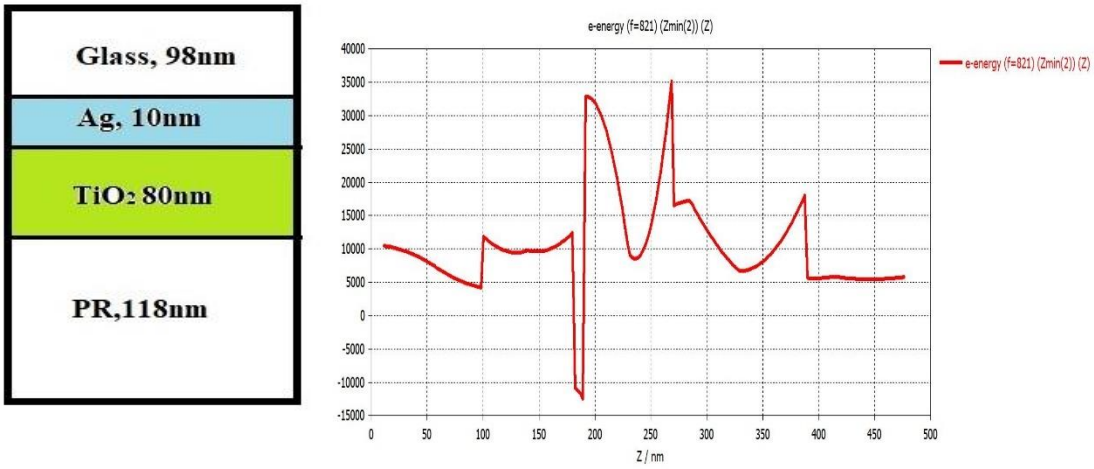

(a)

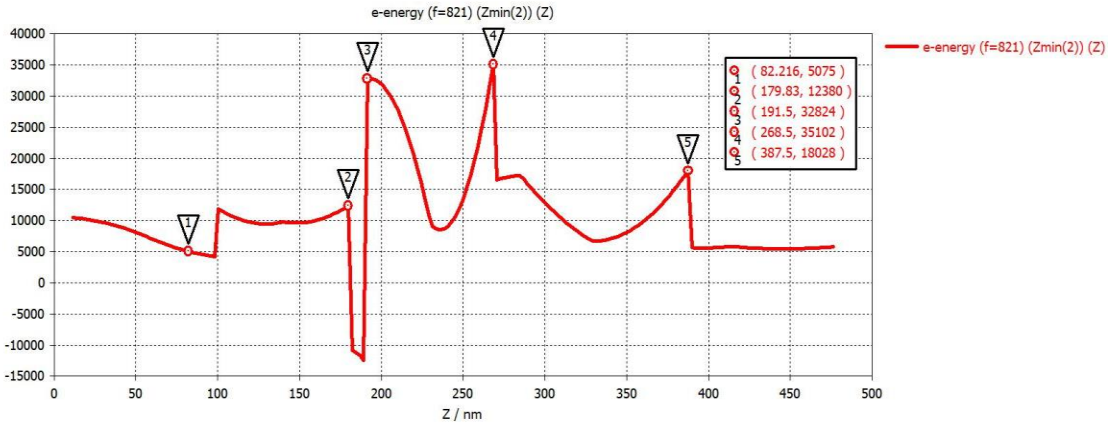

(b)

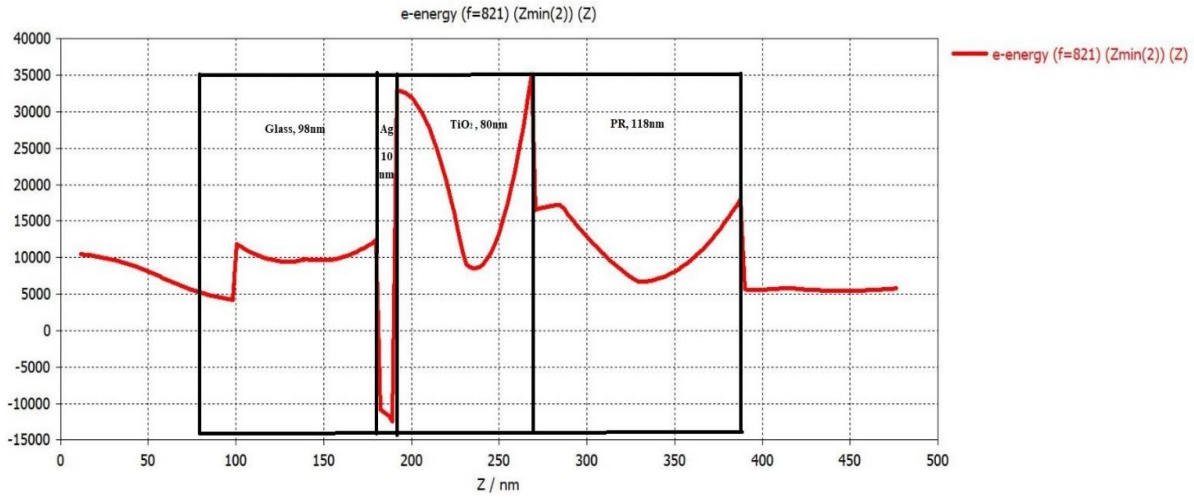

(c)

Figure 4.21: Multi-Layered 1 stack dimension and E-energy density plot

4.5.2: Multi-Layered 2 stack:

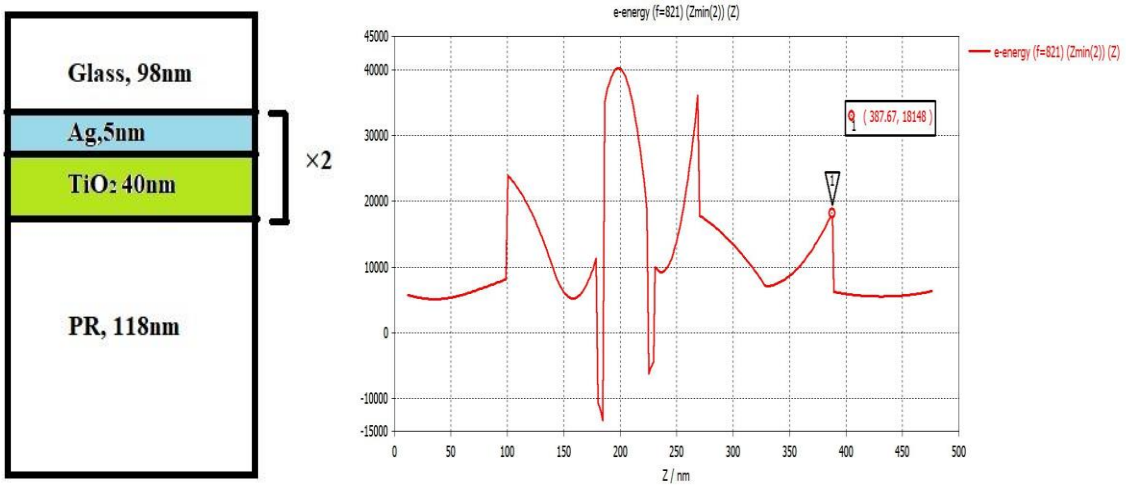

Figure 4.22: Multi-Layered 2 stack dimension and E-energy density plot

4.5.3: Multi-Layered 4 stack:

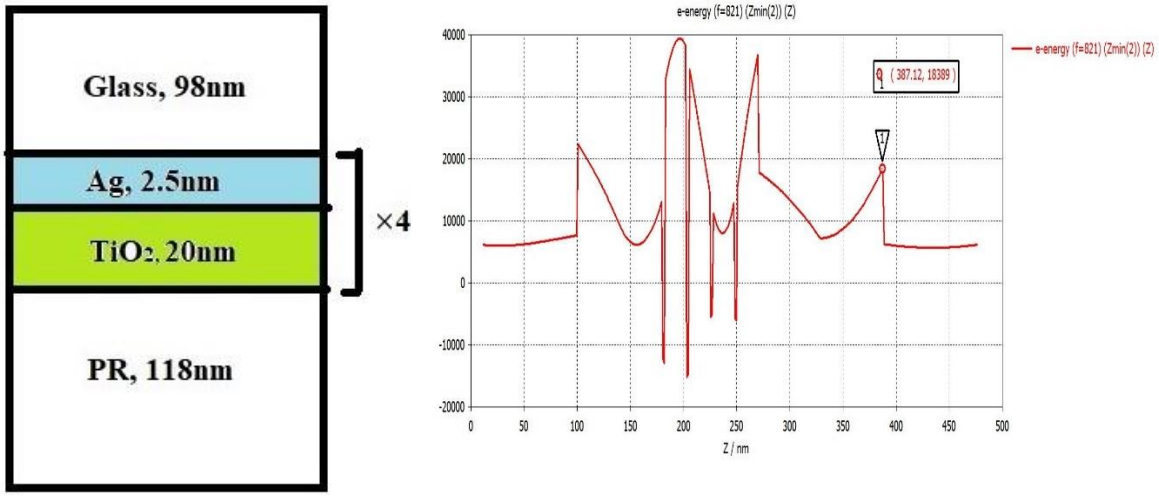

Figure 4.23: Multi-Layered 4 stack dimension and E-energy density plot

4.5.4: Multi-Layered 8 stack:

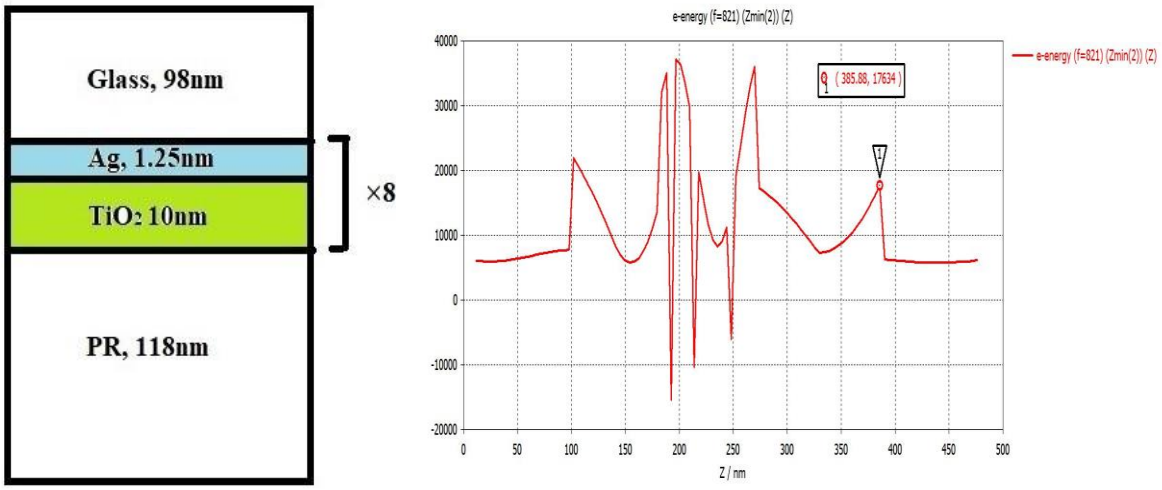

Figure 4.24: Multi-Layered 8 stack dimension and E-energy density plot

4.6: Proposed Multi-Layered Meta-Lens dimension and E-energy density of Multi-Layered Lenses

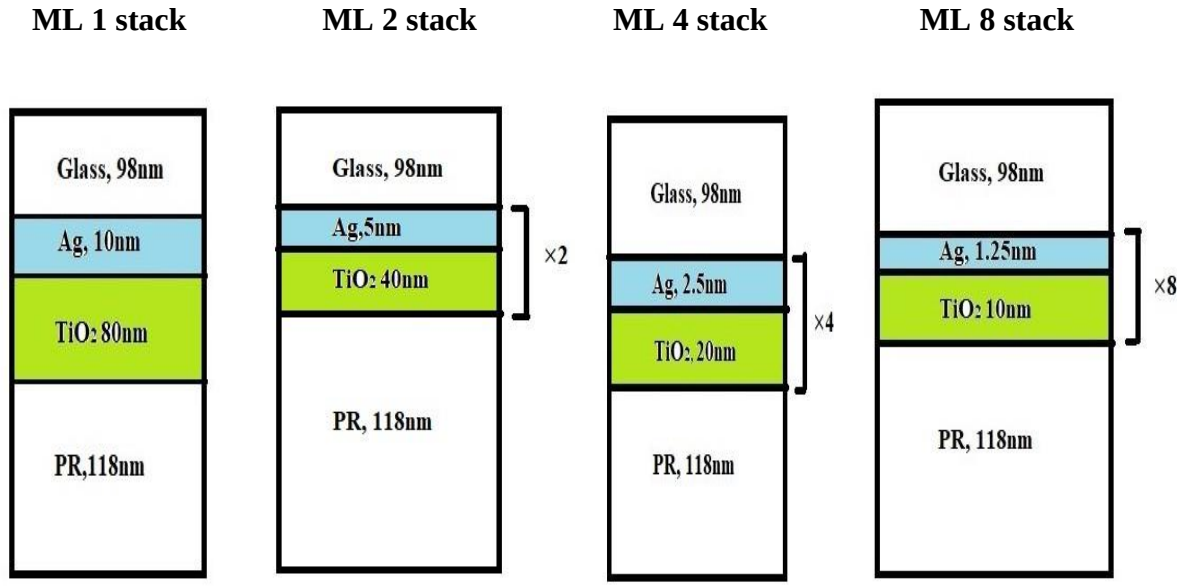

Figure 4.25: Optimized Multi-Layered Lenses

Table: 2

E-energy density of multi-layered lenses

Lens Type (Multi-Layered)	E-energy density (J/m^3) (at point D)
Multi-Layered 1 stack	18028
Multi-Layered 2 stack	18148
Multi-Layered 4 stack	18389
Multi-Layered 8 stack	17634

4.7: Focusing

4.7.1: Focusing through illuminated object (without 40nm thick Ag layer) (validation)

Parameter: Magnetic energy density

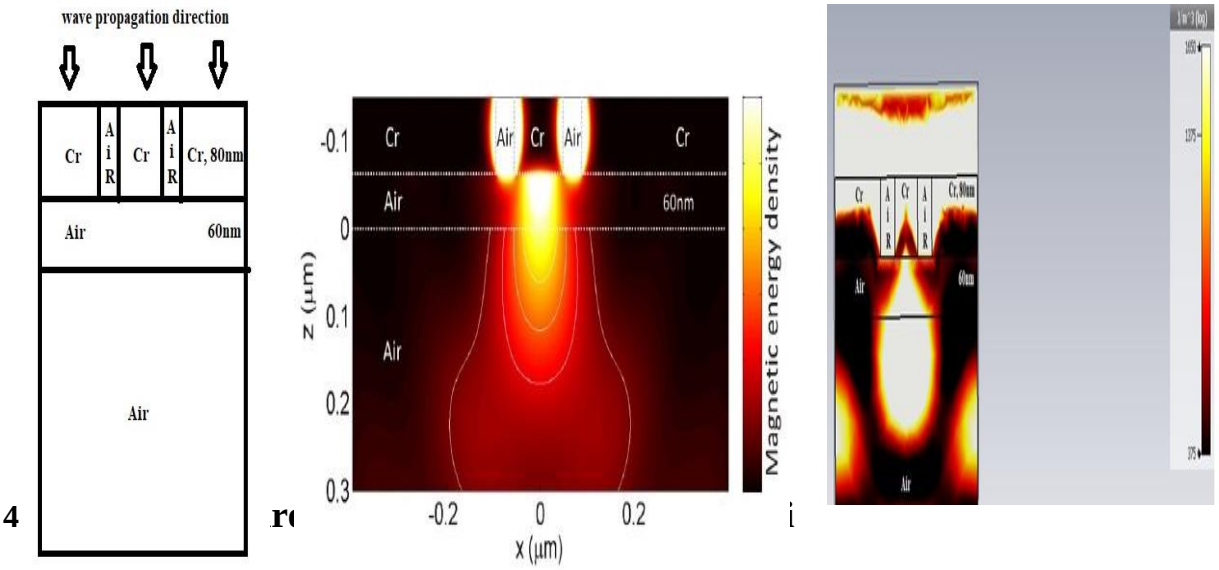

Figure 4.26: Focusing without Lenses

4.7.2: Focusing through illuminated object (with 40nm thick Ag layer) (validation):

Parameter: Magnetic energy density

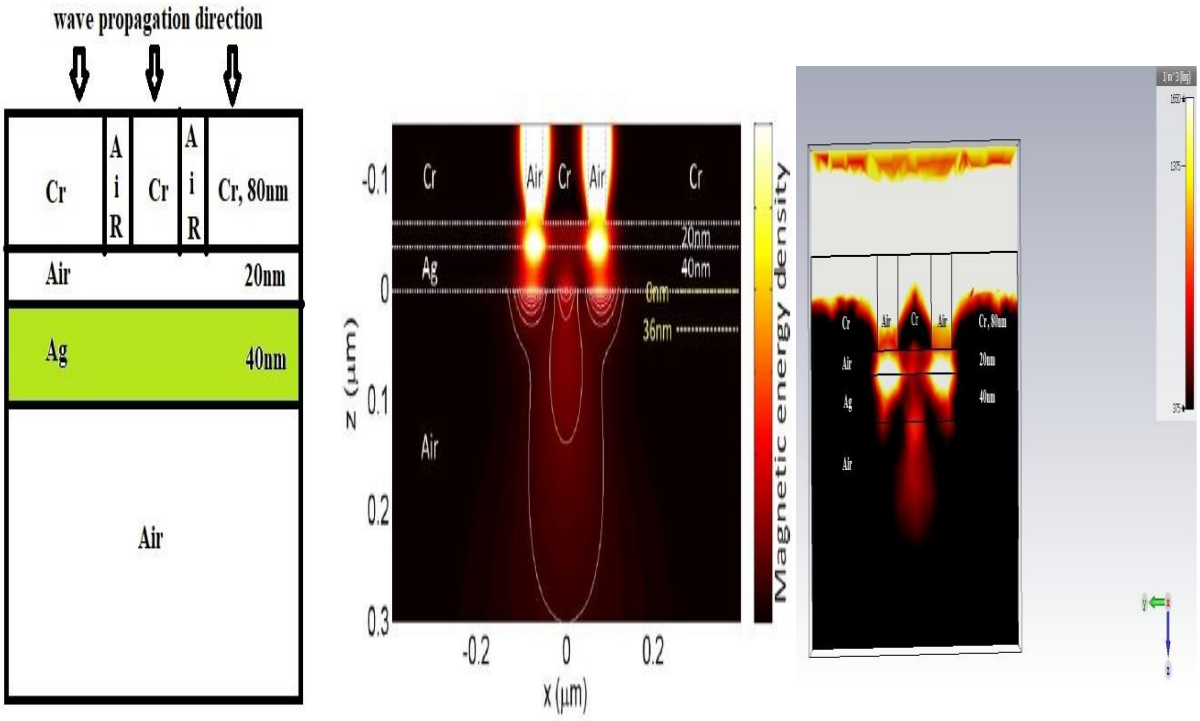

Figure 4.27: Focusing through Ag Lens [30]

4.7.3: Focusing through Pendry's Ag slab:

(a)

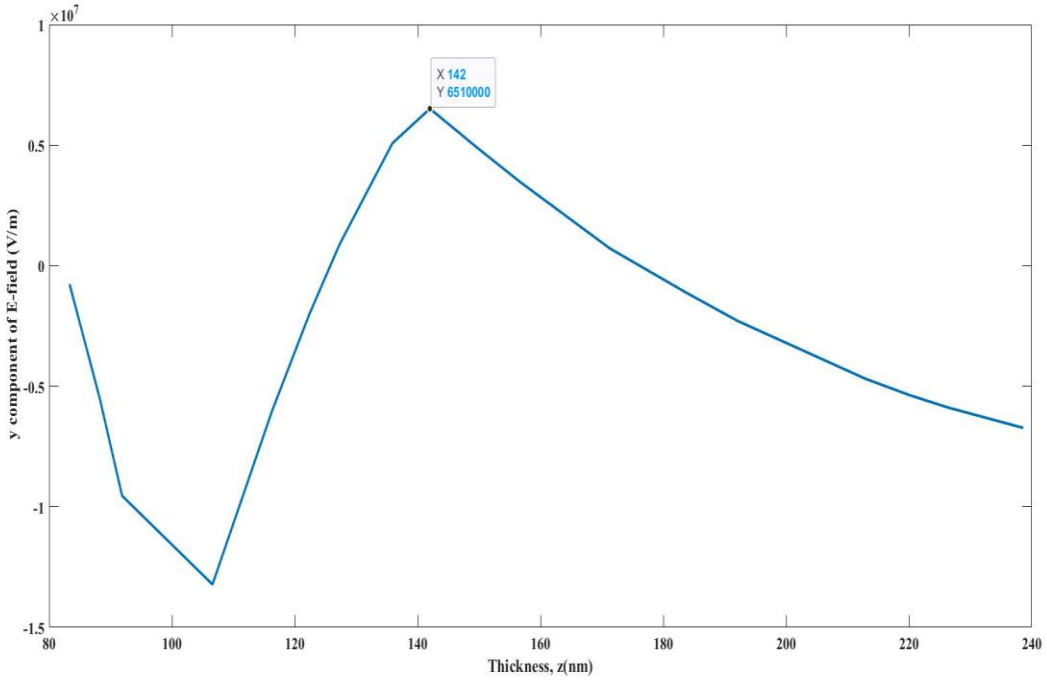
×10^7
1
0.5
0
-0.5
-1
-1.5
X 142
Y 6510000
y component of E-field (V/m)
80
100
120
140
160
180
200
220
240
Thickness, z(nm)

(b)

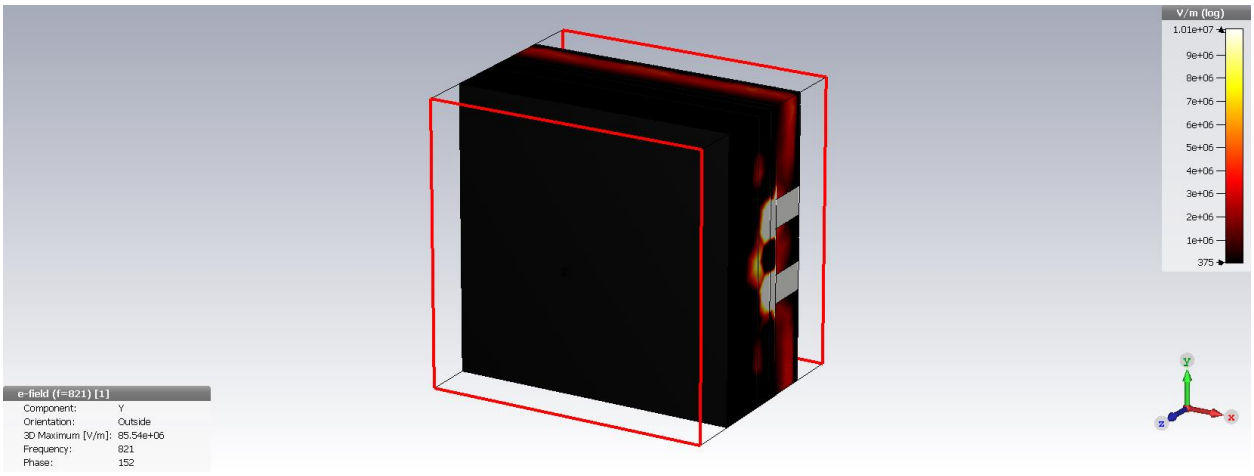
V/m (log)
1.01e+07
9e+06
8e+06
7e+06
6e+06
5e+06
4e+06
3e+06
2e+06
1e+06
375
e-field (f=821) [1]
Component: Y
Orientation: Outside
3D Maximum [V/m]: 85.54e+06
Frequency: 821
Phase: 152

(c)

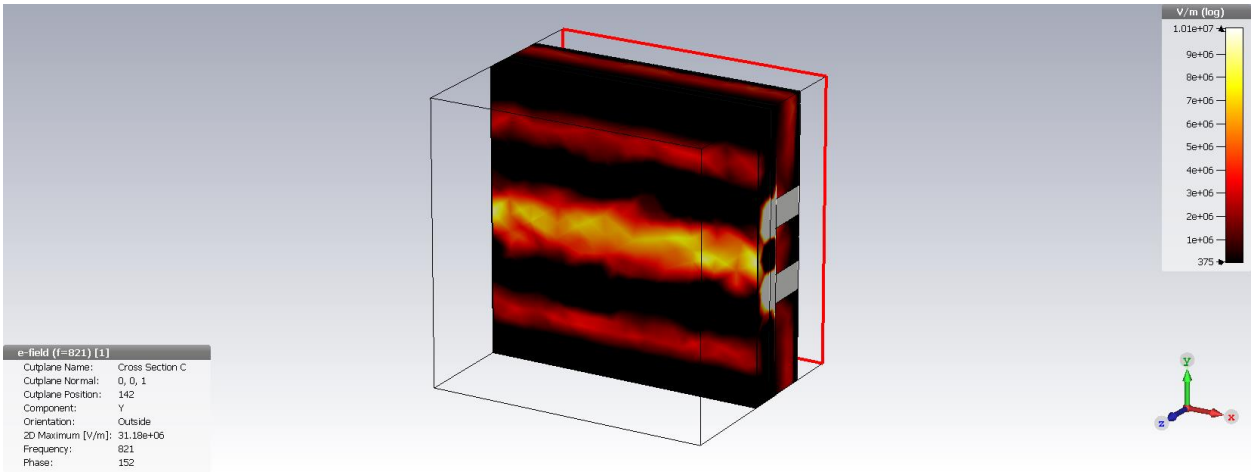

(d)

Figure 4.28: Pendry's Ag Lens (a) Dimension and Right-side cross-sectional view (b) Thickness vs. E-field plot (c) Perspective view (d) Cross-section at highest E-field

4.8: Focal bar

The location of highest E-field has been determined through using **field at cursor** in CST. At the location a cross section has been cut. In the cross sectional view, a focal bar has been observed. It is important to note that usually focal spot (circular shape) is expected. There are mainly two reasons for getting the focal bar:

1. If one aperture is used or a point object is used then circular focal point can be seen. In this structure two apertures or two slits (if boundary condition is not considered) have been used.

2. In this design periodic boundary condition has been used. For this boundary condition, the structure repeats periodically in all sides. As a result, there are infinite number of aperture and infinite number of structures. This infinite combination of structure and slits results in focal bar.

4.9: Focusing through proposed Lenses

4.9.1: Focusing through proposed Ag Lens:

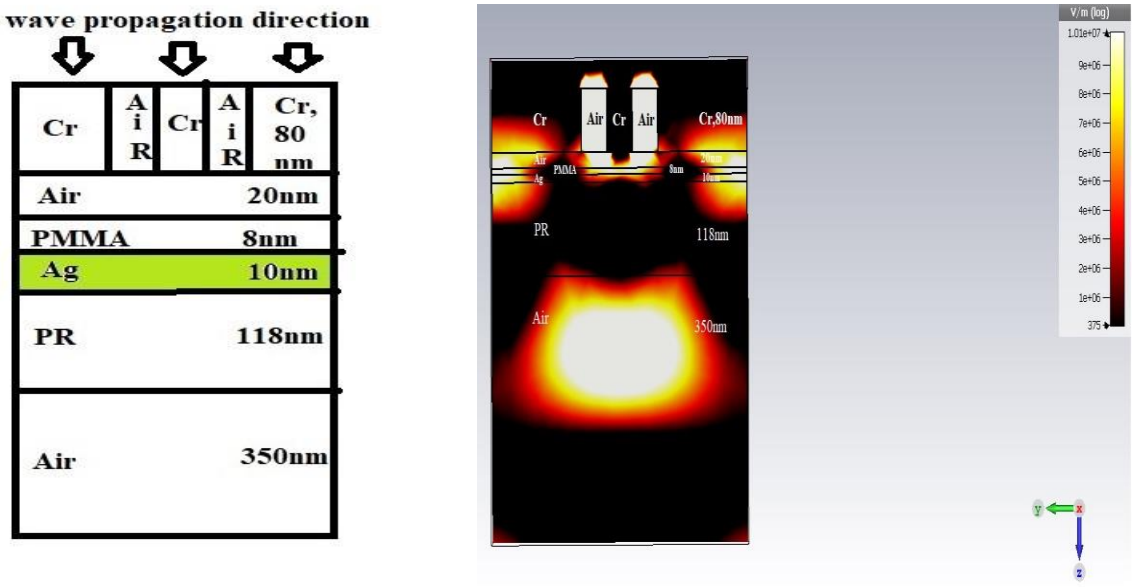

(a)

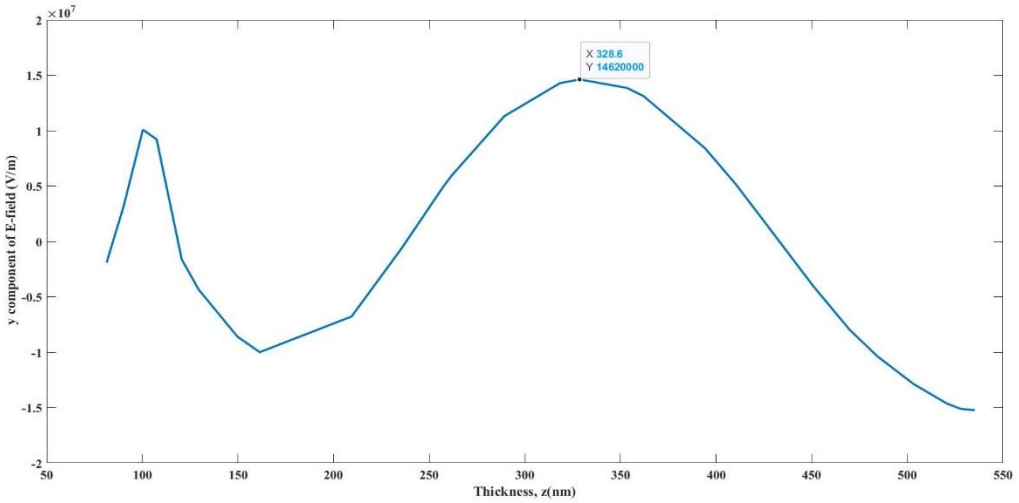
×10^7
2
1.5
1
0.5
0
-0.5
-1
-1.5
-2
X 328.6
Y 14620000
y component of E-field (V/m)
50
100
150
200
250
300
350
400
450
500
550
Thickness, z(nm)

(b)

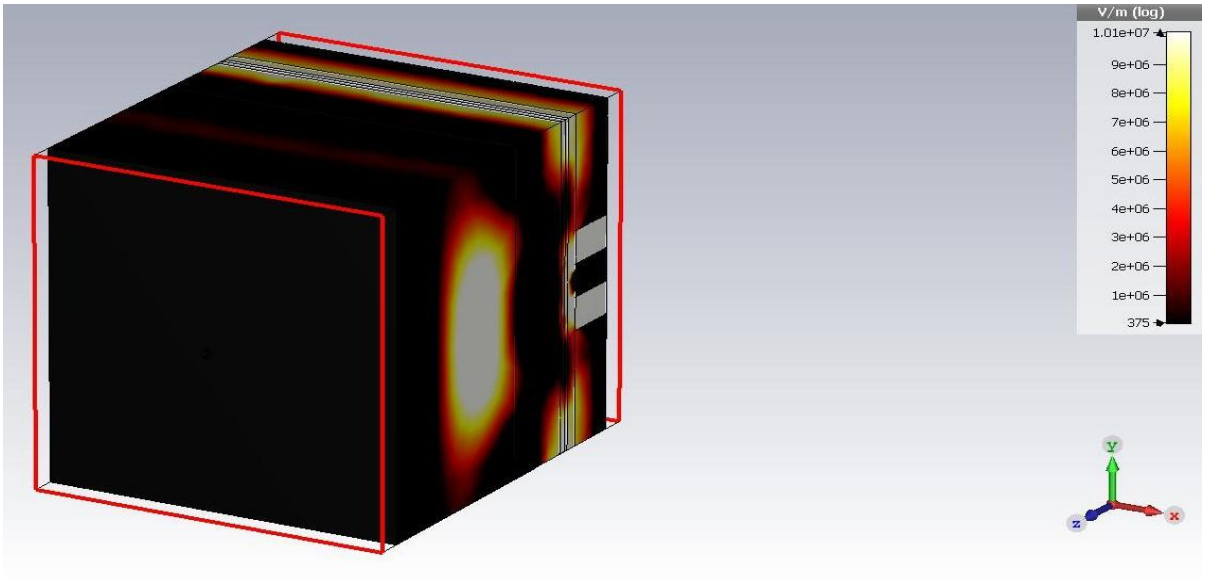
V/m (log)
1.01e+07
9e+06
8e+06
7e+06
6e+06
5e+06
4e+06
3e+06
2e+06
1e+06
375
Y
Z
X

(c)

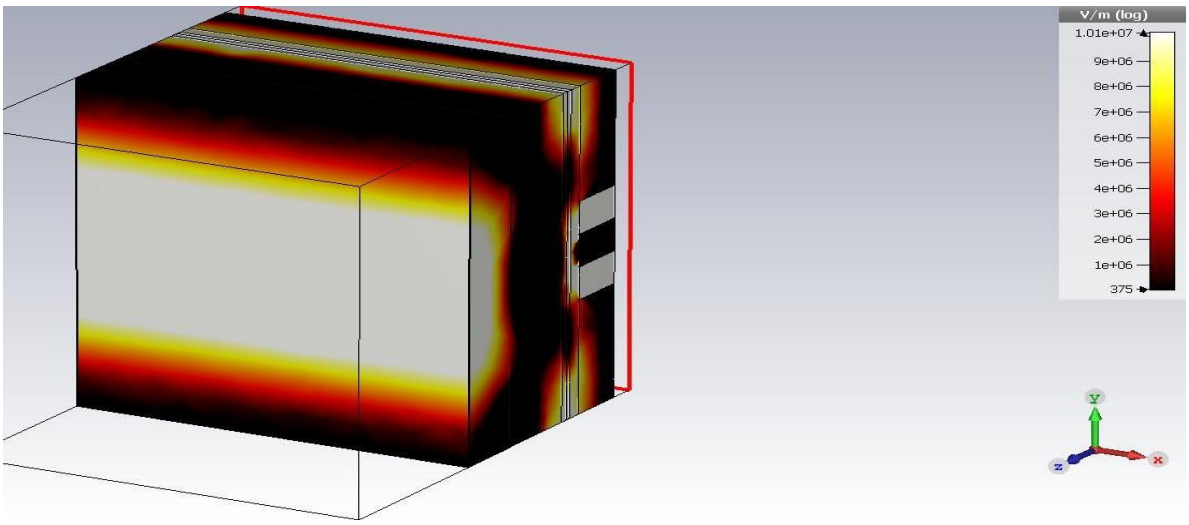

(d)

Figure 4.29: Proposed Ag Lens (a) Dimension and Right-side cross-sectional view (b) Thickness vs. E-field plot (c) Perspective view (d) Cross-section at highest E-field

4.9.2: Focusing through proposed TiO_2 Lens:

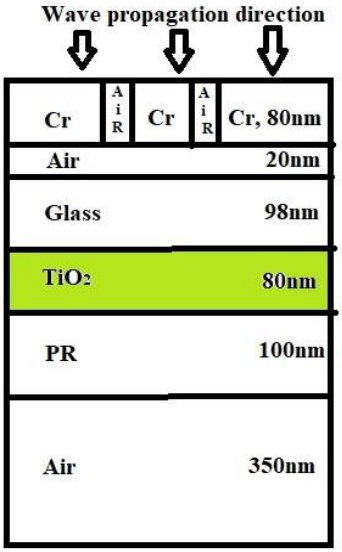

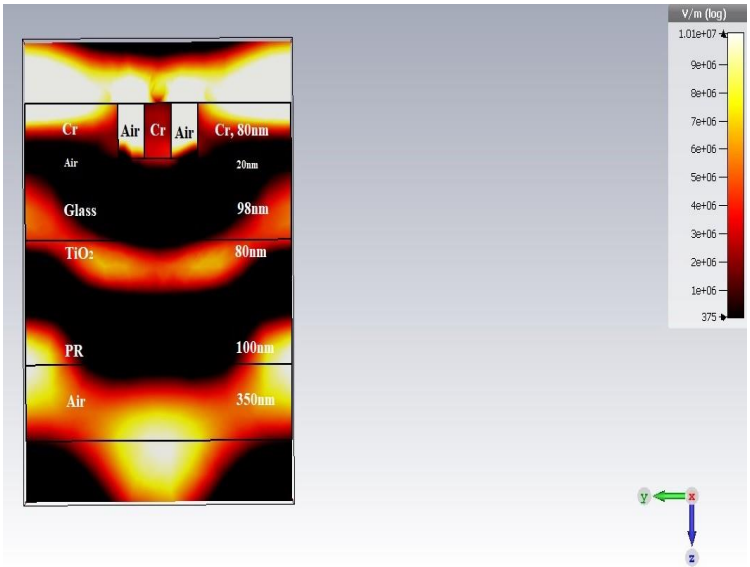

(a)

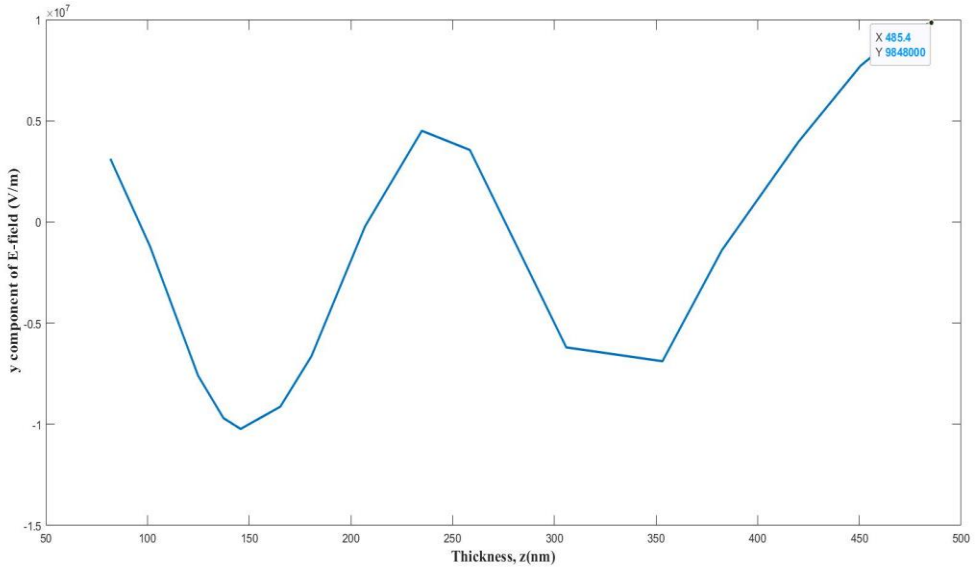
x10^7
1
0.5
0
-0.5
-1
-1.5
50
100
150
200
250
300
350
400
450
500
X 485.4
Y 9848000
y component of E-field (V/m)
Thickness, z(nm)

(b)

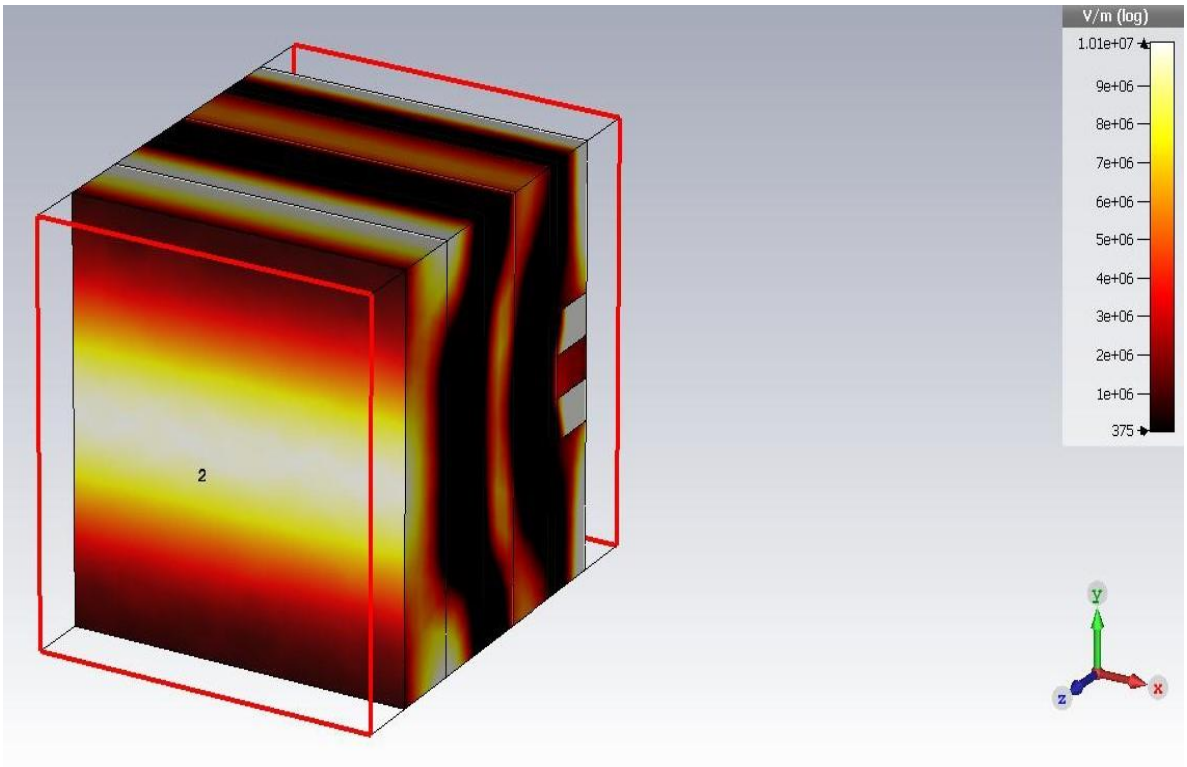
V/m (log)
1.01e+07
9e+06
8e+06
7e+06
6e+06
5e+06
4e+06
3e+06
2e+06
1e+06
375
2
Y
Z
X

(c)

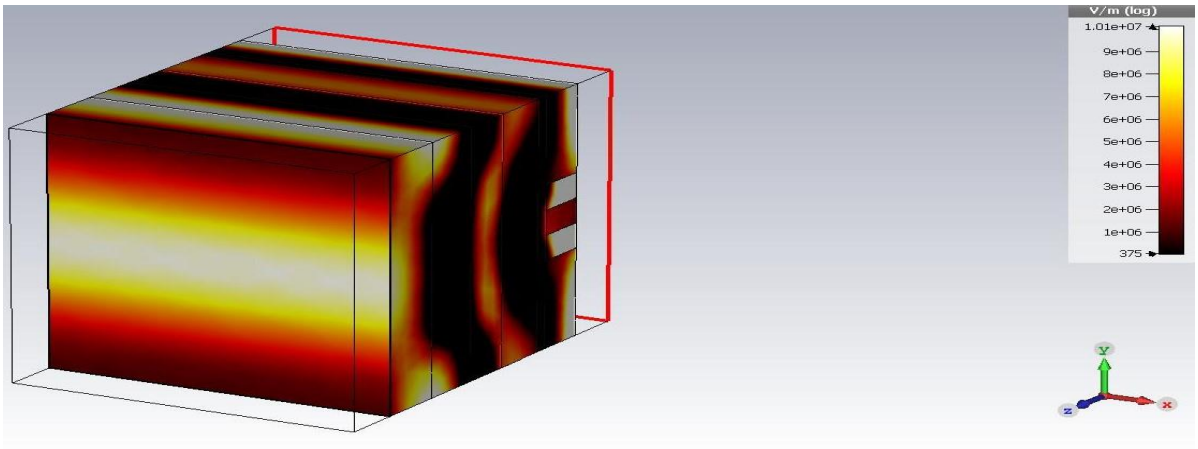

(d)

Figure 4.30: Proposed TiO2 Lens (a) Dimension and Right-side cross-sectional view (b) Thickness vs. E-field plot (c) Perspective view (d) Cross-section at highest E-field

4.9.3: Focusing through proposed Polymer Lens:

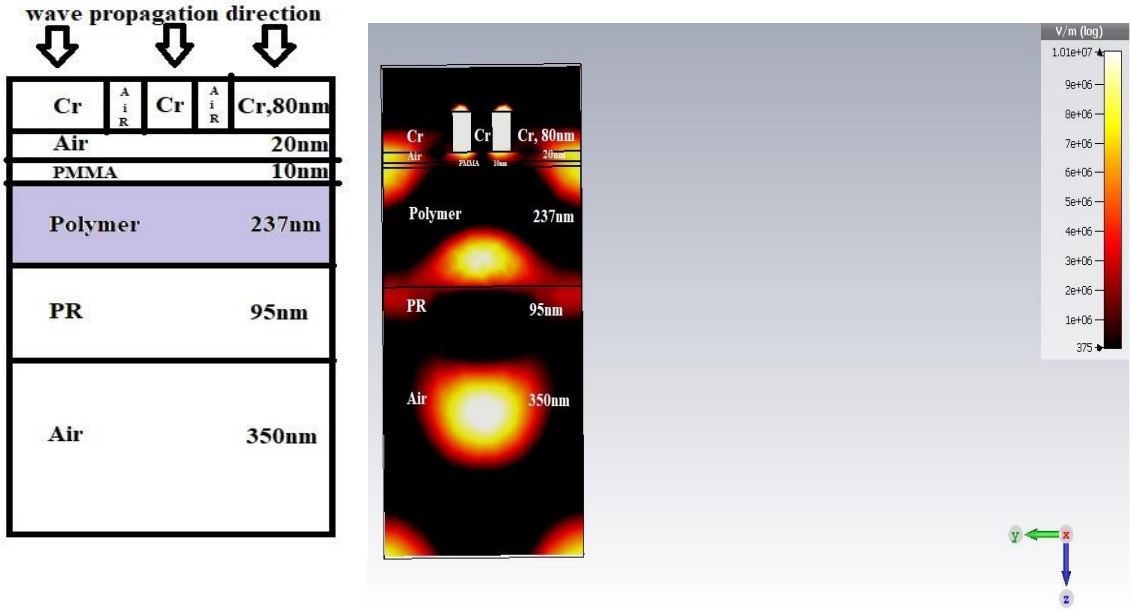

(a)

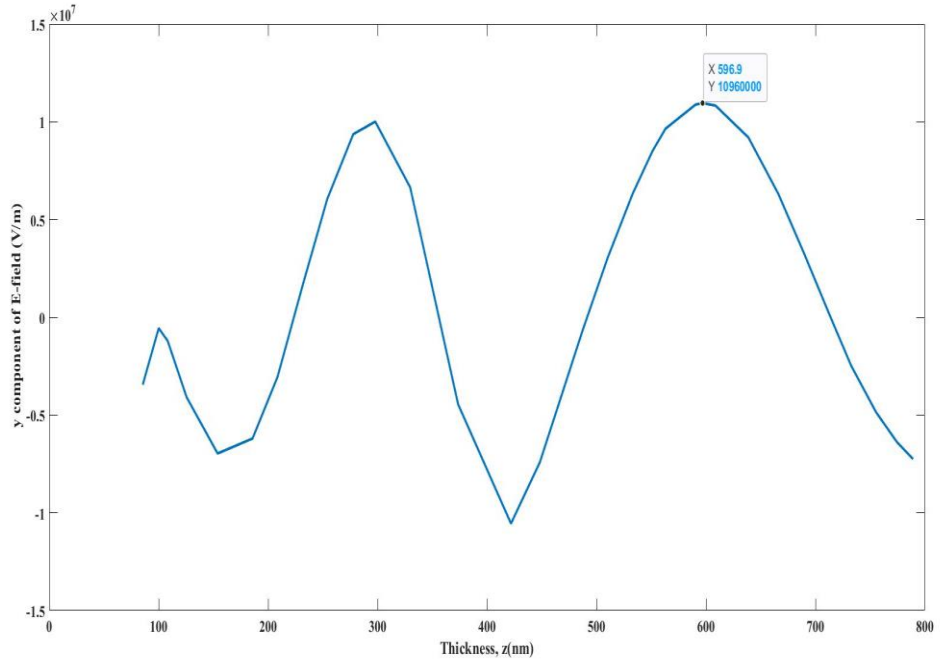
×10^7
1.5
1
0.5
0
-0.5
-1
-1.5
X 596.9
Y 10960000
y component of E-field (V/m)
0
100
200
300
400
500
600
700
800
Thickness, z(nm)

(b)

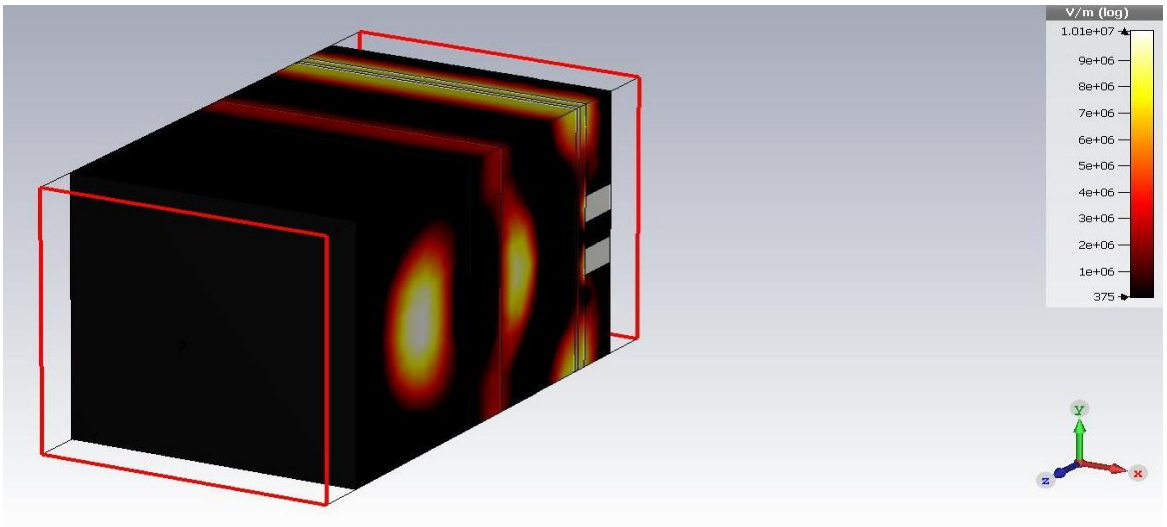
V/m (log)
1.01e+07
9e+06
8e+06
7e+06
6e+06
5e+06
4e+06
3e+06
2e+06
1e+06
375
Y
Z
X

(c)

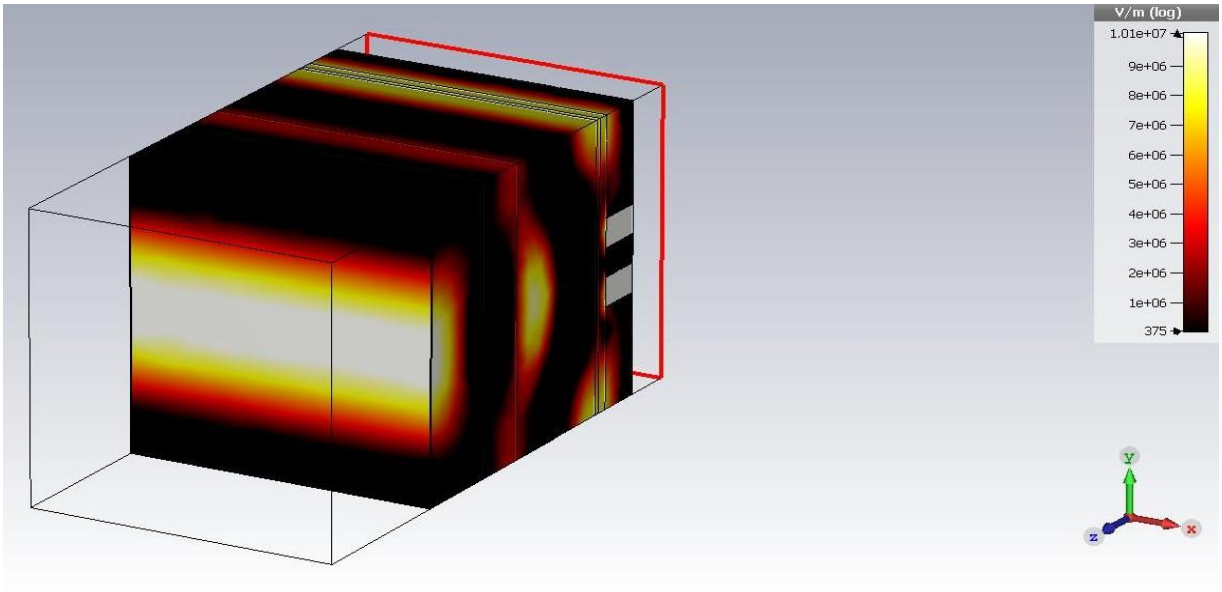

(d)

Figure 4.31: Proposed Polymer Lens (a) Dimension and Right-side cross-sectional view (b) Thickness vs. E-field plot (c) Perspective view (d) Cross-section at highest E-field

4.9.4: Focusing through proposed Multi-Layer (1stack) Lens:

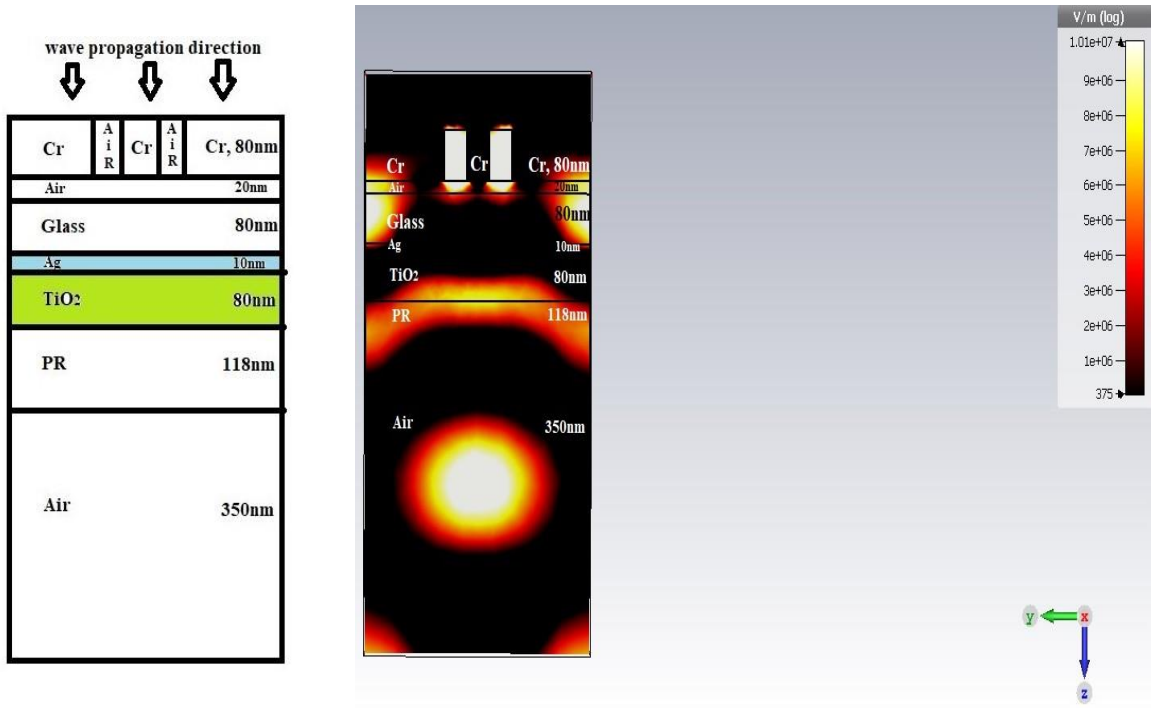

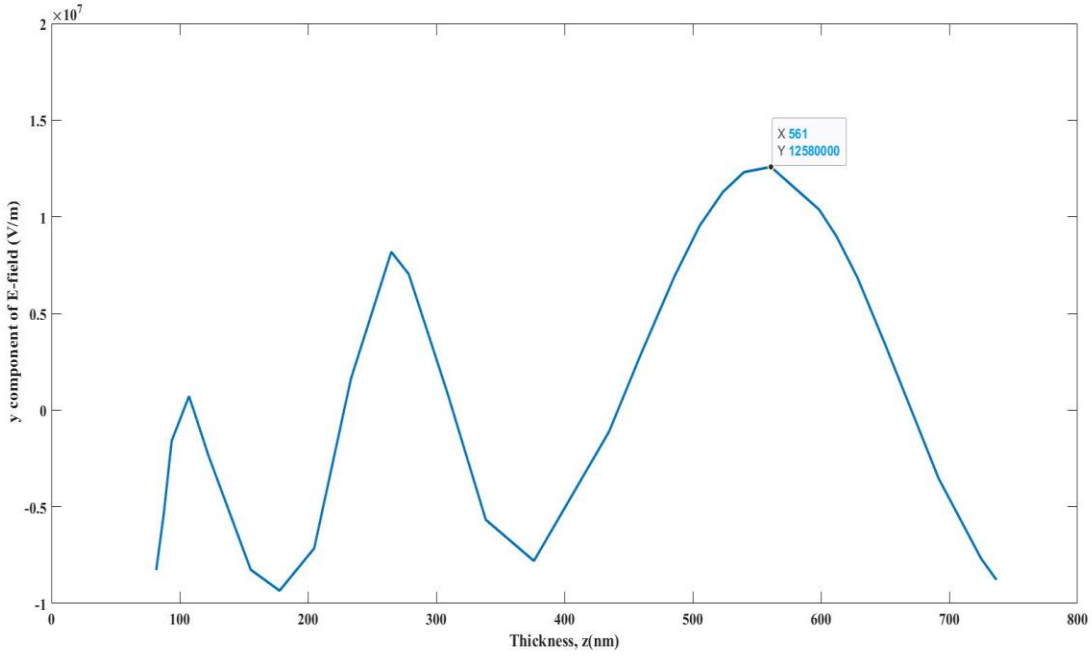
×10^7
2
1.5
1
0.5
0
-0.5
-1
y component of E-field (V/m)
X 561
Y 12580000
0
100
200
300
400
500
600
700
800
Thickness, z(nm)

(b)

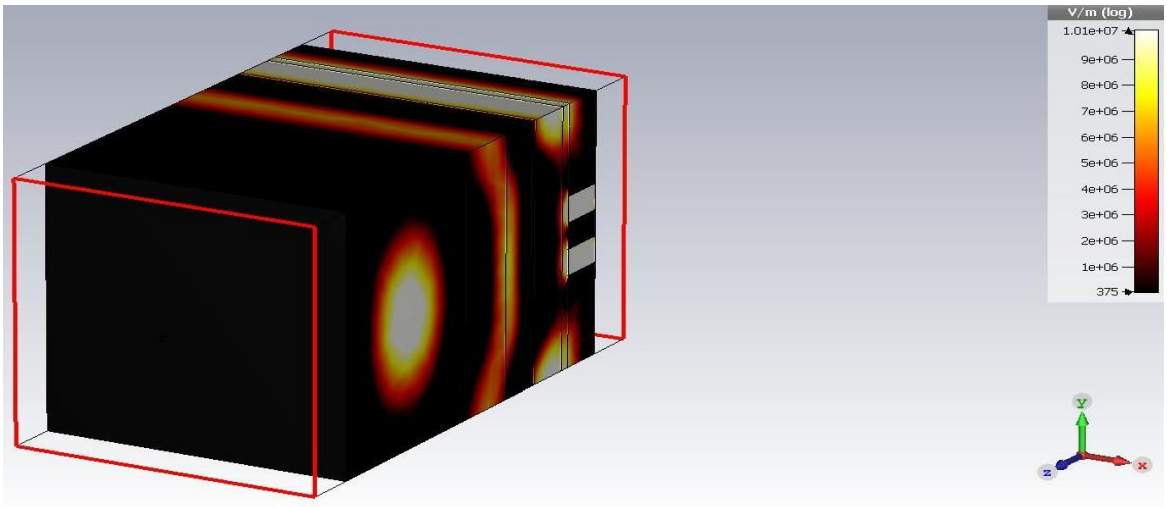
V/m (log)
1.01e+07
9e+06
8e+06
7e+06
6e+06
5e+06
4e+06
3e+06
2e+06
1e+06
375
Y
Z
X

(c)

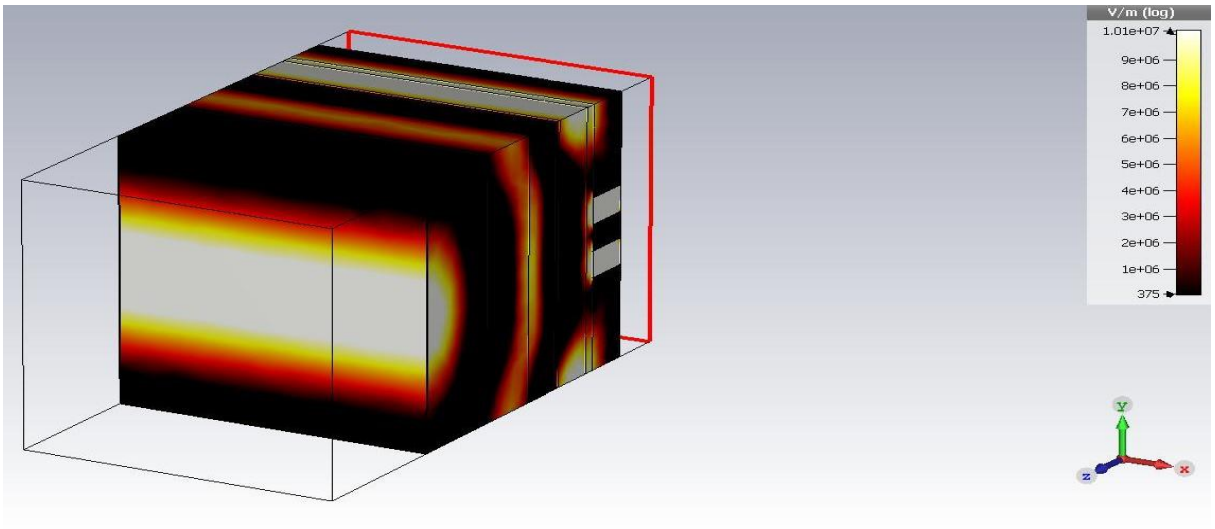

(d)

Figure 4.32: Proposed Multi-Layer (1stack) (a) Dimension and Right-side cross-sectional view (b) Thickness vs. E-field plot (c) Perspective view (d) Cross-section at highest E-field

4.9.5: Focusing through Multi-Layer (2 stack) Lens:

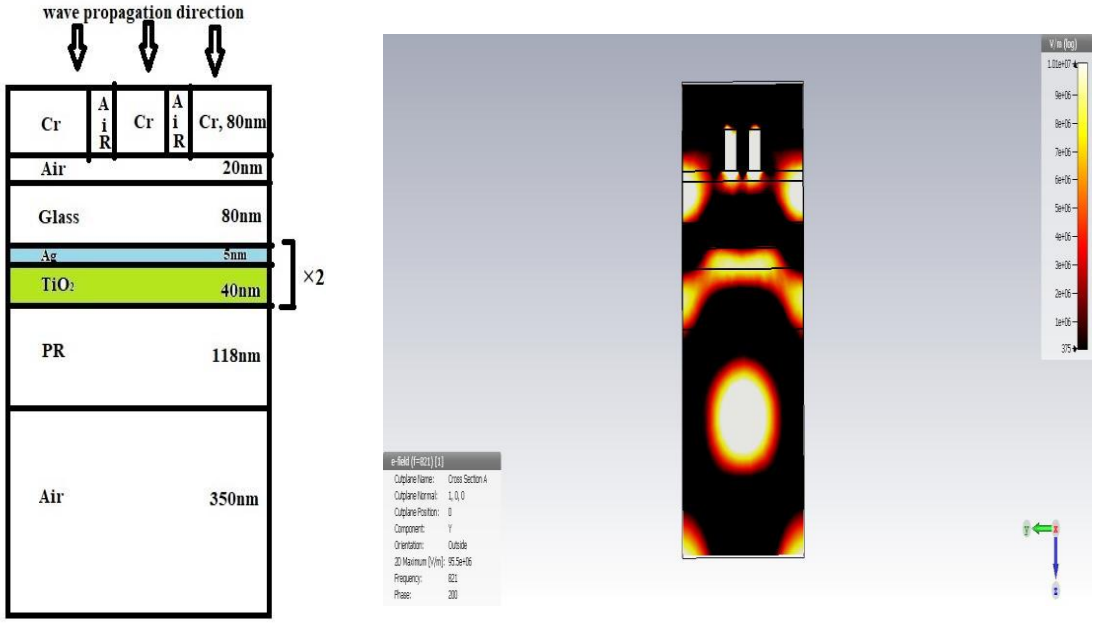

(a)

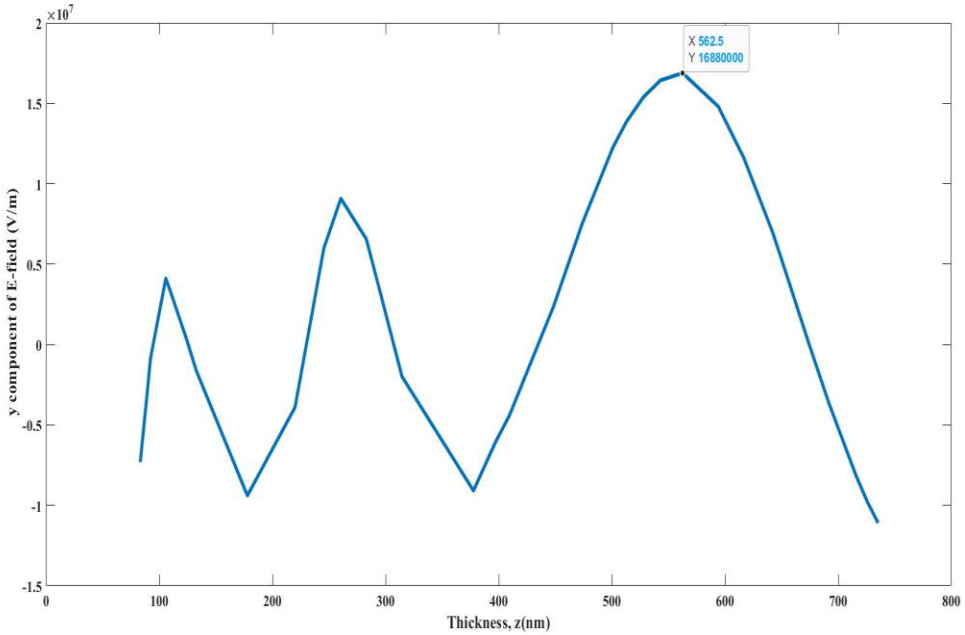
×10^7
2
1.5
1
0.5
0
-0.5
-1
-1.5
y component of E-field (V/m)
X 562.5
Y 16880000
0
100
200
300
400
500
600
700
800
Thickness, z(nm)

(b)

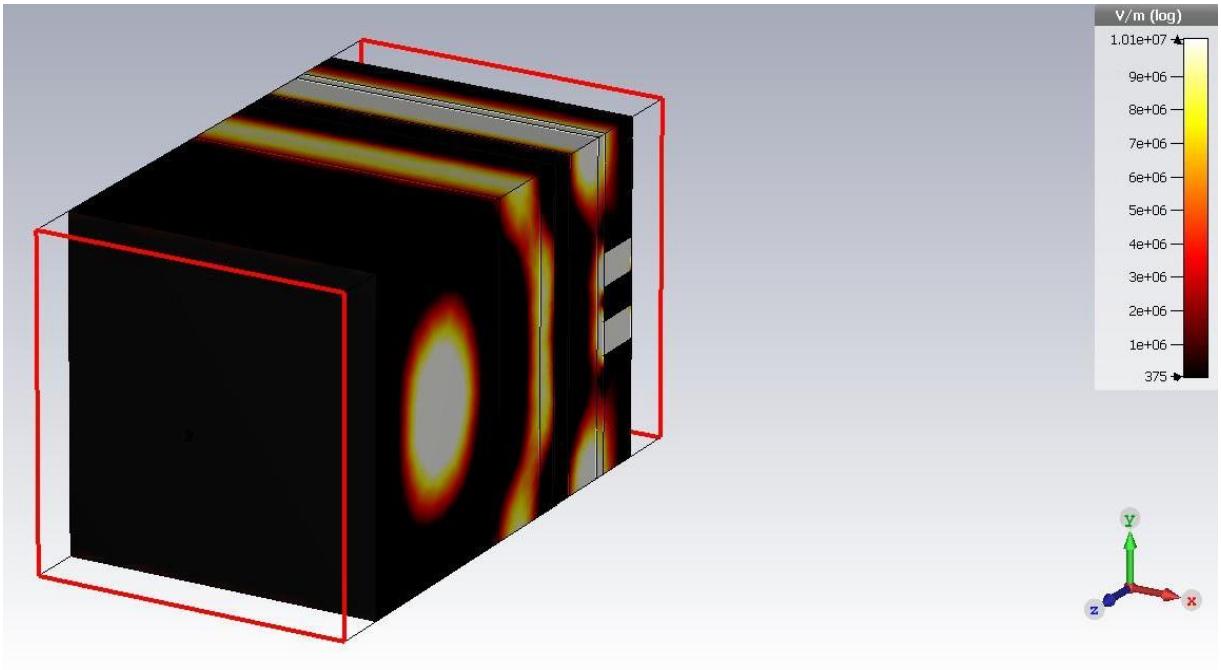
V/m (log)
1.01e+07
9e+06
8e+06
7e+06
6e+06
5e+06
4e+06
3e+06
2e+06
1e+06
375
Y
Z
X

(c)

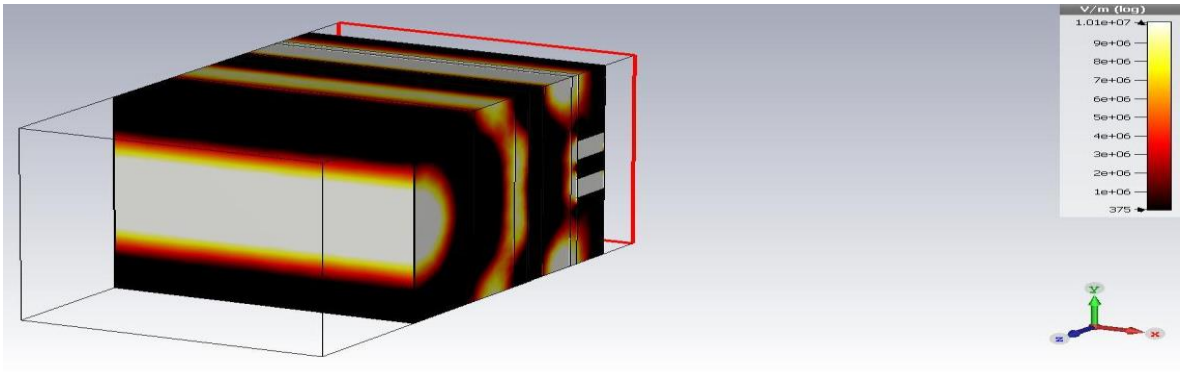

(d)

Figure 4.33: Proposed Multi-Layer (2 stack) (a) Dimension and Right-side cross-sectional view (b) Thickness vs. E-field plot (c) Perspective view (d) Cross-section at highest E-field.

4.9.6: Focusing through Multi-Layer (4 stack) Lens

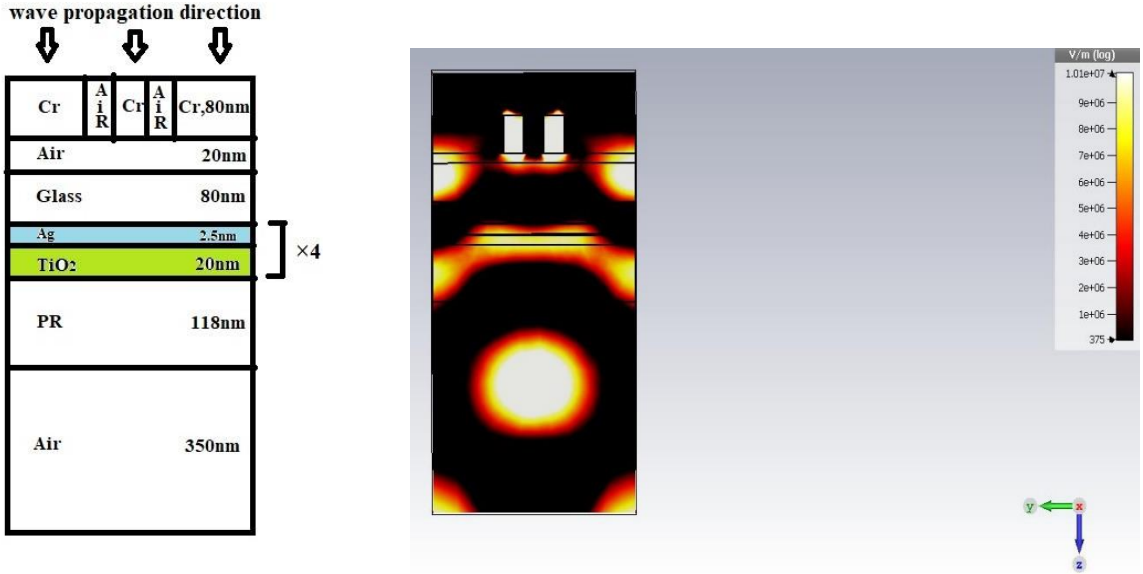

(a)

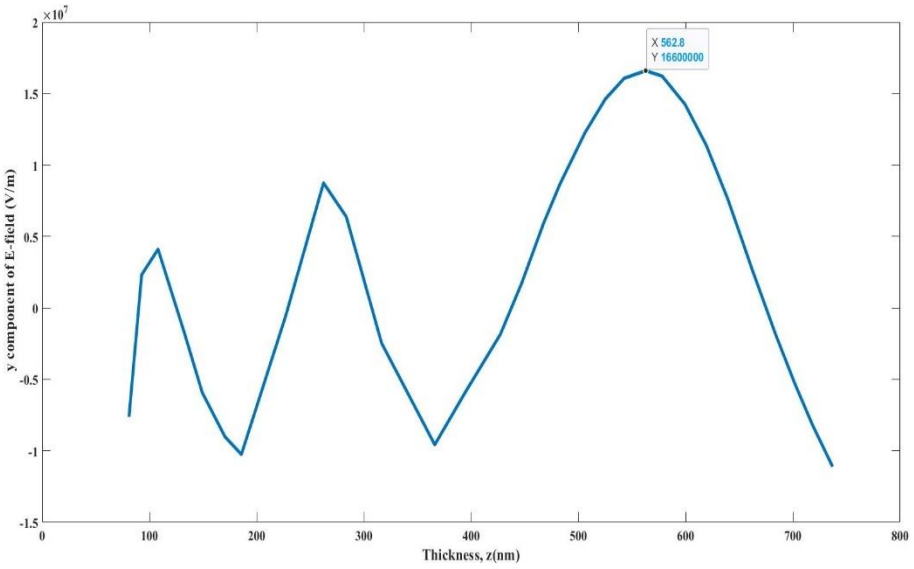
x10^7
2
1.5
1
0.5
0
-0.5
-1
-1.5
X 562.8
Y 16600000
y component of E- field (V/m)
0
100
200
300
400
500
600
700
800
Thickness, z(nm)

(b)

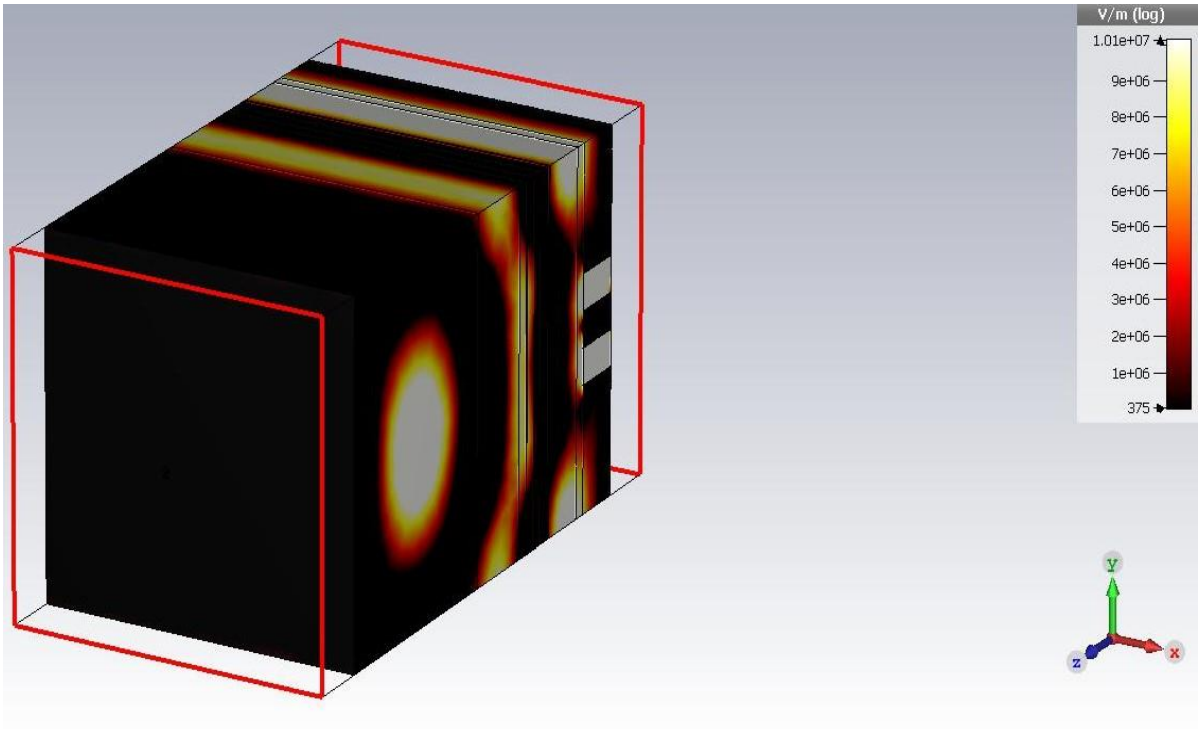
V/m (log)
1.01e+07
9e+06
8e+06
7e+06
6e+06
5e+06
4e+06
3e+06
2e+06
1e+06
375
Y
Z
X

(c)

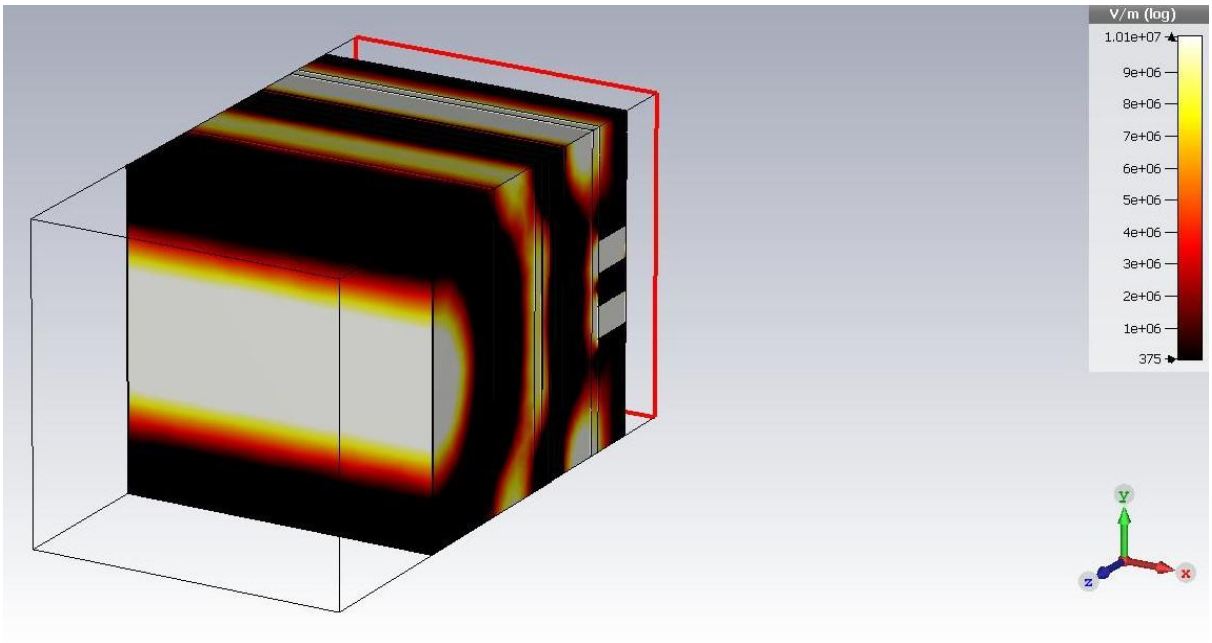

(d)

Figure 4.34: Proposed Multi-Layer (4 stack) (a) Dimension and Right-side cross-sectional view (b) Thickness vs. E-field plot (c) Perspective view (d) Cross-section at highest E-field

4.9.7: Focusing through Multi-Layer (8 stack) Lens

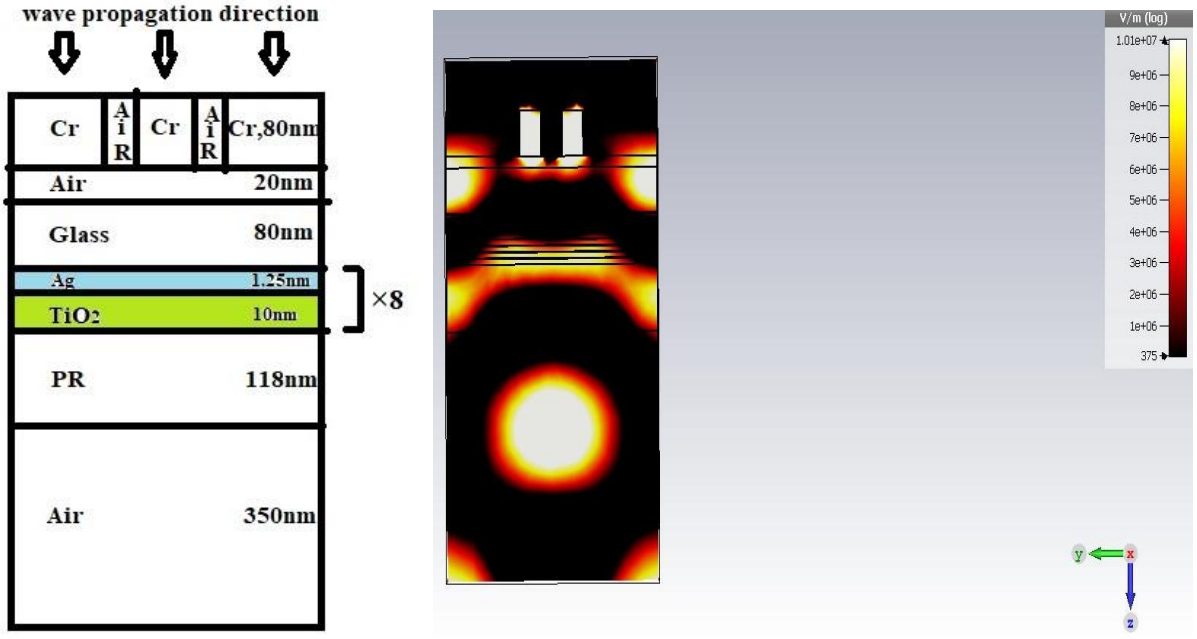

(a)

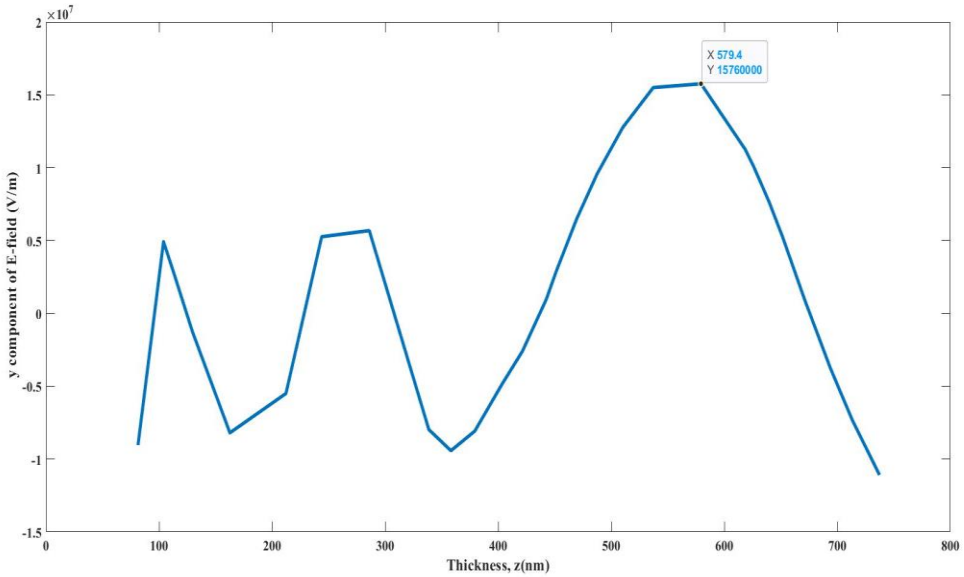
×10^7
2
1.5
1
0.5
0
-0.5
-1
-1.5
y component of E-field (V/m)
X 579.4
Y 15760000
0
100
200
300
400
500
600
700
800
Thickness, z(nm)

(b)

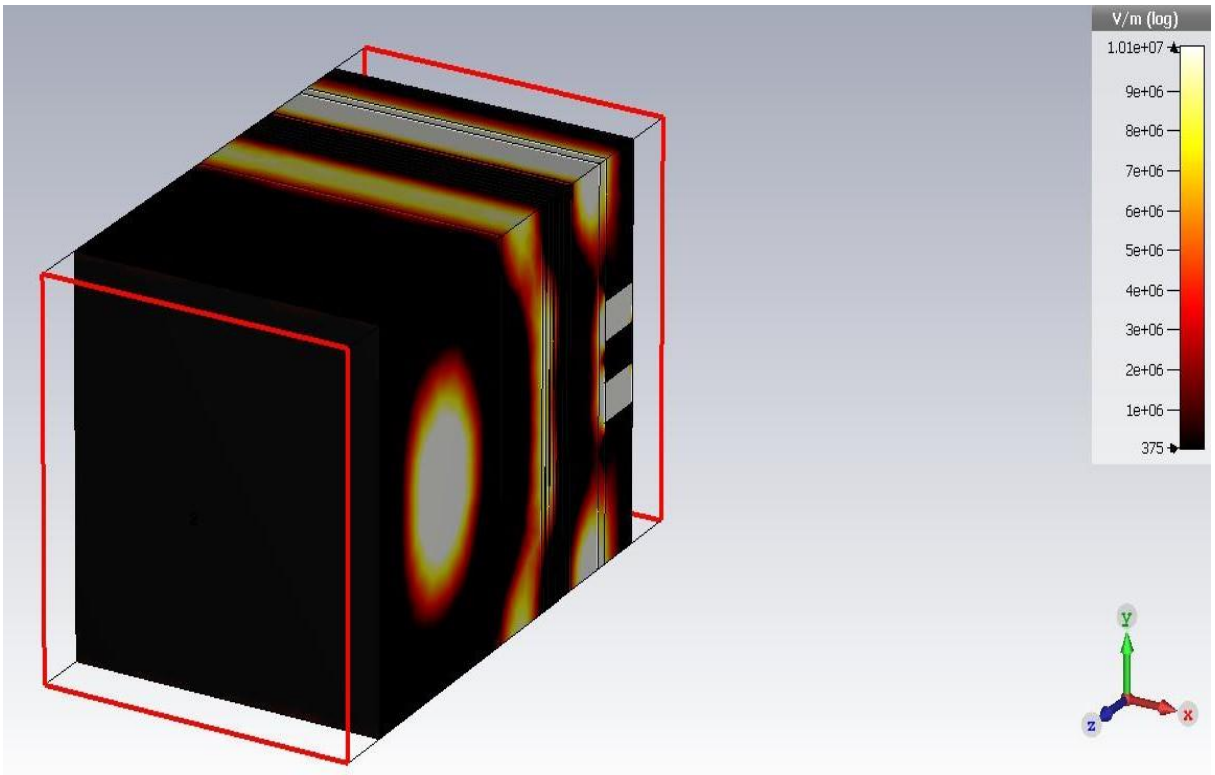
V/m (log)
1.01e+07
9e+06
8e+06
7e+06
6e+06
5e+06
4e+06
3e+06
2e+06
1e+06
375
Y
Z
X

(c)

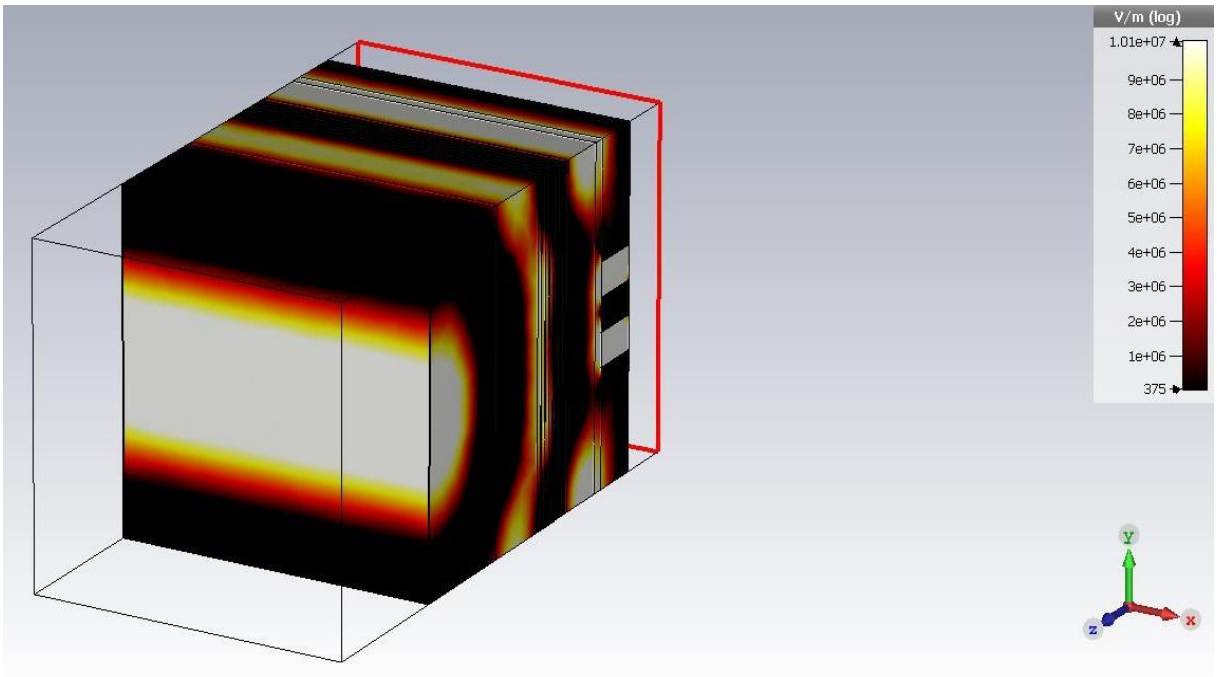

(d)

Figure 4.35: Proposed Multi-Layer (8stack) (a) Dimension and Right-side cross-sectional view (b) Thickness vs. E-field plot (c) Perspective view (d) Cross-section at highest E-field.

Table: 3

Comparison of E-field among various Lenses

Meta-Lenses	E-field (y component) (MV/m)	Normalized E-field (Eout /Ein)	Distance of focal point from last layer
Pendry's Ag Lens from Ott et al.	6.51	0.195	2
Ag Lens	14.62	0.362	98
TiO_2 Lens	9.848	0.523	107.4
Polymer Lens	10.96	0.528	154.9
Multi-Layer 1 stack	12.58	0.625	173
Multi-Layer 2 stack	16.88	0.789	174.5
Multi-Layer 4 stack	16.60	0.802	177.8
Multi-Layer 8 stack	15.76	0.738	191.4

CHAPTER V

CONCLUSIONS AND DISCUSSION

5.1: Conclusion

Proposed Ag Lens and all other meta-lenses (single-layered and multi-layered) provided better E-energy density than the Pendry's Ag slab. It means that proposed meta-lenses can provide better enhancement of evanescent waves consequently better image resolution. In addition to that the proposed meta-lenses also showed better E-field than the Pendry's Ag slab. As a result, these proposed meta-lenses have higher focusing ability than the Pendry's Ag slab.

5.2: Discussion

Amplification of evanescent waves: The Lens properties has been investigated carefully. The simulation has been done to get optimized Lens dimensions. At the optimized dimension, at the end of PR, amplified evanescent waves are restored. To make the lenses' structure practical, substrate and coating material have been used before and after the main lens material. Although, the substrate and coating materials have some losses, but the amplification of the main lens material overcome the losses and in sum amplified evanescent waves can be observed.

Paraxial image vs. Super-resolution: In this research, operating frequency is at 821 THz. The permittivity of a material is related to its property. The permittivity also depends on the

frequency. If the operating frequency is shifted from 821 THz, the permittivity of certain material will change. As a result, optimized dimension will be changed. Consequently, the focal bar will be located to different location with different intensity (E-field). The materials for lens have been selected in terms of their electromagnetic property, availability in nature, possibility of mass production and economic feasibility.

5.3: Future works

5.3.1: Fabrication and measurement:

There are many nanofabrication processes for example Thin film deposition, patterning i.e., Lithography, Film modification i.e., etching and so on. Additionally, 3D printing, sputtering technique that grow material on a substrate can also be an option for fabrication.

5.3.2: Further optimization:

Dimension and Materials: New types of material can be examined or more layers can be added to get better result in future. Furthermore, the internal losses in the layered lenses need to be considered to make the meta-lenses more efficient.

Shape of focal spot: In the proposed lenses, focal bar has been found where two slits have been used as aperture. To get a circular focal spot, aperture shape can be modified, for example, circular shaped aperture can be used.

5.3.3: Application approach:

The proposed meta-lenses can be used in different optical devices, medical instruments, lasers, cameras, and many other devices for imaging.

REFERENCES

[1] THE ELECTRODYNAMICS OF SUBSTANCES WITH SIMULTANEOUSLY NEGATIVE VALUES OF ε AND μ; 1968VG Veselago10.1070/pu1968v010n04abeh003699Soviet Physics Uspekhi

[2] Composite Medium with Simultaneously Negative Permeability and Permittivity, 2000DR Smith, WJ Padilla, DC Vier, SC Nemat-Nasser, Schultz10.1103/physrevlett.84.4184 Physical Review Letters

[3] Superlenses to overcome the diffraction limit; 2008X Zhang, ZLiu10.1038/nmat2141 Nature Materials

[4] Extremely Low Frequency Plasmons in Metallic Mesostructures, 1996JB Pendry, AJ Holden, WJ Stewart, I Youngs10.1103/physrevlett.76.4773Physical Review Letters

[5] Magnetism from conductors and enhanced nonlinear phenomena, 1999 J Pendry, A Holden, D Robbins, W Stewart10.1109/22.798002IEEE Transactions on Microwave Theory and Techniques.

[6] Lu D and Liu Z 2012 Hyperlenses and metalenses for far-field super-resolution imaging *Nat. Commun.* **3** 1–9

[7] Pendry J B 2000 Negative refraction makes a perfect lens *Phys. Rev. Lett.* **85** 3966–9

[8] Superlenses to overcome the diffraction limit, 2008, X Zhang, Z Liu10.1038/nmat2141Nature Materials

[9] Negative Refractive Index Materials, 2006V Veselago, L Braginsky, V Shklover, C Hafner10.1166/jctn.2006.3000Journal of Computational and Theoretical Nanoscience

[10] Design of Multilayered Meta-Lenses for Image Resolution Enhancement, 2019 MA Ruiz, N Wongkasem10.1109/apusncursinrsm.2019.88882902019 IEEE International Symposium on Antennas and Propagation and USNC-URSI Radio Science Meeting

[11] A broadband achromatic polarization-insensitive metalens consisting of anisotropic nanostructures 2019WT Chen, AY Zhu, J Sisler, Z Bharwani, F Capasso 10.1038/s41467-- 019-08305-yNature Communications

[12] A broadband achromatic metalens for focusing and imaging in the visible, 2018WT Chen, AY Zhu, V Sanjeev, M Khorasaninejad, Z Shi, E Lee, F Capasso10.1038/s41565-017-0034-6 Nature Nanotechnology

[13] Flat optics with dispersion-engineered metasurfaces, 2020WT Chen, AY Zhu, F Capasso10.1038/s41578-020-0203-3Nature Reviews Materials

[14] Ultra-compact visible chiral spectrometer with meta-lenses, 2017 AY Zhu, WT Chen, M Khorasaninejad, J Oh, A Zaidi, I Mishra, RC Devlin, F Capasso10.1063/1.4974259APL Photonics

[15] Recent advances in planar optics: from plasmonic to dielectric metasurfaces, 2017P Genevet, F Capasso, F Aieta, M Khorasaninejad, R Devlin10.1364/optica.4.000139Optica

[16] Metalenses: Versatile multifunctional photonic components, 2017M Khorasaninejad, F Capasso10.1126/science.aam8100Science

[17] Subwavelength imaging at optical frequencies using a transmission device formed by a periodic layered metal-dielectric structure operating in the canalization regime 2006PA Belov, Y Hao10.1103/physrevb.73.113110Physical Review B

[18] Directed subwavelength imaging using a layered metal-dielectric system, 2006B Wood, JB Pendry, DP Tsai10.1103/physrevb.74.115116Physical Review B

[19] Imaging the near field, 2003SA Ramakrishna, JB Pendry, MCK Wiltshire, WJ Stewart 10.1080/09500340308235215Journal of Modern Optics

[20] Sub-Diffraction-Limited Optical Imaging with a Silver Superlens, 2005N Fang Fang10.1126/science.1108759Science

[21] Analysis and optimization of multilayer silver superlenses for near-field optical lithography, 2007DO Melville, RJ Blaikie10.1016/j.physb.2006.12.048 Physica B: Condensed Matter

[22] Dual-layered metasurfaces for asymmetric focusing, 2020B Yao, X Zang, Z Li, L Chen, J Xie, Y Zhu, S Zhuang10.1364/prj.387672Photonics Research

[23] Lee H, Xiong Y, Fang N, Srituravanich W, Durant S, Ambati M, Sun C and Zhang X 2005 Realization of optical superlens imaging below the diffraction limit *New J. Phys.* **7**

[24] Bradley J D B, Evans C C, Parsy F, Phillips K C, Senaratne R, Marti E and Mazur E 2010 Low-loss TiO2 planar waveguides for nanophotonic applications *2010 23rd Annu. Meet. IEEE Photonics Soc. PHOTINICS 2010* 313–4

[25] Essalhi Z, Hartiti B, Lfakir A, Siadat M and Thevenin P 2016 Optical properties of TiO2 Thin films prepared by Sol Gel method *J. Mater. Environ. Sci.* **7** 1328–33

[26] Shinen M H, Alsaati S A A and Razooqi F Z 2018 Preparation of high transmittance TiO2 thin films by sol-gel technique as antireflection coating *J. Phys. Conf. Ser.* **1032**

[27] Zhang X, Pint C L, Lee M H, Schubert B E, Jamshidi A, Takei K, Ko H, Gillies A, Bardhan R, Urban J J, Wu M, Fearing R and Javey A 2011 Optically- and thermally-responsive programmable materials based on carbon nanotube-hydrogel polymer composites *Nano Lett.* **11** 3239-44

[28] Panfilova E V., Khlebtsov B N and Khlebtsov N G 2013 Synthesis and optical properties of poly(N-isopropylacrylamide) nanogel containing silver nanoparticles *Colloid J.* **75** 333–8

[29] Brasse Y, Müller M B, Karg M, Kuttner C, König T A F and Fery A 2018 Magnetic and Electric Resonances in Particle-to-Film-Coupled Functional Nanostructures *ACS Appl.Mater. Interfaces* **10** 3133–41

[30] Flat lens criterion by small-angle phase, 2014P Ott, MH Al Shakhs, HJ Lezec, KJ Chau 10.1364/oe.22.029340Optics Express

BIOGRAPHICAL SKETCH

S M Zia Uddin received his B.Sc. in Electrical Engineering from Military Institute of Science & Technology (MIST), Bangladesh in 2017. He has done internship at Atomic Energy Research Establishment (Dhaka, Bangladesh) and Energypac Electronics Ltd. Factory (Dhaka, Bangladesh). He was awarded Presidential Graduate Assistantship (PGRA) from UTRGV (2019-2021). His research interest is in Applied Electromagnetics; Control and Application of Electromagnetic Waves; Theory and Practice of Metamaterials, Optics, Photonics. He was awarded a Master of Science in Engineering: Electrical Engineering from the University of Texas Rio Grande Valley in May of 2021. He can be reached at smziaomi@gmail.com.